



Universitätsklinikum
Hamburg-Eppendorf

UNIVERSITÄTSKLINIKUM HAMBURG-EPPENDORF

Zentrum für Molekulare Neurobiologie Hamburg (ZMNH),
Prof. Dr. Matthias Kneussel

Close Homolog of L1 (CHL1) and its role in the dopaminergic system: biochemical and behavioral consequences of CHL1 and dopamine receptor type 2 interaction

Dissertation

zur Erlangung des Doktorgrades Dr. rer. biol. hum.
an der Medizinischen Fakultät der Universität Hamburg.

vorgelegt von:
Luciana Fernandes, Portugal

Hamburg 2023

UNIVERSITÄTSKLINIKUM HAMBURG-EPPENDORF

Zentrum für Molekulare Neurobiologie Hamburg (ZMNH),
Prof. Dr. Matthias Kneussel

Close Homolog of L1 (CHL1) and its role in the dopaminergic system: biochemical and behavioral consequences of CHL1 and dopamine receptor type 2 interaction

Dissertation

zur Erlangung des Doktorgrades Dr. rer. biol. hum.
an der Medizinischen Fakultät der Universität Hamburg.

vorgelegt von:

Luciana Fernandes, Portugal

Hamburg 2023

**Angenommen von der
Medizinischen Fakultät der Universität Hamburg am: 07.02.2024**

**Veröffentlicht mit Genehmigung der
Medizinischen Fakultät der Universität Hamburg.**

Prüfungsausschuss, der/die Vorsitzende: Prof. Dr. Matthias Kneussel

Prüfungsausschuss, zweite/r Gutachter/in: Prof. Dr. Lars Fester

Prüfungsausschuss, dritte/r Gutachter/in: Prof. Dr. Christian Bernreuther

Contents

Contents	III
Abstract/Zusammenfassung	VII
Chapter I	1
1 Introduction	2
1.1 Cell adhesion molecules superfamilies	2
1.2 Close homolog of L1	3
1.2.1 Structure and expression	3
1.2.2 CHL1 roles in the nervous system	5
1.2.3 Phenotype of CHL1-deficient mice	8
1.2.4 CHL1-related human disorders.....	8
1.2.5 CHL1 and the dopaminergic system – DRD2 connection	10
1.3 Dopamine receptor type-2 in the dopaminergic system	12
1.3.1 Inputs and outputs in midbrain dopaminergic system	12
1.3.2 Dopaminergic receptors: structural features and expression patterns	15
1.3.2.1 DRD2 expression patterns	16
1.3.2.2 DRD2 isoforms	17
1.3.3 DRD2 signal transduction pathways.....	18
1.3.3.1 G protein-dependent pathways of DRD2 signaling	18
1.3.3.2 G protein-independent pathways of DRD2 signaling	21
1.3.4 Physiological roles of DRD2	22
1.3.5 Striatal structure and signaling dichotomy	25
1.3.6 DRD2 functions in striatal-related behaviors	26
1.3.7 DRD2 and neuropsychiatric disorders.....	29
1.4 Aims of the thesis	32
Chapter II	33
2 Materials and Methods	34
2.1 Materials	34
2.1.1 Animals	34
2.1.2 Antibodies.....	34
2.1.3 Solutions, buffers, reagents, and media	35
2.1.3.1 Genotyping and agarose gel electrophoresis	35
2.1.3.2 Cell cultures	36
2.1.3.3 Drug solutions.....	38
2.1.3.4 Biochemical procedures	39
2.1.3.5 Immunofluorescence/histology.....	40
2.1.4 Suppliers of the chemicals, reagents and kits	41

2.2	<i>Molecular biology methods</i>	42
2.2.1	CHL1-deficient mice genotyping	42
2.2.2	Agasore gel electrophoresis	42
2.3	<i>Cell culture methods</i>	43
2.3.1	Coating of coverslips and well plates	43
2.3.2	Culture of ventral midbrain primary neurons	43
2.3.3	Striatal neurons primary culture	44
2.3.4	DRD2-specific compounds and primary cultures treatment.....	45
2.4	<i>Biochemical methods</i>	46
2.4.1	cAMP quantification in ventral midbrain neurons	46
2.4.2	DRD2-specific compounds and animal treatment	47
2.4.3	Protein samples preparation for SDS-PAGE	48
2.4.4	Determination of protein concentration.....	48
2.4.5	SDS-polyacrylamide gel electrophoresis (SDS-PAGE).....	48
2.4.6	Western Blot and relative protein quantification	49
2.5	<i>Immunocytochemistry</i>	50
2.5.1	Immunocytochemistry protocol.....	50
2.5.2	Immunocytochemistry coupled with PLA	50
2.5.3	Quantification of ventral midbrain TH phosphorylation	52
2.5.4	Quantification of striatal DARPP-32 expression.....	52
2.5.5	Sholl analysis of striatal primary neurons	53
2.5.6	Spine analysis of striatal primary neurons	54
2.5.7	Quantification of striatal PSD95 expression.....	55
2.6	<i>Immunohistochemistry and morphology</i>	56
2.6.1	Mouse brain perfusion and cryosectioning.....	56
2.6.2	Antigen retrieval.....	57
2.6.3	Immunohistochemistry coupled with PLA	57
2.6.4	Golgi impregnation technique.....	58
2.6.5	<i>In vivo</i> Sholl analysis and branch order	58
2.7	<i>Behavior protocols</i>	59
2.7.1	Animals and behavioral design.....	59
2.7.2	Animal treatment conditions	60
2.7.3	Handling protocol.....	61
2.7.4	Open field test.....	62
2.7.5	Y-maze: spontaneous alternation	63
2.7.6	Novelty-induced test	64
2.8	<i>Statistical analysis</i>	65

Chapter III	67
3 Results	68
3.1 CHL1 and DRD2 interaction in pre- and postsynaptic dopaminergic neurons	68
3.1.1 CHL1 and DRD2 co-localize pre- and postsynaptically in the striatum of adult mice	68
3.1.2 CHL1 and DRD2 co-localize in cultured TH-positive midbrain neurons and DARPP32-positive striatal neurons.....	70
3.2 Functional consequences of CHL1 and DRD2 interaction in presynaptic dopaminergic and postsynaptic striatal neurons	71
3.2.1 Presynaptic DRD2 signaling cascade is affected by the presence of CHL1 upon pharmacological DRD2-specific modulation	72
3.2.2 Neuronal arborization and dendritic spine morphology of CHL1 KO striatal neurons	77
3.2.2.1 DARPP-32 protein expression in postsynaptic striatal primary neurons is not affected by the absence of CHL1	78
3.2.2.2 DRD2 antagonist and agonist treatment increased dendritic complexity in CHL1 KO striatal neurons <i>in vitro</i>	79
3.2.2.3 CHL1 KO striatal neurons show alterations in dendritic spines after treatment with DRD2 antagonist and agonist	86
3.2.2.4 Lack of CHL1 in striatal neurons prevents the reduction of PSD95 protein levels in the dendritic tree after DRD2 antagonist or agonist treatment	91
3.3 Functional roles of the CHL1 and DRD2 interaction in vivo	95
3.3.1 Decrease of TH (Ser40) phosphorylation in the striatum of CHL1 KO mice is sex- and treatment-dependent.....	95
3.3.2 MSNs of male CHL1 KO mice show a tendency for a lower arbour complexity in the region near the soma	98
3.4 Behavioral characterization of female and male CHL1 KO mice upon DRD2 pharmacological modulation	102
3.4.1 Open field: locomotor, exploratory, and emotional evaluation	103
3.4.2 Y-maze: short-term working spatial memory.....	121
3.4.3 Novelty-induced behavior: the spontaneous exploration of a novel object	126
Chapter VI	133
4 Discussion	134
4.1 CHL1 and DRD2 interact in presynaptic dopaminergic and postsynaptic striatal neurons	134
4.2 Functional impact of the CHL1 interaction with pre- and postsynaptic DRD2	136
4.2.1 CHL1 modulates agonist-induced responses of presynaptic DRD2 while basal DRD2 signaling remains unaffected <i>in vitro</i>	136
4.2.2 Sex- and genotype-dependent modulation of TH phosphorylation in the striatum by DRD2 agonism	138
4.2.3 CHL1 and DRD2 stimulation alters complexity of cultured MSNs.....	139

4.2.4	Interpreting the CHL1 modulation of pre- and postsynaptic DRD2 functions	144
4.2.4.1	CHL1 might act as an allosteric modulator of DRD2 in response to an agonist	144
4.2.4.2	CHL1 might contribute to the maturation of DRD2-dependent signaling during embryonic stages 145	
4.2.4.3	Advantages and limitations of the <i>in vitro</i> models	147
4.3	<i>Behavioral characterization of the CHL1 and DRD2 interaction</i>	148
4.3.1	CHL1 modulates locomotor activity and influences postsynaptic effects of DRD2 antagonism and presynaptic effects of DRD2 agonism in a sex-dependent manner	148
4.3.2	CHL1's role in emotional homeostasis and its influence on sex-specific sensitivity to DRD2 antagonism in females and DRD2 agonism in males	151
4.3.3	Impact of dopaminergic modulation on spontaneous alternation of CHL1 KO mice: working memory is more vulnerable to changes in dopamine triggered by sulpiride in males and by quinpirole in females and males	154
4.3.4	CHL1 does not impact novelty-seeking behavior	157
4.3.5	Sex-dependent behaviors and final assumptions	159
Chapter V	164
5	Conclusion	165
	Abbreviations.....	167
	References	170
	Annex I	188
	Acknowledgements	189
	Curriculum Vitae	190
	Eidesstattliche Erklärung	191

Abstract/Zusammenfassung

Dopamine is a neurotransmitter essential to coordinate biochemical and behavioral functions in the striatum by modulating dopamine receptor signaling, including the dopamine receptor type-2 (DRD2). DRD2 abnormalities are a hallmark of various neuropsychiatric disorders, such as schizophrenia and Parkinson's disease. Genome-wide studies have associated the cell adhesion molecule close homolog of L1 (CHL1) as a risk gene to develop neuropsychiatric disorders. CHL1 and DRD2 were shown to interact and CHL1 KO mice exhibit pre- and postsynaptic dopaminergic dysfunction within the striatum. However, the functional implications of the CHL1-DRD2 interaction remained unexplored so far. Therefore, this thesis aims to functionally characterize the CHL1 and DRD2 interaction, by investigating how their interplay influences both biochemical mechanisms and behavior modulated by these proteins. By employing cultured primary neurons from WT and CHL1 KO mice, the impact of DRD2 pharmacological modulation with the antagonist sulpiride and the agonist quinpirole was assessed on the presynaptic DRD2 signaling pathway and the postsynaptic DRD2-dependent regulation of dendrite and spine morphology.

The ablation of CHL1 in ventral midbrain primary neurons had no impact on presynaptic DRD2 signaling under basal conditions, as shown by similar cAMP levels and total and phosphorylated TH, GSK3 β , and ERK1/2 protein levels. However, in response to quinpirole and sulpiride, the absence of CHL1 increased the neurons' sensitivity, particularly to sulpiride, which reduced phosphorylated TH protein stronger in CHL1 KO neurons compared to WT neurons. In striatal primary neurons, the detailed assessment of neuronal morphology and synaptic plasticity revealed that CHL1 impacted the function of DRD2 in a developmental-dependent manner. Furthermore, the results indicate that the absence of CHL1 does not exert significant effects under basal conditions but alters neuronal sensitivity to DRD2 modulation, thereby affecting both pre- and postsynaptic DRD2 functions.

Behavioral assessment of striatal-dependent functions was conducted using adult female and male WT and CHL1 KO mice, focusing on parameters influenced by presynaptic DRD2 signaling, including locomotor activity, exploration, emotionality, working memory, and novelty-seeking behavior. Sulpiride treatment reduced locomotor activity of CHL1 KO females. Quinpirole treatment resulted in a general reduction in locomotion of WT and CHL1 KO mice, with a delayed effect observed for CHL1 KO mice. Vehicle-treated CHL1 KO males exhibited reduced locomotor activity compared to WT males, while no differences were found in females. CHL1 ablation appeared to diminish reactivity and stress-related behaviors in males, while females showed an unaltered emotional state. Working memory and novelty-seeking behavior remained unaffected by CHL1 ablation, DRD2 modulation, or sex. These findings indicate that CHL1 modulates presynaptic DRD2 functions in a sex-dependent manner, potentially involving reduced presynaptic DRD2 activity.

My findings shed light on the intricate relationship between CHL1 and DRD2 in the context of dopaminergic signaling and its impact on behavior, revealing both sex-dependent and independent parameters. This expands the understanding of the complex mechanisms that could underlying neuropsychiatric disorders and emphasizes the importance of considering sex-specific differences in future investigations of the dopaminergic system and its related pathologies.

Dopamin ist ein Neurotransmitter der biochemische Prozesse im Striatum unerlässlich ist, indem er die Signalübertragung von Dopaminrezeptoren, einschließlich des Dopaminrezeptors Typ 2 (DRD2), moduliert. DRD2-Anomalien sind ein Kennzeichen verschiedener neuropsychiatrischer Erkrankungen wie Schizophrenie und Parkinson. Genomweite Studien haben das Zelladhäsionsmolekül *close homolog of L1* (CHL1) als eines der Risikogene für die Entwicklung vieler neuropsychiatrischer Störungen identifiziert. Außerdem wurde gezeigt, dass CHL1 und DRD2 interagieren und dass CHL1-defiziente Mäuse prä- und postsynaptische dopaminerge Dysfunktionen im Striatum aufweisen. Die funktionellen Auswirkungen der CHL1-DRD2-Wechselwirkung blieben bisher jedoch unerforscht. Daher zielte meine Arbeit darauf ab, die Interaktion von CHL1 und DRD2 funktionell zu charakterisieren. Dabei wurde der Effekt des Zusammenspiels von CHL1 und DRD2 auf dopaminerge Signalwege im Striatum und auf das Verhalten von Mäusen untersucht. Mithilfe kultivierter primärer Neuronen von wildtypischen (WT) und CHL1-defizienten Mäusen wurde der Einfluss der pharmakologischen Modulation von DRD2 mit dem Antagonisten Sulpirid und dem Agonisten Quinpirol auf den präsynaptischen DRD2-Signalweg und die postsynaptische DRD2-abhängige Regulierung der Dendriten- und Spinemorphologie untersucht.

Die Ablation von CHL1 in Primärneuronen des ventralen Mittelhirns hatte unter basalen Bedingungen keinen Einfluss auf den präsynaptischen DRD2-Signalweg, da ähnliche cAMP-Spiegel sowie ähnliche Mengen an phosphoryliertem TH-, GSK3 β - und ERK1/2-Protein sowie deren Gesamtproteinmengen in WT und CHL1-defizienten Neuronen vorlagen. Die Behandlung mit Sulpirid und Quinpirol dagegen führte in CHL1-defizienten Neuronen zu einer verstärkten Reaktion. Insbesondere Sulpirid-Behandlung reduzierte die Menge an phosphoryliertem TH in CHL1-defizienten Neuronen stärker als in WT Neuronen. In striatalen Primärneuronen wurde eine detaillierte Bewertung der neuronalen Morphologie und Synapsenplastizität vorgenommen, welche zeigte, dass CHL1 die Wirkungen von Quinpirol und Sulpirid in einer entwicklungsabhängigen Weise beeinflusst. Darüber hinaus deuten die Ergebnisse darauf hin, dass das Fehlen von CHL1 unter basalen Bedingungen keine signifikanten Auswirkungen hat, aber die neuronale Empfindlichkeit für die Modulation von DRD2

verändert, wodurch sowohl präsynaptische als auch postsynaptische DRD2-Funktionen beeinflusst werden.

Die Bewertung der Fortbewegung und des durch das Striatum vermittelten Verhaltens erfolgte mit erwachsenen weiblichen und männlichen WT und CHL1-defizienten Mäusen. Dabei lag der Schwerpunkt der Untersuchung auf Parametern die von der präsynaptischen DRD2-Signaltransduktion beeinflusst werden, wie die lokomotorische Aktivität, die Exploration, die Emotionalität, das Arbeitsgedächtnis und die Reaktion auf Neues. Sulpiridbehandlung reduzierte selektiv die lokomotorische Aktivität CHL1-defizienter Weibchen. Die Behandlung mit Quinpirol führte sowohl bei WT als auch bei CHL1-defizienten Mäusen zu einer allgemeinen Verringerung der lokomotorischen Parameter, wobei bei CHL1-defizienten Mäusen eine verzögerte Wirkung festgestellt wurde. Diese verzögerte Wirkung war bei CHL1-defizienten Männchen ausgeprägter als bei CHL1-defizienten Weibchen. Mit Vehikel-Lösung behandelte CHL1-defiziente -Männchen zeigten eine reduzierte Locomotoraktivität im Vergleich zu WT Männchen, während bei Weibchen keine Unterschiede festgestellt wurden. Die Ablation von CHL1 verzögerte die Reaktivität auf Quinpirol und das stressbedingte Verhalten bei Männchen, während der emotionaler Zustand der CHL1-defizienten Weibchen unverändert war. Das Arbeitsgedächtnis und die Reaktion auf neue Objekte wurden weder von der Ablation von CHL1 noch von der DRD2-Modulation oder dem Geschlecht beeinflusst.

Meine Ergebnisse werfen ein neues Licht auf die komplexe Beziehung zwischen CHL1 und DRD2 im Zusammenhang mit der dopaminergen Signalgebung und deren Auswirkungen auf das Verhalten, wobei sowohl geschlechtsabhängige als auch -unabhängige Parameter vorliegen. Dies erweitert das Verständnis der komplexen Mechanismen die neuropsychiatrischen Störungen zugrunde liegen könnten und betont die Bedeutung der Berücksichtigung geschlechtsspezifischer Unterschiede bei zukünftigen Untersuchungen des dopaminergen Systems und seiner damit verbundenen Pathologien.

Chapter I

Introduction

1 Introduction

1.1 Cell adhesion molecules superfamilies

Cell adhesion molecules (CAMs) are a group of cell surface proteins that mediate contact between neighboring cells (trans-interaction) or within the same cell (cis-interaction) by homophilic interaction with identical molecules or heterophilic interaction with other binding partners present in the membrane or extracellular matrix (ECM). The homo- and heterophilic interaction of CAMs are essential for the proper development and maintenance of the central nervous system (CNS) architecture and for synaptic transmission^{1,2}. CAMs were originally divided into three superfamilies: cadherins superfamily, integrins superfamily, and immunoglobulin superfamily of cell adhesion molecules (IgSF). Later, other superfamilies have been described in the nervous system: C-type lectin-like domain proteins (CTLDs), neuroligins/neurexins system, and leucine-rich repeat proteins (LRRs)³⁻⁵.

IgSFs are a diverse group of cell-surface proteins that are categorized by at least one extracellular immunoglobulin (Ig)-like domain and these CAMs mediate cell adhesion in a Ca²⁺-independent manner. The extracellular domains of these CAMs typically mediate cell adhesion via homo- and heterophilic interactions with a variety of surface receptors, other CAMs, and ECM proteins^{3,4}. IgSFs can directly or indirectly interact with the cytoskeleton via their intracellular domains or function as downstream mediators in signaling pathways in a wide range of cellular processes. During development, IgSFs play a critical role in regulating the migration and survival of neurons, promoting neurite outgrowth, and facilitating the establishment of synaptic contacts between neurons. In the mature brain, IgSFs are essential for the composition, function, and plasticity of synapses, which are important cell-to-cell contacts⁶⁻⁸.

Most IgSFs are single-span type I transmembrane proteins containing several glycosylation sites and they can be classified into two major groups: those containing one or more Ig-like domain(s) and those with Ig-like domains followed by fibronectin type III repeats (FN-III). Proteins in the first group include P0, Thy-1, and the myelin-associated glycoprotein, while the second group can be further subdivided into two families: neural cell adhesion molecule (NCAM) and L1 subfamilies⁴. The L1 family of CAMs in vertebrates is subdivided into four members: L1, close homolog of L1 (CHL1), neuron-glia-related CAM (NrCAM), and neurofascin (NF, with the two subtypes NF186, and NF155)⁶. These proteins are characterized by a modular structure consisting of six Ig-like domains, three to five FN-III domains, a transmembrane domain, and a short highly conserved intracellular domain (Fig. 1.1).

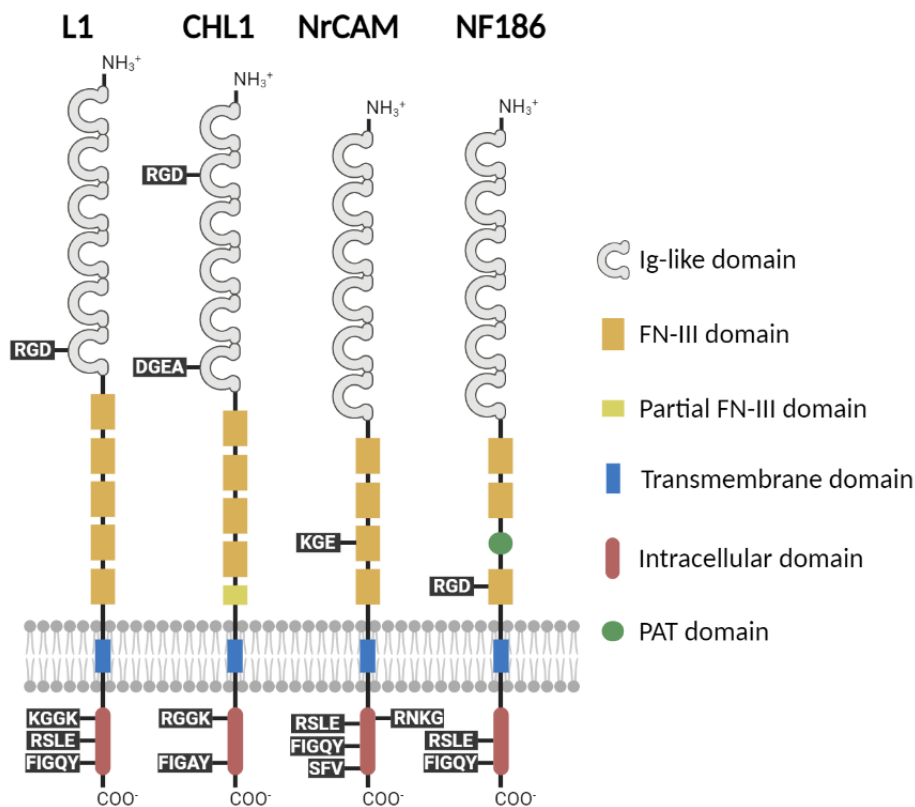


Figure 1.1. Domain structure of L1-CAM family members: L1, CHL1, NrCAM, and NF186. The figure illustrates the overall organization of extracellular Ig-like and FN-III domains, the transmembrane domain, and the cytoplasmic tail. CHL1 contains one partial FN-III domain, and the 186 kDa isoform of neurofascin (NF186) possesses a proline-, alanine-, threonine (PAT)-rich domain. Integrin-binding sites are indicated in the ectodomains, including the Arg-Gly-Asp (RGD) motif in the sixth Ig-like domain of L1, the second Ig-like domain of CHL1, the third FN-III domain of NF186⁹, and the Lys-Gly-Glu (KGE) motif in the third FN-III domain of NrCAM¹⁰. Additionally, CHL1 has an Asp-Gly-Glu-Ala (DGEA) motif in its sixth Ig-like domain, which interacts with $\beta 1$ integrins¹¹. Ezrin-radixin-moesin (ERM) proteins interact with similar membrane-proximal motifs in the intracellular domains of L1-CAM proteins, such as the conserved sequence Arg-Ser-Leu-Glu (RSLE) in L1, NrCAM, and NF186, the KGGK motif in L1, as well as the RGGK motif in CHL1¹², and the RNKG motif in NrCAM¹³. An ankyrin-binding motif, Phe-Ile-Gly-Gln-Tyr (FIGQY), is highly conserved between L1, NrCAM, and NF186, while CHL1 has an alternative sequence with the same functional properties, Phe-Ile-Gly-Ala-Tyr (FIGAY)¹¹. NrCAM presents an additional SFV sequence at the carboxy terminus, which serves as a PZD domain-binding motif for synapse-associated protein (SAP) 90/postsynaptic density 95 (PSD95) and SAP97 proteins¹⁴. The illustration was created using [Biorender](#).

1.2 Close homolog of L1

1.2.1 Structure and expression

CHL1, a member of the L1 family of cell adhesion molecules, was identified through complementary deoxyribonucleic acid (cDNA) library screening using L1 antibodies. In mice, its extracellular domain shares 37% similarity with L1, while its intracellular domain shows the highest homology with L1 (57%) or NrCAM (64%)⁹. CHL1 differs from other family members in several

ways: (i) it has four and a half FN-III domains in the extracellular region, (ii) it features a DGEA motif in the sixth Ig-like domain that is known to interact with $\beta 1$ integrins, (iii) its intracellular FIGAY motif sequence is altered and it is possibly an ankyrin-binding domain, (iv) it lacks the RSLE motif in the intracellular domain but contains an alternative RGGK motif, interacting with ERM proteins (Fig. 1.1)^{9,11,12}.

Three distinct fragments of CHL1 have been identified in brain extracts: a 185 kDa transmembrane form and two soluble forms at 165 kDa and 125 kDa⁹. These forms result from cleavage by ADAM8 (a disintegrin and metalloproteinase)¹⁵. Additionally, a C-terminal fragment is also generated by β -site amyloid precursor protein cleaving enzyme 1 (BACE1) cleavage between Gln1061 and Asp1062 residues upon semaphorin 3A (Sema3A) binding¹⁶. Approximately 15-20% of CHL1's molecular mass comprises N-glycosylated carbohydrates^{9,17}. In humans, CHL1 messenger ribonucleic acid (mRNA) and protein are most abundant in the brain, especially in the cerebral cortex, cerebellum, and caudate, in descending order of expression. Elevated CHL1 expression is also found in various other organs, including the respiratory system, kidneys, skin, soft tissues, and the male and female reproductive organs¹⁸.

In mice, CHL1 shows a unique temporal and spatial expression pattern, being expressed in specific neuronal subpopulations across various structures in the CNS at a slightly different timeframe than other CAMs, such as L1. Immunofluorescence analysis of live cells revealed the presence of CHL1 in primary cultures of hippocampal, cortical, mesencephalic, and spinal cord neurons¹⁷. In the hippocampus, CHL1 mRNA is elevated in interneurons of the proper and hilar regions and in the CA1 and CA3 pyramidal cell layers at postnatal day 7 (P7). At 2-4 weeks of age, CHL1 is prominent in the hilus of the dentate gyrus and mossy fibers of the CA3 region^{17,19}. CHL1 is also seen in neuronal cell bodies in layer V of the cerebral cortex at P7, followed by subsequent downregulation¹⁷. In the thalamus, CHL1 mRNA increases at P7 in various regions except the medial thalamus, then decreases strongly until three weeks after birth¹⁷. CHL1 is expressed in non-myelinating Schwann cells in the PNS, and unlike L1, is also present in glial cells in the CNS such as astrocytes and oligodendrocyte precursors¹⁷. CHL1 expression in the whole brain is first detected on embryonic day 13 (E13), reaches its peak levels around E18 until P7, and then declines to lower but still significant levels during adulthood^{9,17}. Specifically in the midbrain, CHL1 expression varies within neuronal populations of the same brain structure and across the developmental timeline²⁰

Studies in heterozygous transgenic mice have shown that CHL1 exhibits a gene dosage effect²¹. A 50% reduction in CHL1 expression in the hippocampus resulted in a spectrum of histological and behavioral phenotypes, ranging from wild-type (WT) to CHL1 knockout (KO) mice, as well as intermediate phenotypes. Additionally, microdeletions or extra copy variants in the human *CHL1* gene (*CALL*) have been associated with cognitive, behavioral, motor, and coordination deficits²². This emphasizes the importance of the correct *CHL1* gene dosage for normal brain function.

1.2.2 CHL1 roles in the nervous system

The functions of CHL1 in the nervous system are critical for normal brain development and the maintenance of neuronal circuits during adulthood. CHL1 is involved in key processes, such as neuronal outgrowth, proliferation, differentiation, and survival, and is also linked to synapse formation during brain development.

Neurite outgrowth is one of the processes that CHL1 influences, and it has been shown to be cell-specific and to vary depending on the type of interaction established. *In vitro* studies have reported that homophilic CHL1 trans-interactions inhibit neurite outgrowth, whereas heterophilic CHL1 trans-interactions enhance it, as demonstrated by the following literature. Neurite length and branching are higher when hippocampal neurons and astrocytes are co-cultured and CHL1 is expressed in only one type of cells, whereas mutual expression leads to lower outgrowth²³. Similarly, studies using CHL1 as a substrate-bound or soluble form have shown that neurite outgrowth is promoted in cultured mouse cerebellar granule neurons and rat hippocampal neurons^{17,24}. Using the same approach, substrate-bound CHL1 stimulates higher neuritogenesis in P6 to P8 mouse cerebellar neurons deficient in CHL1 than in WT neurons, without affecting neurite length on P4 to P5 cultures. This CHL1-promoted outgrowth is mediated by endogenous vitronectin, which induces the interaction of CHL1 with integrins specifically by its RGD motif, which is not involved in L1-induced neuritogenesis²⁵. The same experimental design was used to examine primary cultures of mouse ventral midbrain neurons, which are frequently employed as a model to study dopaminergic signaling. Interestingly, only dopaminergic neurons expressing CHL1 exhibited increased neurite length and branching in response to substrate-bound CHL1, whereas CHL1 KO dopaminergic neurons or other types of neurons did not show any morphological changes²⁰. These findings contrast with previous results and demonstrate that the homophilic CHL1 interaction induces neuritogenesis specifically in dopaminergic neurons, revealing a cell-specific effect.

Research has also demonstrated CHL1's ability to act as a molecular cue for axon guidance. Studies on CHL1 KO mice have revealed persistent axonal misguidance in several areas, including the cerebellum, hippocampus, cortex, thalamocortical projections, and ventral midbrain^{20,26–29}. In thalamic primary neurons, CHL1 is necessary to promote Sema3A-induced growth cone collapse mediated by its binding to neuropilin1, showing an indirect repellent effect of CHL1 in axon guidance²⁹. However, later studies revealed that a C-terminal fragment of CHL1 cleaved by BACE1 is necessary to restore Sema3A-induced growth cone collapse in CHL1 KO thalamic neurons¹⁶. A similar Sema3A-induced growth cone collapse mechanism for repulsive axon guidance has been described in embryonic cortical neurons and is dependent on CHL1's interaction with ezrin, a filamentous actin-binding protein¹². Moreover, the CHL1-neuropilin1 complex is also thought to interact trans-heterophilically with ALCAM specifically on growth cones of dopaminergic primary neurons to mediate their growth and

branching based on the type of semaphorin present³⁰. A prior *in vitro* study revealed that CHL1 plays a crucial role in dopaminergic fiber guidance not only by providing chemoattractive cues to migrating dopaminergic neuroblasts but also exhibiting a chemorepulsive effect on neurites of ventral midbrain explants²⁰.

The impact of CHL1 on the migration of neurons is influenced by various factors, including the developmental stage or type of neuron. Cultured cerebellar granule neurons from P6 to P8 CHL1 KO mice exhibit a decrease in the number of migrating cells and a slower migration rate compared to WT neurons, with the positive impact of CHL1 on this process relying on heterophilic interactions^{25,31}. Moreover, HEK293 cells transfected with CHL1 show an enhanced migration toward several ECM substrates (e.g., collagen I or vitronectin)¹¹. *In vivo* sections of the cerebellum have revealed that CHL1's positive impact on neuronal migration is present at later stages of postnatal development (P5 to P7), whereas earlier migration is CHL1-independent²⁵. The migration of cerebellar neurons at P6 to P8 is strongly influenced by the heterophilic trans-interactions of CHL1 with vitronectin, β 1 integrins, and plasminogen activator inhibitor-2, which is dependent on the RGD motif in the second Ig-like domain²⁵. However, another study using a non-neuronal cell model reported that CHL1 binding to β 1 integrins is dependent on the DGEA motif present in the sixth Ig-like domain¹¹. Furthermore, a contrasting effect of CHL1 on neuronal migration has been reported when assessing this parameter in neuronal progenitor cells (NPCs) from the cortex of E14.5 embryos³². CHL1 was found to negatively affect the migration of these neurons *in vitro* and *in vivo*, a process that was dependent on the activation of the extracellular signal-regulated kinase 1/2 (ERK 1/2) pathway.

Neuronal differentiation is another important process to which CHL1 is connected. In cultured cortical NPCs, CHL1 has been found to have a negative effect on differentiation³². Similarly, using dissociated cerebellar cells of P4 and cerebellar sections of P5 WT and CHL1 KO mice, it was shown that homophilic CHL1 trans-interactions inhibit differentiation²⁵. Notably, the effect of CHL1 appears to be dependent on the type of neuron, as homophilic interactions enhance the differentiation of E12.5 ventral midbrain primary neurons²⁰.

Several studies have investigated the impact of CHL1 on neuronal survival in culture. Specifically, in cultured postnatal cerebellar granule cells from mice and embryonic hippocampal neurons from rats, the presence of CHL1 in a soluble form has been found to increase neuronal survival^{24,31}. Likewise, the survival of postnatal organotypic cultures of cerebellar granule and Purkinje neurons has been shown to be dependent on CHL1 binding to the hedgehog receptor patched-1 (PTCH1), resulting in higher levels of cell survival³³.

CHL1 is a crucial player in the process of synaptogenesis during neuronal development, as well as in the maturation and maintenance of synapses in adulthood. Dissociated hippocampal neurons exhibit a notably higher level of CHL1 in the plasma membrane of both inhibitory and excitatory presynaptic terminals³⁴. The absence of CHL1 has been linked to impaired γ -aminobutyric acid (GABA)-ergic

signaling in presynaptic terminals in various brain regions. For instance, CHL1 deficiency enhances perisomatic inhibition in the hippocampus by increasing the number of inhibitory parvalbumin-positive interneurons, consequently leading to impaired long-term potentiation in mice¹⁹. Moreover, in the cerebellum of CHL1 KO mice, stellate axons migrate and establish inhibitory synapses with Purkinje dendrites but at significantly reduced efficiency and density, leading to progressive atrophy of these axon terminals²⁶. The determinant role of CHL1 in the maintenance of these presynaptic connections during adulthood has been further strengthened by the notion that CHL1 directly interacts with and positively regulates the activity of chaperones and soluble N-ethylmaleimide-sensitive factor attachment protein receptor (SNARE) complex, promoting the exocytosis and recycling of synaptic vesicles in the presynaptic membrane^{34,35}. Furthermore, CHL1 has been implicated in the regulation and maintenance of postsynaptic terminals. Notably, in pyramidal cortical neurons of adult mice the lack of CHL1 promoted an increase in excitatory synapses and disrupted synaptic strength in postsynaptic terminals³⁶.

Recent publications have revealed CHL1's potential role as a key player in initiating signaling pathways by directly binding to neurotransmitter receptors, suggesting a critical modulation of neural processes in adulthood. One study revealed that CHL1 binds to the serotonin 2c (5-HT_{2c}) receptor via its intracellular domain and modulates serotonergic signaling by reducing the binding of phosphatase and tensin homolog (PTEN) and enhancing the binding of β -arrestin 2 to the receptor³⁷. This interaction occurs in GABAergic interneurons of the striatum, potentially contributing to the hypolocomotion observed in CHL1 KO mice due to 5-HT_{2c} receptor inhibition. A separate study discovered an interaction between the extracellular domain of CHL1 and the first extracellular loop of dopamine receptor type-2 (DRD2)³⁸. Based on the findings of impaired dopaminergic presynaptic signaling in the dorsal striatum and postsynaptic signaling in the ventral striatum, it was proposed that the absence of CHL1 might lead to the constitutive activation of both pre- and postsynaptic DRD2 receptors.

The regeneration of damaged nervous tissue during adulthood is another process in which CHL1 is known to be involved. Following peripheral nerve crush or peripheral nerve grafting into the thalamus, levels of CHL1 mRNA are upregulated in motor, sensory, thalamic neurons, and glial cells, indicating the important role of CHL1 in the regeneration of lesioned nervous tissue^{39,40}. Similarly, after peripheral nerve trauma, CHL1 expression is more pronounced in axons of motor neurons than in Schwann cells, contributing to the guidance of regenerating neurites into the proper nerve branch⁴¹. Moreover, CHL1's impact on axonal growth and spinal circuit remodeling during regeneration after spinal cord injury is evidenced by the faster improvement of CHL1 KO mice compared to their WT littermates²³.

1.2.3 Phenotype of CHL1-deficient mice

The significance of CHL1 in the development and functioning of neuronal pathways has been demonstrated using CHL1 KO mice, where its ablation leads to various morphological and functional impairments.

At the morphological level, CHL1-deficient mice exhibit enlarged lateral ventricles and altered organization of hippocampal mossy fibers and olfactory axon projections as well as abnormal branching and misguidance of pyramidal neurons in neocortical areas, stellate cells in the cerebellum, thalamic projections, and dopaminergic neurons in the ventral midbrain^{20,26–29}. Furthermore, a significant loss of Purkinje cells and granule cells in the mature cerebellum, along with an increased number of parvalbumin-positive hippocampal interneurons during development, but a reduced number in adulthood, has also been observed in CHL1 KO mice^{19,31,42}. Deficits in short- and long-term potentiation at CA3-CA1 excitatory synapses are also present in adult mice^{19,42}. Additionally, spine density is affected since CHL1 KO mice have a smaller number of mature mushroom or stubby spines on the apical dendrites of neurons in the prefrontal and visual cortex of young and adult mice³⁶. Moreover, DRD2 signaling is functionally impaired in CHL1 KO adult mice owing to the reduced phosphorylated levels of tyrosine hydroxylase (TH) and dopamine- and cAMP-regulated phosphoprotein 32 kDa (DARPP-32) proteins in the striatum³⁸.

Behavioral investigations of CHL1 KO mice initially did not reveal any differences in life span, viability, fertility, general behavior, or motor and sensory functions compared with their WT littermates²⁷. However, an altered pattern of exploratory behavior in a novel environment has been described along with indications of a reduced anxiety-like state^{27,43,44}. Cognitive impairments are also found in this mutant, including a general deficit, a slower processing speed while employing working memory and an impaired interval timing^{43–46}. The CHL1 KO mice also exhibit lower levels of aggressiveness, reduced reactivity to novel environmental stimuli, and reduced expression of social behaviors^{21,43,44}. Specifically, the delayed reactivity to novel and social stimuli is supported by the finding that these animals show impaired prepulse inhibition of the acoustic startle response, indicating an inability to gate sensorimotor information, and reduced latent inhibition^{47,48}. Additionally, it has been suggested that CHL1 deficiency in mice can lead to 5-HT_{2c} receptor-related reduction in locomotor activity and reactivity to novelty³⁷.

1.2.4 CHL1-related human disorders

The human gene coding for CHL1, *CALL*, is located on chromosome 3p26.3. Deletions, mutations and duplications of the end of the small p arm of chromosome 3 that contains the locus for *CALL* have been identified in patients exhibiting non-specific and variable forms of cognitive impairment and were occasionally associated with the onset of specific neurological disorders such as autism spectrum

disorders (ASD), major depressive disorder, or schizophrenia^{49–52}. Deletions are the most common type of mutation observed in *CALL*, occurring in 69% of individuals, whereas the remaining 31% display duplications or triplications⁵³. With regard to inherited gene expression patterns of *CHL1*, *de novo* occurrences are the most common ones, observed in 25% of individuals, followed by maternally inherited patterns in 5%, and inheritance from an unaffected parent in 3% of the cases⁵³.

The 3p deletion syndrome is a rare disorder and different genes located within this region can be affected. Individuals with this syndrome display a variable phenotype, but the core features typically include intellectual disability, motor developmental delay, facial dysmorphisms, hypotonia, and other less common symptoms such as congenital heart disease, ASD-related features, or epilepsy⁵⁴. Several clinical reports have demonstrated that deletions on *CALL* might contribute to the impaired cognitive function and non-specific developmental delays seen in the syndrome, while deletions of *Cereblon* (*CRBN*) and/or *Contactin-4* (*CNTN4*) contribute to the development of dysmorphic features and intellectual disability^{21,55–57}. Although isolated deletions on *CALL* are rare, clinical cases have been reported and show variable phenotypes with shared features, including linguistic development delay, learning difficulties, and varying levels of intellectual disability^{58,59}. Isolated microduplications on the chromosomal region 3p26.3, which only involve *CALL*, are extremely rare and have been reported in only a few cases with duplication sizes ranging from 0.66 Mb to 1.07 Mb. Clinical reports of the patients revealed non-syndromic developmental phenotypes characterized by shared features of intellectual disability and global developmental delay, with marked impairments in language and speech development^{53,55,60,61}. Additionally, each individual displayed unique clinical features, such as epilepsy, hyperactivity symptoms, or ASD^{55,60,61}. This evidence implies that *CHL1* is a dosage-sensitive gene, indicating that both deletions and duplications of this gene can cause non-syndromic neurodevelopmental phenotypes^{53,61}.

Genetic alterations in *CALL* have been linked to the development of several neuropsychiatric disorders. Several studies examining the human genome have reported that the presence of various copy number variants in *CHL1*, either alone or in combination with other altered genes, might increase susceptibility to ASD in certain individuals^{49,61,62}. Furthermore, genome-wide expression profiling of human lymphoblastoid cell lines has identified *CHL1* as a potential response biomarker for selective serotonin reuptake inhibitors (SSRI) antidepressants, and further investigations on European individuals have identified specific single nucleotide polymorphisms (SNPs) as potential indicators of treatment-resistant depression, underscoring the importance of this gene in the context of major depressive disorder^{50,63,64}.

Schizophrenia, a complex mental disorder, is believed to result from a combination of prenatal complications, childhood trauma, environmental exposure, or genetic factors^{65,66}. Genetic research has consistently linked polymorphisms in the human *CHL1* gene to the occurrence of schizophrenia in various populations. Notably, a missense polymorphism (Leu17Phe) in *CALL* has been found to be

more prevalent in individuals with schizophrenia than in healthy controls, particularly in Japanese and Qatari populations^{67,68}. This association was further supported by a study of Han Chinese individuals⁶⁹. Genome-wide investigations have also highlighted CHL1's role in schizophrenia susceptibility, identifying a rare deletion variant in the CHL1 gene in the Scottish population and observing dysregulation of the gene in postmortem thalamic neurons of individuals diagnosed with schizophrenia^{51,52}.

Interestingly, the constitutive ablation of CHL1 in mice replicates behavioral traits resembling typical symptoms observed in human neuropsychological disorders, such as reduced response to novel stimuli, altered social preference, and deficits in spatial-temporal integration^{43,44,46}. These observed characteristics are consistent with the core features of ASD and schizophrenia, which include deficits in social interaction and intellectual and learning disabilities^{62,70}. The disturbed prepulse inhibition and latent inhibition exhibited by CHL1 KO mice^{47,48} mirror the abnormal processing of information and attentional deficits observed in individuals with schizophrenia^{48,71}. Furthermore, ablation of CHL1 in mice leads to various morphological anomalies, including enlarged ventricles and reduced levels of parvalbumin-positive neurons in the hippocampus^{27,42}, which are consistently recognized as features associated with the pathophysiology of schizophrenia^{72,73}.

1.2.5 CHL1 and the dopaminergic system – DRD2 connection

A connection between CHL1 and the dopaminergic system was demonstrated in a comprehensive study that reported the impact of CHL1 on the development of the ventral midbrain dopaminergic pathways⁷⁴. Briefly, the development of these pathways involves the migration of dopaminergic neuroblasts from the ventral midbrain to their targets in the dorsolateral ganglionic eminence (developing striatum) and the overlying cortex, forming the nigrostriatal and mesocorticolimbic pathways, respectively⁷⁴. *In vitro* studies conducted by Alsanie et al.²⁰ have elucidated the role of CHL1 in guiding and promoting the migration of ventral midbrain neurons. CHL1 was found to provide chemoattractive cues to migrating dopaminergic neuroblasts and chemorepulsive signals to neurites in ventral midbrain explant cultures. Specifically, the homophilic CHL1-CHL1 interaction positively influenced neurite outgrowth, enhanced branching and length of primary dopaminergic neurons, and further promoted differentiation by increasing the proportion of dopaminergic neurons compared to CHL1-deficient cultures²⁰. The notion of CHL1's novel roles in the establishment of dopaminergic pathways is supported by the observation of the temporo-spatial CHL1 expression pattern during embryonic stages across the multiple substructures of the ventral midbrain²⁰.

Prior to the aforementioned study, studies investigating behavioral phenotypes and brain morphology in WT and CHL1 KO mice suggested a correlation between CHL1 deficiency and the development of psychiatric disorders, with particular emphasis on disorders associated with aberrant dopaminergic system functioning. As mentioned in the previous section, CHL1 has been implicated in

susceptibility for developing ASD and schizophrenia, two disorders which rely heavily on a pronounced impairment of dopaminergic signaling in the mesolimbic and nigrostriatal pathways accordingly to their neurobiological theories^{75,76}. Similarly, a common consequence of *CALL* mutations in humans, such as delayed speech development, strongly depends on the proper functioning and morphological structure of the striatum⁷⁷. Interestingly, the behavioral traits observed in CHL1 KO mice resembling the symptoms observed in ASD or schizophrenia, as described in the previous section, can be influenced or enabled by dysfunction in dopaminergic signaling. For instance, activation of the mesolimbic pathway has been linked to increased exploration of novel stimuli⁷⁸, while prepulse inhibition has been associated with dopaminergic activation of the medial prefrontal cortex⁷⁹. The presence of shared behavioral traits between CHL1 KO mice and psychiatric disorders, along with vulnerability to dopaminergic dysfunction in these conditions, suggests a potential interplay between CHL1 and the dopaminergic signaling pathways. However, the specific neurocircuits or key elements involved in this relationship have yet to be elucidated.

When exploring the intricate pathophysiology of ASD and schizophrenia, one prominent mechanism that strongly contributes to their phenotypes is the impairment of DRD2 signaling, characterized by alterations in the density or sensitivity of the receptor. These changes contribute to subsequent disruptions in the striatal and dopaminergic neurotransmission^{75,76}. Treatment of specific symptoms of schizophrenia often involves the use of first-generation antipsychotic drugs, which are DRD2-specific antagonists⁷⁶. Similarly, atypical antipsychotic drugs targeting DRD2 are sometimes utilized to improve challenging behaviors in ASD, although to a lesser extent⁷⁵. Furthermore, NCAM180, an IgSF, has been shown to interact with and to regulate DRD2 internalization⁸⁰, while CHL1 possesses the capacity to interact with neurotransmitter receptors such as the 5-HT_{2c} receptor³⁷. These findings prompted investigation of the interaction between CHL1 and DRD2 which could potentially influence the neurobiological mechanisms underlying ASD and schizophrenia.

Exploration of the role of CHL1 as a modulator of dopaminergic signaling via DRD2 led to the discovery of the interaction between the extracellular domain of CHL1 and the first extracellular loop of DRD2³⁸. This study revealed a reduction as well in the levels of phosphorylated TH (pTH) in the dorsal striatum and phosphorylated DARPP-32 (pDARPP-32) in the ventral striatum of CHL1 KO mice. These findings suggest that the absence of CHL1 might result in a higher propensity for a constitutively active conformation by pre- and postsynaptic DRD2 isoforms in the dorsal and ventral striatum, respectively³⁸. Nevertheless, the mechanism and functional implications of CHL1's regulation of the dopaminergic system via DRD2 remained unexplored, offering an opportunity to uncover novel roles for CHL1 in neurological circuits and potential insights for developing therapeutic interventions for dopamine-related disorders. The next section delves into the complex structure of the dopaminergic system, with a focus on DRD2's central role.

1.3 Dopamine receptor type-2 in the dopaminergic system

Dopamine or 3,4-dihydroxyphenethylamine, is a main neurotransmitter within the catecholamine group, making up around 80% of the brain's total catecholamine content⁸¹. Dopamine is the precursor for related neurotransmitters like epinephrine and norepinephrine, sharing a common catechol nucleus structure (a benzene ring with two adjacent hydroxyl groups) and a side chain of ethylamine or one of its derivatives⁸¹. Dopamine synthesis occurs in dopaminergic mesencephalic neurons, and it operates through a network of neurons across the brain. At the center of this intricate system lies DRD2, significantly influencing neural circuits and a wide range of physiological and behavioral processes.

1.3.1 Inputs and outputs in midbrain dopaminergic system

Dopamine is synthesized in midbrain neurons and distributed through four pathways: the nigrostriatal, mesolimbic, mesocortical, and tuberoinfundibular pathways. The nigrostriatal pathway originates in the substantia nigra pars compacta (SNc) and primarily projects to the dorsal striatum (caudate putamen, CPU), containing the neurons with the highest concentration of dopamine in the brain and is critical for movement initiation and habit learning (Fig. 1.2)^{82,83}. The mesolimbic pathway, originating in the ventral tegmental area (VTA), and extending to the nucleus accumbens (NAc), amygdala, olfactory tubercle, hippocampus, and other limbic structures, plays a pivotal role in integrating emotional cues into behavioral responses, exerting control over goal-directed behavior, long-term memory processes, emotional behaviors, aversion, and motivation (Fig. 1.2)^{84,85}. Another set of projections from the VTA to the prefrontal cortex (PFC), cingulate cortex, and entorhinal cortex form the mesocortical pathway, associated with cognitive function, working memory, and decision-making (Fig. 1.2)⁸⁶. The mesolimbic and mesocortical pathways synergistically collaborate in the mesocorticolimbic pathway, involved in reward, aversion, cognition, decision-making, and associative memory⁸⁷⁻⁸⁹. Lastly, the tuberoinfundibular pathway, from the hypothalamic arcuate nucleus to the median eminence, regulates prolactin secretion by the pituitary gland⁹⁰.

The classical organization of dopaminergic pathways from the substantia nigra (SN) or VTA is often considered an oversimplification. Recent evidence suggests that these structures are not entirely anatomically or functionally distinct. The classical mesocorticolimbic pathway includes additional projections from the medial SNc to the PFC and dorsal SNc to various limbic and striatal targets, showing that dopaminergic terminals in the brain do not exclusively originate from a single midbrain region^{91,92}. Different subpopulations of projections can also arise within the same structure, with two parallel nigrostriatal dopaminergic projections originating from the SNc, targeting the dorsomedial and dorsolateral striatum, or two distinct populations targeting the medial or lateral NAc from the VTA^{93,94}. The nigrostriatal and mesocorticolimbic pathways are not entirely functionally dissociated and

contribute in parallel to motivational behavior, although with varying roles in reward, aversion, and addiction^{87,92,95}.

In addition to dopaminergic neuronal outputs, midbrain structures house non-dopaminergic populations of GABAergic and glutamatergic neurons that intermingle with dopaminergic fibers, exerting local inhibition/excitation and influencing the dopaminergic midbrain outputs^{96–98}. The substantia nigra pars reticulata (SNr) primarily consists of GABAergic neurons interconnected with dopaminergic neurons from the SNc, projecting to striatal areas, thalamus, and brainstem^{97,99}. Glutamatergic neurons are mainly in the dorsal SNc, targeting the posterior thalamus^{97,99}. Within the VTA, around 30% are GABAergic neurons, more abundant in the anterior part, projecting to NAc and lateral habenula^{96,97}. The VTA also has roughly 20% glutamatergic neurons, concentrated dorsally and medially, forming local synapses with dopaminergic and GABAergic neurons, projecting to NAc, PFC, lateral habenula, ventral pallidum, and olfactory tuberculum^{96–98}. Notably, these neuronal classes exhibit complexity, with some dopaminergic neurons co-releasing GABA or glutamate. GABAergic inputs from VTA to the lateral habenula include dopaminergic marker co-expression, but most VTA neurons innervating the lateral habenula co-express glutamate and GABA markers^{100,101}. Certain dopaminergic neurons co-express vesicular-glutamate transporter 2 (VGluT2) in projections from SNr to the thalamus and VTA to NAc and PFC, although their release often occurs at different sites or distinct synaptic terminals^{99,102,103}.

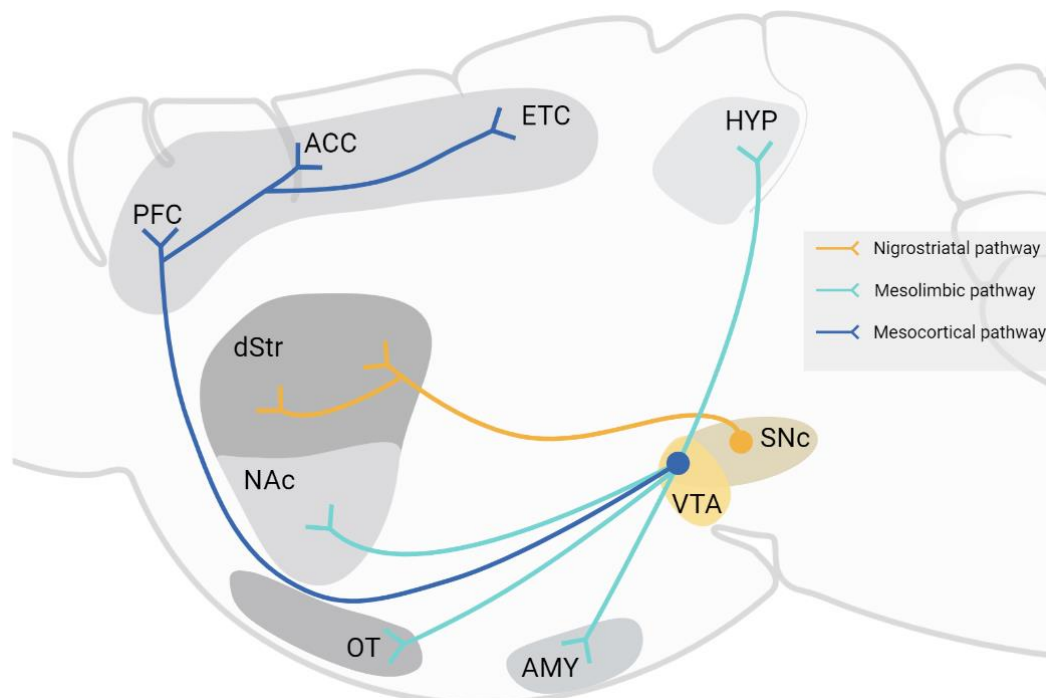


Figure 1.2. Schematic illustration of the major dopaminergic pathways in the mouse brain. The nigrostriatal pathway (yellow) extending from the SNc to the dorsal striatum, the mesolimbic pathway (light blue) from the VTA to the NAc, and the mesocortical pathway (dark blue) from dopaminergic neurons in the VTA to the cortex (ACC: anterior cingulate cortex, AMY: amygdala, dSTR: dorsal striatum, ETC: entorhinal cortex, HYP: hippocampus, NAc: nucleus accumbens, OT: olfactory tubercle, PFC: prefrontal cortex, SNc: substantia nigra pars compacta, VTA: ventral tegmental area). The illustration was created using [Biorender](#).

Dopaminergic pathways are modulated by various neurotransmitter afferents from diverse brain regions. Approximately 70% of the SN receives GABAergic innervation, with the VTA receiving it to a lesser extent (Fig. 1.3)¹⁰⁴. The direct striatal pathway originating in the NAc and dorsal striatum includes GABAergic projections targeting dopaminergic and GABAergic neurons in the VTA and SNr^{105–107}. The indirect striatal pathway, mediated by the subthalamic nucleus (STh), provides glutamatergic inputs to SNr GABAergic neurons^{97,108}. The externus globus pallidus (GPe) primarily sends GABAergic projections to VTA dopaminergic neurons and SNr GABAergic neurons, while these same afferents, although scattered, project to the SNc¹⁰⁹. Additionally, excitatory projections from the PFC reciprocally target VTA dopaminergic neurons projecting to the PFC and GABAergic VTA neurons projecting to the NAc^{104,106}.

Dopaminergic signaling primarily relies on the mentioned main afferents, but other neurotransmitters also play a minor role in its modulation. Cholinergic neurons from the pedunculopontine and laterodorsal tegmental nuclei densely innervate SNc dopaminergic neurons and, to a lesser extent, VTA neurons, with sparse presence in the SNr^{104,109}. Noradrenergic inputs from the

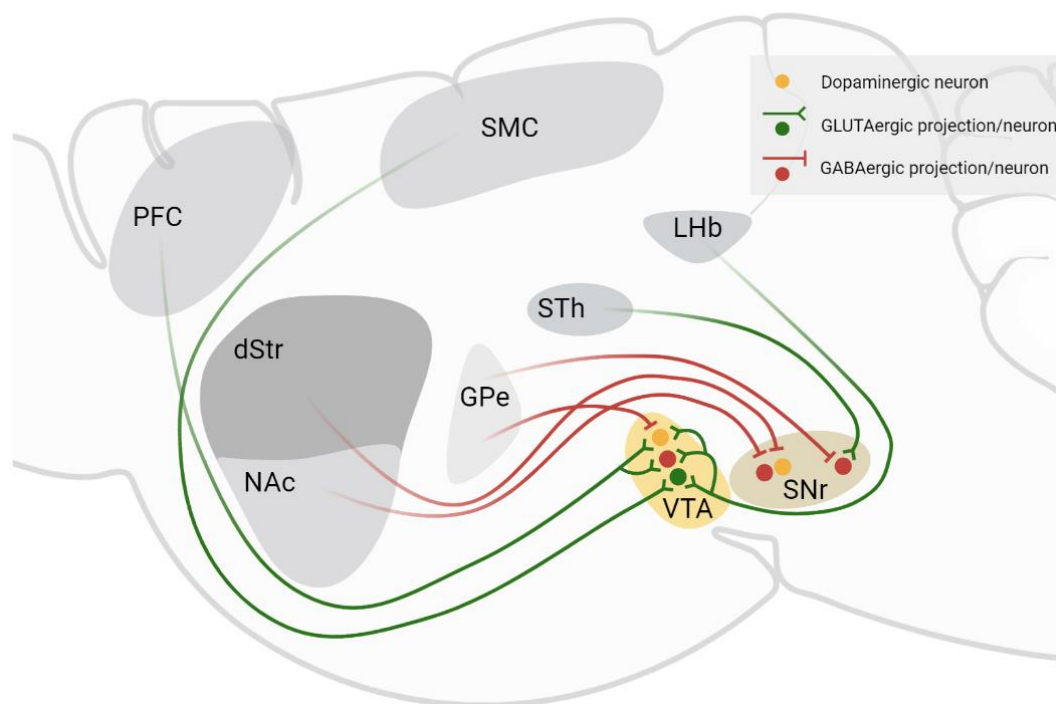


Figure 1.3. Main afferent projections to the midbrain. Neurons of the VTA and SNr receive predominantly glutamatergic (green) and GABAergic (red) projections from different brain regions. The cortex sends excitatory glutamatergic projections to the VTA, establishing connections with dopaminergic (yellow), glutamatergic (green), and GABAergic (red) neurons. The Lhb projects excitatory signals to different VTA neurons, while the STh establishes synapses with GABAergic neurons in the SNr. The primary GABAergic afferents to the VTA originate from the GPe, providing control over dopaminergic neurons. GABAergic neurons in the SNr receive GABAergic projections from both the GPe and the striatum, while dopaminergic neurons primarily receive inputs from the striatum (dSTR: dorsal striatum, GPe: external globus pallidus, Lhb: lateral habenula, NAc: nucleus accumbens, PFC: prefrontal cortex, SMC: sensorimotor cortex, SNr: substantia nigra pars reticulata, STh: subthalamic nucleus, VTA: ventral tegmental area). The illustration was created using [BioRender](#).

locus coeruleus minimally project to VTA dopaminergic neurons^{104,109} and serotonergic fibers from the medial and dorsal raphe nuclei innervate both the SN and VTA¹⁰⁹.

Complex neuronal networks transmit signals through specialized receptors. In dopaminergic pathways, dopamine receptors play a central role by selectively receiving and responding to dopamine, the primary neurotransmitter of this system. Their interaction with dopamine triggers intracellular events, influencing a wide range of physiological and psychological processes.

1.3.2 Dopaminergic receptors: structural features and expression patterns

Dopamine acts through five rhodopsin-like G protein-coupled receptors (GPCRs) that activate both G protein-dependent and -independent pathways. These receptors have seven transmembrane domains linked by three extracellular and three intracellular loops (ICLs). They can be grouped into two families: the dopamine receptor type-1-like family (DRD1 and DRD5), and the DRD2-like family (DRD2, DRD3, and DRD4). While they share a common N-terminal domain, DRD1-like receptors have a shorter ICL3 and a longer C-terminal tail compared to the DRD2-like family^{110,111}.

The DRD1-like family primarily exists in dopaminoceptive regions and is encoded by a single exon. These receptors interact with excitatory $G\alpha$ subunits ($G\alpha_s$ or $G\alpha_{olf}$) to activate adenylyl cyclases (ACs), resulting in the increased production of cyclic adenosine monophosphate (cAMP). This, in turn, leads to the stimulation of protein kinase A (PKA) and the subsequent activation of downstream signaling systems, including the extracellular signal-regulated kinase (ERK) pathway. Alternatively, DRD1-like receptors can also signal through $G\alpha/q$ subunits to activate phospholipase C (PLC)¹¹¹. DRD1 is highly expressed in medium spiny neurons (MSNs) within the striatum, followed by the cerebral cortex, hippocampus, amygdala, and olfactory tubercle^{18,111}. In comparison, the expression profile of DRD5 is more limited within the CNS, and DRD5 is found in brain regions that play a role in mediating the effects of DRD1 stimulation, including the striatum, PFC, and amygdala^{18,111}.

The DRD2-like family distinguishes itself from the previous group in terms of expression patterns and genomic structure. These receptors are found in both dopaminergic neurons (those that produce dopamine) and dopaminoceptive neurons, and their genomic structure includes multiple exons and introns within their coding regions. The canonical signaling pathway associated with these receptors typically produces opposing effects to those of the DRD1-like family. DRD2-like receptors interact with inhibitory $G\alpha$ subunits ($G\alpha_{i/o}$), resulting in ACs inhibition. This leads to the downregulation of cAMP synthesis and further suppression of PKA activity, as well as downstream signaling through the DARPP-32/protein phosphatase 1 (PP1) pathway¹¹¹. DRD3 exhibits the highest expression levels in the limbic striatum, particularly in the NAc, hippocampus, cortex, SN, and VTA^{18,111}. On the other hand, DRD4 has low expression in the brain but can still be detected in the cerebral cortex, hippocampus, and amygdala^{18,111}.

1.3.2.1 DRD2 expression patterns

DRD2 is the second most abundantly expressed dopaminergic receptor in the brain, following DRD1, and it exhibits a widespread expression pattern within the CNS¹¹². The regions containing the highest expression of DRD2 are the striatum, specifically the putamen and the NAc, followed by the pituitary gland, internus/externus globus pallidus (GPI/e), SN, VTA, cerebral cortex, thalamus, and hypothalamus, in descending order of DRD2 abundance^{18,81,113}. Histological and gene expression analysis of human striatal subregions have revealed a homogeneous distribution of DRD2 along the dorso-ventral axis, but a gradual decline in concentration over the rostro-caudal axis of the striatum^{113,114}. On the other hand, autoradiographic experiments assessing DRD2 binding sites (fmol/mg) have revealed distinct variations in the following order among regions: dorsal caudate nucleus (64.2 ± 4.5), ventral caudate nucleus (55.8 ± 4.5), dorsal putamen (67.9 ± 5.5), ventral putamen (63.9 ± 5.2), nucleus accumbens (49.3 ± 7.8) and tail of caudate (48.7 ± 6.1)¹¹³.

In terms of neuronal expression within the striatum, DRD2 is primarily found in non-dopaminergic neurons, including the indirect pathway medium spiny neurons (iMSNs), which make up approximately 48% of striatal GABAergic neurons¹¹⁵. DRD2 is also expressed in cholinergic striatal interneurons (1-3% of striatal neurons) and a subset of GABAergic interneurons¹¹⁵⁻¹¹⁷. Additionally, a subset of GABAergic neurons co-expressing DRD1 and DRD2 are homogeneously distributed throughout the dorsal striatum (1.9% of all MSNs) but heterogeneously scattered and more numerous in the ventral striatum (14.6% in the shell and 7.3% in the core of all MSNs)^{117,118}. In terms of striatal afferents, DRD2 is present on dopaminergic projections from the midbrain^{119,120} and glutamatergic terminals from the corticostriatal projection^{121,122}.

Sex differences in dopaminergic signaling have been observed, and one contributing factor is the differential expression of the DRD2 based on gender. Positron emission tomography (PET) analyses have demonstrated that women generally exhibit higher DRD2 expression than men in the frontal and temporal cortices, as well as the thalamus¹²³. In the striatum, women were described to have a lower DRD2 affinity specifically in the left striatum¹²⁴; however, no gender differences were observed in DRD2 binding potentials or densities in this region^{124,125}. Furthermore, the density of DRD2 in the striatum has been found to decline with age in a sex-specific manner, with a greater decline observed in men compared to women¹²⁶.

Animal studies have provided further support for these sex differences in DRD2 expression. For instance, young male rats tend to exhibit a higher DRD2 density in the cortex, while young female rats exhibit a higher density in the striatum¹²⁷. Moreover, in adult female rats, the expression of DRD1-DRD2 heteromers in the CPu and NAc was found to be higher than in males, despite no differences in DRD2 expression being detected¹²⁸. Interestingly, male rats show a greater increase in striatal DRD2 during early development compared to females¹²⁹. These findings highlight the importance of considering sex-specific differences in DRD2 signaling.

1.3.2.2 DRD2 isoforms

The DRD2 receptor is unique within its receptor family due to the presence of functional splice variants resulting from alternative splicing of the sixth exon, giving rise to two isoforms: DRD2_S (shorter) and DRD2_L (longer). DRD2_L contains an additional 29 amino acids in the ICL3, crucial for G protein interaction^{130–132}. These isoforms differ in signaling pathways, physiological effects, and pharmacological properties. Both isoforms are expressed in various cell types, with tissue-specific ratios. DRD2_S is less abundant, constituting about 2% of total DRD2_L mRNA in the pituitary gland, 12% in the olfactory bulb, 20–25% in several brain regions (striatum, olfactory tubercle, hippocampus, SN, and cortex), and 40–45% in the hypothalamus¹³⁰. In the striatum, both isoforms have a similar level of expression. DRD2_S is more prevalent in the cell bodies and dendrites of midbrain neurons, especially in the SN, whereas DRD2_L is weaker and associated with the cell soma¹³³.

Studies on DRD2 KO mice (lacking both isoforms) reveal insensitivity to dopamine or DRD2 agonist quinpirole-induced firing, as observed through *in vitro* electrophysiological recordings¹³⁴. Similarly, purified striatal synaptosomes from these mice show insensitivity to selective DRD2-agonist inhibition of dopamine release¹³⁵. These findings support the idea that DRD2_S functions as an inhibitory autoreceptor in ventral midbrain dopaminergic neurons and striatal synaptic terminals, regulating dopamine firing at presynaptic sites.

Biochemical and behavioral studies using genetically modified mice lacking DRD2_L have provided further evidence that these mice exhibit a loss of responses associated with postsynaptic striatal DRD2, thus supporting the idea of a preferential role for DRD2_L at the postsynaptic site and DRD2_S at the presynaptic site. A behavioral study demonstrated that both DRD2_L KO and DRD2 KO (lacking both isoforms) mice are resistant to haloperidol (DRD2 antagonist)-induced catalepsy, whereas quinpirole-induced hypolocomotion at low doses was only observed in DRD2_L KO mice^{136,137}. Additionally, Lindgren et al.¹¹⁹ investigated the differential effects of both isoforms on dopaminergic signaling using mouse striatal slices. They found that quinpirole incubation decreased TH phosphorylation at serine 40 (Ser40) in DRD2_L KO mice but not in DRD2 KO (lacking both isoforms) mice¹¹⁹. Likewise, it was observed that a single administration of low or high doses of quinpirole *in vivo* led to a decrease in pTH in the striatum of DRD2_L KO mice, while no significant changes in pTH levels were observed in DRD2_S KO mice¹³⁸. The findings indicating the lack of catalepsy response in DRD2_L KO mice when exposed to DRD2 antagonists, along with the observed inhibitory effects of quinpirole on activity and reduction of presynaptic pTH, provide strong support for the role of DRD2_L as the main heteroreceptor within the striatum, controlling the release of heterologous neurotransmitters (glutamate or GABA)¹³⁹. In contrast, these results suggest that DRD2_S is primarily responsible for autoreceptor-mediated actions on dopamine soma and presynaptic terminals^{119,136,137}. Moreover, it has been demonstrated that the increase in postsynaptic DARPP-32 phosphorylation at threonine 34 (Thr34) induced by a DRD1

agonist remains unaffected by quinpirole in both DRD2_L KO and DRD2 KO (lacking both isoforms) mice¹¹⁹. This finding further solidifies the role of DRD2_L in postsynaptic dopaminergic signaling

Recent studies challenge the idea that DRD2_S is the sole autoreceptor, suggesting that both isoforms can serve this role. Research correlating single-cell gene expression and firing patterns reveals heterogeneous expression of DRD2_S and DRD2_L in TH-expressing neurons, both capable of suppressing firing in SNc dopaminergic neurons⁸². Experiments with viral-mediated reexpression of DRD2_S or DRD2_L in dopaminergic neurons of DRD2 KO mice suggest a functional role for co-expressing DRD2_S and DRD2_L autoreceptors, as DRD2_S alone is insufficient to account for drug-induced plasticity¹⁴⁰. However, subsequent research supports a predominant presynaptic role for DRD2_S, as inhibition of pTH and dopamine synthesis was only prevented in DRD2_S KO mice¹³⁸. Nonetheless, both DRD2_S and DRD2_L contribute to postsynaptic functions at baseline, while DRD2_L signaling is crucial for regulating striatal circuits in response to DRD2-specific drugs¹³⁸.

In summary, while DRD2_L is considered a primary heteroreceptor, both DRD2_S and DRD2_L can act as autoreceptors on dopaminergic neurons to regulate cellular activity and control presynaptic dopamine release. However, it is important to note that the isoforms might exhibit isoform-specific functions under basal conditions or in response to pharmacological stimulation at the cellular and behavioral levels.

1.3.3 DRD2 signal transduction pathways

1.3.3.1 G protein-dependent pathways of DRD2 signaling

G proteins are heterotrimeric complexes composed of three subunits: α , β , and γ that can couple with guanosine triphosphate (GTP) and guanosine diphosphate (GDP). Each subunit of the complex has several subtypes; however, the classification of G proteins is based on the nature of the α -subunit ($G\alpha$), which consists of four broad classes: $G\alpha_s$, $G\alpha_{i/o}$, $G\alpha_q$, and $G\alpha_{12}$. In the resting state, $G\alpha$ is bound to GDP and associates with a $\beta\gamma$ -complex, forming a trimeric complex on the inner membrane surface. Activation of dopamine receptors triggers G protein activation by exchanging GDP for GTP in a nucleotide-binding pocket, leading to the separation of the trimeric complex into $G\alpha$ -GTP and $G\beta\gamma$. The activated GPCR can further activate another G protein, amplifying the signal. Regulators of G protein signaling (RGS) proteins facilitate signal termination by enhancing the GTPase activity of $G\alpha$, converting GTP back to GDP. This process allows the reassociation of α - and $\beta\gamma$ -subunits to initiate the cycle^{111,112,141}. See Fig. 1.4 for a schematic representation of G protein-dependent pathways.

DRD2-like receptors, particularly DRD2, couple with inhibitory $G\alpha$ subunits ($G\alpha_{i/o}$). DRD2 can activate all non-visual $G\alpha_{i/o}$ family members, such as $G\alpha_{i1-3}$, $G\alpha_{oA-B}$, and $G\alpha_z$. The length of the ICL3 influences the interaction between DRD2 and $G\alpha_{i/o}$ proteins, leading to varying affinities of DRD2 isoforms for different G proteins¹³². DRD2_L shows stronger coupling with $G\alpha_o$ compared to $G\alpha_{i1}$, $G\alpha_{i2}$, or $G\alpha_{i3}$ ¹⁴²⁻¹⁴⁴. Recent *in silico* structural models have confirmed this preference, with DRD2_L coupling

more with $G\alpha_{i2}$, while DRD2_S prefers $G\alpha_{i1}$ proteins^{132,145}. Some agonists, like dopamine or quinpirole, exhibit higher efficacy when DRD2 couples with $G\alpha_o$ proteins¹⁴⁴, indicating that each agonist differentially activates the four $G\alpha$ proteins. Additionally, the ratio of receptors and the various $G\alpha_{i/o}$ proteins in cells can influence the binding affinity of the receptor to agonists. For example, the local enrichment of $G\alpha_o$ in the MSNs of the NAc results in higher DRD2 affinity to dopamine^{144,146}.

When DRD2 is activated, it initiates a canonical downstream effect involving the dissociation of the $G\alpha\beta\gamma$ complex, resulting in two independent G-protein subunits that engage in signaling activities. The GTP-bound $G\alpha_{i/o}$ subunit inhibits the enzymatic activity of ACs, preventing the conversion of cAMP into adenosine triphosphate (ATP) and suppressing PKA activity^{112,147}. PKA mainly targets DARPP-32, a protein found predominantly in MSNs, which negatively regulates PP1. Inhibition of PKA reduces DARPP-32 phosphorylation at Thr34, preventing the formation of the pDARPP-32-PP1 complex. Consequently, PP1 becomes free in the cytosol to dephosphorylate its targets, including cAMP response element-binding protein (CREB), N-methyl-D-aspartate (NMDA)- and α -amino-3-hydroxy-5-methyl-4-isoxazolepropionic acid (AMPA)-type glutamate receptors, GABA_{A β 1} receptors, and voltage-gated ion channels such as L/N/P-type Ca^{2+} channels^{112,147-149}. In turn, the inhibitory effect of pDARPP-32 on PP1 acts synergistically with PKA because they share the same targets. Thus, DRD2 activation leads to reduced activity of CREB, ionotropic glutamate receptors, and L/N/P-type Ca^{2+} channels, resulting in decreased intracellular Ca^{2+} levels and neuron excitability. Additionally, DRD2 activation increases the activity of GABA_{A β 1} receptors, Na^+ channels, and the Na^+/K^+ -ATPase^{112,147-150}.

The $G\alpha_{i/o}$ subunit plays a critical role in DRD2_S-mediated extracellular signal-regulated kinase 1/2 (ERK1/2) activation¹⁵¹. ERK1/2 activation through phosphorylation is typically associated with DRD1-expressing MSNs via a DARPP-32-dependent mechanism¹⁵². However, studies have shown that DRD2_S signaling induced by dopamine or quinpirole can also enhance ERK1/2 phosphorylation at Thr202 and tyrosine 204 (Tyr204), respectively^{151,153,154}. This pathway relies on the $G\alpha_{i/o}$ subunit and is mediated by atypical protein kinase C (PKC) proteins activated through phosphoinositide-3 kinase (PI3K) or Src activation via Ca^{2+} -dependent kinases like receptor tyrosine kinases (RTKs)¹⁵¹.

Upon DRD2 activation, the $G\beta\gamma$ subunit separates from the $G\alpha_{i/o}$ subunit and triggers PLC, leading to increased diacylglycerol (DAG) and inositol trisphosphate (IP3) production^{111,112,147}. DAG activates PKC, which, in turn, affects glutamatergic receptors and inhibits the phosphorylation of DARPP-32 at Thr75 by cyclin-dependent kinase 5 (CDK5), potentiating PKA-mediated signaling^{112,147,155}. Simultaneously, the increase in IP3 is responsible for the mobilization of intracellular Ca^{2+} , a mechanism by which the $G\beta\gamma$ subunit regulates intracellular Ca^{2+} levels¹⁵⁶. The increase in Ca^{2+} activates Ca^{2+} -regulated Ser/Thr phosphatases like calcium/calmodulin-dependent protein kinase II (CaMKII) and calcineurin/protein phosphatase 2B (PP2B)^{112,147}. CaMKII enhances glutamate activity via NMDA- and AMPA-type receptors, while PP2B dephosphorylates DARPP-32 at Thr34,

counteracting PKA effects and providing negative feedback for DRD2 signaling^{112,147}. Additionally, the $G\beta\gamma$ subunit reduces intracellular Ca^{2+} levels by negatively influencing voltage-gated ion channels, particularly L/N-type Ca^{2+} channels¹⁵⁶, and promotes DRD2 interaction with G protein-coupled inwardly rectifying potassium channels (GIRKs), causing neuronal hyperpolarization and inhibitory signaling^{112,147,157}. In addition to the role as regulator of RGS proteins in accelerating GTP hydrolysis to terminate G protein signaling, the $G\beta\gamma$ subunit initiates another counteracting mechanism to terminate the activation by recruiting G protein-coupled receptor kinases 2/3 (GRK2/3s) (described in the next section)^{112,147,158}. The PLC pathway induced by DRD2/ $G\beta\gamma$ subunit activation is additionally stimulated by D1-D2 heterodimers, which selectively couple with the $G\alpha_{q/11}$ subunit^{112,147,159}.

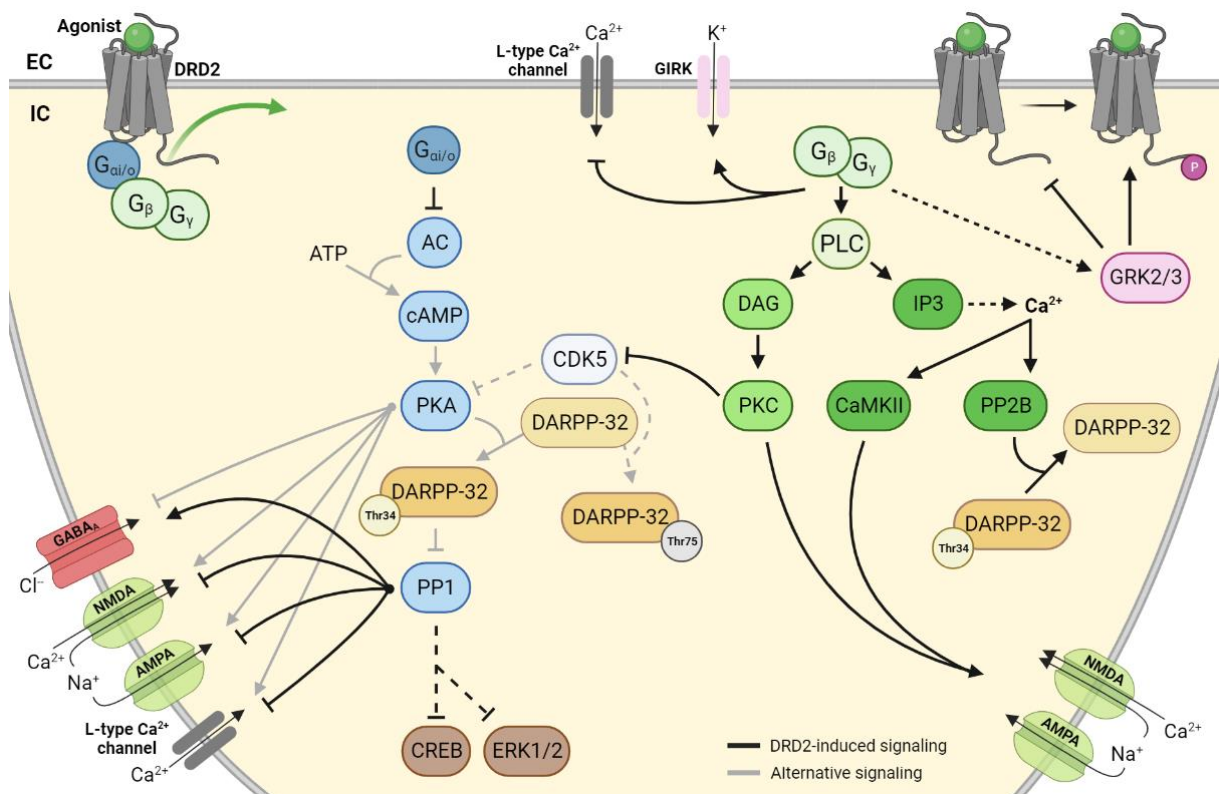


Figure 1.4. G protein-dependent signaling pathways upon stimulation of DRD2. Upon stimulation of DRD2 by dopamine or an agonist (green ball), the receptor undergoes a conformational change, initiating the activation of G protein complexes. The trimeric G protein complex splits into $G\alpha_{i/o}$ and $G\beta\gamma$ subunits upon activation, each responsible for triggering distinct DRD2-induced signaling pathways (black lines). The $G\alpha_{i/o}$ subunit inhibits AC, resulting in reduced levels of cAMP. This inhibition leads to the dephosphorylation of DARPP-32 at Thr34 by PKA and subsequent activation of PP1 that can either activate (\uparrow) or inhibit (\downarrow) PKA targets by dephosphorylating them. This pathway leads to decreased activity of NMDA/AMPA receptors and L-type Ca^{2+} channels, while increasing the activity of $GABA_A$ receptors. The $G\beta\gamma$ subunit activates a PLC pathway, leading to PKA-mediated inhibition of DARPP-32 phosphorylation at Thr75 by CDK5 that acts as a counterbalance to PKA activation. PLC also induces PP2B-mediated dephosphorylation of DARPP-32 at Thr34. In addition, this pathway increases the activity of NMDA/AMPA receptors and GIRK channels, while decreasing the activity of L-type Ca^{2+} channels. The $G\beta\gamma$ subunit can recruit and activate GRK2/3s, which phosphorylates and deactivates DRD2 activity. The illustration was created using [Biorender](#) (black lines: DRD2-induced signaling; grey lines: alternative signaling without DRD2 activation; straight/slashed lines: direct/indirect mechanisms).

1.3.3.2 G protein-independent pathways of DRD2 signaling

In addition to regulating cAMP/PKA and Ca²⁺ pathways through G-protein-mediated signaling, DRD2 is also involved in β -arrestin 2-mediated signaling, which controls several dopaminergic outcomes¹⁴⁷. When DRD2 is stimulated for an extended period or with high agonist concentrations, GRK2/3s are recruited to the membrane. This recruitment can occur through binding to the G $\beta\gamma$ subunit or directly through DRD2 stimulation (G protein-independent recruitment)^{158,160}. GRK2/3s, which are abundant in dopaminergic regions, phosphorylate Ser and Thr residues on the ICL3 of activated DRD2¹⁶¹, leading to receptor desensitization. This desensitization promotes the binding of β -arrestin 2 to the receptor, blocking further G protein interactions^{158,161}. Although β -arrestin 2 prevents G proteins from binding to the phosphorylated DRD2¹⁶², the phosphorylation of the receptor by GRK2/3s was shown to be not critical for β -arrestin 2 recruitment¹⁶¹. Once β -arrestin 2 is coupled to the DRD2, it functions as a scaffold protein for clathrin and clathrin adaptor protein 2 (AP2) that triggers endocytosis of the receptor via clathrin-coated pits^{112,163}.

Another significant pathway controlled by DRD2 and mediated by β -arrestin 2 is the dopamine-regulated inhibition of protein kinase B (Akt)¹⁶⁴. Normally, RTKs and specific GPCRs stimulate PI3K, converting phosphatidylinositol 4,5-bisphosphate (PIP2) to phosphatidylinositol 3,4,5-trisphosphate (PIP3). PIP3 then recruits Akt to the cell membrane by phosphorylation at Thr308 and Ser474, facilitated by phosphatidyl-dependent kinases (PDK), namely PDK1 and PDK2, respectively. Once activated, Akt phosphorylates Ser/Thr residues of various substrates, including GSK3 isoforms, leading to their inhibition^{112,163}. Upon DRD2 activation, β -arrestin 2 is recruited and forms a complex with phosphorylated Akt and protein phosphatase-2A (PP2A). PP2A then dephosphorylates Thr308 of Akt, deactivating Akt (Ser473) and activating GSK3 signaling^{163,164}. This negative regulation of Akt by dopamine, resulting in GSK3 isoform activation, is primarily governed by DRD2 stimulation. While DRD3 appears to modulate this pathway by potentiating DRD2 signaling, DRD1 is not essential for Akt inhibition in response to dopaminergic drugs¹⁶⁵. GSK3 β , the predominant isoform in the brain¹⁶⁶, is commonly associated with DRD2-dependent signaling, either through genetic ablation or reduction upon DRD2 pharmacological activation of Akt^{167,168}.

Furthermore, a specific motif mutation in the N-terminal region of DRD2 ICL3 reduces β -arrestin 3-dependent activation of ERK1/2, indicating an alternative DRD2-mediated pathway involved in ERK1/2 modulation (DRD2/G $\alpha_{i/o}$ -independent pathway)¹⁶⁹. This mutation also inhibits DRD2-mediated β -arrestin 3 translocation and internalization, potentially leading to decreased ERK1/2 phosphorylation¹⁶⁹. This study highlights additional β -arrestin 3-independent mechanisms involved in the regulation of ERK1/2 phosphorylation through DRD2, consistent with previous research indicating that β -arrestin 1/2 does not impact DRD2_S-mediated ERK1/2 activation¹⁵¹. A simplified diagram of the G protein-independent pathways is shown in Fig. 1.5.

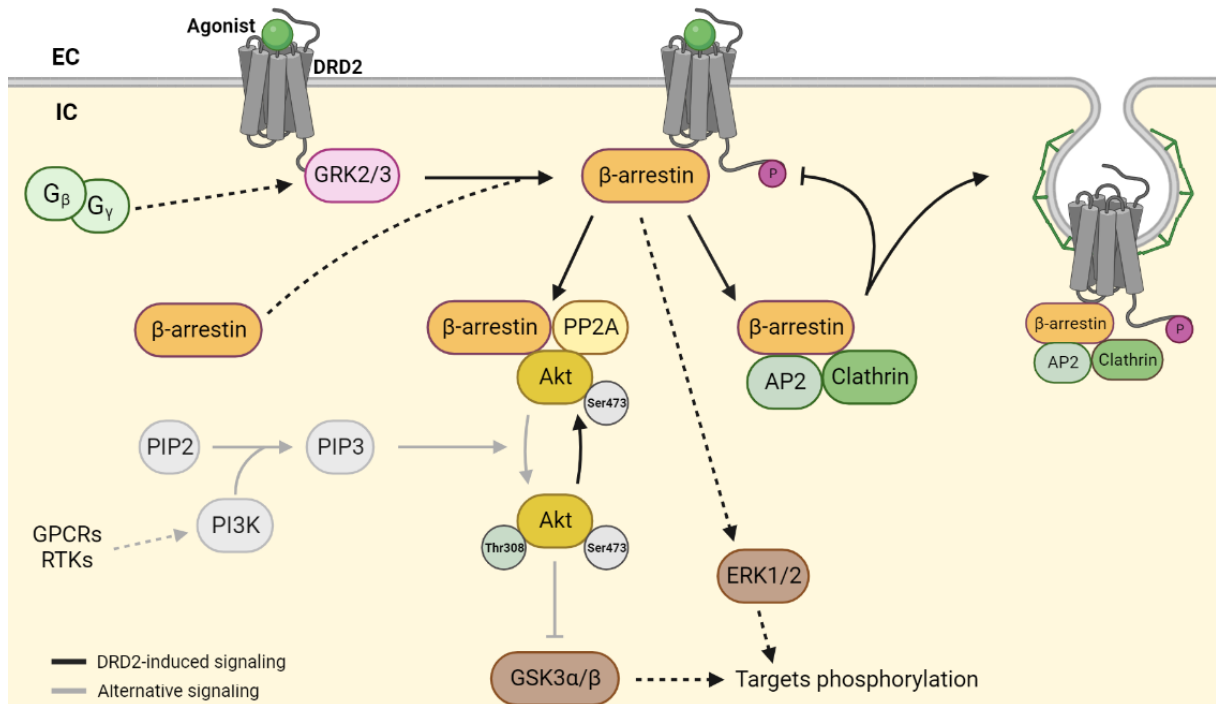


Figure 1.5. G protein-independent signaling pathways upon stimulation of DRD2. Stimulation of DRD2 by dopamine or an agonist (green ball), the activation of the G $\beta\gamma$ subunit contributes to the recruitment of GRK2/3s to the membrane. GRK2/3s phosphorylate specific residues of DRD2, increasing the receptor's affinity for β -arrestin. β -arrestin bound to DRD2 forms a protein complex with PP2A and Akt (Ser473), facilitating the activation of GSK3 α/β . β -arrestin bound to DRD2 enables the downstream target phosphorylation through the activation of GSK3 α/β or ERK1/2. External signaling can activate other GPCRs or RTKs, which in turn activate PI3K and prevent the binding of Akt to the protein complex. Instead, Akt is phosphorylated at Thr388 and is able to inhibit GSK3 α/β actions. β -arrestin bound to DRD2 forms a protein complex with AP2 and clathrin, triggering clathrin-mediated endocytosis of the receptor that acts as a negative regulatory feedback mechanism of DRD2 activation. The illustration was created using [BioRender](#) (black lines: DRD2-induced signaling; grey lines: alternative signaling without DRD2 activation; straight/slashed lines: direct/indirect mechanisms).

1.3.4 Physiological roles of DRD2

The dopaminergic signaling pathway plays a crucial role in embryonic development, and DRD2 has been identified as a significant modulator in this process. Loss of DRD2 reduces the number of TH-expressing neurons without affecting the overall population of midbrain neurons in mice lacking both isoforms of DRD2, indicating its influence on the differentiation of dopaminergic neurons¹⁵³. This reduction is associated with a downregulation of specific transcription factors like Nurr1, regulated by the ERK1/2 pathway. This lower differentiation rate was associated with the downregulation of specific transcription factors such as Nurr1. This downregulation was found to be regulated by the ERK1/2 pathway, as indicated by the increased activation of ERK1/2 and Nurr1 in TH-expressing neurons following quinpirole treatment in WT mice, and the suppression of their activation in the presence of an ERK inhibitor¹⁵³. Regarding migration, activation of DRD2 was found to inhibit the migration of GABAergic neurons from the ganglionic eminences to the cerebral cortex in embryonic brain slices,

accompanied by a redistribution of cytoskeleton elements favoring a cellular localization in the cell body, characteristic of non-migrating neurons¹⁷⁰. Furthermore, DRD2 might have a role in adult neurogenesis, influencing the proliferation and differentiation of neural stem cells in the ventricular subependyma into various mature cell types (e.g., striatal or other cells), a process impacted in neurodegeneration¹⁷¹. Notably, neural stem cells express DRD2, and its antagonism has been shown to stimulate their proliferation *in vitro* and *in vivo*¹⁷².

Similar to CHL1, DRD2 signaling affects neuronal outgrowth during neurodevelopment, and this effect has been linked to vulnerability for neurological and/or neuropsychiatric disorders. Selective upregulation of DRD2 in MSNs in adult mice or chronic stimulation of DRD2 using quinpirole in cultured striatal neurons leads to a reduction in the complexity and length of dendritic arbors^{173,174}. This decreased arborization complexity *in vivo* was accompanied by an increase in membrane excitability, and both effects were regulated by the downregulation of inward rectifying potassium 2 (Kir2) channels as a consequence of DRD2 overexpression¹⁷³. Interestingly, studies conducted in primary striatal cultures showed an interaction between DRD2 and disrupted-in-schizophrenia 1 protein (DISC1), which is also a binding partner of CHL1¹⁷⁴. This interaction was observed in the soma, dendrites, and spines, and it was found that the quinpirole-induced decrease in neurite length and branching was associated with the excessive formation of the DRD2-DISC1 complex¹⁷⁴. Additionally, the same study demonstrated that the quinpirole-induced DRD2-DISC1 complex was responsible for a significant reduction in synaptic spine density, likely due to the downregulation of synaptophysin and postsynaptic density 95 (PSD95) expression¹⁷⁴. Previous studies have also reported a decrease in spine density caused by quinpirole in hippocampal brain slices and neuronal culture. This inhibitory effect on spine density was attributed to DRD2-induced activation of NMDA receptors, specifically when the GluN2B subunit was present¹⁷⁵. Furthermore, studies focusing on DRD2 autoreceptor function in dopaminergic neurons have demonstrated that selective deletion of DRD2 leads to an increase in axonal arborization of SNc neurons¹⁷⁶. Moreover, chronic activation of DRD2 with quinpirole results in a reduction in the number of axonal terminals and a decrease in dopamine release through direct inhibition of PKA¹⁷⁷. These findings offer valuable insights into the regulatory role of DRD2, both pre- and postsynaptically, in modulating morphological characteristics, such as dendritic arborization and synaptic spine density, across various types of neurons.

Presynaptic autoreceptors, mainly DRD2_s, located on the nerve terminals of midbrain dopaminergic neurons, are involved in inhibitory feedback mechanisms that decrease vesicular dopamine release and synthesis in response to changes in extracellular dopamine levels¹⁷⁸. One common mechanism for regulating dopamine release is the inhibition of voltage-gated calcium channels via Gβγ-mediated signaling^{179,180}. Following dopamine release, DRD2 autoreceptors promote clearance from the extracellular space by increasing the activity of dopamine transporter (DAT), as another regulatory mechanism. This clearance can occur through an increase in DAT cell surface expression via the

activation of an ERK1/2-dependent pathway during periods of excessive DRD2 stimulation, or possibly through changes in the voltage dependence the dopamine uptake^{154,181,182}. As a final regulatory mechanism, DRD2 activation regulates dopamine synthesis by inhibiting TH activity through reduced cAMP-PKA-mediated phosphorylation at Ser40^{139,183}. The prolonged autoreceptor activation leads to decreased phosphorylated TH levels, affecting presynaptic dopamine vesicle filling, as well as the expression and distribution of the vesicular monoamine transporter (VMAT)^{184,185}. Notably, DRD2 heteroreceptors (long isoform) on MSNs also contribute to dopamine release regulation, with greater efficiency observed in the dorsal striatum compared to the NAc¹³⁹.

DRD2 autoreceptors in the somatodendritic region of dopaminergic neurons regulate action potential firing by activating GIRK conductance^{178,186}. When dopaminergic neurons fire, local dopamine release in the somatodendritic sites activates DRD2 autoreceptors, leading to robust hyperpolarization and a temporary pause in firing^{187,188}. This hyperpolarization is induced by GIRK channel activation through the G $\beta\gamma$ subunit, resulting in potassium efflux and decreased neuronal excitability^{157,178,189}. Additionally, DRD2 is found in somatodendritic compartments and synaptic terminals of iMSNs, where it can suppress inhibitory synaptic transmission within the striatum¹⁸⁶.

Another regulatory mechanism that prevents continuous dopaminergic signaling through DRD2 activation involves receptor desensitization and internalization. β -arrestin 2 activation is associated with DRD2 homologous desensitization and clathrin-mediated endocytosis of the receptor^{163,190}. Internalization can occur in the endosomal compartment, where the receptor is dephosphorylated and recycled to the cell surface, or it can undergo degradation via the lysosomal pathway^{163,190}. Interestingly, upon internalization, phosphorylation of the receptor by GRK2/3s is thought to be important in promoting recycling pathways¹⁶¹. Additionally, PKC has been reported to mediate receptor desensitization and internalization by phosphorylating specific sites in ICL3 of DRD2, leading to β -arrestin- and dynamin-dependent endocytosis¹⁹¹. It is worth noting that CHL1 interacts with both DRD2 isoforms, but only agonist-induced internalization of DRD2_S is inhibited in the absence of CHL1³⁸.

The dopaminergic control of DRD2 extends beyond neurotransmission and influences various physiological processes, including insulin control, hormone secretion, and body temperature regulation. The Akt/GSK-3 pathway mediates the intracellular actions of insulin, insulin-related peptides, and neurotrophins that exert their biological functions by stimulating RTKs^{112,163}. DRD2 also controls hormone secretion from glands like the pituitary and adrenal glands, impacting the release of prolactin, growth hormone, and adrenocorticotrophic hormone⁸¹. Furthermore, DRD2 in the hypothalamus is involved in regulating body temperature through modulation of thermoregulatory circuits¹⁹².

The involvement of the DRD2 in modulating synaptic plasticity, neurotransmission, and neuronal excitability emphasizes its crucial role in regulating a diverse array of behaviors. These behaviors

include motor control, cognitive functions, or reward-related processes, which are tightly governed by the interplay between DRD2 and striatal signaling.

1.3.5 Striatal structure and signaling dichotomy

The striatum, a pivotal component of the basal ganglia, integrates dopaminergic and glutamatergic signals to modulate diverse behaviors. In rodents, it comprises two primary regions: the dorsal striatum (CPu), further divided into dorsomedial and dorsolateral sections, and the ventral striatum with the NAc, consisting of the core and shell subdivisions. The striatum is primarily composed of GABAergic MSNs, which make up about 95% of striatal neurons and these can be categorized into two partially separated populations: direct pathway MSNs (dMSNs) expressing DRD1, substance P, and dynorphin, and indirect pathway MSNs (iMSNs) expressing DRD2, adenosine receptor 2a, and enkephalin¹⁹³. While dMSNs and iMSNs are broadly distributed throughout the striatum, some topographical variation exists: DRD1-expressing dMSNs are more abundant in the caudal dorsal striatum, whereas the medial/ventral NAc has a higher proportion of DRD2-expressing iMSNs^{194,195}. Recent research suggests the presence of a small population of MSNs co-expressing both DRD1 and DRD2 receptors, uniformly distributed in the dorsal striatum (comprising around 1.9% of MSNs) but with varying densities, notably 14.6% in the shell and 7.3% in the core of the ventral striatum^{118,193}.

In addition to MSNs, the striatum comprises about 5% of other neurons, primarily consisting of tonically active cholinergic interneurons (0.5-1%) and a diverse array of GABAergic interneurons (3-4%). GABAergic interneurons display distinct features based on markers and firing patterns, such as parvalbumin-positive fast-spiking interneurons, neuropeptide Y-positive neurogliaform interneurons, somatostatin/neuropeptide Y-positive low-threshold spiking interneurons, TH-positive interneurons with diverse firing patterns, and calretinin-positive interneurons. These interneurons modulate MSN excitability directly or indirectly, and ongoing research continues to identify additional subpopulations of cells within this diverse group^{193,196}.

As the main basal ganglia input center, the striatum receives excitatory glutamatergic cortical inputs and dopaminergic projections from the SNc and VTA. In the dorsal striatum, dMSNs form the striatonigral pathway, directly inhibiting neurons at the GPi and SNr. This inhibition of GABAergic neurons at the GPi/SNr stops the inhibitory effect that GPi/SNr exerts over the thalamus and activates the thalamic glutamatergic projections to the cortex, facilitating movement and action. Conversely, iMSNs in the dorsal striatum contribute to the striatopallidal pathway. They indirectly affect the GPi/SNr through the GPe and STh, suppressing GABAergic neurons at the GPe and allowing activation of STh glutamatergic neurons. These neurons stimulate SNr GABAergic projections to the thalamus, inhibiting thalamocortical neurons and suppressing movement¹⁹³. In the NAc, though less distinct, a similar dichotomy between direct and indirect pathways exists. dMSNs project to the ventral pallidum

and basal ganglia output nuclei (SNr and VTA), while iMSNs pass through the ventral pallidum and STn before reaching the output nuclei^{193,197}.

1.3.6 DRD2 functions in striatal-related behaviors

The control of voluntary and automatic motor behavior relies on the striatum's ability to integrate sensory and associative information from excitatory inputs originating from the cortex, as well as limbic cues provided by midbrain dopaminergic projections. This integration enables the striatum to play a crucial role in the selection, planning, refinement, and implementation of motor actions. Owing to the distinct inputs it receives from different brain regions, the striatum exhibits both anatomical and functional segregations. Additionally, direct and indirect pathways play opposing roles in the control of behaviors; however, sometimes, their interactions can be complex and dependent on the context in which they occur.

The dorsomedial striatum serves as an associative region that plays a crucial role in coordinating goal-oriented behaviors, reward processing, and general movement signaling^{198,199}. This region is particularly significant during the initial phase of acquiring the action-outcome value and later in the capacity to select between different anticipated outcomes based on the desired outcome, considering the nature of the rewards and the animal's current motivational state. These behaviors demonstrate flexibility and adaptability as they can be modified in response to changing circumstances or new information^{199,200}. In this context, the activation of dMSNs reinforces and initiates a selected behavior upon a rewarding stimulus, while iMSNs stimulation acts as a signal of punishment/avoidance or an inhibitory brake on a certain behavior when unrewarded stimuli are encountered^{199–202}. Furthermore, various behavioral paradigms investigating working memory have identified the distinct and important contributions of dMSNs and iMSNs to executive function^{86,203,204}, where the dorsomedial striatum plays a crucial role in spatial working memory²⁰⁵.

The dorsolateral striatum is considered to be more closely associated with sensorimotor functions, particularly habit-based behaviors and movement^{198,199}. As a set of events is repeated over time, resulting in positive outcomes, stimulus-response associations are acquired during the learning process. With repeated learning, the action sequence becomes automated and responses become sensory-driven and no longer dependent on changes in reward value or contingency^{198,200}. During habit learning, both the direct and indirect pathways in the dorsolateral striatum are involved in positive reinforcement, but they support different action strategies in a time-specific manner²⁰⁶. It has been observed that the recruitment of dMSNs primarily occurs during the early learning stage, supporting actions that are associated with goal-directed behaviors or outcome-based behaviors^{206,207}. As learning progresses, there is a shift in stimulation towards iMSNs, which contributes significantly to habit formation or stimulus-driven behaviors^{206,207}.

In comparison to other subregions, the ventral striatum stands out as a limbic-related structure that plays a crucial role in controlling motivation and incentive-reward responses associated with various stimuli, including novel, social, hedonic, stressful, or aversive stimuli^{199,208}. Specifically, the NAc core is more closely connected with reinforcement learning and motivation, while the shell region is involved in hedonic responses, pleasure, and addiction^{199,208}. Studies in the ventral striatum have demonstrated that optogenetic stimulation of dMSNs promotes reward-related responses, whereas stimulation of iMSNs induces aversion^{209,210}. However, recent research has shown that both dMSNs and iMSNs possess the capability to inhibit or disinhibit thalamic activity, challenging the assumption that the segregation observed in the dorsal striatum applies identically to the NAc^{199,211}. Furthermore, studies have indicated that the activation of iMSNs in both the dorsolateral and ventral striatum can promote a more exploratory behavioral tendency rather than exploitative behavior, which is a descriptor of value-based decision-making processes²¹². Other behavioral paradigms have shed light on the involvement of both direct and indirect pathways in value-based decision-making²¹³. Alongside the dorsal striatum, the NAc also plays a role in motor function, as selective deletion of DRD2 in the entire NAc or in NAc MSNs significantly increases locomotor and exploratory-like behavior measures^{214,215}.

Research involving genetic or pharmacological manipulation of DRD2 in mice has provided valuable insights into receptor function within striatal circuits and its role in behavioral control. Notably, DRD2 ablation in the mouse brain, affecting both isoforms, leads to significant motor dysfunction, including reduced motor activity and coordination, and exploratory behavior^{216,217}. Similarly, the selective deletion of DRD2_L in the brain or iMSNs reflects the motor impairments observed in DRD2 KO (lacking both isoforms) mice^{137,139}. However, other studies on DRD2_L KO mice suggest that the presence of DRD2_S can compensate for the loss of the long isoform and maintain normal motor performance^{136,138}. In contrast, the loss of presynaptic DRD2_S in dopaminergic neurons or in the entire brain appears to have minimal impact on the basal motor abilities of mice^{138,139}. Furthermore, a hyperactive state induced by a novel environment (during the initial minutes of exposure to a new arena) or by acute cocaine administration has been reported in mice with DRD2_S-deficient dopaminergic neurons^{138,218}. In contrast, the ablation of DRD2_L in iMSNs results in a blunted response to the motor-stimulating effects of the same drug¹³⁹. These hyper-responsive states observed in DRD2_S KO mice might be explained by elevated dopaminergic synthesis and release²¹⁸. These findings emphasize the crucial role of DRD2_S in regulating dopamine release in response to environmental and drug-induced motor effects, as well as the essential requirement of DRD2_L in iMSNs for translating dopaminergic signaling into motor activity.

The differential actions of both DRD2 isoforms in various neuron types are not only evident under basal conditions but also in relation to drug-induced effects. Pharmacological activation of DRD2 with the agonist quinpirole elicits a characteristic biphasic locomotor response in a dose-dependent manner. Low doses of quinpirole induce an immediate hypolocomotive state that persists throughout the entire

test, whereas high doses result in a gradual decrease in locomotion followed by a sustained hyperactive state starting approximately 60 minutes (min) after administration, which is known as the biphasic effect. Intermediate doses produce an intermediate level of excitation preceded by a brief period of reduced locomotion²¹⁹. The impact of low doses of quinpirole on motor activity in mice and rats has been well documented, with effects typically observed within the first minutes of administration^{136,137,219}. Additionally, the administration of a low dose of quinpirole to DRD2_S KO mice fails to induce the sustained locomotor decrease seen in WT or DRD2_L KO mice^{138,139}. It has been suggested that the hypolocomotor effect derives from the activation of higher-affinity presynaptic DRD2 autoreceptors, leading to a reduction in striatal dopamine release. On the other hand, hyperactivity is attributed to the activation of less sensitive DRD2 receptors on iMSNs^{112,117}.

Consistent with this notion, it has been demonstrated that DRD2_L is necessary for the cataleptic effect induced by haloperidol (DRD2 antagonist), while the absence of DRD2_S in mice does not affect this response^{136,138,139}. Moreover, as DRD2_S exhibits a higher affinity for benzamides than DRD2_L^{220,221}, sulpiride (DRD2 antagonist) is another compound with pre- or postsynaptic-dependent effects. Low doses of sulpiride are believed to block DRD2_S^{222,223} and enhance dopamine turnover in the striatum, limbic system and NAc^{224,225}. In contrast, high doses of sulpiride predominantly result in the postsynaptic blockade and reduction of dopamine signaling^{226,227}. Although a reduction in locomotor activity is frequently observed with DRD2 antagonists²²⁶, significant decreases in locomotor activity appear to be more recurrent with higher doses of sulpiride in rats^{228,229}.

Disruption of DRD2 signaling has been linked to impairments in specific aspects of executive function, particularly working memory²³⁰. To replicate the moderate increase in striatal DRD2 density observed in schizophrenic patients²³¹, a transgenic mouse model was created with a 15% overexpression of DRD2 in MSNs²³². This model exhibited deficits in working memory tasks and cognitive flexibility, resembling the cognitive symptoms seen in patients. Working memory's dynamic update and maintenance relies on a prefrontal-basal ganglia model that includes a "go" circuit mediated by DRD1 (striatal direct pathway) and a "no-go" circuit mediated by DRD2 (striatal indirect pathway)^{233,234}. Elevated striatal dopamine levels activate DRD2, inhibiting the striatal indirect pathway, ultimately alleviating the suppressive effect of the "no-go" signaling and facilitating cortical actions. In turn, low striatal dopamine levels relieve the striatal indirect pathway from its tonic DRD2 inhibition, promoting "no-go" signaling and suppressing cortical actions^{233,234}. In healthy individuals, treatment with a DRD2 agonist during working memory tasks lowered the threshold for working memory updates, increasing distractibility and reducing "no-go" signaling^{234,235}. Furthermore, the differential DRD2 pre- and postsynaptic binding affinities of sulpiride might contribute to discrepant effects on spatial working memory. While a high dose of sulpiride administered to healthy volunteers causes impairments in spatial working memory²³⁶, lower doses were found to either have an impact or show no effect on this parameter^{237,238}.

DRD2 also plays a role in regulating motivational and reward-related behaviors, where an individual's motivational state influences their engagement in rewarding activities. Constitutive DRD2 ablation in mice not only reduces spontaneous locomotion but also results in deficits in motivation, particularly reducing the effectiveness of food reinforcement^{239,240}. The absence of DRD2 leads to diminished responses to drugs of abuse, resembling the blunted reactions observed with natural rewards, as it reduces sensitivity to the rewarding and reinforcing properties of cocaine, ethanol, and morphine^{117,193}. Similarly, transgenic mice with approximately 15% overexpression of DRD2 in MSNs exhibit deficits in various motivational tasks due to a decreased willingness to exert effort to obtain rewards, potentially stemming from an imbalance in cost/benefit computation^{241,242}. Interestingly, the overexpression of DRD2_L in the CPu or NAc using a non-cell-type-specific viral strategy in adult mice revealed that the upregulation in the NAc enhanced motivation and animals' willingness to work for food²⁴³. However, variations in regional specificity, developmental onset, and the degree of DRD2 upregulation can induce contrasting effects on reward and motivation, underscoring the significance of DRD2 in the development of dopaminergic pathways.

Novelty-seeking behavior is strongly linked to motivation to seek new experiences and is closely tied to the reward system. This behavior is considered a personal trait that is inversely associated with the availability of DRD2 receptors in the ventral midbrain in both humans and rodents^{244,245}. Indeed, mice lacking DRD2 in dopaminergic neurons display hyperactivity in novel environments and increased motivation to seek rewards²¹⁸. Furthermore, rodents with high responsiveness to novelty exhibit higher levels of extracellular dopamine in the NAc, both under baseline conditions and when stimulated^{246,247}.

1.3.7 DRD2 and neuropsychiatric disorders

The literature extensively documents genetic or functional impairments in DRD2 across a range of neurological and psychiatric disorders, including schizophrenia, ASD, major depressive disorder, Parkinson's disease, Huntington's disease, and addiction. In some cases, targeting DRD2 constitutes a pharmacological approach to cure or ameliorate the symptoms associated with these conditions.

Schizophrenia is a psychiatric disorder with a global prevalence of approximately 0.33%, affecting both men and women²⁴⁸. It is characterized by three core symptom types: positive symptoms (e.g., delusions and hallucinations), negative symptoms (e.g., anhedonia and social withdrawal), and cognitive dysfunction (e.g., learning deficits and attention difficulties)⁷⁶. While most theories concerning the pathophysiology of schizophrenia focus on the neurotransmitter imbalances of dopamine, serotonin, and glutamate, the dopamine hypothesis has significant prominence and acceptance. Recent models propose that hyperactive dopaminergic transmission in mesolimbic areas contributes to positive symptoms, while hypoactive dopaminergic transmission in the nigrostriatal and mesocortical pathways affects the extrapyramidal system (motor symptoms) and elicits negative

symptoms and cognitive deficits^{76,249}. Postmortem and *in vivo* neuroimaging studies have consistently found an increased DRD2 density and occupancy in the striatum of patients^{250,251}. Interestingly, all typical antipsychotics prescribed to schizophrenic patients aim to block DRD2 and alleviate the severity of positive symptoms^{252,253}. Upregulation of DRD2 in a high-affinity state in the striatum is a consistent feature in mouse models of schizophrenia²⁵⁴⁻²⁵⁶, which often display a range of schizophrenic-like behaviors, including spontaneous hyperlocomotion, hyperreactivity to stress, impaired working memory, deficits in novel object recognition, and reduced social interactions^{70,230}. Additionally, impaired DRD2 signaling has been specifically associated with deficits in various subcomponents of working memory in both animal models^{203,241} and in patients, which has been attributed to compromised cortico-striatal-thalamic loop functioning^{257,258}. Genetic studies have linked various polymorphisms in the DRD2 coding region (rs2283265 or rs1076560) to the development of schizophrenia and their potential influence on inter-individual variations in schizophrenic phenotypes²⁵⁹⁻²⁶². While typical antipsychotics (DRD2 antagonists) were initially the standard treatment, atypical antipsychotics (second-generation) have become the preferred choice due to their lower incidence of extrapyramidal symptoms⁶⁶. However, preclinical rodent studies have shown that both typical and atypical antipsychotics can induce sex-dependent alterations in DRD2 expression within the hypothalamus²⁶³.

ASD is a prevalent developmental disorder affecting approximately one in 100 children and has a higher prevalence in males with a reported male-to-female ratio of approximately 4 to 1^{248,264,265}. Recent research suggests potential diagnostic biases in ASD diagnosis, with females potentially needing more intense or numerous symptoms for diagnosis^{264,265}. ASD is characterized by delayed language, repetitive behaviors, social interaction challenges, and varying degrees of motor skill impairments, including eye movement, fine and gross motor skills, balance, coordination, action sequencing, and inhibitory control^{248,266}. In individuals with ASD, elevated levels of DRD2 mRNA have been observed in the caudate and putamen, indicating dysfunction in the indirect motor pathway, which contributes to motor dysfunction, stereotypy, and repetitive behaviors²⁶⁶. These symptoms can be ameliorated with classical antipsychotic pharmacotherapy involving DRD2 antagonism, such as haloperidol or risperidone, indicating that increased dopamine levels play a role in motor abnormalities associated with ASD^{75,267}.

Major depressive disorder is characterized by persistent anhedonia, low motivation, fatigue, and occasional delusions/hallucinations and affects approximately 4% of men and 6% of women²⁴⁸. Anhedonia has been linked to dysfunction in the reward system, particularly in dopaminergic transmission²⁶⁸. Specifically, the different availability of DRD2/DRD3 in the NAc has been associated with higher anxiety symptoms and is inversely correlated with the severity of motivational anhedonia²⁶⁹. Patients with depression have shown increased DRD2 binding in the striatum²⁷⁰, and blocking DRD2 with raclopride in rats has been demonstrated to partially enhance depressive-like

symptoms²⁷¹. Additionally, common treatments for this disorder include SSRIs or serotonin/norepinephrine reuptake inhibitors, which aim to increase serotonin and noradrenaline levels in the synaptic cleft. However, certain medications also incorporate partial agonists of DRD2 (e.g., aripiprazole) or selective agonists of DRD2-like receptors (e.g., pramipexole)²⁶⁸.

Parkinson's disease is the second most prevalent neurodegenerative disorder, which is 1.5 times more incident in men than in women^{248,272}. Recent studies have shown gender-related differences in disease progression, with men often experiencing more pronounced impairments in motor function and cognitive abilities. The disease is characterized by motor symptoms like tremors, bradykinesia, muscular rigidity, and impaired balance, potentially influenced by a combination of genetic, environmental, and hormonal factors^{272,273}. These symptoms result from the degeneration of dopaminergic neurons in the SNc, leading to reduced dopamine levels in the dorsal striatum, which overactivates the indirect pathway and reduces the direct pathway. Intracellular accumulation of Lewy bodies containing aggregated α -synuclein is a hallmark of the disease¹⁷¹. Specific DRD2 polymorphisms, including those associated with schizophrenia, have been linked to Parkinson's disease¹⁷¹. L-DOPA is a common therapy, but chronic use can lead to motor side effects. DRD2 agonists like bromocriptine and cabergoline are used as alternatives for both early and advanced stages of the disease¹⁷¹.

Huntington's disease is a neurodegenerative disorder caused by a dominantly inherited mutation in the huntingtin gene, affecting around 5-7 individuals per 100,000 people, with variations in epidemiology across populations and sexes²⁷⁴. A recent longitudinal study highlighted gender differences in disease manifestation, with women showing worsened motor and depressive symptoms²⁷⁵. The disease is characterized by chorea, cognitive deficits, and psychiatric disturbances that worsen over time²⁷⁴. Of note, mutated huntingtin proteins aggregate in the CNS, initiating mechanisms of neuronal dysfunction and cell death. The initial signs are observed in the dorsal striatum iMSNs that express DRD2, resulting in an initial hyperkinesia phenotype^{274,276}. The interplay between dopamine and glutamate signaling, particularly the reduction in NMDA receptor response due to DRD2 activation, plays a neuroprotective role in this disorder^{277,278}.

Addiction is characterized by compulsive behavior, often involving substances or activities like drugs, alcohol, gambling, or sex, despite their negative and detrimental consequences²⁷⁹. It is more prevalent in men than women, with clinical studies indicating lower DRD2 availability in the striatum in men and higher DRD2 binding in the VTA in women²⁸⁰⁻²⁸². Initially, addictive substances or activities trigger an increase in dopamine release, followed by a decrease in striatal DRD2 availability²⁸³. Repeated exposure to addictive stimuli leads to synaptic changes in the mesolimbic pathway due to persistent downregulation of DRD2 in the VTA and NAc^{117,283}. In rodents, reduced dopamine levels and decreased DRD2 activity result in a preference for less effortful and smaller

immediate rewards²⁴³. Similarly, low DRD2 density in the striatum is associated with higher impulsivity and an increased risk of addiction in humans^{284,285}.

Understanding the relationship between DRD2 and other binding partners like CHL1 is crucial. Investigating the functional interactions offers valuable insights into the complex mechanisms of dopaminergic signaling and the pathophysiology of related disorders.

1.4 Aims of the thesis

The investigation of the connection between CHL1 and the dopaminergic system has attracted interest due to the strong association between *CALL* polymorphisms and neuropsychiatric disorders, such as ASD and schizophrenia^{49,51,52,61}, as well as CHL1's pivotal role in guiding the development of ventral midbrain structures^{20,74}. Although the specific neurocircuits and key elements involved in this connection are not fully understood, DRD2 signaling impairments in neuropsychiatric disorders are linked to *CALL* mutations which suggests that DRD2 could interact with CHL1 to modulate dopaminergic functions.

Based on this hypothesis, our research group conducted experiments that revealed a direct interaction between CHL1 and DRD2. Results showed that CHL1 regulates the internalization of DRD2 isoforms and that CHL1 deficiency affects pre- and postsynaptic dopaminergic signaling in the striatum³⁸. However, the specific mechanisms or functional consequences of the CHL1-dependent modulation of dopaminergic signaling through DRD2 remained unexplored. Therefore, my thesis aims to provide a comprehensive functional characterization of the interaction between CHL1 and DRD2, exploring how their interplay influences both biochemical and behavioral mechanisms that are typically regulated by these proteins. In pursuit of this objective, my research had the following aims:

- i. Investigate the co-localization of CHL1 and DRD2 in the striatum and in cultured neurons to determine their association with pre- and postsynaptic neurons involved in dopaminergic transmission.
- ii. Identify the functional consequences of CHL1 and DRD2 interaction on DRD2-dependent signaling pathways in presynaptic dopaminergic neurons and striatal tissue.
- iii. Characterize the functional impact of CHL1 on DRD2-induced morphological changes of the dendritic tree of postsynaptic MSNs in culture and in the striatum of WT and CHL1-deficient mice.
- iv. Assess the implications of the CHL1 and DRD2 interaction on DRD2 antagonist/agonist-induced behavioral responses in striatal-dependent behaviors.

Chapter II

Materials and Methods

2 Materials and Methods

2.1 Materials

2.1.1 Animals

The CHL1 KO mice were generated in 2002 by removing the first exon and part of the first intron of the CHL1 gene²⁷. The mice were backcrossed onto a C57BL/6J background for more than eight generations. The CHL1 KO mice and their age-matched WT littermates derived from heterozygous breeding or from C57BL/6J mice were bred and maintained at the animal facility of the *Zentrum für Molekulare Neurobiologie Hamburg*. Mice were kept at a temperature of 25 °C, on a 12 h light-dark cycle and ad libitum access to food and water. For all the experiments, 3- to 5-month-old adult female and male WT and CHL1 KO mice were used. All procedures used were approved by the responsible authorities of the State of Hamburg (*Behörde für Justiz und Verbraucherschutz*; animal permit numbers N061/2019 and ORG_1022), and conducted in agreement to the ARRIVE guidelines and standards set by the European Union and Germany.

2.1.2 Antibodies

The primary and secondary antibodies used in this study are presented in Tables 2.1 and 2.2, respectively. The tables include information about the antibody dilutions used for the various applied techniques, as well as information about the supplier.

Table 2.1. List of primary antibodies. Abbreviations: PLA – proximity ligation assay, IHC – immunohistochemistry, ICC – immunocytochemistry, WB – western blot, GAPDH - glyceraldehyde-3-phosphate dehydrogenase, MAP2 - microtubule-associated protein 2.

Antibody (company)	Dilution
Goat polyclonal anti-CHL1 (AF2147, R&D Systems)	PLA/IHC 1:50 PLA/ICC 1:100
Mouse monoclonal anti-DRD2 (B-10, Santa Cruz Biotechnology)	PLA/IHC 1:50 PLA/ICC 1:100
Rabbit polyclonal anti-TH (AB152, Millipore)	PLA/IHC 1:200 PLA/ICC 1:100
Mouse monoclonal anti-TH (F-11, Santa Cruz Biotechnology)	ICC 1:400 WB 1:1,000
Rabbit polyclonal anti-phospho TH (Ser40) (AHP912, Bio-Rad)	ICC 1:200 WB 1:1,000
Mouse monoclonal anti-GSK3 β	WB 1:1,000

Chapter II Materials and Methods

(E-11, Santa Cruz Biotechnology)	
Rabbit polyclonal anti-phospho GSK3 β (Ser 9) (9336, Cell Signaling Technology)	WB 1:1,000
Mouse monoclonal anti-ERK1/2 (4696, Cell Signaling Technology)	WB 1:1,000
Rabbit polyclonal anti-phospho ERK1/2 (Thr202/Tyr204) (9101S, Cell Signaling Technology)	WB 1:1,000
Mouse monoclonal anti-DARPP-32 (H-3, Santa Cruz Biotechnology)	ICC 1:300 WB 1:1,000
Rabbit monoclonal anti-DARPP-32 (2306, Cell Signaling Technology)	PLA/IHC 1:200 PLA/ICC 1:100
Mouse monoclonal anti-GAPDH (6C5, Santa Cruz Biotechnology)	WB 1:2,000
Rabbit polyclonal anti-MAP2 (GTX133110, GeneTex)	ICC 1:1000
Guinea pig polyclonal anti-PSD95 (124014, Synaptic Systems)	ICC 1:500

Table 2.2. List of secondary antibodies. Abbreviations: IRDye – infrared dye, HRP – horseradish peroxidase, Cy – cyanine fluorescent dyes.

Antibody (company)	Dilution
IRDye800CW goat anti-rabbit (LI-COR)	WB 1:10,000
IRDye680RD goat anti-mouse (LI-COR)	WB 1:10,000
HRP-conjugated goat anti-rabbit (LI-COR)	WB 1:10,000
HRP-conjugated goat anti-mouse (LI-COR)	WB 1:10,000
Cy2-conjugated donkey anti-mouse (Jackson ImmunoResearch)	IF 1:200
Cy3-conjugated donkey anti-guinea pig (Jackson ImmunoResearch)	IF 1:200
Cy5-conjugated donkey anti-rabbit (Jackson ImmunoResearch)	IF 1:200

2.1.3 Solutions, buffers, reagents, and media

2.1.3.1 Genotyping and agarose gel electrophoresis

A list of solutions, buffers, and reagents used for the genotype of mice and agarose gel electrophoresis is presented and described in Table 2.3. Supplier information is disclaimed whenever important.

Table 2.3. List of solutions, buffers, and reagents used for the genotype of mice and agarose gel electrophoresis. Abbreviations: EDTA - ethylenediaminetetraacetic acid, TAE - tris-acetate-EDTA buffer, w – weight, v – volume.

Solutions, buffers, or reagents	Ingredients / Company
Phire Animal Tissue Direct PCR Kit	Thermo Fisher Scientific
RNase-free water	Qiagen
CHL1 A primer (forward, 5'-AATTGATCGAGGCAGCACTACTTTCTG-3')	Metabion International
CHL1 5 primer (reverse, 5'-CATTCCCAGAAAGGAGGCAACGTG-3')	Metabion International
Neo primer (reverse, 5'-CTAAAGCGCATGCTCCAGACTGCC-3')	Metabion International
50 × TAE solution	2 M Tris 1M acetic acid 50 mM EDTA pH 8.0
Agarose gel	2.5% (w/v) agarose powder (Carl Roth) 1 × TAE 0.07 µl/ml Roti-Safe GelStain (Carl Roth)
6 × Loading dye	Thermo Fisher Scientific
GeneRuler 1 kb DNA Ladder	Thermo Fisher Scientific

2.1.3.2 Cell cultures

A list of solutions, buffers, reagents or media used for the primary cultures is presented and described in Table 2.4. Supplier information is provided for the most important materials.

Table 2.4. List of solutions, buffers, reagents and media used for primary cell cultures. Abbreviations: PDL - Poly-D-lysine, ddH₂O – double distilled water, HBSS - Hanks' Balanced Salt Solution, DMEM - Dulbecco's Modified Eagle Medium, FBS - fetal bovine serum, BSA - bovine serum albumin, PNGM - Primary Neuron Growth medium, PNBM - Primary Neuron Basal medium, DNase – deoxyribonuclease, NSF-1 - Neural Survival Factor-1, NGF-β - nerve growth factor β, AP – alkaline phosphatase, ELISA, enzyme-linked immunosorbent assay.

Solutions, buffers, reagents or media	Ingredients / Company
12 mm glass coverslips	Carl Roth

Chapter II Materials and Methods

PDL coating solution	5 µg/ml PDL (Sigma-Aldrich) in ddH ₂ O
Laminin coating solution	5 µg/ml of laminin (Sigma-Aldrich) in HBSS
HBSS	without Ca ²⁺ and Mg ²⁺ , containing 0.35 g/l NaHCO ₄ and phenol red (Sigma-Aldrich)
Culture medium	10% (v/v) FBS 100 U/mL penicillin 100 µg/ml streptomycin 25 mM HEPES 4 mM glutamine 30 mM glucose in DMEM (Gibco)
Supplemented-DMEM	1% (v/v) N2 supplement 10 µg/ml BSA in DMEM
Trypsin-EDTA	0.05% trypsin and 0.02% EDTA (PAN Biotech)
FBS-HBSS	10% (v/v) FBS in HBSS
PNGM BulletKit (Lonza)	PNBM, glutamine, gentamicin-amphoterin and NSF-1
PNBM medium	2 mM glutamine 50 µg/ml Gentamicin 37 ng/ml Amphoterin in PNBM medium
Supplemented PNBM medium (ventral midbrain culture)	2% (v/v) NSF-1 in PNBM medium
DNase solution	200 U/ml DNase (Sigma–Aldrich) in PNBM medium
NGF-β supplemented PNBM medium (striatal culture)	2% (v/v) NSF-1 100 ng/ml NGF-β (ImmunoTools) in PNBM medium
Direct cAMP ELISA kit	(Enzo Life Sciences) Anti-rabbit pre-coated Microtiter plate cAMP standard stock Acetylating buffer Neutralizing reagent AP-conjugated cAMP Rabbit polyclonal cAMP antibody Washing buffer pNpp substrate Stop solution

2.1.3.3 Drug solutions

A list of solutions and reagents used to treat primary neurons or mice with DRD2-specific compounds is presented and described in Table 2.5 and 2.6, respectively. Supplier information is provided for the most important materials.

Table 2.5. List of solutions and reagents used for primary culture treatment. Abbreviations: DMSO - dimethyl sulfoxide.

Solutions or reagents	Ingredients
Vehicle treatment	0.9% (w/v) NaCl 10% (v/v) sterile DMSO in ddH ₂ O
(S)-(-)-Sulpiride (Tocris)	stock: 10 mM in sterile DMSO
(-)-Quinpirole hydrochloride (Tocris)	stock: 3.9 mM in ddH ₂ O with 0.9% NaCl
Sulpiride solution	working solution: 1 mM (10 mM stock diluted in ddH ₂ O with 0.9% NaCl) 30 μM final concentration for cell treatment
Quinpirole solution	working solution: 666.66 μM (3.9 mM stock diluted in ddH ₂ O with 0.9% NaCl and 10% DMSO) 20 μM final concentration for cell treatment

Table 2.6. List of solutions and reagents used for mice treatment.

Solutions	Ingredients
Vehicle treatment	0.9% (w/v) NaCl 0.5% (v/v) sterile DMSO in ddH ₂ O
Sulpiride stock solution	20 mg/ml in sterile DMSO
Quinpirole stock solution	0.2 mg/ml in ddH ₂ O
Sulpiride treatment	1 mg/kg (20 mg/ml stock diluted in ddH ₂ O with 0.9% NaCl)
Quinpirole treatment	0.02 mg/kg (0.2 mg/ml stock diluted in ddH ₂ O with 0.9% NaCl and 0.5% DMSO)

2.1.3.4 Biochemical procedures

A list of solutions, buffers, and reagents used across the several biochemical techniques is presented and described in Table 2.7. Supplier information is provided for the most important materials.

Table 2.7. List of solutions, buffers or reagents used for the biochemical procedures. Abbreviations: PBS - phosphate-buffered saline, RIPA - radioimmunoprecipitation assay, Tris – trisaminomethane, PMSF - phenylmethylsulfonyl fluoride, EGTA - ethylene glycol tetraacetic acid, SDS - sodium dodecyl sulfate, BCA - bicinchoninic acid protein, BSA - bovine serum albumin, dH₂O- distilled water, TBS - tris-buffered saline, TBS-T – tris-buffered saline with Tween 20, ECL - enhanced chemiluminescence.

Solutions, buffers, or reagents	Ingredients / Company
PBS	13.7 mM NaCl 0.27 mM KCl 0.8 mM Na ₂ HPO ₄ 0.15 mM KH ₂ PO ₄ pH 7.4
RIPA buffer	20 mM Tris-HCl, pH 7.5 150 mM NaCl 1 mM EDTA 1 mM EGTA 1% (v/v) Triton-X 100
Inhibitory cocktail (freshly prepared)	1 mM PMSF 1 × PhosSTOP™ tablet (Roche) 1 × cOmplete™, EDTA-free Protease Inhibitor Cocktail tablet (Roche) in 10 ml RIPA buffer
Laemmli buffer (4 x)	250 mM Tris-HCl, pH 6.8 8% (w/v) SDS 40% (v/v) glycerol 0.04% (w/v) bromphenol blue 5% (w/v) β-mercaptoethanol
BCA Protein Assay Reagent Kit	Thermo Fisher Scientific
BSA standard solutions	BSA (Thermo Fisher Scientific) in 62.5, 125, 250, 500, 1,000 and 2,000 µg/µl in dH ₂ O
PageRuler™ Plus Prestained Protein Ladder	Thermo Fisher Scientific
Running buffer (10 x)	250 mM Tris-HCl, pH 8.3 1.9 M glycine 1% (w/v) SDS Dilute in dH ₂ O to 1 × running buffer
Blotting buffer (10 x)	250 mM Tris-HCl, pH 8.3

Chapter II Materials and Methods

	1.9 M glycine
Blotting buffer (1 x)	10% Blotting buffer (10 x) 20% (v/v) methanol in dH ₂ O
TBS (10 x)	100 mM Tris-HCl, pH 8.0 1.5 M NaCl Dilute in dH ₂ O to 1 × TBS
TBS-T	10% TBS (10 x) 0.1% (v/v) Tween-20 in dH ₂ O
Blocking buffer	5% skim milk powder (Carl Roth) in TBS-T
ECL select and ECL prime reagents	GE Healthcare
Revert™ 700 Total Protein Stain Kit	LI-COR

2.1.3.5 Immunofluorescence/histology

A list of solutions, buffers, and reagents used in immunofluorescence and histology techniques is presented and described in Table 2.8. Supplier information is provided for the most important materials.

Table 2.8. List of solutions, buffers or reagents used for the biochemical procedures. Abbreviations: PFA – paraformaldehyde, DAPI - 4',6-diamidino-2-phenylindole, PLA - proximity ligation assay, O.C.T., optimal cutting temperature,

Solutions, buffers, or reagents	Ingredients / Company
8% PFA solution	8% (w/v) PFA in 10 ml PBS pH 7.5
PBS (0.02% NaN ₃)	0.02% (w/v) NaN ₃ in PBS
Blocking and permeabilizing buffer	10% (v/v) normal donkey serum (Dianova) 0.2% (v/v) Triton X-100 in PBS
DAPI stain	stock solution: 500 µg/ml DAPI (Thermo Fisher Scientific) in ddH ₂ O 1 µg/ml final concentration
Epredia™ Shandon™ Immu-Mount™	Thermo Fisher Scientific
Permeabilizing solution	0.2% (v/v) Triton X-100 in PBS

Duolink® In Situ Detection Reagents Red	(Sigma-Aldrich) Duolink blocking solution Washing buffers A and B Ligation solution Ligase Amplification solution Polymerase
Duolink® In Situ PLA® Probes	(Sigma-Aldrich) Anti-goat minus Anti-mouse plus Duolink antibody diluent
30% sucrose solution	30% (w/v) sucrose in ddH ₂ O
Tissue-Tek™ O.C.T. Compound	Sakura Finetek™
Superfrost Plus glass slides	Thermo Fisher Scientific
Antigen retrieval buffer	10 mM tri-sodium citrate dihydrate pH 9.0
FD Rapid GolgiStain™ Kit	(FD NeuroTechnologies) Solution A, B, C and E
Gelatin-Coated Microscope Slides	FD NeuroTechnologies
Eukitt® Quick-hardening mounting medium	Sigma-Aldrich

2.1.4 Suppliers of the chemicals, reagents and kits

All chemicals, reagents and kits were purchased from the following companies: Abcam (Cambridge, UK), Abnova (Taipei, Taiwan), Bioline (London, UK), Bio-Rad Laboratories (Munich, Germany), BioTek (Winooski, VT, USA), Biozol (Eching, Germany), Carl Roth (Karlsruhe, Germany), Cayman Chemical (Ann Arbor, MI, USA), Cell Signaling Technology via New England BioLabs (Frankfurt am Main, Germany), Corning (Wiesbaden, Germany), Dianova (Hamburg, Germany), Eppendorf AG (Hamburg, Germany), ENZO Life Sciences (Farmingdale, NY, USA), FD NeuroTechnologies (Columbia, USA), GE Healthcare (Braunschweig, Germany), Herolab GmbH (Wiesloch, Germany), ImmunoTools (Friesoythe, Germany), Invitrogen (Waltham, MA, USA), Jackson ImmunoResearch (West Grove, UK), LI-COR (Lincoln, NE, USA), Lonza (Basel, Switzerland), Macherey-Nagel (Düren, Germany), Merck Chemicals (Darmstadt, Germany), Metabion (Munich, Germany), Millipore (Schwalbach, Germany), PAN Biotech (Aidenbach, Germany), Promega (Madison, WI, USA), Qiagen (Venlo, The Netherlands), R&D Systems (Wiesbaden, Germany), Roche Diagnostics (Mannheim, Germany), Santa Cruz Biotechnologies (Dallas, TX, USA), Sigma-Aldrich (Taufkirchen, Germany), Synaptic Systems (Göttingen, Germany), ThermoFisher Scientific (Waltham, MA, USA), Tocris (Bristol, UK).

2.2 Molecular biology methods

2.2.1 CHL1-deficient mice genotyping

The genotyping of mice used in this study was performed using tail biopsies from newborns and the Phire Animal Tissue Direct PCR Kit. First, the tail cuts were lyzed in a mixture of Dilution Buffer (20 μ l/sample) and DNA Release solution (0.5 μ l/sample) for 10 min)at room temperature. The reaction was then stopped by incubating the samples for 5 min at 98 °C using the SimpliAmp Thermal Cycler (Life Technologies). A polymerase chain reaction (PCR) reaction was prepared by combining two μ l of the extracted DNA, 2 \times Phire Tissue buffer (10 μ l/sample), Phire II Polymerase (0.4 μ l/sample), primers (CHL1 A, forward primer at 2.5 pM; and CHL 5 and Neo, reverse primers at 1.25 pM), and RNase-free water (to adjust the final volume of 20 μ l). The conditions used for PCR in the SimpliAmp Thermal Cycler were described in Table 2.9.

Table 2.9. PCR cycling scheme for genotyping CHL1-deficient mice.

Steps	Temperature	Time	Steps
Initial denaturation	98 °C	1 minute	1
Denaturation	98 °C	5 seconds	35
Annealing	68 °C	1 minute	
Extension	72 °C	1 minute	
Final extension	72 °C	10 minutes	1
Cooling	4 °C	until use	

2.2.2 Agasore gel electrophoresis

The PCR products were analysed with electrophoresis on a 2.5% agarose gel. To prepare the gel, the agarose is dissolved in 1 \times TAE buffer by heating the solution, and Roti-Safe GelStain was added for fluorescent staining of DNA (7 μ l/100 ml of solution). The solution was then poured into a gel tray and loading wells were created with a well comb. After polymerization, the gel was transferred to a horizontal electrophoresis chamber (BioRad) immersed in 1x TAE buffer. PCR products were mixed with 6 \times Loading dye and added to loading wells along with one well of GeneRuler 1 kb DNA Ladder. The electrophoresis was performed for 30 to 40 min at a constant voltage of 180 V. A picture of the gel was taken using the E.A.S.Y. UV-light documentation system (Herolab) and the genotypes were distinguishable by the presence of a single band at 450 kb for the WT genotype, a single band at 380 kb for the CHL1 KO genotype, and the presence of both bands for the heterozygous genotype.

2.3 Cell culture methods

2.3.1 Coating of coverslips and well plates

To perform immunocytochemistry of ventral midbrain and striatal primary neurons, 12 mm glass coverslips were cleaned and sterilized. First, the coverslips were placed inside an Erlenmeyer flask and gently agitated in a 3 M hydrochloric acid solution for 30 min. After two washes with ddH₂O, the coverslips were submerged in acetone for 3 hours with gentle shaking. They were then washed five more times with ddH₂O and twice with absolute ethanol for 10 min. Next, the coverslips were heated to 160 °C for 2 hours. All subsequent steps were conducted in a sterile environment using a laminar flow hood. The coverslips were coated with sterile PDL at a concentration of 50 µg/ml in ddH₂O overnight at 4 °C with gentle shaking. The excess PDL was removed by washing the coverslips three times with ddH₂O and they were dried at room temperature under the hood. The coverslips were placed in a sterile 50 ml Falcon tube and stored until use. The day before the cell culture, PDL-coated coverslips were coated with laminin at a concentration of 5 µg/ml in HBSS. The coverslips were pre-incubated overnight at 4 °C and the solution was only removed immediately prior to cell seeding.

For cell lysates, 12-well plates were coated with sterile PDL at a concentration of 50 µg/ml in ddH₂O overnight at 4 °C with gentle shaking. The excess PDL was removed by washing the wells three times with ddH₂O and the plates were dried at room temperature under the hood.

2.3.2 Culture of ventral midbrain primary neurons

On embryonic day 14 (E14), pregnant female mice were sacrificed using CO₂, and embryos were extracted from the uterus using sterilized tools. Two protocols to prepare ventral midbrain primary cultures were used in this thesis.

A modified version of the protocol described by Choi et al. (2013)²⁸⁶ to evaluate CHL1 and DRD2 co-localization in ventral midbrain neurons was applied. The embryos were cleaned with ice-cold DMEM before being fixed onto a Sylgard dish with fresh ice-cold DMEM. Brains were extracted from the skull and meninges and superficial blood vessels were removed. The ventral midbrain was dissected and incubated with 5 ml of fresh DMEM for 10 min in a 37 °C water bath. Following this, the DMEM was discarded and the tissue was mechanically dissociated with a 1 ml pipette tip in 5 ml of warmed culture medium. The cell suspension was allowed to settle for 2 min, and the supernatant was separated from the remaining tissue. To determine the cell number, 10 µl of the cell suspension was mixed with 0.4% trypan blue solution at a 1:1 ratio and counted under a microscope using a glass Neubauer chamber. The cells were diluted in culture medium to a density of 8×10^6 cells/ml, and 100 µl was added per coverslip to form a micro-island. The cells were then incubated overnight in a humidified incubator with 5% CO₂ and 95% air at 37 °C. The following day, 900 µl of warmed culture medium was carefully added to the wells, and the cells were incubated again. Half of the medium was replaced

by fresh culture medium on 3 day *in vitro* (div) and by supplemented-DMEM on 5 div. The neurons were kept in culture until 7 div, as this allowed for the expression of TH protein (Choi 2013, Gaven 2014).

To study the DRD2 upstream signaling pathway in the ventral midbrain neurons, a protocol described by Weinert et al. (2015)²⁸⁷ was adapted. The embryos were three times washed with ice-cold HBSS before being fixed onto a Sylgard dish with new ice-cold HBSS. Brains were removed from the skull and meninges and superficial blood vessels were removed. The ventral midbrain was dissected, transferred under a hood to 3 ml of warmed Trypsin-EDTA, and later incubated for 10 min in a 37 °C water bath with occasional gentle agitation. The solution was then removed, and digestion was stopped with 3 ml of FBS-HBSS for 1 min with gentle shaking. The tissue was washed twice with 1 ml warmed PNB medium and then mechanically disrupted in 2 ml warmed supplemented PNB medium using two fire-polished glass Pasteur pipettes with rounded tips, from wider to a thinner diameter, until a single cell suspension was obtained. The cells were centrifuged at $400 \times g$ for 5 min at room temperature, the supernatant was removed, and cells were resuspended in 2 ml of warmed supplemented PNB medium. To determine the cell number, 10 μ l of the cell suspension was mixed with 0.4% trypan blue solution at a 1:3 ratio and counted under a microscope using a glass Neubauer chamber. Cells were diluted in supplemented PNB medium using the following conventions: for immunocytochemistry, 500 μ l was added per well at a density between $1.6-1.2 \times 10^5$ cells/ml; for the AMP assay, a density of 4×10^5 cells per well was used; for WB, a density of 1×10^6 cells per well was used. The cells were incubated overnight in a humidified incubator with 5% CO₂ and 95% air at 37 °C. The following day, the same volume of supplemented PNB medium was added to the wells, and half of the medium was replaced with fresh culture medium on 3 div. The neurons were kept in culture until 7 div.

2.3.3 Striatal neurons primary culture

To prepare primary cultures of mouse striatum, a protocol described by Schock et al. (2010)²⁸⁸ was adapted. At E16/16.5, pregnant female mice were euthanized using CO₂ asphyxiation and embryos were extracted from the uterus using sterilized tools. After washing the embryos with ice-cold HBSS three times, their heads were separated and fixed onto a Sylgard dish with new ice-cold HBSS. The brains were extracted from the skull, meninges and superficial blood vessels were removed, and the striatum was dissected from each hemisphere and reserved in ice-cold HBSS. The tissue was then centrifuged for 5 min at $400 \times g$ at room temperature and the solution was aspirated off. Mechanical dissociation in 5 ml of warmed DNase solution was performed using a fire-polished glass Pasteur pipette with rounded tips, with no more than ten triturations until a single cell suspension was obtained. The suspension was allowed to settle for 2 min and the neurons in the supernatant were transferred to a new falcon. To determine the cell number, a 1:1 ratio of 10 μ l of the cell suspension and 0.4% trypan

blue solution was mixed and counted under a microscope using a glass Neubauer chamber. Neurons were diluted and plated using NGF- β supplemented PNB medium and incubated in a humidified incubator with 5% CO₂ and 95% air at 37 °C. Fresh NGF- β supplemented PNB medium was added every 3 to 4 days, replacing half of the existing medium. For WB, cultures were seeded at a density of 1×10^6 cells per well and maintained until 12 div. Neurons used for immunocytochemistry were plated on coverslips at a density of $5-7 \times 10^4$ cells per coverslip for 12 div cultures, and at a density of $2-4 \times 10^4$ cells per coverslip for 21 div cultures.

In previous studies, primary cultures of mouse striatal neurons were found to exhibit reduced neurite length upon treatment with the DRD2 agonist quinpirole at 7 div²⁸⁹. At 9 div, these neurons were shown to express DARPP-32 in MSNs, despite retaining an immature morphology²⁹⁰. Given that by 14 div striatal neurons had developed into morphologically complex cells^{290,291}, we selected the 12 div time point for this thesis to represent an intermediate stage of morphological complexity. This stage is characterized by good neuronal connectivity and dendritic spines, as previously described²⁹². Additionally, dendritic morphology and spine complexity were analyzed in fully developed neurons at 21 DIV, a time point when dendritic and spine maturation have plateaued and remained stable until 28 DIV, following their maximal complexity at 19 DIV according to prior studies^{290,293}.

2.3.4 DRD2-specific compounds and primary cultures treatment

The vehicle solution used as saline control consisted of 0.9% NaCl and 10% sterile DMSO in ddH₂O. For sulpiride (DRD2 antagonist), a stock solution of 10 mM was prepared in sterile DMSO, which was then freshly diluted in ddH₂O (0.9% NaCl) to a working solution of 1 mM containing 10% DMSO. Quinpirole (DRD2 agonist) was initially dissolved to a stock solution of 3.9 mM in ddH₂O (0.9% NaCl) and further diluted to a fresh working solution of 666.66 μ M in ddH₂O (0.9% NaCl and 10% sterile DMSO). Stock solutions were aliquoted and stored at -20 °C until use.

The primary neurons were then treated with freshly prepared solutions of the vehicle and DRD2-specific compounds, at a final concentration of 30 μ M sulpiride and 20 μ M quinpirole. The same volume of treatments was added to the medium and the plate was gently swirled for 5 seconds and the final DMSO concentration was 0.3%. The plate was then returned to the humidified incubator until the incubation period was over. The incubation period for ventral midbrain neurons at 7 div was 20 min, while for striatal neurons at 12 or 21 div, it was 30 min or 24 hours, respectively. The incubation was carried out prior to the lysis or fixation of the neurons. To ensure consistent treatment conditions, the same volume of the compounds and DMSO concentration were added to the neuronal cultures. To prevent cytotoxicity, the concentration of DMSO in all treatment conditions was maintained below 0.3%.

The concentrations and incubation times for the treatments were optimized through a combination of previous studies and preliminary pilot tests. Specifically, previous studies demonstrated that DRD2

stimulation with 10 μ M quinpirole in the midbrain and striatal neurons changes the upstream portion of the signaling pathway within the first 5 to 30 min^{289,294,295}. Dendritic morphology and spine density were shown to change in striatal neurons after 24 hours of treatment with the same quinpirole concentration¹⁷⁴. Additionally, studies treating HEK293 cells or striatal neurons with sulpiride used working concentrations between 10 to 30 μ M^{296,297}. Therefore, as a result of combining these data with our pilot tests, neurons were treated with 30 μ M sulpiride or 20 μ M quinpirole and shorter periods of treatment were used to study early effects on the signaling pathway, whilst longer incubation times were employed to study changes in neuronal morphology. Since some studies reported morphological changes occurring in primary neurons in less than 30 min^{298,299} and the first striatal cultures produced in the laboratory were treated with the compounds for 30 min at 12 div, it was chosen to investigate the existence of morphological changes at this time point as well.

2.4 Biochemical methods

2.4.1 cAMP quantification in ventral midbrain neurons

The Direct cAMP ELISA kit was used to determine the cAMP levels in cell lysates of WT and CHL1 KO ventral midbrain cultures at 7 div, following the manufacturer's acetylated version of the protocol. This is a colorimetric competitive enzyme immunoassay for the quantitative determination of extracellular cAMP, with a 10-fold increase in sensitivity achieved through the acetylation procedure. Briefly, samples containing cAMP are first incubated with a cAMP antibody and an AP-conjugated cAMP protein on a pre-coated plate that has been coated with a species-specific secondary antibody. This setup allows the cAMP in the sample to compete with the AP-conjugated cAMP for binding to the antibody-coated plate. Later, a substrate for the AP enzyme is added, and the enzymatic reaction produces a distinct yellow color. The amount of cAMP in the sample is quantified by measuring the absorbance of the colorimetric signal.

Following treatment with DRD2-specific compounds treatment for 20 min, neurons were washed with PBS and lysed in 0.1 M HCl with 0.2% Triton X-100 for 10 min at room temperature. The lysed cells were then centrifuged at 600 \times g for 10 min to remove cellular debris, and the resulting supernatants were either used directly or snap-frozen in liquid nitrogen for later analysis. Total protein concentration of each sample was determined using the BCA protein assay ([section 2.4.4](#)), and cAMP content was measured as follows.

First, cAMP standard stock (2 nmol/ml) was diluted serially in 0.1 M HCl with 0.2% Triton X-100 to obtain concentrations of 20, 5, 1.25, 0.312, and 0.078 pmol/ml. The samples and standards were treated with acetylating buffer. Next, the following mixture was added to the wells of a 96-well goat anti-rabbit pre-coated microtiter plate: neutralizing reagent, acetylated sample or cAMP standard, cAMP conjugated with AP, and rabbit polyclonal cAMP antibody. The plate was sealed and incubated

for 2 hours at room temperature on a plate shaker (≈ 500 rpm). The wells were washed three times with washing buffer, and then pNpp substrate (AP substrate) was added and incubated for 1 hour at room temperature without agitation. Stop solution was subsequently added, and the plate absorbance was measured at 405 nm using a μ Quant spectrophotometer (Bio-Tek Instruments). The resulting yellow color was indicative of the enzymatic reaction, and the optical density was inversely proportional to the cAMP concentration of the sample. The concentrations (pmol/ml) were calculated from the cAMP standard curve, normalized to the total protein content of each sample (pmol of cAMP per mg of total protein), and expressed relative to the control (WT vehicle group). Samples were run in duplicates with the following controls: wells without cAMP antibody as negative control for nonspecific binding, 0.1 M HCl with 0.2% Triton X-100 as the 0 pmol/ml standard, wells with only AP-conjugated cAMP and AP substrate as the positive control, and blank wells only with stop solution to eliminate background signal. The experiment used cells from 5 independent cultures.

2.4.2 DRD2-specific compounds and animal treatment

The vehicle solution used as saline control consisted of 0.9% NaCl and 0.5% sterile DMSO in ddH₂O. For sulpiride, a stock solution of 20 mg/ml was prepared in sterile DMSO, which was then diluted in ddH₂O (0.9% NaCl) to the final concentration of 1 mg/ml containing 0.5% DMSO. Quinpirole was initially dissolved to a stock solution of 0.2 mg/ml in ddH₂O and further diluted to a final concentration of 0.02 mg/ml in ddH₂O (0.9% NaCl and 0.5% sterile DMSO). All materials and solutions used were sterile and prepared shortly before use.

Female and male WT and CHL1 KO mice received an intraperitoneal (i.p.) injection of 300 μ l solution per 30 g of body weight using a 27 G needle. The solutions consisted in the vehicle (0.9% NaCl, 0.5% DMSO), sulpiride (1 mg/kg) or quinpirole (0.02 mg/kg). After a 15-min interval, the animals were euthanized through cervical dislocation, and striatal homogenates were subsequently prepared for protein content analysis. Animals previously used in behavioral procedures were utilized for this purpose.

In line with the behavioral tests, the early onset of effects was the main focus for analysing the protein content. Earlier studies have shown that i.p. injection of low doses of quinpirole into male mice for either 15 min (0.2 mg/kg) or 30 min (0.02/0.2 mg/kg) can impact phosphorylation events in the DRD2-induced signaling pathway in striatal homogenates^{138,300,301}. The same events are similarly affected in the striatum by high doses of quinpirole treatment in male mice (1 mg/kg, i.p.) with the maximal effect observed 15 min after treatment, starting from the first 3 min³⁰², and in male rats (5 mg/kg, subcutaneous) after 15 min³⁰³. Additionally, striatal changes in CREB phosphorylation content were reported after a high dose of i.p. sulpiride treatment (50 mg/kg) after 10 min in male mice. Hence, a treatment for 15 min was chosen to ensure that the signaling pathway did not completely unwind, while still providing enough time for phosphorylation events to be triggered.

2.4.3 Protein samples preparation for SDS-PAGE

Cell lysates were prepared from primary cultures treated with DRD2-specific compounds. The culture plates were placed on ice and rinsed three times with cold HBSS, and the neurons were incubated with an appropriate amount of cold RIPA buffer containing the protease phosphatase inhibitory cocktail for 10 min with gentle agitation. The cells were subsequently scraped off, collected in a tube and centrifuged at $600 \times g$ for 10 min at 4 °C to remove cellular debris. The supernatant was collected.

Striatal homogenates were prepared from female and male WT and CHL1 KO mice treated with the DRD2-specific compounds for 15 min ([section 2.4.2](#)). Striata were bilaterally dissected out on an ice-cold surface and immediately snap-frozen in liquid nitrogen and saved at -80 °C until use. Tissue was later homogenized by trituration twice with a 20 gauge needle and four times with a 24 gauge needle in 200 μ l of cold RIPA buffer containing the inhibitory cocktail. The homogenates were transferred to a new tube and subjected to centrifugation at $10,000 \times g$ for 10 min at 4 °C. The supernatant was collected.

The protein concentration in tissue and cell supernatants was determined using the BCA protein assay ([section 2.4.4](#)). Solutions with the same protein concentrations were prepared for each sample by diluting a specific volume of the supernatant in Laemmli buffer (4 x). The proteins were then denatured by heating the samples at 95 °C for 5 min. The remaining supernatant was frozen at -80 °C.

2.4.4 Determination of protein concentration

For the determination of protein concentrations, the BCA Protein Assay Reagent Kit was used. Standard solutions of BSA were prepared in dH₂O at concentrations of 62.5, 125, 250, 500, 1,000 and 2,000 μ g/ μ l. Different dilutions of the homogenates were also prepared in dH₂O. Microtiter 96-well plate was loaded with 10 μ l/well of blank control, standards, or diluted samples, along with 200 μ l of a mixture of solutions A and B from the Protein Assay Kit in a ratio of 1:50. The plate was then incubated for 30 min at 37 °C, and the absorbance was measured at 562 nm using a μ Quant spectrophotometer (Bio-Tek Instruments). The calibration of the absorbance curve of the BSA standards provided the necessary information for determining the protein concentration of the samples.

2.4.5 SDS-polyacrylamide gel electrophoresis (SDS-PAGE)

The cell lysates were subjected to protein separation via SDS-PAGE using a Mini-Protean II system with 15-well 4-20% Criterion™ Tris-HCl gels (Bio-Rad). The gels were loaded with the same volume of sample per well containing 20 μ g protein, and the estimation of molecular masses was achieved using the PageRuler™ Plus Prestained Protein Ladder. The chamber was filled with running buffer, and

the gels were run using a Power Pac 200 (Bio-Rad) at an initial voltage of 80 V for 20 min, followed by 120 V until good separation was obtained between 70 to 30 kDa proteins.

For the striatal lysates, a Criterion™ Vertical Electrophoresis cell with 26-well 8–16% Criterion™ TGX™ Precast Midi Protein gels (Bio-Rad) was used. The same sample volume per well containing 40 µg protein was loaded onto the gels and they were run initially at 80 V for 20 min and then at 150 V until good protein resolution was obtained.

2.4.6 Western Blot and relative protein quantification

Western Blot analysis was used in order to examine the relative quantity of proteins. Proteins separated in the SDS-PAGE were transferred from the gel to a 0.45 µm nitrocellulose Amersham™ Protran™ (GE Healthcare). Before assembling the blotting sandwich, membranes were incubated in ice-cold blotting buffer for at least 30 min. The transfer was performed in a Bio-Rad transfer apparatus placed on ice and filled up with ice-cold blotting buffer. The proteins were transferred at a constant voltage of 90 V for 1 hour.

After electrophoretic transfer, the membranes were positioned in a glass container with the protein-binding side facing upwards and were blocked with blocking buffer while gently shaken for 1 hour at room temperature. Next, the primary antibodies were diluted in blocking buffer and incubated with the membranes overnight at 4 °C with agitation. The next day, the membranes were washed three times for 5 min at room temperature with TBS-T and then incubated with either HRP- or IRDye-conjugated secondary antibodies in blocking buffer for 1 hour. Throughout the subsequent steps, the membranes incubated with IRDye-conjugated secondary antibodies were kept protected from light. After being washed three times for 10 min with TBS-T, HRP-conjugated antibodies were visualized on the membrane using an ECL select or ECL prime mixture according to the manufacturer's protocol with the LAS 4000 Mini camera (GE Healthcare). IRDye-conjugated secondary antibodies were detected using an Odyssey Infrared Imager (LI-COR).

To determine relative protein levels, Image Studio Lite software (LI-COR) was utilized. For the quantification of phosphorylation levels, the signal of the phosphorylated protein was normalized to the total protein. To quantify total protein levels, the signal was normalized to a housekeeping protein such as GAPDH or to the total protein content of the immunoblot following the manufacturer's instructions for the Revert™ 700 Total Protein Stain Kit (Fig. 2.1). Protein quantification via WB involved the use of three independent cultures for ventral midbrain cultures and 7-8 animals per condition for striatal homogenates.

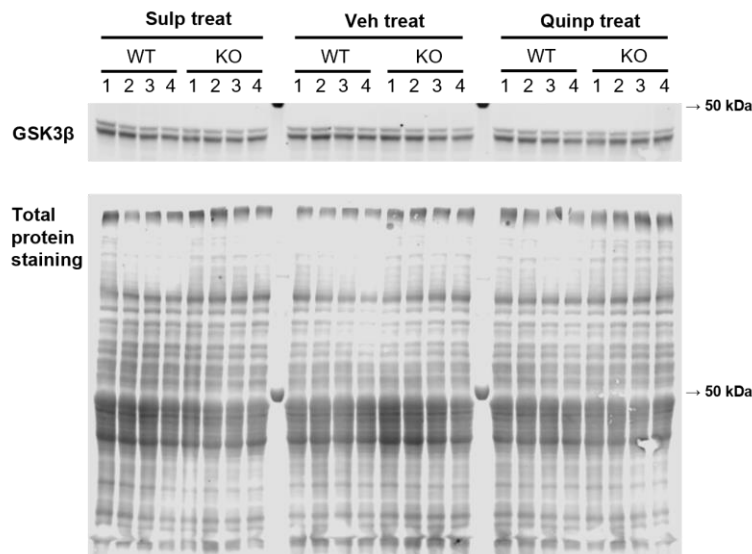


Figure 2.1. Representative immunoblot of total protein normalization. Example of an immunoblot loaded with four striatal homogenates for each genotype per treatment (sulpiride, sulp; vehicle, veh; quinpirole, quinp) and probed with GSK3 β primary antibody followed by an IRDye680RD secondary antibody. Before the blocking procedure, the membrane was submitted to the Revert™ 700 Total Protein Stain Kit, and staining of the total protein content was obtained.

2.5 Immunocytochemistry

2.5.1 Immunocytochemistry protocol

Primary cultures in glass coverslips were fixed for 20 min at room temperature using an 8% PFA solution diluted in the maintenance medium at a 1:1 ratio and washed three times for 5 min with PBS. Coverslips were either stained or saved in PBS containing 0.02% NaN₃ at 4 °C until use. Prior to immunostaining, the neurons were incubated with a blocking and permeabilizing solution for 1 hour at room temperature with gentle shaking. Primary antibodies in PBS were added and incubated overnight at 4 °C with gentle agitation. The next day, the neurons were washed three times for 5 min with PBS and then incubated with Cy-conjugated secondary antibodies against the species of the primary antibody and DAPI stain at a concentration of 1 μ g/ml for 1 hour at room temperature with gentle agitation. The neurons were protected from light from this point onward. The coverslips were then washed three times for 10 min with PBS, shortly dried and mounted on glass slides using EpreDia™ Shandon™ Immu-Mount™. To control for nonspecific binding of the fluorescent antibodies, negative control coverslips were incubated solely with Cy-conjugated secondary antibodies.

2.5.2 Immunocytochemistry coupled with PLA

PLA technology was used to investigate the close proximity of CHL1 and DRD2 in WT ventral midbrain and striatal neurons immunostained with dopaminergic markers, TH and DARPP-32. This

assay is designed to detect interactions between two proteins. Primary antibodies raised in different species are used to recognize the target proteins and species-specific secondary antibodies conjugated with oligonucleotides, called PLA probes, are then added to bind to the primary antibodies. Short DNA strands are later added to hybridize to the PLA probes only if they are in close proximity (< 40 nm), forming a closed-circle DNA template that is used for rolling-circle amplification. The PLA probe acts as a primer for a DNA polymerase, resulting in the production of several-hundredfold DNA circle replicates. These replicates are labeled with fluorescent complementary oligonucleotide probes, making each signal visible as an individual discrete spot (PLA signal) when analyzed by microscopy. The Duolink[®] In Situ Detection Reagents Red kit was utilized for performing the PLA, following the manufacturer's instructions and a previously published protocol³⁰⁴.

Firstly, neurons in glass coverslips were fixed as previously detailed, permeabilized for 30 min with a permeabilizing solution, and followed by a blocking step for 40 min at 37 °C with Duolink blocking solution. The coverslips were then incubated in a humid chamber overnight at 4 °C with the primary antibodies anti-CHL1 (goat, 1:100), anti-DRD2 (mouse, 1:100), and either anti-TH (rabbit, 1:100) in ventral midbrain neurons or anti-DARPP-32 (rabbit, 1:100) in striatal neurons, diluted in Duolink antibody diluent. The cells were washed twice for 5 min with washing buffer A and incubated with two PLA probes – Duolink[®] In Situ PLA[®] Probe anti-goat minus and anti-mouse plus, diluted 1:5 in Duolink antibody diluent in a humid chamber at 37 °C for 70 min. After washing twice for 5 min with washing buffer A, the ligation step was conducted at 37 °C for 50 min using ligation solution diluted 1:5 and ligase diluted 1:40 in RNase-free water. The same washing step was repeated, followed by the amplification step, in which amplification solution diluted 1:5 and polymerase diluted 1:80 in RNase-free water was added to the coverslips and incubated in a dark humid chamber at 37 °C for 120 min. From this point onward, the neurons were protected from light. The coverslips were then washed for 10 min with washing buffer B and incubated with Cy5-conjugated donkey anti-rabbit (1:200) and DAPI stain (1 µg/ml) for 1 hour at room temperature. After an additional washing step, twice with washing buffer B and once with PBS for 10 min each, the coverslips were shortly dried and mounted on glass slides using Eprelia[™] Shandon[™] Immu-Mount[™].

High magnification fields were imaged using the Olympus Fluoview FV1000 confocal microscope in sequential mode, with a 60 × objective plus 2/5 × digital magnification. The acquired images were processed for brightness and contrast using the ImageJ software. Negative controls were included in the experiment, using striatal sections from male CHL1 KO littermate mice for the PLA, and incubating striatal sections solely with Cy-conjugated secondary antibodies to detect nonspecific binding. The experiment used cells from 3 independent cultures.

2.5.3 Quantification of ventral midbrain TH phosphorylation

The immunofluorescent protocol ([section 2.5.1](#)) was carried out on WT and CHL1 KO ventral midbrain cultures at 7 div that had been treated with DRD2-specific compounds for 20 min to assess phosphorylation levels of TH. The primary antibodies against pTH (rabbit, 1:200) at Ser 40 and total TH (mouse, 1:400) were used, followed by the application of Cy5-conjugated donkey anti-rabbit and Cy2-conjugated donkey anti-mouse (1:200) as fluorescent dyes.

Z-stacked images of individual neurons (0.5/1 μm) at high magnification were obtained using the Olympus Fluoview FV1000 confocal microscope in sequential mode with a 60 \times objective. A maximum intensity Z-projection of the neurons was manually delineated using ImageJ software and values for integrated density, area of the cells, and mean grey value average from two background areas were obtained. The corrected total cell fluorescence (CTCF) was then calculated by subtracting the product of cell area and background mean grey value from the integrated density. A ratio between pTH and total TH CTCF was obtained, and CTCF from pTH or total TH was also plotted. The intensities were measured from 5 independent cultures, consisting of 68 to 115 neurons per condition in total.

2.5.4 Quantification of striatal DARPP-32 expression

The immunofluorescent protocol ([section 2.5.1](#)) was performed on WT and CHL1 KO striatal cultures at 12 and 21 div using primary antibodies against DARPP-32 (mouse, 1:300) as the morphological marker and MAP2 (rabbit, 1:1000) as the control neuronal marker. This was followed by labelling with Cy2-conjugated donkey anti-mouse and Cy5-conjugated donkey anti-rabbit (1:200) as fluorescent dyes. MAP2 was used as a neuron-specific cytoskeletal marker.

Low magnification fields were captured from striatal cultures at 12 div using the Olympus Fluoview FV1000 confocal microscope in sequential mode with a 20 \times objective. A pipeline (code) was constructed in CellProfiler software to automatically outline DARPP-32-positive neurons and measure the fluorescent signal of DARPP-32 and MAP2 for each cell (within the outline) (Fig. 2.2 A). Confocal Z-stacks (0.5 μm) of the entire neuronal tree were acquired at 21 div using the Olympus Fluoview FV1000 microscope in sequential mode with a 60/40 \times objective. The Z-stacks were processed to obtain a maximum intensity Z-projection in ImageJ software. A macro was then developed to automatically outline the DARPP-32 signal using the outline function and to obtain DARPP-32 and MAP2 fluorescent signal within the outlined area using the "analyze particles" command, yielding specific results for each neuronal tree (Fig. 2.2 B). CTCF values were calculated for each marker, and DARPP-32 intensity was normalized to MAP2. Intensities were measured from 3 independent cultures at 12 div for a total of 376 WT neurons and 381 CHL1 KO neurons, and at 21 div for 92 WT neurons and 59 CHL1 KO neurons.

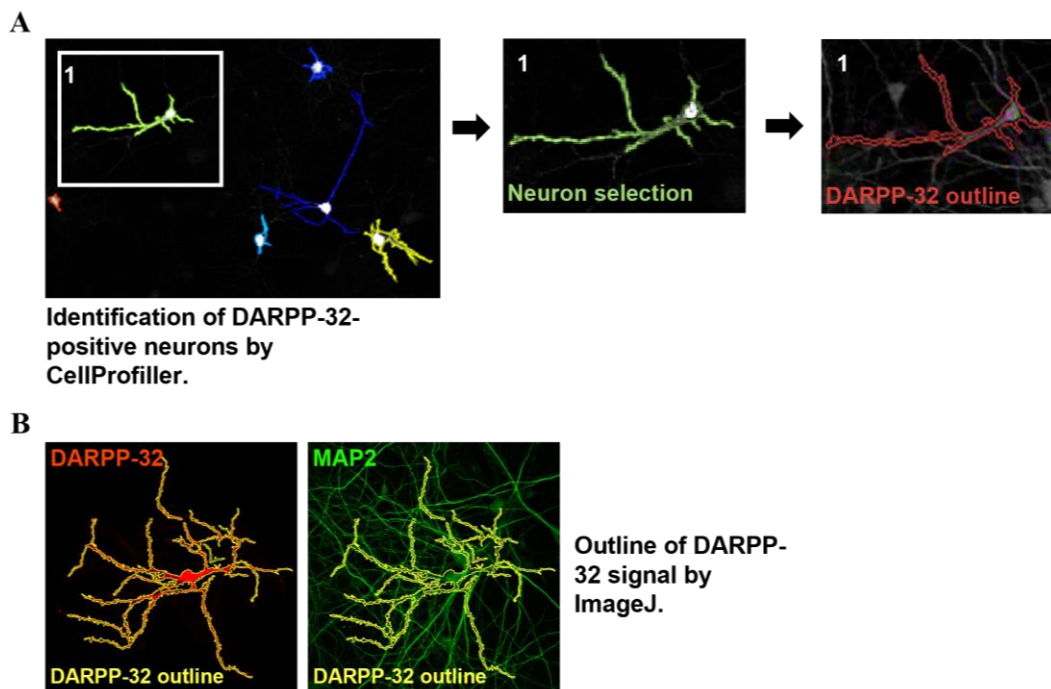


Figure 2.2. Schematic representation of outline strategies of DARPP-32 signal in MSNs. Striatal neurons were co-stained with DARPP-32 and MAP2 antibodies. **(A)** Low magnification confocal fields (20 x objective) were acquired at 12 div and analyzed with a CellProfiler pipeline. **(B)** High magnification Z-stacks (60/40 x) were obtained at 21 div and a macro in ImageJ software was developed to analyze DARPP-32 expression. Both programs were capable of detecting DARPP-32-positive neurons and automatically outlining the DARPP-32 fluorescent signal. The signals for DARPP-32 and MAP2 were measured for each neuron within the outline.

2.5.5 Sholl analysis of striatal primary neurons

Sholl analysis was the method used to assess the complexity of striatal neuronal trees and determine whether treatment conditions had an effect on neuronal morphology. This method involves placing concentric circles of pre-specified radius around the neuronal soma, and counting the number of dendrites intersecting each circle until the end of the neuron is reached (Fig. 2.3). Initially, the length of a straight line from the center of the soma to the end of the longest dendrite is used to define the ending radius or the ending point of the analysis. A starting radius and a radius step are then defined, representing the distance from the center of the soma where the analysis begins and the increase in radius for each subsequent circle. The following parameters are commonly measured: ending radius, the largest intersecting radius; primary branches, the number of dendrites emerging directly from the soma; maximum intersections number, the greatest number of intersections that occurs at any radius; radius of maximum intersections, the radius at which the largest number of intersections occurs; and the number of intersections graphed as a function of radial distance from the soma, an index of how neurite density varies spatially^{305–307}.

Intermediately and fully developed WT and CHL1 KO striatal neurons at 12 and 21 div were treated with DRD2-compounds for 30 mins and 24 hours, respectively. Immunofluorescence was performed on the neurons using DARPP-32 antibody (mouse, 1:300) and MAP2 antibody (rabbit, 1:1000), followed by fluorescent-labeled secondary antibodies as Cy2-conjugated donkey anti-mouse and Cy5-conjugated donkey anti-rabbit (1:200). High magnification Z-stacks ($0.5\ \mu\text{m}$) from individual neurons were imaged with the Olympus Fluoview FV1000 confocal microscope in sequential mode with a $40/60\times$ objective. Z-stacks were analyzed in ImageJ by binarizing maximum intensity Z-projections using Default Dark's thresholding method and manually erasing non-specific signals or traces of other dendrites' neurons.

Sholl analysis was performed with ImageJ plug-in³⁰⁸, using a starting radius of $7\ \mu\text{m}$ and a radius step of $1\ \mu\text{m}$. All the metrics mentioned above were obtained for each neuron and presented as an average per condition. Furthermore, to improve the accuracy of intersection location, a polynomial fitting with the best fitting degree option was used to the maximum intersections number, the radius of maximum intersections and the number of intersections/radial distance from the soma. The experiment was done with 2 independent cultures at 12 div (59 to 76 neurons per condition) and 3 independent cultures at 21 div (58 to 84 neurons per condition).

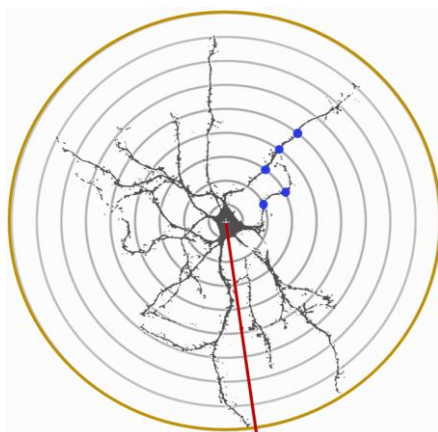


Figure 2.3. Sholl analysis of the neuronal tree morphology. Concentric circles (grey) were placed at $1\ \mu\text{m}$ apart, starting at $7\ \mu\text{m}$ from the cell soma. The red line represents the straight line from the cell soma until the end of the longest dendrite which defines the ending radius (yellow circle), the ending point of the analysis. The blue points represent the intersections, whenever a dendrite crosses the circles.

2.5.6 Spine analysis of striatal primary neurons

A spine analysis in fully developed WT and CHL1 KO striatal neurons at 21 div was carried out to quantify and classify dendritic spines morphology. After a 24-hour treatment with DRD2-compounds, neurons were immunostained with anti-DARPP-32 (mouse, 1:300) and anti-MAP2 (rabbit, 1:1000) antibodies, followed by Cy2-conjugated donkey anti-mouse and Cy5-conjugated donkey anti-rabbit (1:200) secondary antibodies. High magnification super-resolution Z-stacks ($0.1\text{-}0.2\ \mu\text{m}$) were acquired from spines located in secondary or tertiary dendrites, with a maximum of 2 segments per neuron being imaged. An Abberior multichannel confocal/STED microscope based on a Nikon Ti-E microscope was used with a $60\times$ objective. The images were first pre-processed using ImageJ by

subtracting the background with a rolling ball radius of 100 pixels, and all subsequent analysis was performed using Imaris software (Belfast, United Kingdom).

The dendritic branches were 3D reconstructed using the Filament Tracer tool with the Autopath algorithm through the DARPP-32 channel. The spines were then reconstructed initially with the Autopath mode and later refined with the manual method. They were defined as having a minimum head width of $\geq 0.3 \mu\text{m}$ and a maximum length of $\leq 2 \mu\text{m}$. Spine morphology was determined and classified from the 3D reconstruction of spines using Xtension extension in Imaris, based on the following default criteria: stubby, spine length $< 1 \mu\text{m}$; mushroom, spine length $< 3 \mu\text{m}$ and maximum head width $> (\text{mean neck width} \times 2) \mu\text{m}$; long thin, mean head width $\geq \text{mean neck width}$; filopodia/dendrite, the rest of the identified spines (Fig. 2.4)³⁰⁹. The total number, percentage and density for each spine class were determined, as well as the mean and total (accumulative values) of geometric metrics including spine area, length, neck length, and spine volume, for each spine class. For this experiment, 18-20 dendritic branches were analyzed per condition using 3 independent cultures.

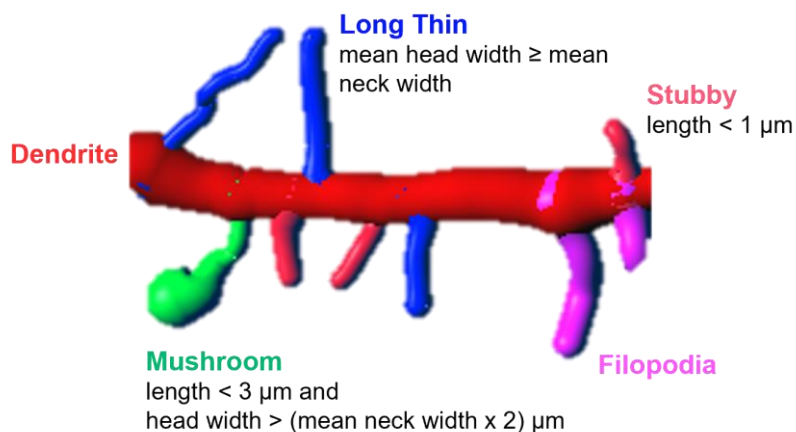


Figure 2.4. Representative 3D reconstruction of spines and their classification in Imaris software.

2.5.7 Quantification of striatal PSD95 expression

The expression of PSD95 protein was measured via immunofluorescence in the whole neuronal tree or specifically in dendritic spines of WT and CHL1 KO striatal neurons exposed to a 24-hour treatment with DRD2-compounds at 21 div. In addition to the previously presented co-staining of striatal neurons with DARPP-32 and MAP2 antibodies, the neurons were also stained with anti-PSD95 (guinea pig, 1:500) and Cy3-conjugated donkey anti-guinea pig (1:200) antibodies.

For the analysis of PSD95 expression in the whole neuronal tree, individual neurons were imaged using high magnification Z-stacks ($0.5 \mu\text{m}$) with the Olympus Fluoview FV1000 microscope in sequential mode with a $40/60 \times$ objective. The Z-stacks were then processed to obtain a maximum intensity Z-projection in ImageJ software, and a macro was developed to automatically outline the

DARPP-32 signal using the outline function. The fluorescent signals of PSD95 and MAP2 were subsequently measured within the outlined area using the analyze particles function, yielding specific results for each neuronal tree. CTCF values were calculated for each protein, and the PSD95 intensity was normalized to MAP2. For this experiment, 92 to 60 neurons per condition were analyzed using 3 independent cultures.

PSD95 expression was as well specifically measured for each class of dendritic spines. Following the 3D reconstruction and spine morphology classification of striatal dendritic branches ([section 2.5.6](#)), the PSD95 immunofluorescent signal was measured in Imaris software using the Surface tool. This involved creating a 3D surface from the DARPP-32 channel's 3D reconstruction of spines and measuring the fluorescent signal through the overlay of this surface on PSD95 and MAP2 channels. Maximum, mean and total values of PSD95 intensity (UA) were normalized to the MAP2 signal. For this experiment, 18 to 20 dendritic branches were analyzed per condition using 3 independent cultures.

2.6 Immunohistochemistry and morphology

2.6.1 Mouse brain perfusion and cryosectioning

The adult male WT and CHL1 KO mice were anesthetized with a ketamine and xylazine mixture (80 mg/kg ketamine and 10 mg/kg xylazine per body weight) and administered via intraperitoneal injection. Surgical tolerance was assessed using the pinch-response method, and once no response was detected, the mice were secured to a plastic surface using adhesive tape. Following careful opening of the rib cage and exposure of the heart, the posterior end of the left ventricle was punctured using an olive-tipped perfusion needle, which was then passed through into the ascending aorta. The transcardiac perfusion started by making a small incision on the right atrium. A plastic outlet was attached to the needle and 10 ml of PBS was first pumped at a constant rate, followed by 50 ml of 4% paraformaldehyde solution for fixation. The brain was meticulously removed from the skull and subsequently post-fixed overnight at 4 °C in a 4% paraformaldehyde solution, followed by cryopreservation in 15% sucrose for 1 day and 30% sucrose for 2 days at 4 °C. The brains were then frozen in 80 °C-cold isopentane for 1 min and stored at -80 °C for future use.

To prepare for cryosectioning, the chamber of the CryoStar™ NX70 cryostat (Thermo Fisher Scientific) was first cooled to -20 °C, and the frozen brain was allowed to stabilize within the chamber for 30 min. The blade of the cryostat was cooled down to -18 °C. The caudal pole of the brain was attached to the cold tissue holder using a Tissue-Tek OCT Compound and covered with the same solution, being careful to avoid the formation of air bubbles. Once the Tissue-Tek OCT Compound was frozen, the ventral portion of the brain was positioned to face the cryostat knife edge, and serial coronal sections with 40 µm thickness were cut. Sections were collected and stored free-floating in PBS (0.02% NaN₃) at 4 °C until use.

2.6.2 Antigen retrieval

The coronal sections, which had been stored in PBS (0.02% NaN₃), were transferred to a tube containing pre-warmed antigen retrieval buffer and incubated for 15 min at 80 °C (up to a maximum of 3 slices per tube). Following this step, the slices were allowed to cool down to room temperature before being mounted on glass slides (Superfrost Plus) with PBS and left to dry completely at room temperature.

2.6.3 Immunohistochemistry coupled with PLA

PLA was used to investigate the close proximity of CHL1 and DRD2 in coronal striatal sections of 3- to 4-month-old male WT mice immunostained with antibodies against the dopaminergic markers TH and DARPP-32. For this experiment, coronal striatal sections were prepared by mounting 40 µm-thick slices on glass slides after antigen retrieval. A PLA protocol, based on the one previously described for primary neurons, was used with minor modifications.

All the incubations were carried out in a humidity chamber. The slices were blocked with Duolink blocking solution for 1 hour at 37 °C, followed by incubation with the primary anti-CHL1 (goat, 1:50), anti-DRD2 (mouse, 1:50), and either anti-TH (rabbit, 1:200) or anti-DARPP-32 (rabbit, 1:200) antibodies in Duolink antibody diluent for 3 days at 4 °C. The slices were washed three times for 5 min with washing buffer A and incubated with Duolink[®] In Situ PLA[®] Probe anti-goat minus and anti-mouse plus, diluted 1:5 in Duolink antibody diluent in a humid chamber at 37 °C for 70 min. After washing twice for 5 min with washing buffer A, the ligation step was conducted at 37 °C for 60 min using ligation solution diluted 1:5 and ligase diluted 1:30 in RNase-free water. The same washing step was repeated, followed by the amplification step, in which amplification solution diluted 1:5 and polymerase diluted 1:60 in RNase-free water was added to the slides and incubated at 37 °C for 150 min. From this point onward, the neurons were protected from light. The coverslips were then washed for 10 min with washing buffer B and incubated with Cy5-conjugated donkey anti-rabbit (1:200) secondary antibody and DAPI stain (1 µg/ml) for 1 hour at room temperature. After an additional washing step, twice with washing buffer B and once with PBS for 10 min each, the slices were then allowed to dry completely and covered with a glass cover using Eprelia[™] Shandon[™] Immu-Mount[™].

High magnification fields were imaged in the whole striatal area using the Olympus Fluoview FV1000 confocal microscope in sequential mode, with a 60× objective plus 2/5× digital magnification. The acquired images were processed for brightness and contrast using the ImageJ software. Negative controls were included in the experiment, using striatal sections from male CHL1 KO littermate mice for the PLA, and incubating striatal sections solely with Cy-conjugated secondary antibodies to detect nonspecific binding. The experiment was done on striatal slices from 3 animals.

2.6.4 Golgi impregnation technique

The Golgi impregnation technique was used to compare the striatal morphology of MSNs in coronal striatal sections from 4-month-old male WT and CHL1 KO mice. This method is based on the impregnation of potassium dichromate and silver nitrate in brain tissue, which results in a chemical reaction that creates intracellular precipitates of silver chromate. The technique selectively stains a small percentage of neurons (3-5%), enabling the complete visualization of the complex neuronal structure.

After euthanizing the mice via CO₂ inhalation and isolating their brains, the tissue was immediately processed using the FD Rapid GolgiStain™ Kit according to the manufacturer's instructions. The brains were rinsed with ddH₂O and placed in a 15 ml falcon containing 6 ml of a mixture of solutions A and B in a 1:1 ratio for 2 weeks at room temperature in the dark, with the solution being changed after the first 24 hours and the brains being gently swirled twice per week. Following this, the brains were transferred into new 15 ml falcons containing solution C, a sucrose-cryoprotectant solution, and kept in the dark for 4 days at 4 °C, with the solution being changed again after the first 24 hours. The brains were then frozen in 80 °C-cold isopentane for 1 min and stored at -80 °C for future use.

To prepare for cryosectioning, the chamber of the CryoStar™ NX70 cryostat (Thermo Fisher Scientific) was first cooled to -25 °C, and the frozen brain was allowed to stabilize within the chamber for 30 min. The cryostat blade was then cooled to -27 °C. To attach the caudal pole of the brain to the cold tissue holder, only a base of Tissue-Tek OCT Compound was used, without completely covering the brain. Serial coronal sections with a thickness of 100 µm were collected and immediately mounted onto gelatin-coated slides with small drops of solution C. The slides were then air-dried at room temperature for 24 hours in the dark.

Slices were rinsed in ddH₂O (2 × 4 min) and subsequently stained in a developing solution (25% solution C and 25% solution E) for 10 min. After rinsing the slices again in ddH₂O (2 × 4 min), slices were dehydrated in successively higher ethanol concentrations for 4 min each, 50%, 75% and 95%, and then in 100% ethanol (4 × 3 min). Slides were cleared with xylene (3 × 4 min), then covered by a glass cover with Eukitt® Quick-hardening mounting medium. The entire process was carried out in a dark environment.

2.6.5 *In vivo* Sholl analysis and branch order

The morphological complexity of the MSNs was compared by applying Sholl analysis to coronal striatal slices that had been processed for Golgi impregnation staining ([section 2.6.4](#)) of 4-month-old male WT and CHL1 KO mice. In addition, a branch hierarchy analysis was employed to have a closer look at the specific organization and architecture of the neuronal tree. Dendrites were classified with

incremental values at every bifurcation away from the soma using this analysis, allowing for a comparison of the complexity and different geometric metrics between the different orders of branches.

MSNs located in the dorsal striatum were imaged under bright-field illumination using the Olympus Fluoview FV1000 confocal microscope and high magnification Z-stacks (0.5 μm) were acquired from the whole neuronal tree using a 40/60 \times objective. Only neurons well-impregnated with no evidence of incomplete or artificial staining were utilized. The Filament Tracer tool in Imaris software was used to 3D reconstruct the complete neuronal tree. First, an approximate radius of the soma was measured and reconstructed in a sphere form. Then, using the Autodepth mode, dendrites were drawn and adjusted in diameter along the way. The diameter and shape of the dendrites were manually corrected whenever necessary.

The 3D reconstruction of the neurons was later subjected to a Sholl analysis with a radius step size of 5 μm using Filament No. Sholl intersections tool in Imaris. The same metrics described in Sholl analysis for primary neurons (section 2.5.5) were extracted and analyzed for this experiment (ending radius, primary branches, maximum intersections number, radius of maximum intersections and number of intersections as a function of radial distance from the soma). The branch order of the dendrites was as well analyzed with the Branch Hierarchy extension in Imaris, where dendrites were classified into 4 orders of complexity, and morphological parameters of area, length, or volume were obtained per order of complexity. Individual data sets were extracted for each neuron and averaged for each genotype condition. This experiment consisted of a pilot test using 2 animals per genotype in a total of 12 WT neurons and 10 CHL1 KO neurons analyzed.

2.7 Behavior protocols

2.7.1 Animals and behavioral design

Three-month-old female and male WT and CHL1 KO mice were used in behavioral experiments. At two months of age, mice were transferred from the pathogen-free breeding facility to the *vivarium* with a reversed 12-hour light-dark cycle (7:00 AM light on) and maintained in standard conditions (21 \pm 1 $^{\circ}\text{C}$, 40-50% humidity, food and water *ad libitum*). Animals were housed in groups of 3 to 4 littermates, consisting of one heterozygotic and at least one WT and one CHL1 KO mouse. To control for litter effects, no more than 2 males of the same genotype per litter were used. After a two-week adjustment period in the behavioral facility, mice underwent an intensive handling protocol and daily body weight monitoring for additional two weeks.

At 3-month-old, mice were subjected to several behavioral paradigms once per week during their dark cycle in a room adjacent to the *vivarium*. Tests were conducted between 9:00 am and 4:00 pm with care to minimize discomfort to the animals. To minimize stress impacts, the behavioral tests were performed in an ascending order of stress with a one-week gap between each, starting with the open

field test, followed by the Y-maze test, and ending with the novelty-induced test (Table 2.10). Mice were acclimated to the behavioral room for 30 min before each test under dim red light. Testing began with manual restraint of the mouse using the scruffing technique and a single i.p. injection of the treatment (later explained). The mouse was then returned to its home cage, and the behavioral trial began 2 min later. After each test, fecal boli and urine drops were counted, and all equipment was thoroughly cleaned with a sequence of ethanol (30%), soap solution, and water. Each mouse had a one-week rest period before undergoing the next behavioral test. The execution and analysis of the behavioral tests were performed blind to the genotype and treatment to prevent any unconscious bias. The sample size was 11 to 13 mice per group.

The animals' welfare was regularly assessed throughout the behavioral timeline using a score sheet ([Annex 1](#)) that evaluated body weight, general condition, reaction to the handling and specific criteria related to the i.p. injection.

Table 2.10. Time course of the behavioral experiments. Prior to the behavioral tests, the mice were acclimated to the behavioral facility and subjected to an intensive handling protocol. The tests were then conducted in an ascending order with a one-week break between each to minimize stress impact.

Week	Experiments
0-2	Acclimatization
2-4	Intensive handling protocol
4-5	Open field test
5-6	Y-maze test
6-7	Novelty-induced test

2.7.2 Animal treatment conditions

The i.p. injection consisted of 300 μ l vehicle (0.9% NaCl, 0.5% DMSO) as the control saline solution, sulpiride solution (1 mg/kg), or quinpirole solution (0.02 mg/kg) per 30 g of body weight using a 27 G needle. All materials and solutions were sterilized and prepared shortly before use, as explained previously ([section 2.4.2](#)).

Compared to the long form of DRD2, the short form of the receptor has a higher binding affinity for dopamine and benzamides like sulpiride^{220,221}. As a result, sulpiride exhibits primarily a presynaptic action when administered at lower doses (1 mg/kg) in rats during conditioned avoidance response tests^{226,310}. Similarly, treatment with low concentrations of quinpirole (0.03 mg/kg) results in a rapid decrease in locomotor activity in mice within minutes of the open field test due to a presynaptic activation of DRD2, persisting for approximately 2 hours after treatment²¹⁹. The impact of low concentrations of quinpirole on motor activity in mice and rats has been well documented, with effects typically being observed within the first minutes after intraperitoneal or subcutaneous

administration^{136,137,219}. Therefore, in the present thesis lower doses of DRD2-specific compounds were used to specifically target the presynaptic DRD2 and evaluate their effect on the different behaviors, rather than higher doses of DRD2 antagonist and agonist that would elicit postsynaptic DRD2 effects.

Furthermore, all the behavioral observations were started 2 min after the administration of the compounds. This time point was initially chosen because it targets the early onset of presynaptic DRD2 effects elicited by low doses of quinpirole. However, it is important to note that sulpiride has a slower pharmacokinetic profile compared to quinpirole, which can be attributed to its lower lipophilicity or higher molecular weight^{228,311}. This short time window of 2 min might pose a challenge when studying the behavioral effects of sulpiride. In fact, only some studies have administered low doses of sulpiride to rodents 15 min to 1 hour before behavioral tests. For instance, mice treated with a low dose of sulpiride (3 mg/kg) 15 min before a motor task showed a trend for initial lower activity compared to controls³¹², while another study demonstrated that pre-treatment with sulpiride (1.25 mg/kg) 1 hour before quinpirole injection (0.2 mg/kg) prevented a decrease in locomotion after the second injection²²⁸. As the time-window of sulpiride effects is not extensively described in the literature, this thesis adopted a short 2-min period between compound administration and behavioral analysis, combined with behavioral tasks lasting for at least 15 min. This approach ensures that the observations include the effects of sulpiride and allow the investigation of how soon these effects are triggered.

Additionally, the 2 min period also grants time for the animals to recover from the stress induced by the i.p. injection procedure while keeping the stress effects constant across the different treatment groups. If behavior were to be analyzed at different times between compounds, additional control groups would need to be included to account for the effect of stress. However, this would not comply with the 3Rs ethics in animal studies, which promote Replacement, Reduction, and Refinement. Therefore, the decision to analyze the behavior at the same time point was also made to ensure the ethical treatment of animals in the study.

2.7.3 Handling protocol

To reduce stress and interindividual variability in the experimental data related to manual restraint during i.p. injections, a 2-week handling protocol was implemented prior to any interventions^{313,314}. The present protocol was inspired by practices recommended by Gouveia et al. (2019)³¹⁵ on non-aversive handling methods.

The protocol involved twice-daily handling of the mice from each cage for approximately 5 min under dim red light. During the first week, a plexiglass beaker was introduced to the mice by weighing, transporting them inside, or placing it within the cage for exploration. The hand with glove and sleeve was also placed inside the cage to acclimate the mice to human presence. In the second week, the scruffing restraint technique was additionally introduced once a day. Mice were first picked up by the

hand/sleeve, then held by the tail on a cage grid and restrained for at least 5 seconds, followed by voluntary play-time with the hand as positive reinforcement. Body weight was monitored daily.

Mice were not handled the day before testing and had one or two days without handling after each behavioral test. Handling sessions during this time were limited and lighter, only involving hand/sleeve exposure and restraint. Throughout the procedures, mice were only briefly picked up by the tail for transport via sleeve after i.p. administration, if necessary.

2.7.4 Open field test

The open field test is a widely used behavioral test for assessing motor activity, exploratory behavior, and anxiety-like behavior in rodents^{316,317}. The test was performed in a square open-field arena (50 × 50 × 50 cm) illuminated by 50 lux. Two minutes after the i.p. injection, the mouse was carried in a plexiglass beaker and placed in one corner of the arena. The trial started 2 seconds after the movement was detected in the arena and was recorded for a duration of 30 min with a sample rate of 12.5 frames per second using Ethovision XT software (Noldus, Wageningen, Netherlands). The center of the mouse's body was tracked throughout the test (Fig. 2.5 A). The arena was divided into the center, medial and outer zones (Fig. 2.5 B).

The movement in the entire arena and in each zone were analyzed with a series of parameters, either across the entire duration of the test or in specific time intervals, including distance moved, time spent in the area, time moving, latency, average speed, and average distance from the wall. During the first 10 min of the test, The Observer software (Noldus, Wageningen, Netherlands) was used to analyze the frequency, duration and latency of stereotyped behaviors, including supported and unsupported rearing, grooming, and jumping. Supported rearing describes a type of vertical exploration in which the mouse stands on its hind legs with one or two front paws touching the wall, while unsupported rearing refers to the same posture without any wall support.

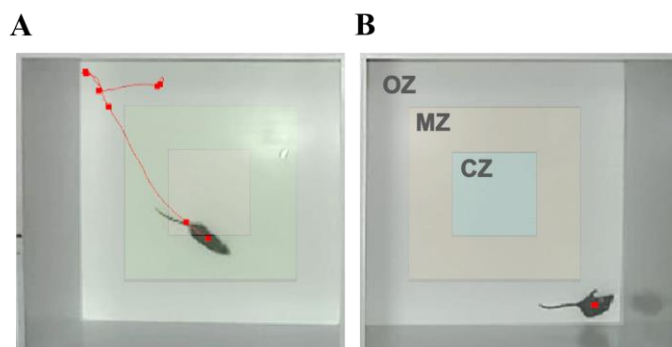


Figure 2.5. Arena and tracking settings of the open field test using Ethovision XT software. (A) The movement of the mouse was tracked using the center of its body as a reference and is represented by the red line. **(B)** The arena was divided into center zone (CZ), medial zone (MZ), and outer zone (OZ).

2.7.5 Y-maze: spontaneous alternation

The Y-maze test aims to assess short-term memory retention and manipulation, particularly spatial working memory, through spontaneous alternation in a free-trial procedure^{318,319}. Rodents exhibit a natural curiosity to explore new areas. In a three-arm maze, an intact working memory will allow them to recall which arm was previously visited, resulting in a preference for entering an arm that was less recently visited^{319,320}.

The maze was a Y-shaped structure comprised of three identical opaque arms orientated at 120° angles and connected in the center, measuring 30 × 7 cm each, and illuminated by 10 lux during the test. The mouse was placed at the end of an arm of the Y-maze two minutes after receiving an i.p. injection, and the trial began only when the mouse reached the center (Fig. 2.6 A). The spontaneous movement of the mouse was recorded for 15 min at a sample rate of 12.5 frames per second using Ethovision XT software. The Y-maze was divided into four zones, one for each arm and one for the center, and the center of the mouse's body was tracked throughout the test.

Throughout the experiment, the animals display different levels of spontaneous alternation (Fig. 2.6 B). Correct alternation was defined as consecutive entries into each of the three arms of the Y-maze (e.g. A-B-C), while repetitive entries were considered incorrect (e.g. A-B-C-B or A-B-B-C). Spontaneous alternation was evaluated by considering the first 24 alternations for a maximum of 15 min, as illustrated in the sample scoring sheet (Fig. 2.6 C). The test would be terminated after 15 min,

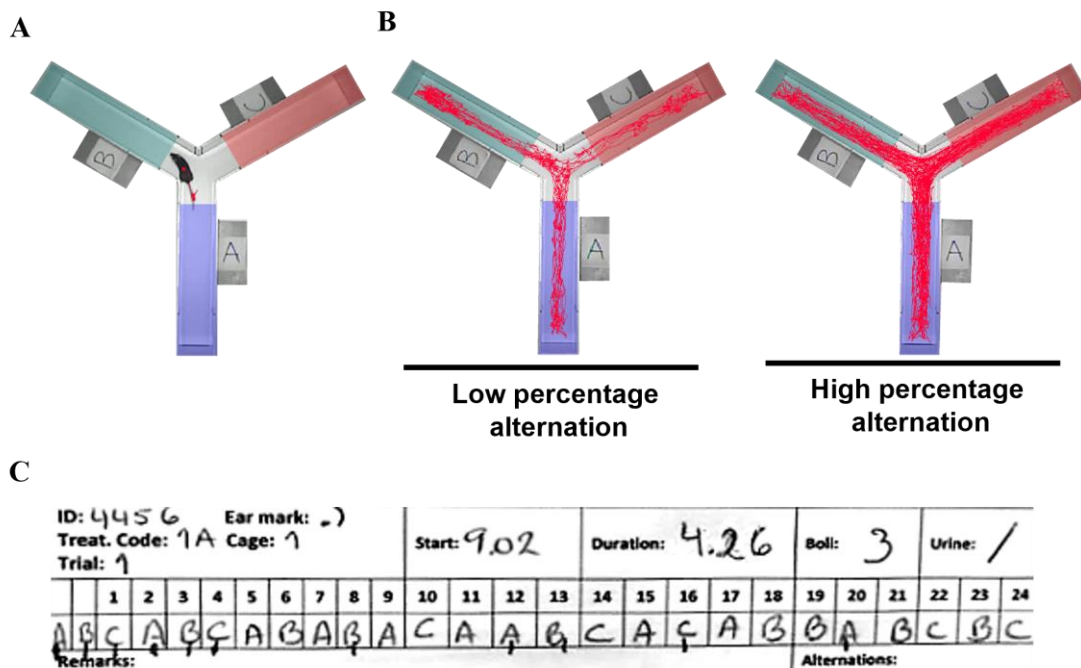


Figure 2.6. Spontaneous alternation test settings. (A) The Y-maze is divided into three arms (blue, green, and red) and the trial starts once the mouse reaches the center. (B) Representative images of tracking lines (red) showing low and high percentages of alternation in the Y-maze. (C) Example of a scoring sheet for counting the number of correct alternations.

even when 24 alternations were not completed. An entry was counted when the mouse stepped into one arm with its hind paws and the beginning of its tail.

To analyze spontaneous alternation, number of correct alternations, percentage of correct alternations and time to complete 24 alternations were obtained. The locomotion was analyzed in the whole Y-maze, including distance moved and time moving, either across the entire duration of the test or in designated time intervals.

2.7.6 Novelty-induced test

The release of dopamine in the most caudal portion of the striatum plays a crucial role in the risk assessment response during approach/avoidance conflicts, for example in the presence of a novel stimulus³²¹. The current approach to the novel-induced test differs from the traditional method, which relies on the animal's previous recollection of the object. Instead, it specifically targets the novelty-seeking behavior triggered by a new stimulus for which there is no pre-existing recognition memory, the stimulus novelty³²². The protocol is a simplified version of the one described by Akiti et al. (2022)³²¹.

The test was performed in a square open-field arena (50 × 50 × 50 cm) illuminated by 5 lux. The test included a habituation phase of the mouse to the empty arena for 5 min. Afterwards, the mouse was injected with the respective treatment and the object was inserted in the middle of the arena. Two minutes after the i.p. injection, the mouse was carried in a plexiglass beaker and placed in one corner of the arena. The trial started 2 seconds after the first movement was detected in the arena and was recorded for 20 min, with the Advanced Model-based (XT 6) detection mode, and a sample rate of 12.5 frames per second using Ethovision XT software. The mouse's movement was tracked using its nose, body center or tail base as a reference (Fig. 2.7 A). The area of the object was withdrawn from the detection, and an 8cm radius was set around it, defining the object zone. To evaluate the mouse's direct interaction with the object, its nose movement (nose-point) was tracked within the object area (area between concentric circles) (Fig. 2.7 B). The nose-point movement within the object zone was analyzed to obtain parameters such as distance moved, time spent in the area, time moving, and latency to approach the object, either over the entire duration of the test or in specific time intervals. The center-point movement in the whole arena (excluding the object area) was also analyzed to study locomotion, with parameters such as distance moved and time moving, across the entire duration of the test or in designated periods.

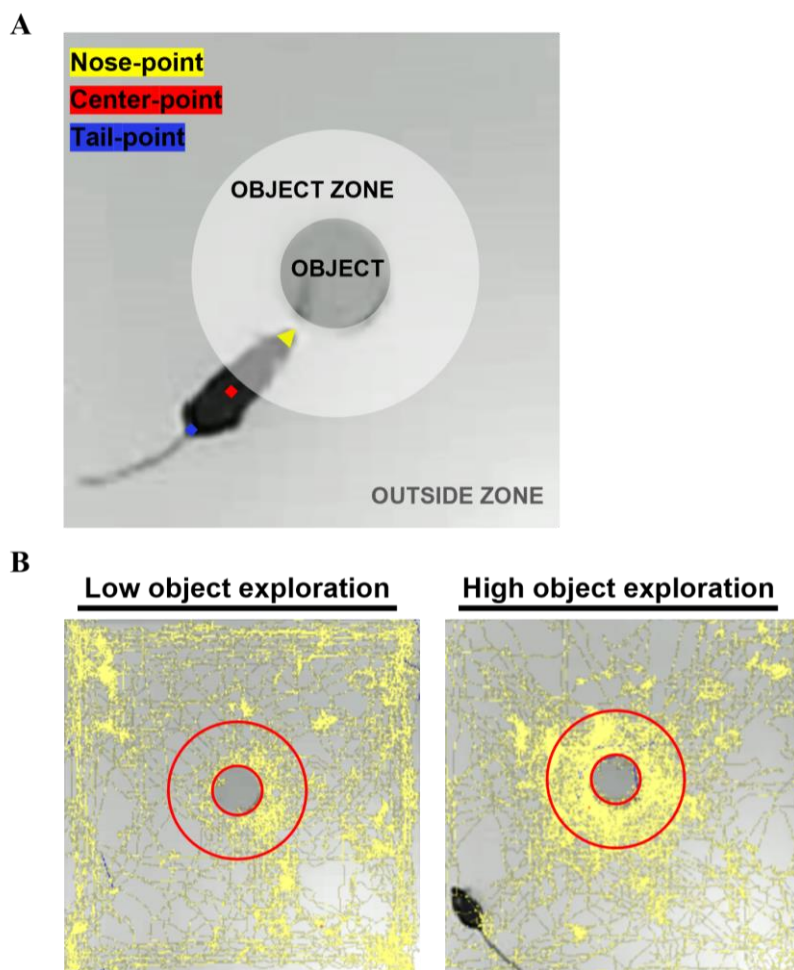


Figure 2.7. Novelty-induced test settings. (A) The mouse's movement was tracked using the nose (yellow), body center (red), and tail base (blue) as reference points. The object area was excluded from the detection zone, and an 8 cm radius around the object was defined as the object zone. (B) Object exploration was assessed by tracking the movement of the nose-point (yellow tracking) within the object zone, indicating low or high levels of exploration.

2.8 Statistical analysis

The IBM SPSS Statistics 25 software (Chicago, USA) was used to conduct the statistical analyses. Firstly, the Tukey's fences test was applied to identify outliers, which were later removed from the analysis. Next, the assumption of normal distribution was tested using the Shapiro-Wilk test, and the verification of equality of variances was performed with Levene's Test of Equality of Error Variances ($\alpha = 0.05$, for both).

When two independent variables were present (e.g. genotype and treatment), two-way analysis of variance (ANOVA) was applied to data that fulfilled the normality and homogeneity assumptions. ANOVA with Welch's correction was used when the data did not pass Levene's test for homogeneity of variance. The Kruskal-Wallis test for k-independent samples was used if the data did not follow a

Gaussian-like distribution but still exhibited homogeneous variance. Otherwise, the Brown-Forsythe ANOVA would be employed.

Number of intersections across the radial distance from the soma (repeated measure) were compared using two-way repeated measures ANOVA, with genotype and treatment considered as between-subjects factors. If no main effect of treatment was detected but a tendency was graphically visible for only one of the genotypes, this factor would be nested (only test either WT or CHL1 KO), and one-way repeated measures would be employed to investigate the possible effect of treatment only in one genotype group. One-way repeated measures were also utilized when genotype was the only factor present.

Regarding the behavioral analysis, three-way ANOVA was employed when the data demonstrated normal distribution and homogeneity of variance, with genotype, treatment, and sex (female and male) considered as between-subjects factors. If no interaction between factors was observed but an indication of interaction existed for one of the factors, the groups of that factor were separated, and further analysis was conducted using two-way ANOVA. Then, the influence of genotype and treatment on either the female or male group, in case of sex split, would be explored. If the data did not follow a normal distribution and failed Levene's test for homogeneity of variance, the Brown-Forsythe ANOVA was employed. This was achieved by analyzing one of the sex groups and grouping genotype and treatment into a single variable with 6 groups.

Student's t-test was used to compare the percentage of correct alternations for each group with the 50% chance level of performance.

Three-way repeated measures ANOVA was applied to compare behavioral parameters across different time points, with time being the repeated measure, and genotype, treatment, and sex as the between-subjects factors. In cases where no main effect of treatment was observed but a tendency was visually noticeable in one of the treatments, the same analysis of variance was conducted by considering only vehicle and either sulpiride or quinpirole as treatment factors.

For pairwise comparisons, Bonferroni correction post-hoc test was performed if statistically significant main effects were identified in any of the ANOVAs or Kruskal-Wallis test. In cases where Brown-Forsythe ANOVA detected any difference, the Games-Howell post-hoc test was used for multiple comparisons.

Chapter III presents only the most relevant results, while the statistical results of parameters with significant pairwise comparisons can be found in the figure captions or designated tables. Data yielding statistical values with an associated probability of $p < 0.05$ were interpreted as statistically significant.

Only the most relevant results are presented in Chapter III and the statistical results of parameters with significant pairwise comparisons can be found in the figure captions or designated Tables. Statistical significance was determined for all tests with a significance level set at $p \leq 0.05$.

Chapter III

Results

3 Results

3.1 CHL1 and DRD2 interaction in pre- and postsynaptic dopaminergic neurons

Prior research suggests that mutations in the CHL1 gene are correlated with a higher susceptibility to develop certain psychiatric disorders, such as depression, ASD, and schizophrenia⁴⁹⁻⁵². Since DRD2 plays a prominent role in the pathophysiology of these disorders^{70,266,268}, our group started to explore whether CHL1 could interact with DRD2 or influence the signaling via DRD2.

A previous study by our group³⁸ revealed an interaction between the extracellular domain of CHL1 and the first extracellular loop of DRD2 in a biochemical assay. The close proximity of the proteins was also demonstrated *in vivo* using striatal sections of adult mice employing both immunofluorescence and proximity ligation assay techniques. To gain a deeper understanding of CHL1 and DRD2 interactions, it was crucial to investigate whether these molecules interact in close proximity, either pre- and/or postsynaptically, to regulate dopaminergic signaling at the pre- or postsynaptic level. The following data that I obtained was published together with the previous work of the group³⁸.

3.1.1 CHL1 and DRD2 co-localize pre- and postsynaptically in the striatum of adult mice

The striatum is the ideal structure for the study of dopaminergic signaling at the pre- and postsynaptic sides because it is the brain structure of the basal ganglia with a major input of dopaminergic neurons emerging from the midbrain structures, namely the SNc and VTA³²³. Dopaminergic efferents from the midbrain targeting different parts of the striatum can be identified by immunostaining for TH³²³. Specifically, these dopaminergic terminals can form synapses with GABAergic MSNs that are distinguished from other neuron types by immunostaining for DARPP-32³²⁴. Therefore, in this study, TH was used as a presynaptic marker of dopaminergic terminals, and DARPP-32 as a postsynaptic marker of MSNs, the main neurons responsible for dopaminergic signaling in the striatum.

With the goal of analyzing whether the CHL1 and DRD2 interaction takes place pre- and/or postsynaptically, coronal sections from the striatum of 3- to 4-month-old male WT mice were prepared. Sections were stained with the PLA technique using CHL1- and DRD2-specific antibodies combined with immunofluorescence staining for TH or DARPP-32. The interaction between CHL1 and DRD2 was observed by the red dots given by fluorescently labeled oligonucleotide probes from the PLA kit, whenever the distance between the proteins was 40 nm or less. Striatal sections from male CHL1 KO littermate mice were used as negative controls.

Red spots indicative of an interaction between CHL1 and DRD2 in striatal sections were observed on TH- and DARPP-32-positive neurons (Fig. 3.1 A and B, respectively), indicating that CHL1 and DRD2 interact presynaptically on dopaminergic neurons, and postsynaptically on MSNs.

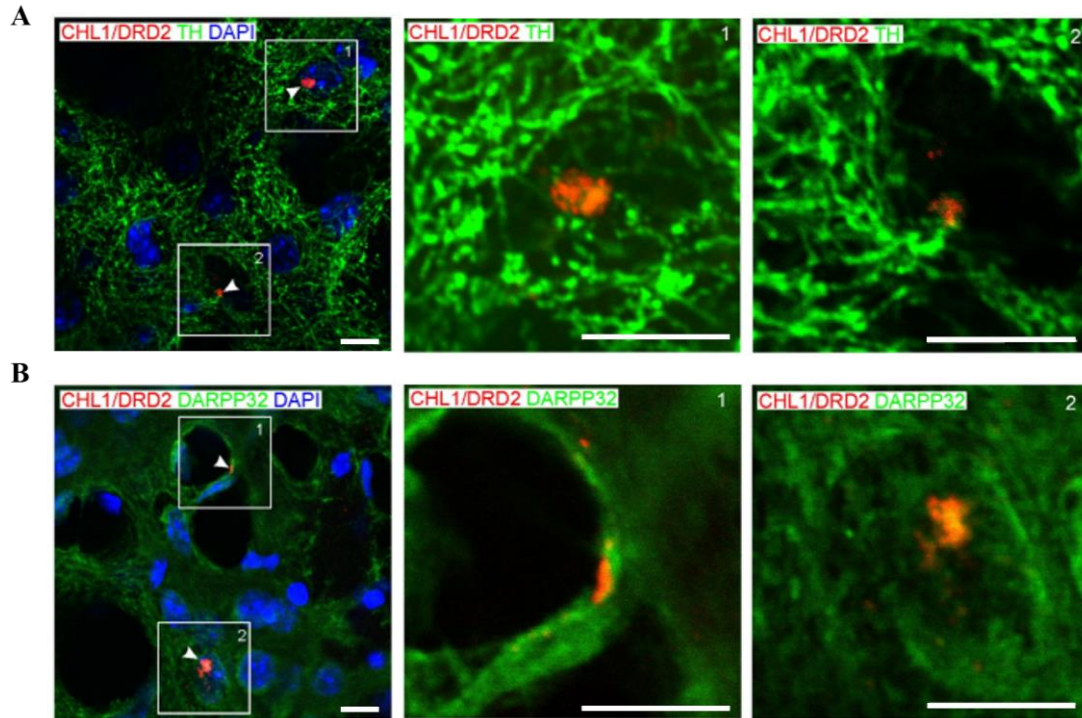


Figure 3.1. Close proximity of CHL1 and DRD2 in TH- and DARPP-32-positive neurons in striatal sections. 40 μm -thick coronal striatal sections from 3- to 4-month-old male WT mice were subjected to PLA with goat anti-CHL1 and mouse anti-DRD2 antibodies (red staining). Slices were then immunostained with rabbit anti-TH (A) or anti-DARPP-32 (B) antibodies (green staining). Representative confocal images are presented. Red spots indicate close molecular interactions of CHL1 and DRD2 on both types of neurons. Close-ups (rectangles 1 and 2) show that the interaction is present nearby the neurons. Nuclei are stained with DAPI stain (blue). Scale bars: 10 μm . The experiment was done on striatal slices from 3 animals.

3.1.2 CHL1 and DRD2 co-localize in cultured TH-positive midbrain neurons and DARPP32-positive striatal neurons

To complement the analysis of CHL1 and DRD2 interaction in striatal sections of adult mice, primary cultures from embryonic ventral midbrain and striatal neurons were analyzed by PLA and immunostaining.

Development of dopaminergic neurons in the ventral midbrain region of mice starts around E10 and TH immunoreactivity is found in the murine midbrain at E12. The outgrowth of TH-positive dopaminergic axons in the direction of the telencephalon, specifically to the precursor region of the striatum, the ganglionic eminences, starts between E13.5-14.5 and until E18 connections of these axons with neurons in the ganglionic eminences are formed^{74,325}. Ventral midbrain neurons isolated from E14 mice lack fully developed axons and allow to study the growth and maturation of postmitotic dopaminergic neurons in culture^{286,326-328}. Therefore, mixed-sex ventral midbrain primary cultures from E14 embryos were used to analyze the presynaptic interaction of CHL1 and DRD2.

The mature structure of the striatum is developed between E18-18.5 in mice^{74,325}. At E16 striatal neurons are not entirely developed and preparation of neurons at this stage yields cultures with higher neuronal survival and differentiation potential^{288,290,292}. Thus, mixed-sex striatal primary cultures from E16 embryos were used to analyze the postsynaptic CHL1 and DRD2 interaction.

At 7 div, for ventral midbrain culture, and 12 div, for striatal culture, cultures were stained with the PLA technique using CHL1 and DRD2 specific antibodies combined with immunofluorescent staining for TH, in the case of the ventral midbrain neurons, or DARPP-32, for striatal neurons (Figure 3.2 A and B). Primary cultures from female CHL1 KO littermates were used as a negative control and showed no PLA signal (data not shown).

Red spots which indicate the close proximity of CHL1 and DRD2 were found in TH-positive ventral midbrain cells (Fig. 3.3 A) and DARPP-32-positive striatal cells (Fig. 3.3 B).

In summary, these results show that CHL1 and DRD2 are in close proximity allowing them to interact *in vivo* and *in vitro* in TH-positive dopaminergic neurons and DARPP-32-positive MSNs, suggesting that pre- and postsynaptic CHL1 and DRD2 interactions could modify dopaminergic circuit communication between midbrain structures and the striatum.

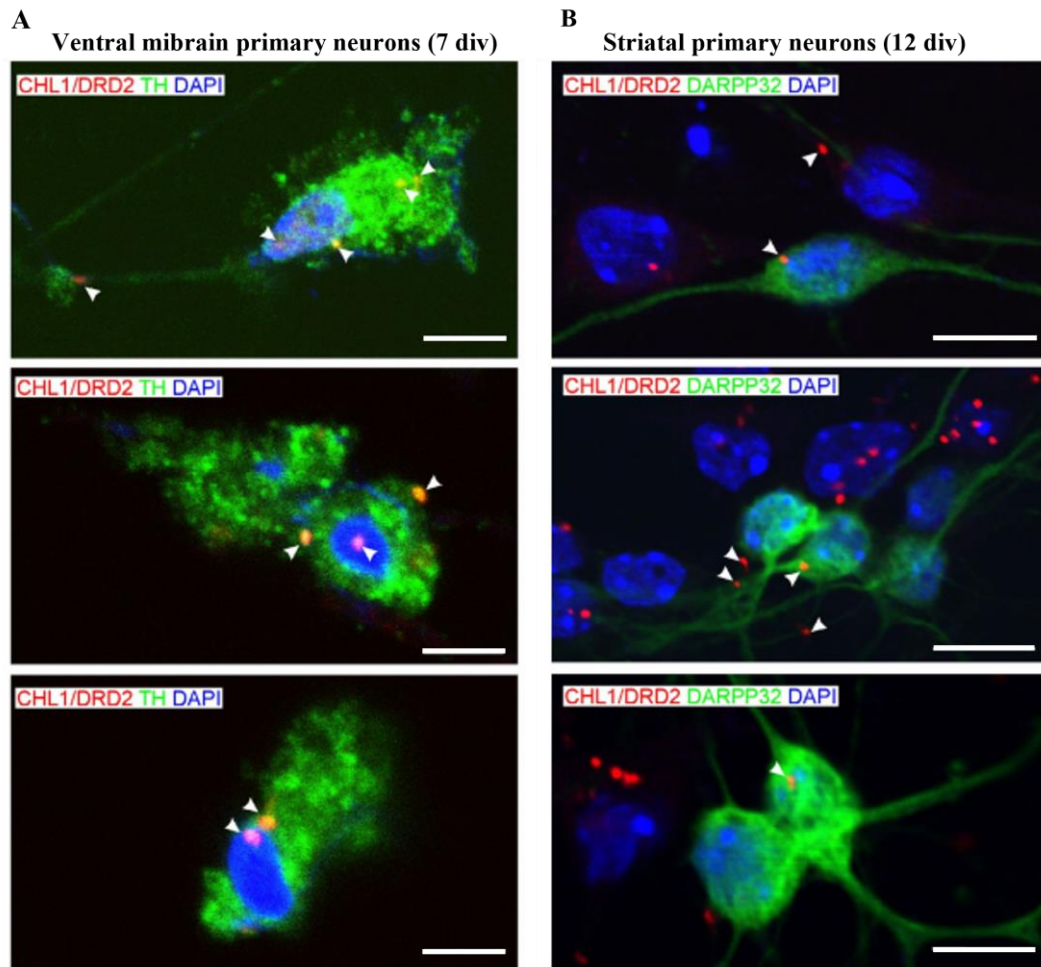


Figure 3.3. Close proximity of CHL1 and DRD2 in TH- and DARPP-32-positive cells in cultures of ventral midbrain and striatum. Cultures of ventral midbrain (A) or striatal (B) neurons were maintained for 7 or 12 div, fixed and analyzed by PLA using goat anti-CHL1 and mouse anti-DRD2 antibodies (red staining) combined with immunofluorescent staining using rabbit anti-TH or anti-DARPP-32 antibodies (green staining). Representative confocal images of different cells are shown. Red spots (white arrows) indicate close molecular interaction of CHL1 and DRD2 on both types of neurons. Nuclei are stained with DAPI stain (blue). Scale bars: 10 μm . The experiment was performed with cultures from 3 animals.

3.2 Functional consequences of CHL1 and DRD2 interaction in presynaptic dopaminergic and postsynaptic striatal neurons

Previous results by Kotarska et al. (2020)³⁸ using CHL1 KO mice revealed a functional impairment of DRD2 signaling, including reduced phosphorylation level of TH at Ser40 in the dorsal striatum and phosphorylation level of DARPP-32 at Thr34 in the ventral striatum. These findings strengthen the notion that CHL1 could play a role in regulating the mechanisms underlying pre- and postsynaptic DRD2-dependent signaling.

To investigate the impact of CHL1 on DRD2-dependent signaling, primary neuron cultures from WT and CHL1 KO mice were treated with the DRD2 antagonist sulpiride and the DRD2 agonist quinpirole. To specifically examine the effect of CHL1 on presynaptic DRD2 signaling, the expression of proteins involved in the presynaptic DRD2-signaling pathway was analyzed in ventral midbrain primary cultures. For postsynaptic DRD2 signaling, morphological analysis was performed using striatal neuron cultures.

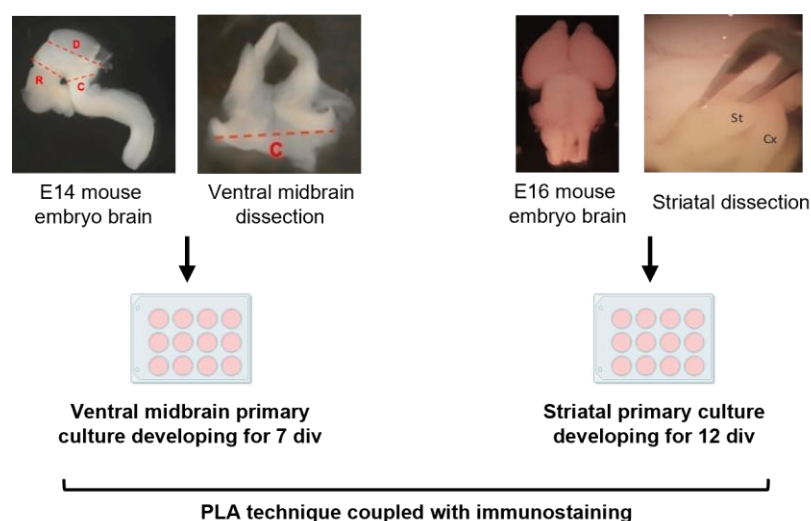


Figure 3.2. Schematic representation of the preparation of ventral midbrain and striatal primary cultures. Ventral midbrain was dissected from embryonic brains at E14 (remaining tissue after cutting along R, D, and C lines) and striatum from embryonic brains at E16 (St: striatal tissue; Cx: cortex region). At div 7 or 12, neurons were fixed and subjected to PLA with goat anti-CHL1 and mouse anti-DRD2 antibodies. Ventral midbrain and striatal cultures were then immunostained against TH or DARPP-32, respectively. Ventral midbrain pictures were adapted from Gaven et al. (2014)³²⁸, striatum pictures from Naia et al. (2018)²⁹², and scientific animations from [Biorender](#).

3.2.1 Presynaptic DRD2 signaling cascade is affected by the presence of CHL1 upon pharmacological DRD2-specific modulation

After having shown that CHL1 co-localizes with DRD2 in murine striatal and ventral midbrain cultures, I investigated if the DRD2 signaling pathways are altered in the presence or absence of CHL1. For this aim, cultured neurons from WT and CHL1 KO mice were treated with DRD2 antagonist or agonist. Experiments using rat striatal slices showed that the DRD2 agonist quinpirole decreases the Ser40 phosphorylation of TH through the reduction of AC activity, thereby inhibiting the production of cAMP¹⁸³. Hence, WT and CHL1 KO ventral midbrain cultures at 7 div were used to measure TH phosphorylation state and cAMP levels. Cells were treated for 20 min with vehicle solution (veh) as control or with the DRD2-specific compounds, sulpiride (sulp) and quinpirole (quinp). In addition, proteins involved in downstream DRD2 signaling were assessed by Western blot.

To determine the basal levels of Ser40 phosphorylation of TH (pTH), neurons treated with vehicle, sulpiride, or quinpirole were fixed and subjected to immunostaining using antibodies targeting Ser40-phosphorylated TH and the total TH protein. Confocal Z-stacked images were used to measure values for integrated density, area of the cells and mean grey value of the background. After determining the CTCF for each fluorescent signal, the ratio between pTH CTCF and total TH CTCF was calculated. Representative images of TH and pTH staining are shown (Fig 3.4 A), and representative images of neurons from each condition are presented in Fig 3.4 B.

The results revealed no statistical difference in phosphorylation level of TH at Ser40 between WT and CHL1 KO ventral midbrain neurons treated with vehicle (Fig.3.4 C). In contrast, sulpiride and quinpirole treatments reduced pTH levels relative to total TH levels in both genotypes. CHL1 KO neurons were more sensitive to sulpiride treatment and showed a stronger reduction in pTH levels compared to the WT neurons. Quinpirole treatment caused a similar reduction of pTH levels in WT and CHL1 KO neurons when compared to levels in vehicle-treated neurons. Interestingly, only sulpiride treatment increased total TH CTCF in WT neurons compared to vehicle treatment (Fig. 3.4 D), without affecting pTH CTCF in WT or CHL1 KO neurons compared to their respective vehicle-treated group (Fig. 3.4 E).

It was noticeable that CHL1 KO neurons showed an overall tendency to have lower levels of total TH (veh WT x CHL1 KO: $p = 0.072$).and pTH (veh WT x CHL1 KO: $p = 0.078$; quinp WT x CHL1 KO: $p = 0.083$) protein than the WT neurons in all treatments.

The next step was to analyze whether cAMP levels were affected by the treatment with quinpirole and sulpiride. It is expected that the DRD2 agonist quinpirole inhibits the production of cAMP and therefore, decreases TH phosphorylation events. The cAMP levels were determined in lysates of WT and CHL1 KO ventral midbrain neurons after 20 min of treatment with vehicle solution, sulpiride, or quinpirole using the Direct cAMP ELISA kit from Enzo (Fig. 3.5 A).

Levels of cAMP were similar in vehicle-treated WT or CHL1 KO neurons and only showed a tendency to be smaller in CHL1 KO neurons ($p = 0.066$) (Fig. 3.5 B). Treatment of cells with sulpiride and quinpirole did not change cAMP levels significantly when compared to vehicle treatment. However, cAMP levels were reduced in CHL1 KO neurons after sulpiride and quinpirole treatment when compared to levels in WT cells with the respective treatment (Fig. 3.5 B).

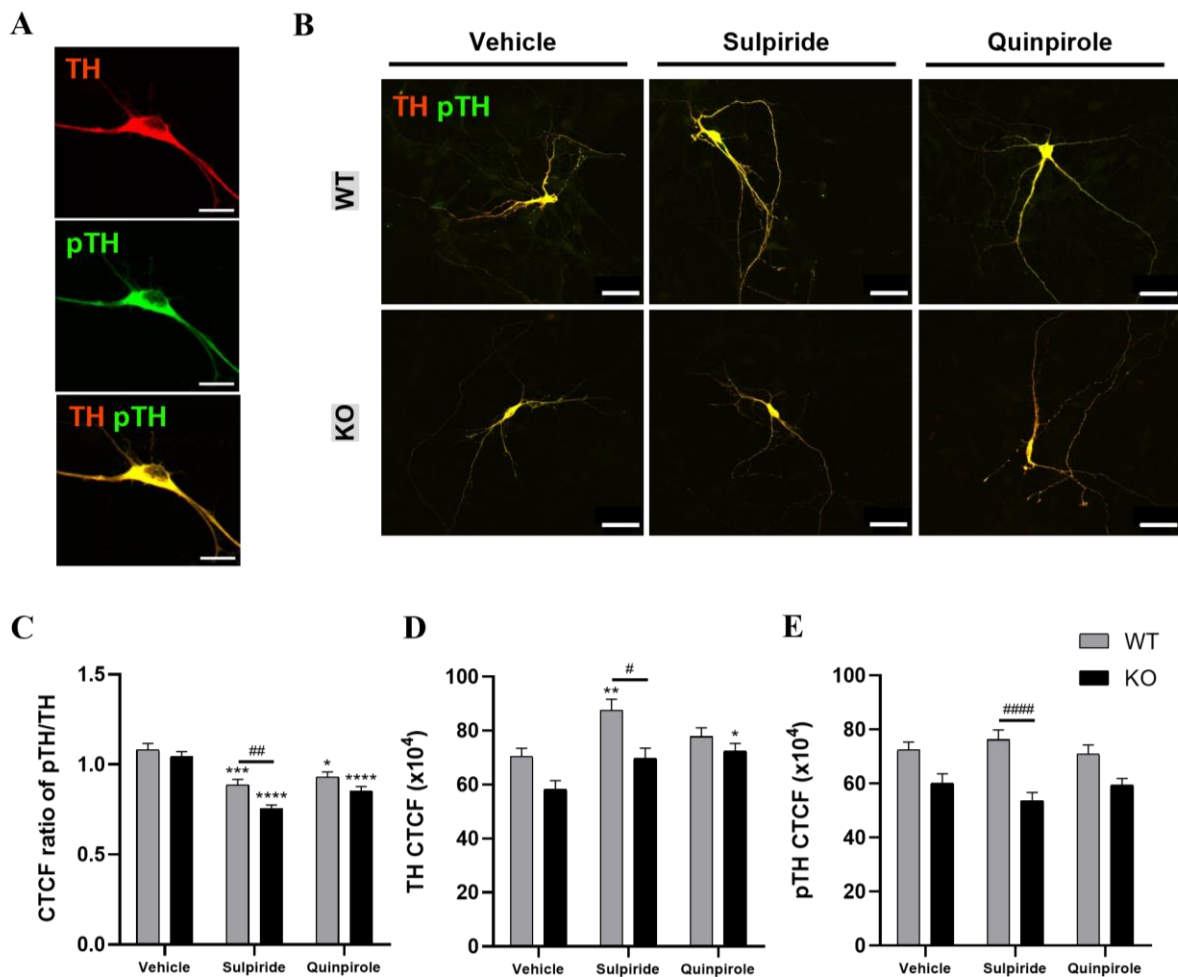


Figure 3.4. Effect of the sulpiride and quinpirole on TH phosphorylation at Ser40 in cultured WT and CHL1 KO ventral midbrain neurons. WT and CHL1 KO ventral midbrain neurons at 7 div were incubated with vehicle, sulpiride (30 μ M), and quinpirole (20 μ M) for 20 min, and stained with antibodies against Ser40-phosphorylated TH or total TH. (A) Example of a neuron immunolabeled with TH (red) or pTH (green) antibody. The overlay of the red and green signals in yellow is also shown. Scale bars 10 μ m. (B) Representative neurons with TH and pTH staining showing merged signals. Scale bars 30 μ m. The CTCF ratios of pTH and total TH (C) and the CTCF values for total TH (D) and pTH (E) were determined. Values are presented as mean + SEM (n = 3 independent cultures, 68-115 neurons per condition) and were analyzed with Brown-Forsythe ANOVA followed by Games-Howell post-hoc test ((C): $F(5,507.91) = 17.97$, $p = 0.0001$; (D): $F(5,537.01) = 8.46$, $p = 0.0001$; (E): ($F(5,532.37) = 7.04$, $p = 0.0001$) (* $p < 0.05$, ** $p < 0.01$, *** $p < 0.001$ and **** $p < 0.0001$, statistical difference from vehicle-treated correspondent genotype; # in case of genotype difference within treatment).

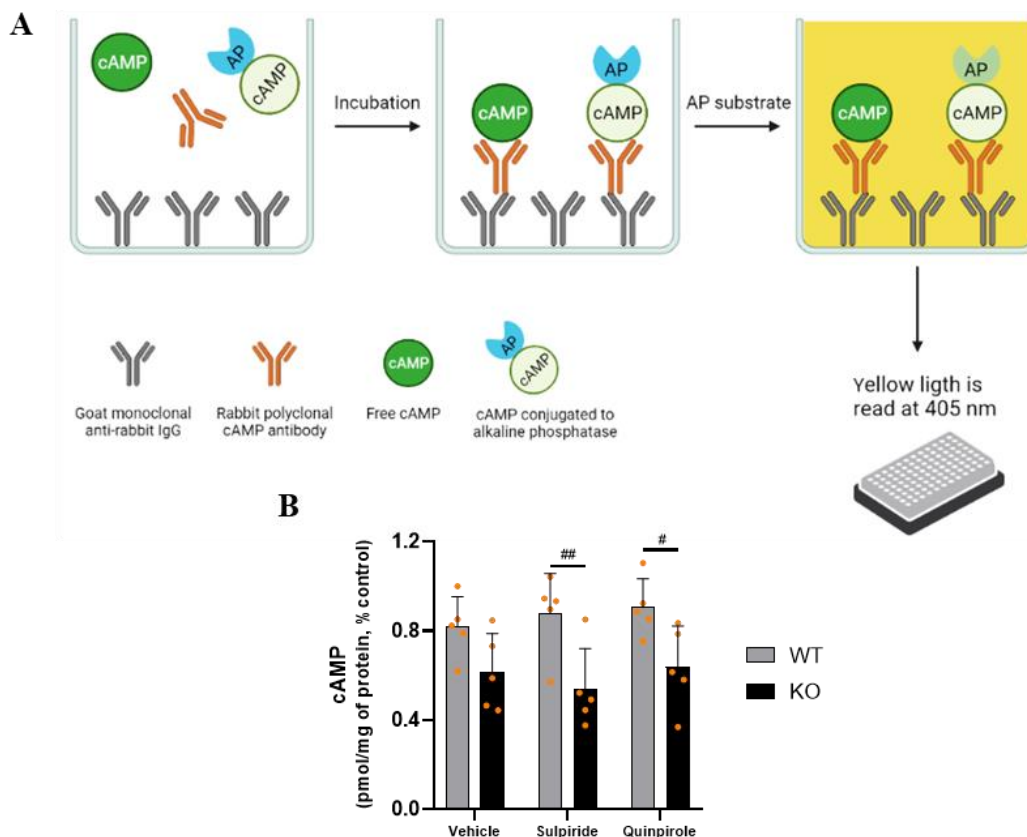


Figure 3.5. Determination of cAMP levels in cultured WT and CHL1 KO ventral midbrain neurons after treatment with sulpiride and quinpirole. WT and CHL1 KO ventral midbrain neurons at 7 div were incubated with vehicle, sulpiride (30 μ M), and quinpirole (20 μ M) for 20 min. Cells were lysed and cAMP levels were determined in the lysates (A). Samples were incubated with rabbit polyclonal cAMP antibody and a conjugate of cAMP with AP in a plate pre-coated with goat monoclonal anti-rabbit antibody. A substrate of the AP is added, and the product of this enzymatic reaction is measured. (B) cAMP concentration (pmol/mg of total protein) is calculated relative to the control (WT vehicle group). Values are presented as a bar scatter plot with mean + SEM ($n = 5$ independent cultures) and were analyzed with two-way ANOVA (genotype: $F(1,24) = 19.88$, $p < 0.0001$) followed by Bonferroni correction post-hoc test (# $p < 0.05$ and ## $p < 0.01$).

Activation of DRD2, suppresses Akt phosphorylation, and downregulates GSK3 β activity through Ser9 phosphorylation^{165–167}. Furthermore, activation of DRD2s signaling either by quinpirole or dopamine, was described to increase ERK1/2 (Thr202/Tyr204) activation^{151,153,154}. Hence, phosphorylation levels of GSK3 β (pGSK3 β) and ERK1/2 (pERK1/2) were quantified by western blot analysis. Cells from ventral midbrain cultures were treated with vehicle, sulpiride, and quinpirole for 20 min, and lysates were subjected to Western blot analysis using antibodies targeting the phosphorylated and total GSK3 β and ERK1/2 proteins.

No differences in phosphorylation levels of GSK3 β (Fig. 3.6 A) and ERK1/2 (Fig. 3.6 B) were detected. Additionally, the normalized levels of total GSK3 β and ERK1/2 showed no differences between genotypes or treatments.

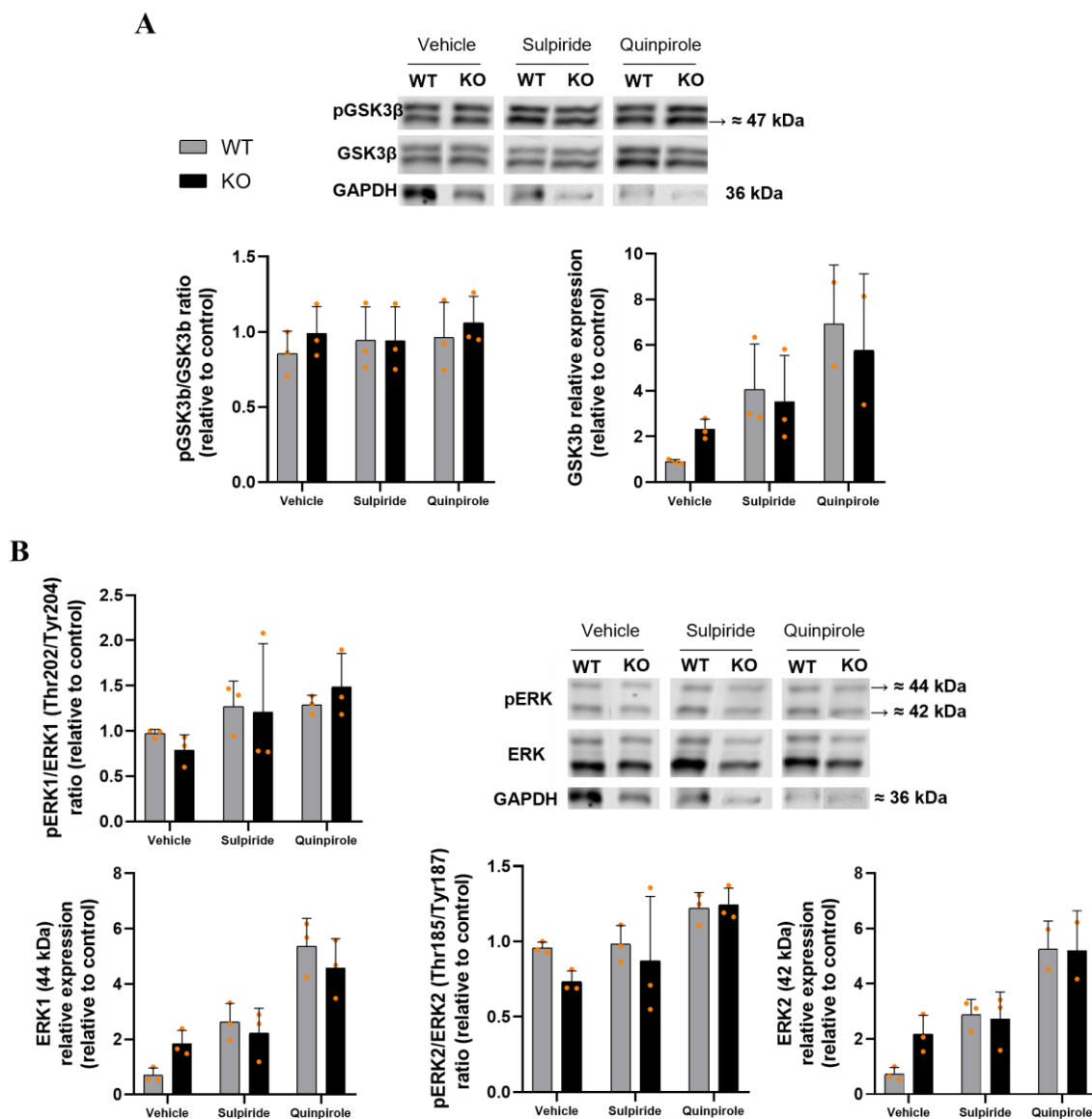


Figure 3.6. DRD2 downstream pathway proteins are not altered by treatment of WT and CHL1 KO ventral midbrain neurons with quinpirole and sulpiride. WT and CHL1 KO ventral midbrain neurons at 7 div were incubated with vehicle, sulpiride (30 μ M), and quinpirole (10 μ M) for 20 min. Lysates from each condition were subjected to protein quantification by Western blot using antibodies targeting the phosphorylated and total form of the proteins. The luminescence signal of phosphorylated proteins was normalized relative to the signals of the total proteins. Total protein levels were calculated relative to levels of the housekeeping protein (GAPDH) using Image Studio Lite software. **(A)** pGSK3 β (Ser9) and GSK3 β representative Western blot bands and pGSK3 β (Ser9)/GSK3 β protein ratio (left) and GSK3 β relative expression to GAPDH (right). **(B)** pERK1/2 (44/42 kDa) and ERK1/2 representative Western blot bands and pERK1 (Thr202/Tyr204)/ERK1 protein ratio (upper left) and ERK1 protein level relative to GAPDH level (lower left). pERK2 (Thr185/Tyr187)/ERK2 protein ratio (lower middle) and ERK2 relative expression normalized to GAPDH (right). Values are presented as a bar scatter plot with mean + SD and as a relative percentage to the control (WT vehicle group) ($n = 3$ independent cultures). Statistical analysis with one-way ANOVA ($p > 0.05$).

In summary, these results from ventral midbrain neurons treated with the D2DR antagonist sulpiride and agonist quinpirole indicate that the presynaptic absence of CHL1 affects signaling pathways upstream of DRD2. Although no differences were found in TH phosphorylation at Ser40 or cAMP levels between WT and CHL1 KO neurons treated with vehicle, CHL1 KO neurons showed a stronger decrease in TH phosphorylation after sulpiride treatment while quinpirole treatment decreased TH phosphorylation in both genotypes to the same extent.

3.2.2 Neuronal arborization and dendritic spine morphology of CHL1 KO striatal neurons

CHL1 was shown to affect the neuronal morphology of dopaminergic neurons from the ventral midbrain where it increased neurite length and complexity of branching and played a role in neurite elongation and directional growth³⁰. Moreover, CHL1 was described as a promotor of differentiation for mouse embryonic stem cells driving the cells to a dopaminergic phenotype²⁰. These results attribute a strong role to CHL1 in the development of dopaminergic pathways in the midbrain. However, as the striatum is one of the main targets of the midbrain dopaminergic fibers, the question of whether CHL1 also plays a part in striatal development or in the MSN's functionality has not yet been addressed in the scientific literature.

Interestingly, DRD2 was suggested to be involved in the regulation of neuronal architecture and spine density. Loss of striatal volume constitutes a morphological trait in schizophrenia³²⁹, which can be reversed with chronic antipsychotic treatment with DRD2 antagonists⁷² and was found to be associated with decreased complexity and length of dendritic arbors of MSNs in mice overexpressing DRD2¹⁷³. This atrophy of dendritic arbors and spine loss in MSNs are also present in animal models of Parkinson's disease³³⁰. In addition, CHL1 and DRD2 share DISC1 as a mutual interaction partner: CHL1 rescued DISC1's inhibitory effect in the initial phase of neurite outgrowth from cortical neurons³³¹, and D2DR overactivation reduced neurite length and branching, and total spine density in early postnatal striatal neurons through interaction with DISC1¹⁷⁴. Also, decreased spine density was reported as a trait in animal models of schizophrenia and Parkinson's disease^{332,333}.

In summary, changes in the dendritic morphology and spine density of MSNs can disrupt normal communication between neurons, leading to the development of psychiatric disorders. Therefore, to investigate whether an interaction of CHL1 and DRD2 affects these mechanisms, MSNs from WT and CHL1 KO striatal cultures were subjected to morphological analysis of the neuronal structure and of dendritic spines upon treatment with DRD2 antagonist and agonist.

3.2.2.1 DARPP-32 protein expression in postsynaptic striatal primary neurons is not affected by the absence of CHL1

In order to use DARPP-32 as a morphological marker it was important to check if DARPP-32 expression was not altered in non-treated CHL1 KO MSNs. WT and CHL1 KO striatal neurons at 12 or 21 div were co-stained with antibodies targeting DARPP-32 and MAP-2. Confocal images were acquired and the intensity of staining was measured for each neuron individually (Fig. 3.7 A). Representative images are presented in Fig. 3.7 B for 12 and 21 div neurons.

No differences were found in the basal levels of DARPP-32 from MSNs between WT and CHL1 KO neurons either at 12 div or 21 div (Fig. 3.7 C left and right, respectively). After this assessment, DARPP-32 is confirmed as a marker to look into MSNs morphological changes.

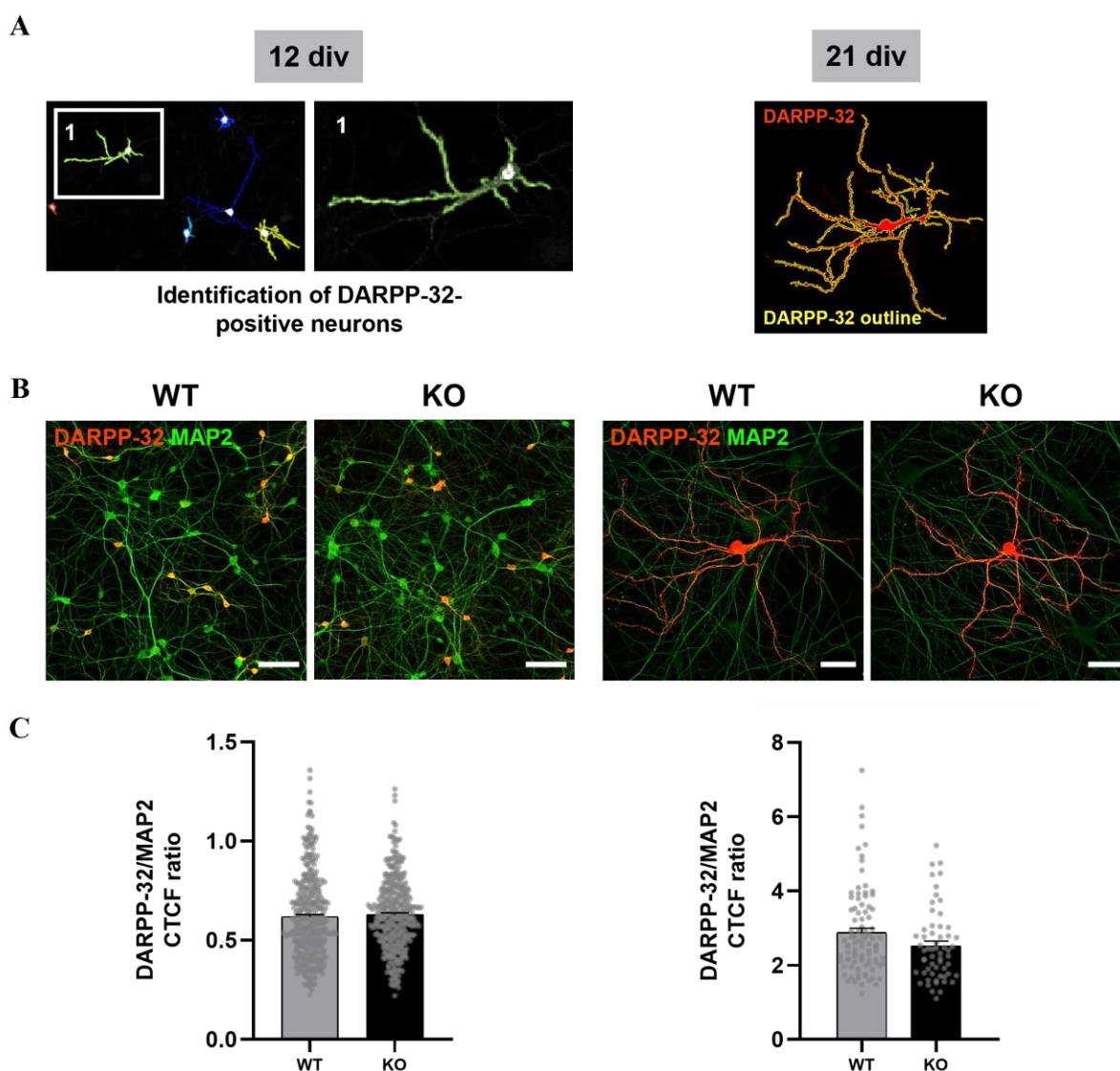


Figure 3.7. DARPP-32 protein expression is not affected by CHL1 absence in MSNs from striatal neurons. WT and CHL1 KO striatal neurons were co-stained with DARPP-32 and MAP2 antibodies at 12 or 21 div. (A) At 12 div, low-magnification confocal fields were analyzed by CellProfiler, and DARPP-32-positive neurons were automatically outlined to obtain the fluorescent intensity of the markers.

(**Figure 3.7**) At 21div, confocal Z-stacks of complete neurons were acquired and the DARPP-32 signal was automatically outlined by ImageJ to obtain the fluorescent intensity of the markers for each neuron. (**B**) Representative images of confocal fields from WT and CHL1 KO MSNs at 12 div (scale bars 50 μm) and maximum-intensity Z-projections from WT and CHL1 KO MSNs at 21 div (scale bars 25 μm) are shown (DARPP-32, red; MAP2, green). (**C**) DARPP-32 signal was normalized to MAP2. Values are presented as a bar scatter plot with mean + SEM (n = 3 independent cultures, 12 div: 376 WT and 381 KO neurons, 21 div: 92 WT and 59 KO neurons) and were analyzed with Mann–Whitney U test ($p > 0.05$).

3.2.2.2 DRD2 antagonist and agonist treatment increased dendritic complexity in CHL1 KO striatal neurons *in vitro*

In this study, Sholl analysis allowed a closer look at specific details of the dendritic organization in a neuron and, consequently, of its morphological complexity. Using DARPP-32 as the morphological marker of MSNs, the goals of this approach were on one side to check whether the dendritic tree of CHL1 KO MSNs differs from WT neurons, and to determine how DRD2 antagonist and agonist treatments affect the dendritic tree development of WT and CHL1 KO MSNs. To this end, WT and CHL1 KO striatal neurons at 12 or 21 div were treated with vehicle, sulpiride, or quinpirole for 30 min or 24 h, respectively, and were stained with DARPP-32 antibody. Confocal Z-stacks from the whole neuronal tree of MSNs were acquired, and the DARPP-32 signal was traced and subjected to Sholl analysis. From this analysis, several parameters of the dendritic arborization were determined: ending radius of the dendritic tree, number of primary branches, maximum number of intersections, and radius where the maximum number of intersections occurred (radius of max. intersections). Representative Sholl masks of neurons for each condition are shown at 12 or 21 div (Fig. 3.8 A and B). The results of the statistical analysis of variance are presented in Table 3.1.

The ending radius of the dendritic tree (Fig. 3.8 C) was not altered in vehicle-treated CHL1 KO MSNs relative to WT MSNs. At 12 div, only sulpiride-treated CHL1 KO neurons showed an increased radius of the dendritic tree when compared with vehicle-treated CHL1 KO neurons, while quinpirole treatment did not induce any changes in neurons from both genotypes. At 21 div, only the WT neurons treated with sulpiride and quinpirole exhibited an increased radius compared to the vehicle-treated WT MSNs.

The number of branches originating from the cell soma was also determined and no differences were found between the vehicle-treated WT and CHL1 KO MSNs at 12 div and 21 div (Fig. 3.8 D). At 12 div, quinpirole-treated CHL1 KO neurons exhibited a higher number of primary branches than quinpirole-treated WT neurons. At 21 div, the number of primary branches of sulpiride-treated MSNs from both genotypes showed a tendency to be increased (WT vehicle x sulpiride: $p = 0.187$, CHL1 KO vehicle x sulpiride: $p = 0.052$) and the number of primary branches of WT and CHL1 KO MSNs was significantly increased after quinpirole treatment relative to vehicle treatment.

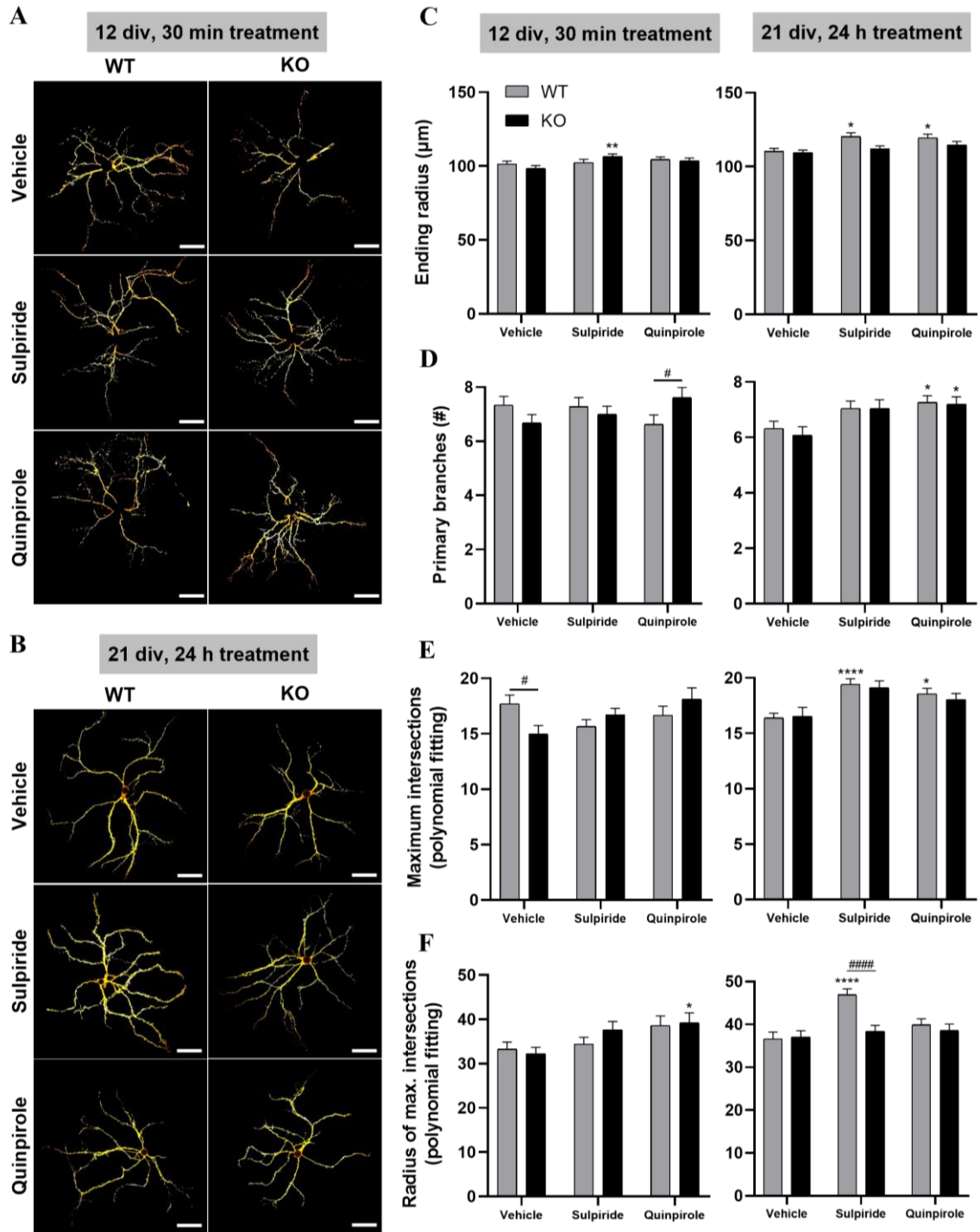


Figure 3.8. DRD2 antagonist and agonist treatment increases dendritic tree complexity of CHL1 KO MSNs at different developmental stages. WT and CHL1 KO striatal neurons were treated with vehicle, sulpiride (30 μM), or quinpirole (20 μM) for 30 min at 12 div or 24 h at 21 div. Neurons were stained with DARPP-32 antibody and high-magnification confocal Z-stacks were acquired from the whole neuronal tree. Maximum-intensity Z-projections of the DARPP-32 signal were traced and the dendritic tree was analyzed with the Sholl analysis plugin from ImageJ, using a starting radius of 7 μm and a radius step of 1 μm. Sholl masks show a representative dendritic tree for each genotype and treatment condition at 12 div (A) and 21 div (B) (scale bars: 30 μm). Ending radius (μm) (C), number of primary branches (D), and the polynomial fitting of the maximum number of intersections (E) and of the radius of maximum number of intersections (F) were obtained and compared across the groups for the neurons at 12 div or 21 div.

(Figure 3.8) Values are presented as mean + SEM (12 div: n = 2 independent cultures, 59-76 neurons per condition; 21 div: n = 3 independent cultures, 58-84 neurons per condition) and were analyzed with two-way ANOVA or Kruskal-Wallis followed by Bonferroni correction test or Brown-Forsythe ANOVA followed by Games-Howell test (*p < 0.05, **p < 0.01 and ****p < 0.0001, statistical difference from vehicle-treated correspondent genotype; # in case of genotype difference within treatment). For detailed statistics see Table 3.1.

Table 3.1. Statistical tests of analysis of variance were used to identify relevant differences in Sholl parameters. Results of parametric and non-parametric ANOVA tests are presented, followed by the respective post-hoc test used to analyze each parameter of the Sholl analysis.

		Test	Results	Post-hoc test
Ending radius (µm)	12 div	Two-way ANOVA	Genotype: F(1,377) = 0.0001, p = 0.995 Treatment: F(2,377) = 3.882, p = 0.021 Gen x treat: F(2,377) = 1.930, p = 0.147	Bonferroni correction
	21 div	Brown-Forsythe ANOVA	F(5,430.84) = 4.354, p = 0.001	Games-Howell
Number of primary branches	12 div	Two-way ANOVA	Genotype: F(1,377) = 0.004, p = 0.948 Treatment: F(2,377) = 0.090, p = 0.914 Gen x treat: F(2,377) = 3.328, p = 0.037	Bonferroni correction
	21 div	Two-way ANOVA	Genotype: F(1,452) = 0.200, p = 0.655 Treatment: F(2,452) = 7.406, p = 0.001 Gen x treat: F(2,452) = 0.109, p = 0.896	Bonferroni correction
Max. intersections (poly. fitting)	12 div	Kruskal-Wallis	H(4) = 12.131, p = 0.016	Bonferroni correction
	21 div	Brown-Forsythe ANOVA	F(5,370.78) = 5.062, p = 0.0001	Games-Howell
Radius of max. intersections (poly. fitting)	12 div	Two-way ANOVA	Genotype: F(1,373) = 0.225, p = 0.636 Treatment: F(2,373) = 4.812, p = 0.009 Gen x treat: F(2,373) = 0.490, p = 0.613	Bonferroni correction
	21 div	Two-way ANOVA	Genotype: F(1,452) = 6.854, p = 0.009 Treatment: F(2,452) = 8.097, p = 0.0001 Gen x treat: F(2,452) = 5.456, p = 0.005	Bonferroni correction

12 div: n = 2 independent cultures, 59-76 neurons per condition

21 div: n = 3 independent cultures, 58-84 neurons per condition

At 12 div, vehicle-treated CHL1 KO MSNs showed a lower maximum number of intersections compared to WT neurons (Fig. 3.8 E, polynomial fitting). Treatment with the DRD2-specific compounds sulpiride and quinpirole did not increase the number of dendritic intersections of WT neurons and led to slightly enhanced numbers in CHL1 KO neurons (CHL1 KO vehicle x sulpiride: $p = 0.181$, CHL1 KO vehicle x quinpirole: $p = 0.089$). At 21 div, vehicle-treated WT and CHL1 KO neurons showed the same maximum number of dendritic intersections, and DRD2 antagonist and agonist treatment significantly increased this parameter in WT MSNs compared to the vehicle treatment. The same effect was present as a tendency in sulpiride-treated CHL1 KO neurons relative to vehicle treatment (CHL1 KO vehicle x sulpiride: $p = 0.105$).

Analysis of the radius where the maximum number of intersections occurred (Fig. 3.8 F, polynomial fitting) did not reveal any differences between vehicle-treated neurons of both genotypes at 12 or 21 div. At 12 div, quinpirole-treated CHL1 KO MSNs had the maximum number of intersections at a higher radius than vehicle-treated MSNs. In contrast, at 21 div quinpirole treatment did not change this parameter, while sulpiride shifted the radius where maximum intersections occur to a higher value only in WT MSNs relative to CHL1 KO neurons and vehicle-treated MSNs.

To further investigate the overall complexity of the dendritic arbor in respect of ramification and branching, the number of dendritic intersections at each circle of the Sholl analysis was analyzed along the radius.

When comparing the number of intersections along the neuronal tree between WT and CHL1 KO neurons at 12 div, a significant decrease in the number of intersections was observed at a radius of 25-60 μm for the neuronal tree of vehicle-treated CHL1 KO neurons (Fig. 3.9 A). Treatment with DRD2-specific compounds for 30 min increased the number of intersections in the neuronal tree of CHL1 KO neurons compared to the neuronal tree of WT neurons, specifically from the middle until the end part of the tree in the case of sulpiride treatment (50-100 μm) and only at the ending of the tree with quinpirole treatment (75-85 and 95-100 μm). In contrast, CHL1 KO and WT neurons showed a similar branching complexity at 21 div (Fig. 3.9 B). Compared to the WT group, after 24 h of sulpiride treatment, CHL1 KO neurons showed a decrease in the number of intersections at a radius interval of 60-80 μm , while quinpirole treatment did not affect the neuronal structure of CHL1 KO neurons.

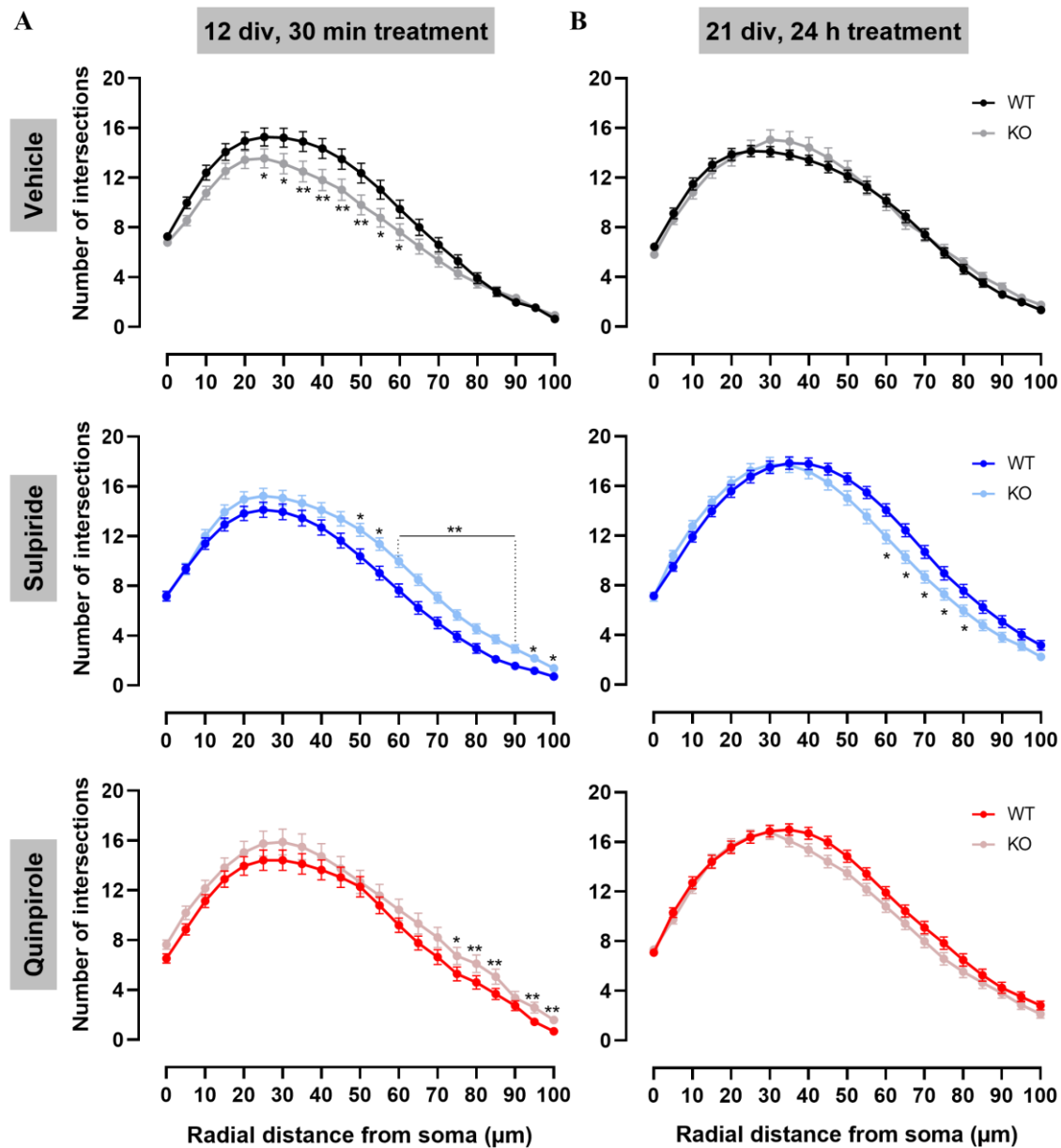


Figure 3.9. CHL1 KO MSNs show alterations of the neuronal tree after treatment with DRD2 antagonist and agonist. WT and CHL1 KO striatal neurons were treated with vehicle, sulpiride (30 μM), or quinpirole (20 μM) for 30 min at 12 div or 24 h at 21 div. Neurons were stained with DARPP-32 antibody and high-magnification confocal Z-stacks were acquired from the whole neuronal tree. Maximum-intensity Z-projections of DARPP-32 signal were traced and the dendritic tree was analyzed with Sholl analysis adopting a starting radius of 7 μm and a radius step of 1 μm . The number of dendritic intersections at each circle was counted and modeled by polynomial regression. The results were plotted as a function of the radial distance from the soma per 5 μm . Curves along the radius were statistically compared between genotypes for each treatment condition at 12 div (A) or 21 div (B). Values are presented as mean \pm SEM (12 div: $n = 2$ independent cultures, 59-76 neurons per condition; 21 div: $n = 3$ independent cultures, 58-84 neurons per condition) and were analyzed with two-way repeated measures ANOVA followed by Bonferroni post-hoc comparisons (* $p < 0.05$ and ** $p < 0.01$). For detailed statistics see table 3.2.

Comparisons of the number of intersections along the neuronal tree between the different treatment conditions at 12 div revealed that the dendritic tree of WT neurons is only partially affected by sulpiride treatment at the end of the tree (65-75 μm) and is not altered by quinpirole treatment, relative to vehicle treatment (Fig. 3.10 A). Interestingly, CHL1 KO neurons depict strong changes in the dendritic tree after treatment with DRD2-specific compounds. Compared to vehicle-treated neurons, sulpiride treatment increased the number of intersections in the middle part of CHL1 KO neurons (40-65 μm) and quinpirole treatment caused a wider effect by changing the dendritic tree in the middle and at the

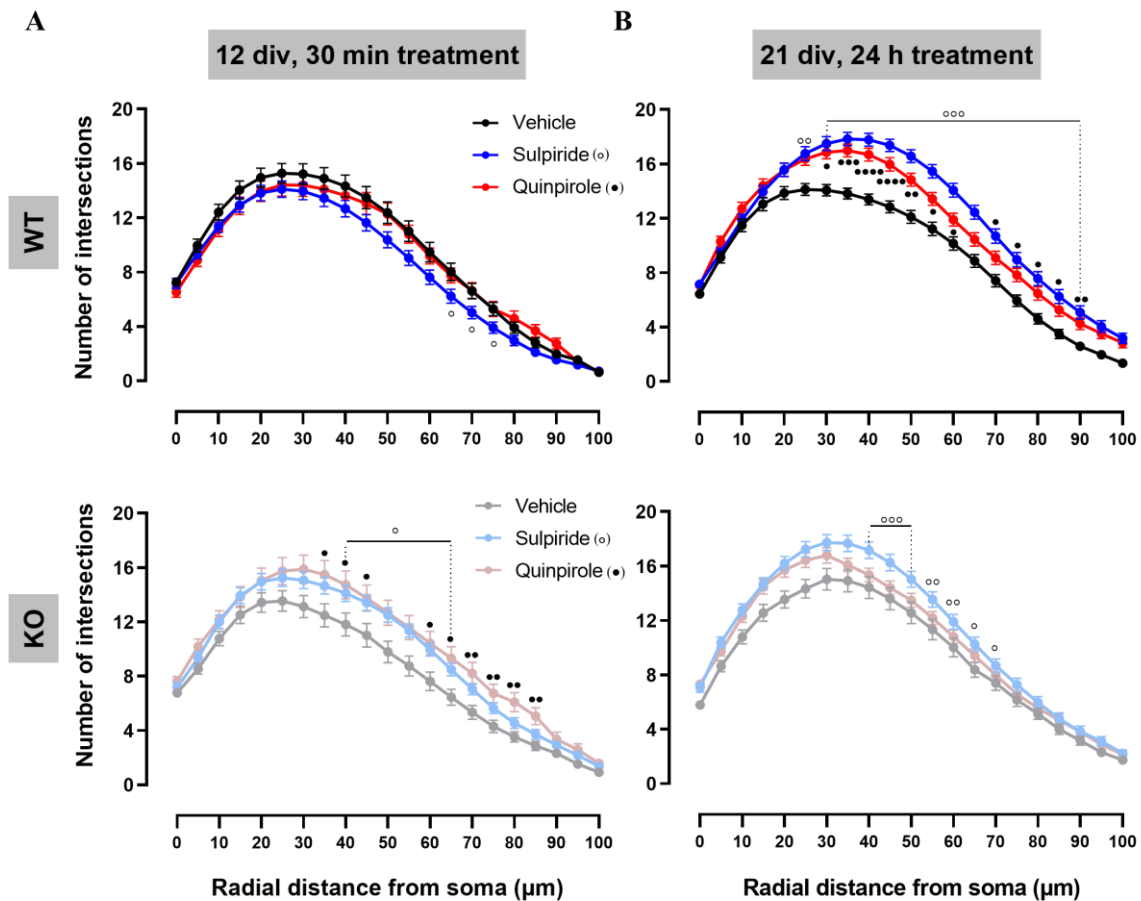


Figure 3.10. WT and CHL1 KO MSNs show alterations of the neuronal tree after treatment with sulpiride and quinpirole. WT and CHL1 KO striatal neurons were treated with vehicle, sulpiride (30 μM), or quinpirole (20 μM) for 30 min at 12 div or 24 h at 21 div. Neurons were stained with DARPP-32 antibody and high-magnification confocal Z-stacks were acquired from the whole neuronal tree. Maximum-intensity Z-projections of DARPP-32 signal were traced and the dendritic tree was analyzed with Sholl analysis adopting a starting radius of 7 μm and a radius step of 1 μm . The number of dendritic intersections at each circle was counted and modeled by polynomial regression. The results were plotted as a function of the radial distance from the soma per 5 μm . Curves along the radius were statistically compared between treatments for each genotype group at 12 div (A) or 21 div (B). Values are presented as mean \pm SEM (12 div: n = 2 independent cultures, 59-76 neurons per condition; 21 div: n = 3 independent cultures, 58-84 neurons per condition) and were analyzed with repeated measures two- or one-way ANOVA followed by Bonferroni post-hoc comparisons ($^{\circ}p < 0.05$, $^{\circ\circ}p < 0.01$, $^{\circ\circ\circ}p < 0.001$ and $^{\circ\circ\circ\circ}p < 0.0001$, statistical difference between vehicle and sulpiride; \bullet in case of comparison between vehicle and quinpirole). For detailed statistics see table 3.2.

end (35-45 and 60-75 μm). At 21 div, WT neurons treated with sulpiride or quinpirole showed an increased number of intersections starting from the middle part until the ending part of the neuronal tree relative to the vehicle group (25-90 μm or 30-60 and 70-90 μm , respectively) (Fig. 3.10 B). In CHL1 KO neurons, sulpiride treatment caused an increase in intersections in the middle part of the neurons (40-70 μm), while quinpirole treatment did not lead to any changes.

Table 3.2. Analysis of variance of the number of intersections across the radial distance from the soma (μm). Two-way repeated measures ANOVA was used to analyze the effect of genotype and treatment on the number of dendritic intersections obtained from Sholl analysis across the radial distance from the soma. To test the effect of treatment within a genotype group (Fig. 3.10), some cases required the nesting of the genotype group and one-way repeated measures ANOVA was used. The radius interval used for the tests is indicated and all the tests were followed by Bonferroni post-hoc comparisons.

div	Test		Radius interval	Results
12	Two-way RM ANOVA (Genotype comparisons within treatment)		25-100 μm	Radius x Gen: $F(2.2,791.4)=1.858$, $p=0.153$ Radius x Treat: $F(4.3,791.4)=0.351$, $p=0.858$ Radius x Gen x Treat: $F(4.3,791.4)=2.544$, $p=0.034$
	Treatment comparisons within genotype	One-way RM ANOVA nesting WT group	65-95 μm	Radius x Treat: $F(3.1,279.1)=2.883$, $p=0.035$
21	Two-way RM ANOVA (Genotype comparisons within treatment)		0-100 μm	Radius x Gen: $F(2.7,734.3)=3.413$, $p=0.020$ Radius x Treat: $F(5.6, 734.3)=1.699$, $p=0.124$ Radius x Gen x Treat: $F(5.6, 734.3)=0.633$, $p=0.692$
	Treatment comparisons within genotype	One-way RM ANOVA nesting WT group	0-90 μm	Radius x Treat: $F(4.8,448.4)=2.798$, $p=0.018$
	Treatment comparisons within genotype	One-way RM ANOVA nesting CHL1 KO group	40-95 μm	Radius x Treat: $F(3.5,267.9)=3.024$, $p=0.023$

12 div: n = 2 independent cultures, 59-76 neurons per condition

21 div: n = 3 independent cultures, 58-84 neurons per condition

Based on this result, I conclude that the lack of CHL1 in MSNs does not affect the normal development of the neuronal tree under basal physiological conditions. Despite a lower complexity found in the middle part of CHL1 KO neuron's dendritic tree at 12 div relative to WT neurons, none of the other parameters reveals genotype differences. No differences between vehicle-treated neurons from both genotypes were observed when cells were cultured for 21 div. In addition, the results also indicate that the effects of DRD2-pharmacological modulation on the complexity of the dendritic tree of striatal MSNs are dependent on the genotype and developmental stage. CHL1's absence in younger developed MSNs (12 div) seems to influence the pharmacological sensitivity for both compounds since a higher complexity of dendritic branching is induced only in CHL1 KO neurons. This feature seems to disappear with the neuronal development as WT MSNs at 21div show even a higher branching

complexity than CHL1 KO neurons. Interestingly, both compounds induce similar effects on the dendritic morphology of the striatal MSNs.

3.2.2.3 CHL1 KO striatal neurons show alterations in dendritic spines after treatment with DRD2 antagonist and agonist

After unveiling that the complexity of the dendritic branching of MSNs is affected by the absence of CHL1's and the phase of development when MSNs are exposed to DRD2-specific antagonism and agonism, the next step was to find out whether the density and morphology of dendritic spines are also affected. To this end, cultured WT and CHL1 KO striatal neurons at 21 div were treated with vehicle, sulpiride, or quinpirole for 24 h and were stained with DARPP-32 antibody. Confocal Z-stacks of secondary/tertiary dendrites of different neurons were acquired and the DARPP-32 stained neuronal tree was reconstructed into a 3D structure. This structure was subjected to spine quantification and spines were classified by their morphology as stubby, mushroom, long thin, or filopodia shaped spines. From this analysis, parameters of spine morphology classification and quantification were obtained: percentage, total number, and density per spine class; mean and total values of spine area (μm^2), length (μm), neck length (μm), and spine volume (μm^3) of each spine type. Representative maximum intensity Z-projections of the DARPP-32 signal and 3D reconstructions of the dendritic spines per condition are shown (Fig. 3.11 A).

Spine percentage for each spine class (Fig. 3.11 B) was calculated relative to the total number of spines for each condition, and certain statistical differences were observed between genotype and treatments. The percentages of stubby spines were similar on dendrites of vehicle- and sulpiride-treated WT and CHL1 KO neurons, while quinpirole-treated CHL1 KO neurons showed a decreased percentage of stubby spines relative to dendrites of WT neurons (WT 34.96%, CHL1 KO 29.66%). A higher percentage of mushroom spines was observed in dendrites of vehicle-treated CHL1 KO neurons (WT 3.00%, CHL1 KO 4.52%), while there were no differences between numbers of mushroom spines on dendrites of WT and CHL1 KO MSNs after sulpiride and quinpirole treatment. The percentage of long thin spines was decreased by sulpiride treatment in CHL1 KO neurons relative to WT neurons (WT 55.56%, CHL1 KO 49.18%), and was increased by quinpirole treatment in CHL1 KO neurons relative to WT neurons and vehicle condition (quinpirole: WT 51.26%, CHL1 KO 56.51%; vehicle CHL1 KO 49.73%). Filopodia spines did not show changes between treatments or genotypes. Of note, no differences in the total number of spines (Fig. 3.11 C) were detected between genotypes or treatments.

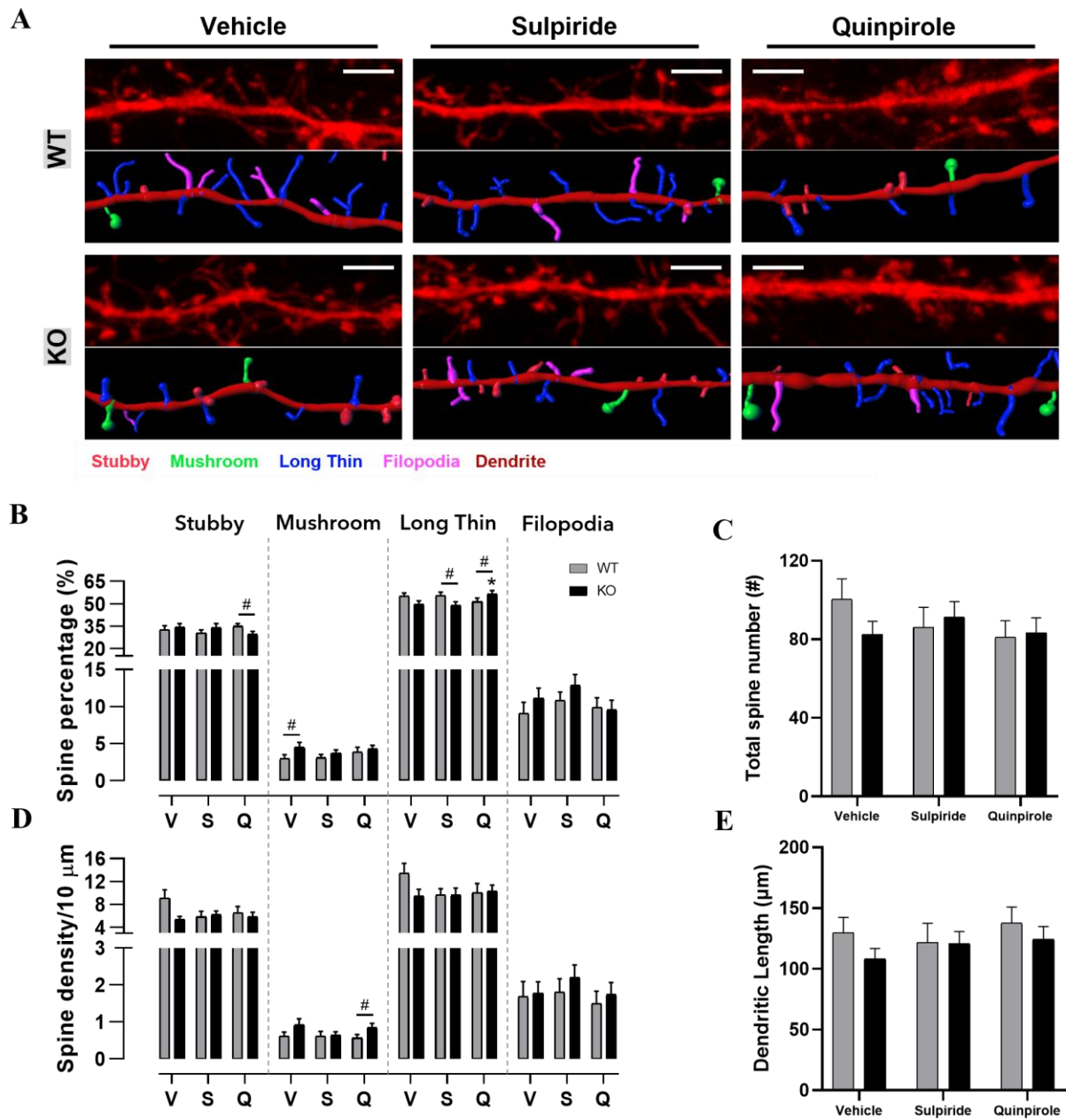


Figure 3.11. DRD2 antagonist and agonist treatment for 24h induces changes in dendritic spine shape and density of CHL1 KO MSNs. WT and CHL1 KO striatal neurons were treated with vehicle (V), sulpiride (S, 30 μM), or quinpirole (Q, 20 μM) for 24 h at 21 div. Neurons were stained with DARPP-32 antibody and high-magnification confocal Z-stacks of secondary/tertiary dendrites were acquired. Dendrites and spines were 3D reconstructed and spines were quantified and morphology was scored as stubby (light red), mushroom (green), long thin (blue), or filopodia (purple) using Imaris software. (A) Representative images of DARPP-32 fluorescent signal (red) and its 3D reconstructions of dendritic spines per condition are shown (scale bars: 3 μm). (B) For each neuron, the number of spines was normalized to the total number of spines, and percentages for each group are presented. (C) Spine density across 10 μm of dendrite was obtained for each condition. (D) Total spine number for each condition. (E) Dendrite length (μm) analyzed on average for each condition.

(Figure 3.11) Values are presented as mean + SEM (n = 3 independent cultures, 18-20 dendrites per condition) and were analyzed with two-way ANOVA for each type of spine followed by Bonferroni post-hoc comparisons ((B) stubby spines (genotype x treatment: $F(2,106) = 3.62$, $p = 0.03$), mushroom spines (genotype: $F(1,106)=5.38$, $p = 0.02$), and long thin spines (genotype x treatment: $F(2,106)=5.67$, $p = 0.005$); (D) mushroom spines (genotype: $F(1,92)=5.98$, $p = 0.016$)) (* $p < 0.05$, statistical difference from vehicle-treated correspondent genotype; # in case of genotype difference within treatment).

Determination of the spine number for each spine class per 10 μm along the dendrites (Fig. 3.11 D) showed no alteration in spine density, except a higher density of mushroom spines in dendrites of quinpirole-treated CHL1 KO neurons relative to WT neurons (WT 0.56 and CHL1 KO 0.85 spines per 10 μm). No differences in the dendritic length (Fig. 3.11 E), area, or volume (data not shown) analyzed for each condition were detected between genotypes or treatments.

Since alterations induced by quinpirole and sulpiride were found in the quantification of dendritic spines in CHL1 KO MSNs, morphological parameters per spine class were analyzed.

The morphology of stubby spines was not influenced by the lack of CHL1 or the treatment by DRD2-specific compounds as seen by no changes in the mean or total evaluated measures (Fig. 3.12 and 3.13 A-D, stubby spines). On the contrary, mushroom spines showed morphological changes with an increased spine volume in sulpiride-treated CHL1 KO neurons relative to WT neurons, while quinpirole treatment induced an increase in mean and total values of spine area, length, neck length, and volume in CHL1 KO neurons compared to WT neurons (Fig. 3.12 and 3.13 A-D, mushroom spines). To a lower extent, long thin spines were mainly affected by quinpirole treatment with an increase in mean spine area, length, and volume in CHL1 KO neurons compared with WT neurons (Fig. 3.12 A, B, and D, long thin spines). Similarly, filopodia spines were only affected by quinpirole treatment with an increase in mean spine length and neck length in CHL1 KO neurons relative to the WT group (Fig. 3.12 B and C, filopodia spines).

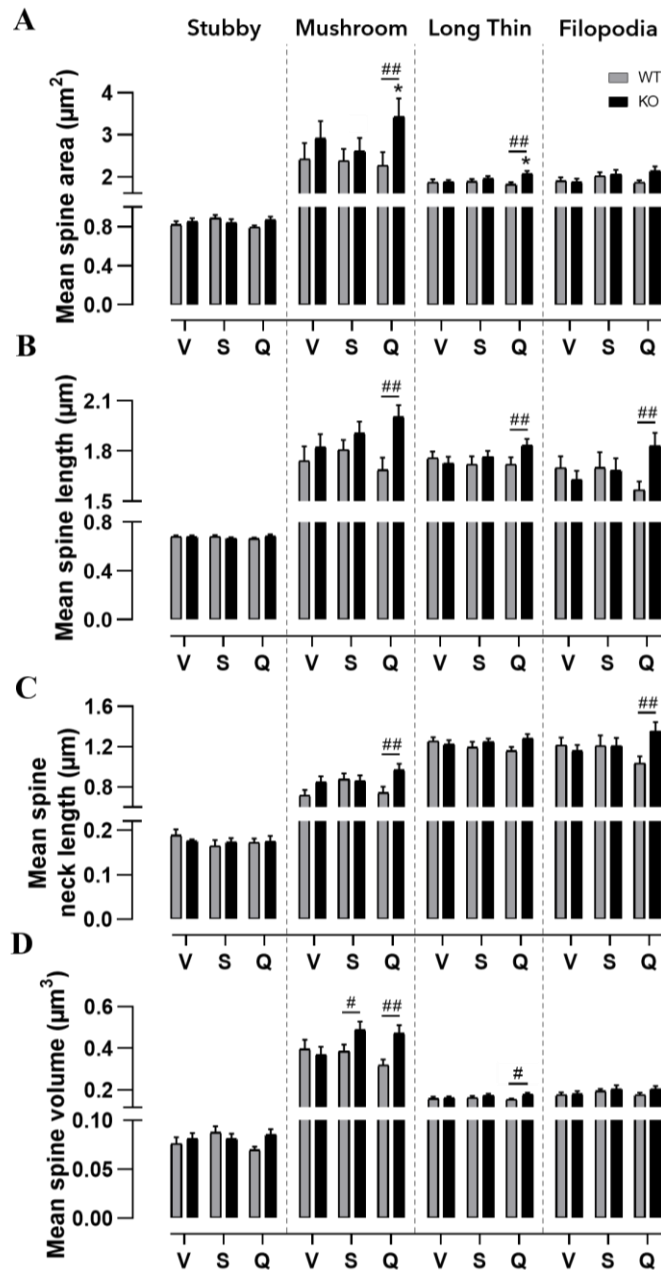


Figure 3.12. DRD2 antagonist and agonist treatment for 24 h induces morphological changes in dendritic spines of CHL1 KO MSNs. WT and CHL1 KO striatal neurons were treated with vehicle (V), sulpiride (S, 30 μM), or quinpirole (Q, 20 μM) for 24 h at 21 div. Neurons were stained with DARPP-32 antibody and high-magnification confocal Z-stacks of secondary/tertiary dendrites were acquired. Dendritic spines were 3D reconstructed and their morphology was analyzed and scored as stubby, mushroom, long thin, or filopodia using Imaris software. Mean values of spine area (μm^2) (A), spine length (μm) (B), spine neck length (μm) (C), and spine volume (μm^3) (D) were obtained for each spine class. Values are presented as mean + SEM ($n = 3$ independent cultures, 18-20 dendrites per condition) and were analyzed with two-way ANOVA for each type of spine followed by Bonferroni post-hoc comparisons ((A) mushroom spines (genotype: $F(1,98)=5.24$, $p = 0.024$), and long thin spines (genotype: $F(1,107)=6.00$, $p = 0.016$); (B) mushroom spines (genotype: $F(1,100)=7.80$, $p = 0.006$), long thin spines (genotype: $F(1,97)=3.94$, $p = 0.05$), and filopodia (genotype x treatment: $F(2,104)=3.19$, $p = 0.045$); (C) mushroom spines (genotype: $F(1,99)=6.24$, $p = 0.014$), and filopodia (genotype x treatment: $F(2,105)=3.24$, $p = 0.043$); (D) mushroom spines (genotype: $F(1,98)=6.68$, $p = 0.011$), and long thin spines (genotype: $F(1,97)=7.12$, $p = 0.009$)) (* $p < 0.05$ and ** $p < 0.01$, statistical difference from vehicle-treated correspondent genotype; # in case of genotype difference within treatment).

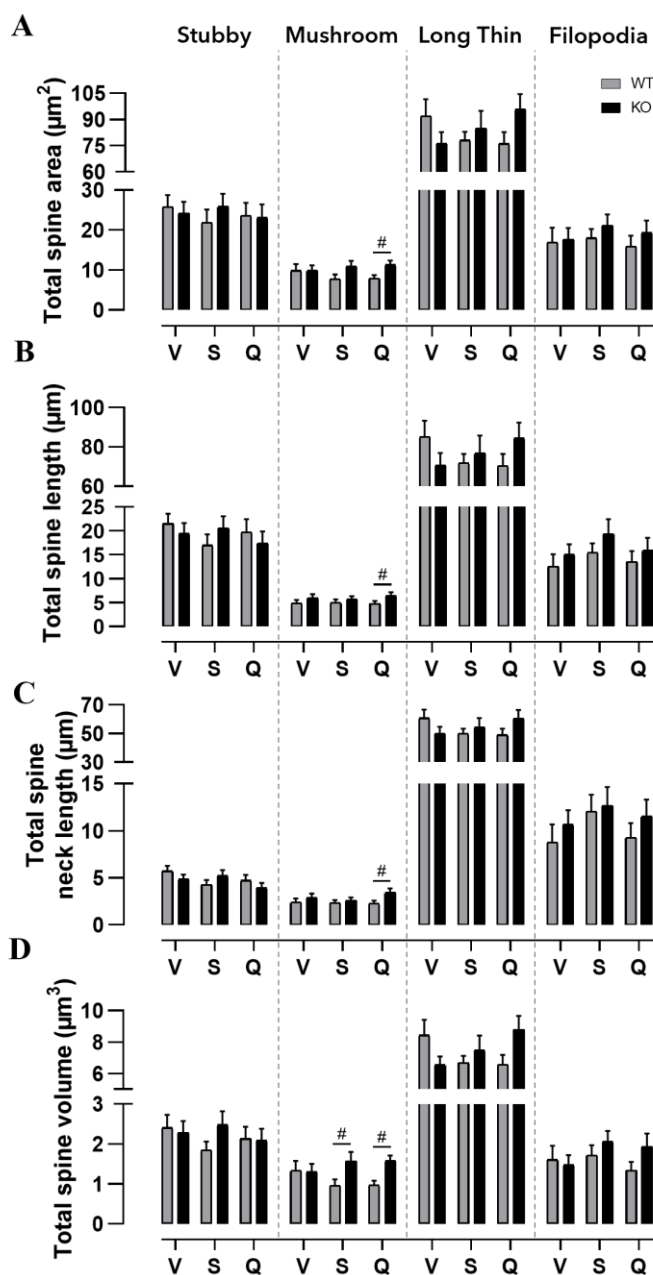


Figure 3.13. DRD2 antagonist and agonist treatment for 24 h induces morphological changes in mushroom spines of CHL1 KO MSNs. WT and CHL1 KO striatal neurons were treated with vehicle (V), sulpiride (S, 30 μ M), or quinpirole (Q, 20 μ M) for 24 h at 21 div. Neurons were stained with DARPP-32 antibody and high-magnification confocal Z-stacks of secondary/tertiary dendrites were acquired. Dendritic spines were 3D reconstructed and their morphology was analyzed and scored as stubby, mushroom, long thin, or filopodia using Imaris software. Total values of spine area (μ m²) (A), spine length (μ m) (B), spine neck length (μ m) (C), and spine volume (μ m³) (D) were obtained for each spine class. Values are presented as mean + SEM (n = 3 independent cultures, 18-20 dendrites per condition) and were analyzed with two-way ANOVA for each type of spine followed by Bonferroni post-hoc comparisons ((A) mushroom spines (genotype: $F(1,85)=8.24$, $p = 0.005$); (B) mushroom spines (genotype: $F(1,85)=7.50$, $p = 0.008$); (C) mushroom spines (genotype: $F(1,85)=6.29$, $p = 0.014$); (D) mushroom spines (genotype: $F(1,97)=7.79$, $p = 0.009$)) (# $p < 0.05$, statistical difference within treatment).

The results indicated that under basal physiological conditions, the development of dendritic spines was not affected by the genotype since WT and CHL1 KO MSNs show similar levels of each spine class, with the exception of a slight increase of mushroom spines in dendrites of CHL1 KO MSNs. When DRD2-specific compounds were used, striatal MSNs showed higher reactivity to the treatments when CHL1 was absent, displaying substantial changes in the number and morphology of specific classes of dendritic spines. Antagonism of DRD2 with sulpiride caused a decrease of long thin spines percentage in CHL1 KO MSNs. The activation of DRD2 with quinpirole impacted specifically the morphology of mushroom spines by increasing several spine parameters in CHL1 KO MSNs, and also increased the percentage and the morphological measures of long thin spines in CHL1 KO MSNs.

3.2.2.4 Lack of CHL1 in striatal neurons prevents the reduction of PSD95 protein levels in the dendritic tree after DRD2 antagonist or agonist treatment

My results indicate that the absence of CHL1 in striatal MSNs changes the morphology of mushroom and long thin spines and affects DRD2-postsynaptic signaling upon DRD2 antagonism or agonism. Therefore, it might be possible that protein rearrangements in the postsynaptic density occur in excitatory synapses of CHL1 KO striatal MSNs.

PSD95 is a scaffold protein responsible for interacting, recruiting, and trafficking proteins like NMDA and AMPA receptors to the postsynaptic membrane of dendritic spines. PSD95 has been described to be an important regulator of synaptogenesis since the lack of this protein disrupts synaptic function during juvenile periods in medial prefrontal and visual cortex neurons, and induces impairments in sociability and working memory in mice^{334,335}. Moreover, PSD95 has been reported to be involved in all of the subsequent processes of neuronal spine development, such as spine maturation or plasticity in the primary prefrontal cortex and hippocampal neurons³³⁶⁻³³⁸. Furthermore, since PSD95 and DRD2 share DISC1 as a binding partner, previous work supports the assumption that PSD95 can indirectly modulate spine structure via DRD2 signaling. In primary cortical neurons, prolonged knockdown of DISC1 decreased Ka1-7/PSD95 binding, markedly reducing spine size³³⁹. In HEK-293 cells and neonatal striatal neurons, D2DR overactivation by quinpirole led to an excessive DRD2-DISC1 interaction and downregulation of PSD95 protein expression, resulting in a reduction of dendritic spine density in the striatal neurons¹⁷⁴. Hence, to investigate whether the absence of CHL1 leads to alterations in the postsynaptic density of striatal MSNs after treatment with DRD2 antagonist or agonist, the levels of PSD95 protein were determined in the cell soma and in the dendritic spines of primary neurons.

For this purpose, cultured WT and CHL1 KO striatal neurons at 21 div were treated with vehicle, sulpiride, or quinpirole for 24 h and were co-stained with DARPP-32, PSD95, and MAP2 antibodies. MAP2 protein was used as control morphological marker. To evaluate the PSD95 signal in the neuronal tree of striatal MSNs, confocal Z-stacks from the whole neuronal tree of MSNs were acquired, the

DARPP-32 signal was outlined and PSD95 and MAP2 intensities were measured in the same area corresponding to the DARPP-32 signal. Representative confocal images of MSNs stained with DARPP-32, PSD95, and MAP2 are presented, and PSD95 close-ups of the cell soma are displayed (Fig. 3.14 A).

No genetic differences in PSD95 levels were observed between vehicle-treated WT and CHL1 KO MSNs (Fig. 3.14 B), while a significant reduction in the PSD95 level was observed in sulpiride- and quinpirole-treated WT neurons compared to vehicle-treated WT neurons. Although sulpiride treatment of CHL1 KO neurons showed a tendency to reduce PSD95 levels compared to levels in CHL1 KO vehicle-treated neurons ($p = 0.074$), quinpirole treatment did not induce a change in PSD95 levels in CHL1 KO neurons. No differences in MAP2 intensities were found between genotype and treatments (Fig. 3.14 C).

To evaluate the PSD95 signal in the dendritic spines of striatal MSNs, confocal Z-stacks of secondary/tertiary dendrites were acquired and the DARPP-32 stained neuronal tree was reconstructed into a 3D structure. This structure was subjected to spine analysis according to the spine morphology and PSD95 and MAP2 fluorescent signals were measured in the 3D reconstruction of spines. Representative images of DARPP-32, PSD95, and their signal merged with the MAP2 signal are presented, as well as a 3D spine reconstruction with each spine class and the 3D surface for measuring the PSD95 signal (Fig. 3.15 A).

No differences in maximum, mean, or total PSD95 fluorescence intensity were detected between genotypes or treatments for each spine class (Fig. 3.15 B-D).

Determination of the PSD95 immunofluorescence signal in WT and CHL1 KO striatal MSNs revealed that PSD95 protein levels were similar between genotypes under basal conditions. Although sulpiride treatment showed a tendency to reduce PSD95 levels in CHL1 KO neurons, DRD2-specific compounds significantly reduced the overall levels of PSD95 only in the neuronal tree of WT neurons. In contrast, the PSD95 protein content remained unaffected by genotype or treatment in all spine classes.

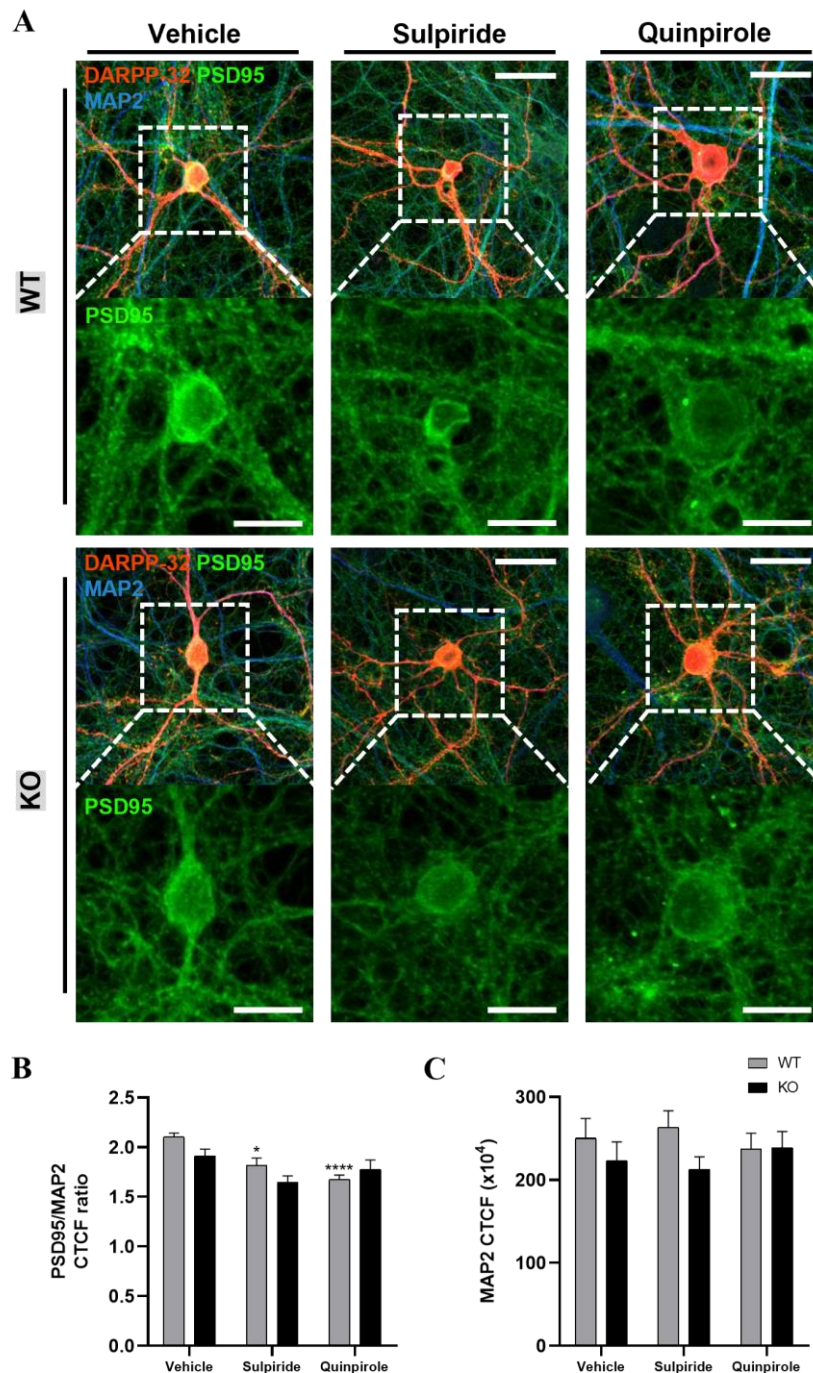


Figure 3.14. The absence of CHL1 in striatal MSNs prevents the reduction of PSD95 protein levels in the neuronal tree after sulpiride or quinpirole treatment. WT and CHL1 KO striatal neurons were treated with vehicle, sulpiride (30 μ M), or quinpirole (20 μ M) for 24 h at 21 div. Neurons were co-stained with DARPP-32, PSD95, and MAP2 antibodies and high-magnification confocal Z-stacks were acquired from the whole neuronal tree. MSNs stained with DARPP-32 were outlined and PSD95 and MAP fluorescent signals were measured within this area using ImageJ. (A) Representative confocal images of DARPP-32 (red), PSD95 (green), and MAP2 (blue) fluorescent signals (scale bars: 20 μ m) and close-ups of PSD95 signal in the soma of the neurons (scale bars: 10 μ m) are shown. (B) PSD95 signal present in MSNs was normalized to MAP2 fluorescent signal. (C) Average of MAP2 CTCF in MSNs. Values are presented as mean + SEM (n = 3 independent cultures, 92-60 neurons per condition) and were analyzed with Brown-Forsythe ANOVA followed by Games Howell post-hoc test ((B): $F(5,351.76) = 6.92$, $p = 0.0001$) (* $p < 0.05$ and **** $p < 0.0001$, statistical difference from vehicle-treated correspondent genotype).

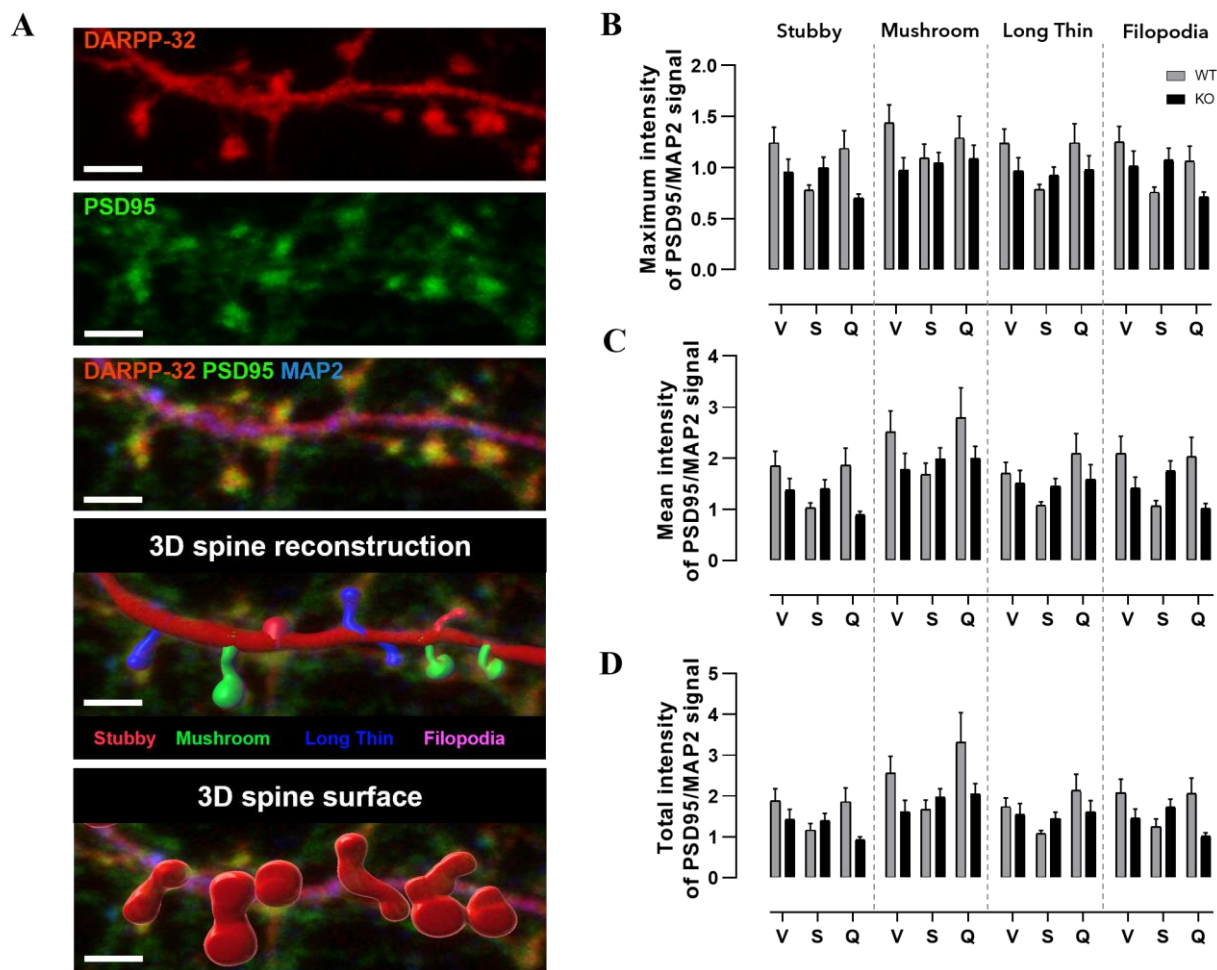


Figure 3.15. PSD95 protein levels are not affected in dendritic spines of CHL1 KO MSNs after DRD2 antagonist or agonist treatment. WT and CHL1 KO striatal neurons were treated with vehicle (V), sulpiride (S, 30 μ M), or quinpirole (Q, 20 μ M) for 24 h at 21 div. Neurons were co-stained with DARPP-32, PSD95, and MAP2 antibodies, and high-magnification confocal Z-stacks of secondary/tertiary dendrites were acquired. Using Imaris software, dendritic spines were 3D reconstructed, their morphology analyzed and a 3D surface was built on the spines to measure PSD95 and MAP2 signals. (A) Representative confocal images of DARPP-32 (red), PSD95 (green), and their signal merged with MAP2 (blue) are shown. 3D reconstructions of dendritic spines per class and the resultant 3D surface to measure fluorescent signal is presented (scale bar 2 μ m). Maximum intensity (B), mean intensity (C), and total intensity (D) of PSD95 were normalized to the MAP2 signal. Values are presented as mean + SEM (n = 3 independent cultures, 18-20 dendrites per condition) and were analyzed with Welch's test or Brown-Forsythe ANOVA ($p > 0.05$).

3.3 Functional roles of the CHL1 and DRD2 interaction *in vivo*

In the preceding sections, I have discussed studies focused on the functional implications of CHL1 and DRD2 interaction within the presynaptic dopaminergic signaling pathway in cultured ventral midbrain neurons, as well as its role in regulating neuronal architecture and dendritic spine morphology in cultures of MSNs. To establish a connection between the findings obtained from cell culture models and the *in vivo* function of CHL1 and DRD2 interaction, the DRD2-dependent signaling pathway and the morphology of MSNs were analyzed in the brains of adult WT and CHL1 KO mice.

3.3.1 Decrease of TH (Ser40) phosphorylation in the striatum of CHL1 KO mice is sex- and treatment-dependent

For the majority of proteins, phosphorylation is tightly linked with protein activity and is a key factor in regulating protein function. It has been reported that changes in phosphorylation levels of downstream players of the DRD2 signaling pathway can be influenced by CHL1 or by DRD2-specific agonism. Reduced phosphorylation levels of TH at Ser40 were found in the dorsal striatum of male CHL1 KO mice and striatal slices of male rats incubated with quinpirole^{38,183}. In CHL1 KO mice, a reduction in DARPP-32 phosphorylation at Thr34 was described for the ventral striatum³⁸ and in striatal lysates of DRD2-deficient mice, phosphorylation of GSK3 β at Ser9 was found to be highly increased¹⁶⁸. Lastly, increased phosphorylation of ERK1 and ERK2 at Thr202/Tyr204 and Thr185/Tyr187 by DRD2 stimulation with quinpirole or dopamine has been reported^{153,154}. Thus, to investigate whether CHL1 absence *in vivo* can interfere with the DRD2-signaling pathway, an analysis of protein expression and phosphorylation of kinases involved in DRD2 signaling was performed in striatal homogenates of female and male WT and CHL1 KO mice.

For this purpose, adult animals were treated with a single i.p. injection of vehicle, sulpiride, or quinpirole. After 15 min, striata were dissected out, striatal homogenates were prepared and subjected to Western blot analysis using antibodies targeting total TH and TH phosphorylated at Ser40, total GSK3 β and GSK3 β phosphorylated at Ser9, total ERK2 and ERK2 phosphorylated at Thr185/Tyr187, and total ERK1 and ERK1 phosphorylated at Thr202/Tyr204.

In female mice, no differences in phosphorylation levels of TH, GSK3 β , or ERK1/2 in striatal homogenates of vehicle-treated WT and CHL1 KO mice were found (Fig. 3.16 A). Decreased levels of phosphorylated TH were detected in the striatal homogenates of sulpiride-treated WT females relative to vehicle treatment, while CHL1 KO females did not show this decrease. Quinpirole treatment did not affect phosphorylation levels of TH, GSK3 β , or ERK1/2 in WT and CHL1 KO females.

In male mice, no differences in phosphorylation levels were detected in striatal homogenates of vehicle-treated WT and CHL1 KO mice (Fig. 3.16 B). Sulpiride treatment did not affect the

phosphorylation of TH, GSK3 β , or ERK1/2 in striatal homogenates from WT and CHL1 KO males. A decrease of phosphorylated TH induced by quinpirole was found only in striatal homogenates from CHL1 KO males relative to the WT group and vehicle treatment, while levels of phosphorylated GSK3 β and ERK1/2 remained unaffected.

No differences were found in the total protein levels of TH, GSK3 β and DARPP-32 in striatal homogenates of vehicle-, sulpiride-, or quinpirole-treated WT and CHL1 KO females and males (Fig. 3.17 A and B).

In general, the results indicate that after DRD2 antagonism or agonism phosphorylation levels and total protein levels of downstream players of DRD2 signaling are similar in striatal homogenates of female and male WT and CHL1 KO mice. However, decreased phosphorylation levels of TH at Ser40 were found in sulpiride-treated WT females and quinpirole-treated CHL1 KO males, exposing sex- and genotype-dependent effects of the DRD2-specific compounds.

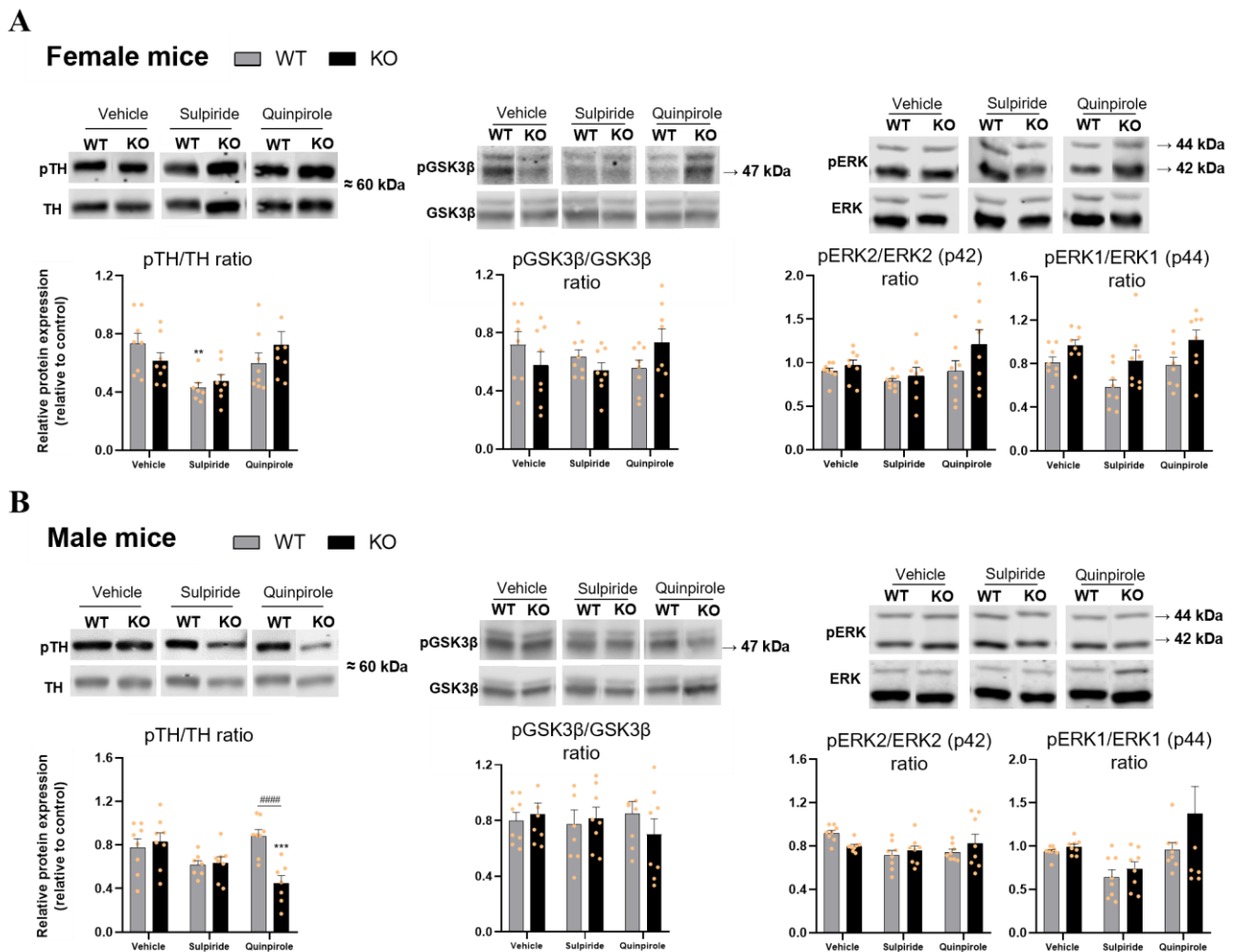
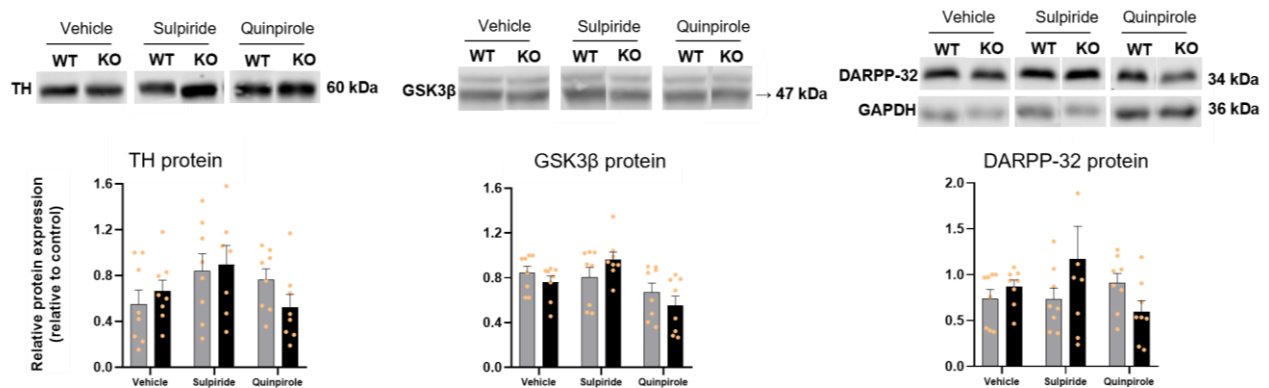


Figure 3.16. Alterations of TH phosphorylation are induced in WT females by sulpiride treatment and in CHL1 KO males by quinpirole treatment. 4-month-old WT and CHL1 KO mice were treated with a single i.p. injection of vehicle, sulpiride (1 mg/kg), or quinpirole (0.02 mg/kg) for 15 min, and homogenates were prepared from the striatum and subjected to Western blot analysis. Antibodies against the total and phosphorylated TH (Ser40), GSK3 β (Ser9), ERK2 (Thr185/Tyr187), and ERK1 (Thr202/Tyr204) were used and the signal obtained for phosphorylated proteins was normalized relative to the signal obtained for the total protein using Image Studio Lite software. Representative Western blot bands and respective protein ratio for pTH/TH, pGSK3 β /GSK3 β , pERK2/ERK2, and pERK1/ERK1 are presented for female (**A**) and male (**B**) mice for each genotype and treatment group. Values are presented as a bar scatter plot with mean + SEM ($n = 7/8$ mice) and were analyzed with two-way ANOVA followed by Bonferroni correction post-hoc test ((A) pTH/TH ratio: treatment: $F(2,41)=6.75$, $p = 0.003$; (B) pTH/TH ratio: genotype x treatment: $F(2,40)=7.99$, $p = 0.001$ and pGSK3 β /GSK3 β ratio) or Welch's test ANOVA ($p > 0.05$) (* $p < 0.05$ and ** $p < 0.01$, statistical difference from vehicle-treated correspondent genotype; # in case of genotype difference within treatment).

A

Female mice WT KO

B

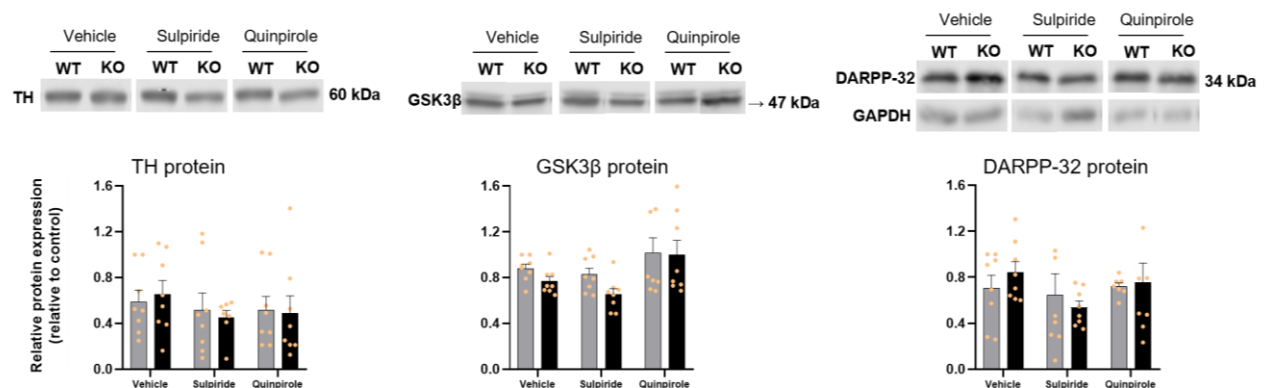
Male mice WT KO

Figure 3.17. DRD2 antagonist and agonist treatment do not affect total levels of DRD2-signaling pathway proteins in female and male CHL1 KO mice. 4-month-old WT and CHL1 KO mice were treated with a single i.p. injection of vehicle, sulpiride (1 mg/kg), or quinpirole (0.02 mg/kg) for 15 min, and homogenates were prepared from the striatum and subjected to Western blot analysis. Total protein levels of TH and GSK3β were normalized against the total protein content of the immunoblot, and DARPP-32 was normalized to the housekeeping protein GAPDH using Image Studio Lite software. Representative Western blot bands and respective protein expression for TH, GSK3β, and DARPP-32 are presented for female (A) and male (B) mice for each genotype and treatment group. Values are presented as a bar scatter plot with mean + SEM (n = 7/8 mice) and were analyzed with two-way (TH protein) or Welch's test ANOVA (GSK3β and DARPP-32 protein) ($p > 0.05$).

3.3.2 MSNs of male CHL1 KO mice show a tendency for a lower arbour complexity in the region near the soma

Considering the previous *in vitro* experiments together with the preceding analysis of the dopaminergic signaling pathway *in vivo*, the constitutive ablation of CHL1 in mice displays a moderate phenotype that does not evidently impair the daily life of these animals compared with the WT mice. Since the morphological analysis of cultured MSNs at 21 div did not reveal any differences between

WT and CHL1 KO neurons, it was important to investigate if MSNs exhibit any major differences *in vivo*. Additionally, several studies have identified morphological impairments in the cerebral cortex, hippocampus, and cerebellum of CHL1-deficient mice^{27,28,31}, whereas morphological impairments in the striatum have not been described yet. Thus, to investigate whether the morphology of striatal MSNs is altered in the absence of CHL1, brains from adult male WT and CHL1 KO littermates were subjected to a detailed morphological analysis of the MSNs neuronal tree using the Golgi-impregnation technique.

For this purpose, brains from 4-month-old male littermates were exposed to a Golgi impregnation procedure and were cut into serial coronal sections. MSNs at the dorsal striatum were imaged under a bright-field illumination and Z-stacks were taken from whole neurons. The neuronal tree was 3D-reconstructed and subjected to Sholl and branching analysis. From Sholl analysis, several parameters of the dendritic arborization were determined: ending radius of the dendritic tree, number of primary branches, maximum number of intersections, and radius where the maximum number of intersections occurred (radius of max. intersections). From branching analysis, the dendrites were classified into 4 orders of complexity, and morphological parameters of area, length, or volume were obtained. The Fig. 3.18 A displays representative images of Z-projections of Golgi-stained neurons and the respective 3D reconstruction of the neuronal tree of MSNs of male WT and CHL1 KO mice. In Fig. 3.19 A, a representation of the dendrites classified by branching order is shown for each group.

No differences were found for the ending radius (μm), number of primary branches, maximum number of intersections, or radius of maximum intersections (Fig. 3.18 B-E). When comparing the number of intersections along the neuronal tree (Fig. 3.18 F), CHL1 KO neurons tended to have a lower number of intersections in the region near the cell soma in the intervals 5-25 μm and 10-20 μm ($p = 0.094$ and $p = 0.089$, respectively).

For the branching analysis, the size of dendrites compared between WT and CHL1 KO neurons was similar with no differences detected in total dendritic area (μm^2) and length (μm) (Fig. 3.19 B and C). No differences were found in the number of dendrites, total dendritic area (μm^2), or volume (μm^3) of each branching order between WT and CHL1 KO neurons (Fig. 3.19 D, E, and G). However, CHL1 KO neurons showed a tendency for a higher total dendritic length (μm) of fourth-order branches ($p = 0.089$) (Fig. 3.19 F).

Based on the results, I conclude that the absence of CHL1 in MSNs of adult male mice does not affect the morphology of the dendritic tree significantly. However, strong statistical tendencies were found showing a trend for a lower number of intersections located near the cell soma in CHL1 KO MSNs and a tendency for longer 4th-order dendrites compared to WT MSNs.

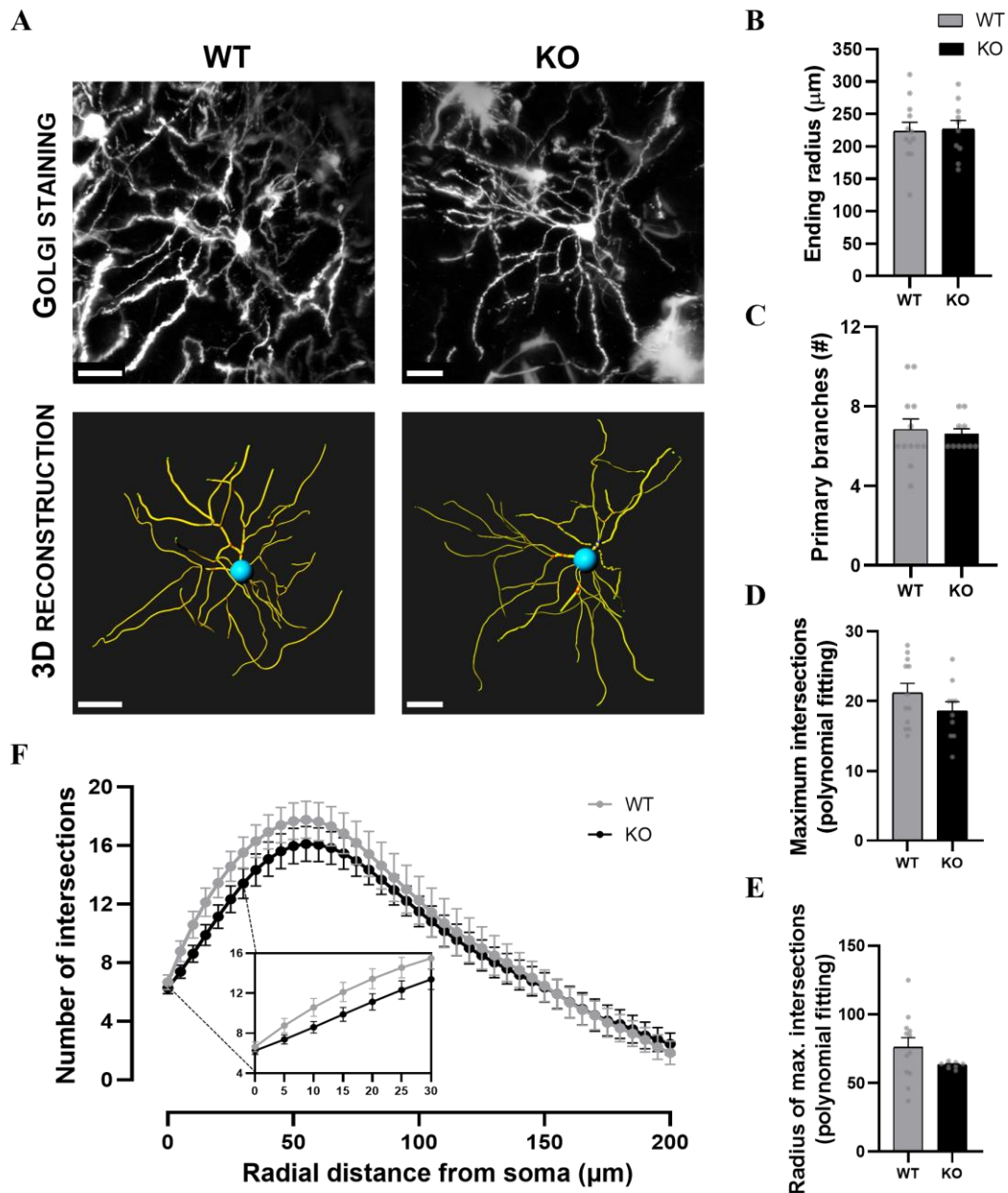


Figure 3.18. Striatal MSNs in CHL1 KO mice show a tendency to have a lower level of complexity in a region near the cell soma. 100 μm -thick coronal brain slices from 4-month-old male WT and CHL1 KO mice were processed for Golgi impregnation with the FD Rapid GolgiStain™ Kit. MSNs located in the dorsal striatum were imaged under bright-field illumination and high-magnification Z-stacks with 0.5 μm step size were acquired from the whole neuronal tree. A 3D reconstruction of the neuronal skeleton was done and subjected to Sholl analysis with a radius step size of 5 μm using the Imaris software. (A) Representative images of sum intensity Z-projection of the Golgi staining and their 3D reconstruction of WT and CHL1 KO MSNs (scale bars: 50 μm). Morphological parameters such as the ending radius (μm) (B), number of primary branches (C), and the polynomial fitting of the maximum number of intersections (D) and of the radius of max. number of intersections (E) were obtained. (F) Polynomial data fitting of the number of intersections as a function of the radial distance from the soma per 5 μm . A close-up of the region near the cell soma shows the radius interval where a statistical tendency was detected (5-25 μm , $p = 0.094$ and 10-20 μm , $p = 0.089$). Values are presented as a bar scatter plot with mean \pm SEM ($n = 2$ animals per genotype, total of 12 WT and 10 CHL1 KO neurons) and were analyzed with Student's t-test (B-E) and one-way repeated measures ANOVA followed by Bonferroni correction post-hoc analysis (F) ($p > 0.05$).

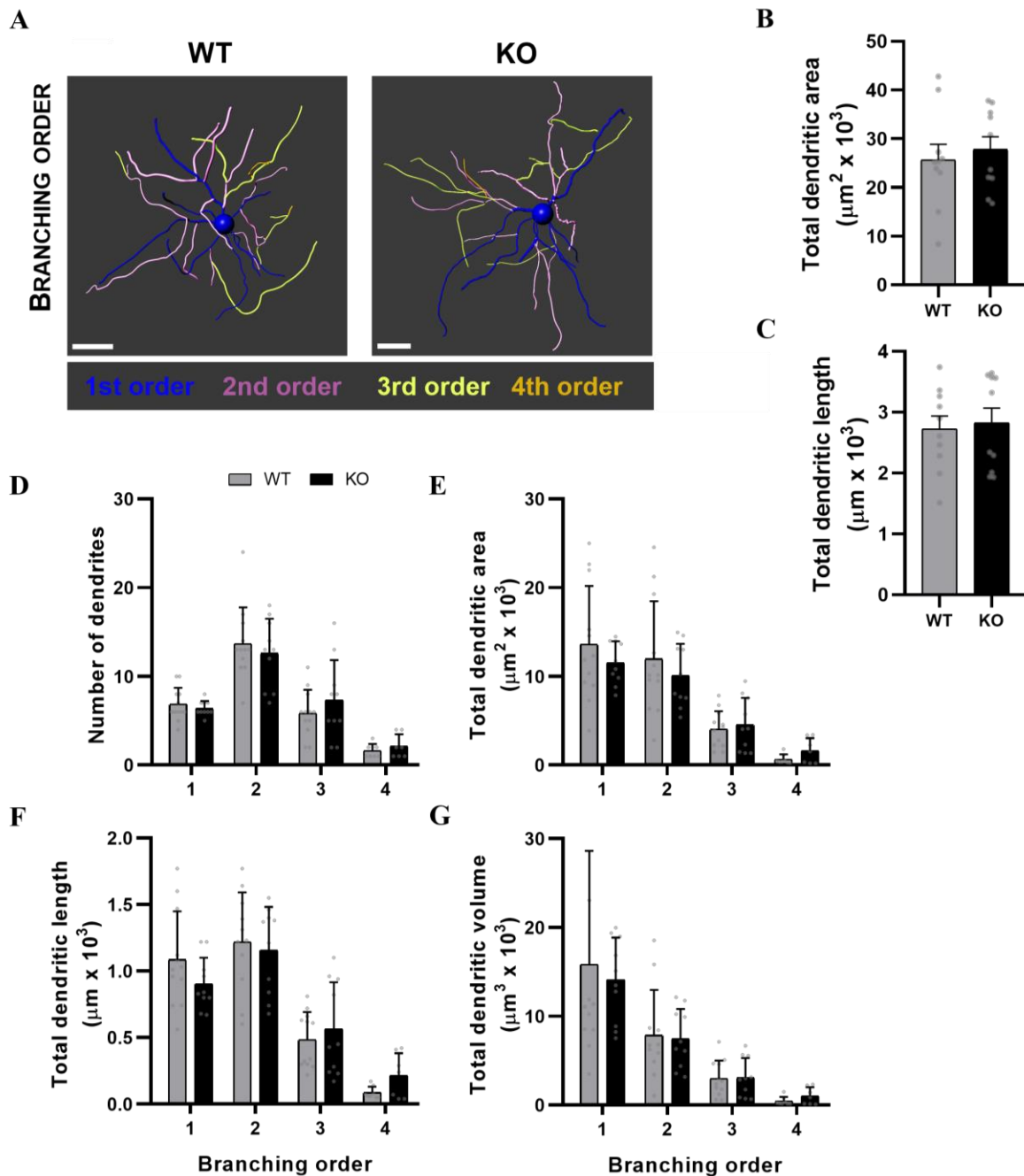


Figure 3.19. Branching order in striatal MSNs is not found altered in CHL1 KO mice. 100 μm -thick coronal brain slices from 4-month-old male WT and CHL1 KO mice were processed for Golgi impregnation with the FD Rapid GolgiStain™ Kit. MSNs located in the dorsal striatum were imaged under bright-field illumination and high-magnification Z-stacks with 0.5 μm step size were acquired from the whole neuronal tree. A 3D reconstruction of the neuronal skeleton was done and subjected to a branching order analysis by Imaris software. (A) Representative images of the 3D reconstruction of WT and CHL1 KO MSNs showing dendrites classification into 4 orders of complexity (1st order, blue; 2nd order, purple; 3rd order, green; 4th order, orange) (scale bars: 50 μm). Total dendritic area (μm^2) (B) and length (μm) (C) were analyzed for each genotype. For each branching order, the number of dendrites (D), total dendritic area (μm^2) (E), length (μm) (F), and volume (μm^3) (G) were calculated. Values are presented as a bar scatter plot with mean + SEM (n = 2 animals per genotype, total of 12 WT and 10 CHL1 KO neurons) and were analyzed with Welch's test ANOVA ($p > 0.05$).

3.4 Behavioral characterization of female and male CHL1 KO mice upon DRD2 pharmacological modulation

Alongside the functional impairments of CHL1-deficient neurons at a molecular and morphological level described previously in the literature and the present thesis, defects in CHL1 expression result in cognitive and locomotor impairments. In humans, mutations in the CHL1 gene were identified as a susceptibility factor in the development of psychiatric disorders such as major depressive disorder, ASD, or schizophrenia^{49–52}. The behavioral phenotype of CHL1 KO mice mimics some of the symptoms present in these disorders, showing a different pattern of exploratory behavior^{27,43,44}, a slower processing speed while employing working memory, a reduced reactivity to novelty⁴⁴, or lower levels of aggressiveness^{21,44}.

Interestingly, genetic or functional impairments of DRD2 are part of the pathophysiology of the same disorders, depression, ASD, or schizophrenia as previously discussed^{70,266,268}. An impaired dopaminergic circuitry is responsible for a wide range of symptoms observed in these disorders and thus can be implied as well in triggering, influencing, or facilitating the behavioral traits exhibited in the CHL1 KO mice. While the association between DRD2 signaling and the aforementioned pathophysiological phenotypes is well-established, the correlation with the CHL1 protein remains unexplored. Thus, my thesis aims to investigate the involvement of CHL1 in the dopaminergic system, starting with understanding the extent to which this protein specifically interferes with DRD2 signaling functions in striatal-dependent behaviors. To achieve this, WT and CHL1 KO mice were treated through direct pharmacological modulation of the receptor with sulpiride or quinpirole to block or activate DRD2.

The battery of behavioral tests targeting striatal-dependent functions included the following goals: evaluate motor and exploratory aptitude through spontaneous locomotion in the open field test (OF), assess short-term working memory through spontaneous alternation in a Y-maze test (YM), explore the reactivity to and interest for the unknown through the novelty-induced test (NI) by an object and take a look at general parameters of anxiety-like behaviors across all the previous tests. The behavioral paradigms used in this study included minimal intervention by the investigator, easy reproducibility, clear endpoints, and are widely considered sensitive to detect behavioral phenotypes related to depression, autism spectrum disorders, and schizophrenia disease. Furthermore, to reduce restraint-induced stress and fear during i.p. administration, a handling protocol was used^{313,314}.

Before the behavioral assessment, 2-month-old female and male WT and CHL1 KO littermates were acclimatized for 2 weeks to the behavioral facility (inverted 12 h light/dark cycle, room temperature of $21\pm 1^{\circ}\text{C}$, with food and water supplied *ad libitum*) and were housed in 3-4 mice per cage. Afterwards, mice were subjected to a repetitive handling protocol for two weeks. The order of the tests was

specifically designed to limit potential stress impacts with a one-week gap between them, starting with the OF test, and ending with the NI test. For all tests, the behavioral protocol started with a single i.p. injection of vehicle, sulpiride, or quinpirole solution 2 min before each behavioral session. Figure 3.20 shows a diagram of the experimental design.

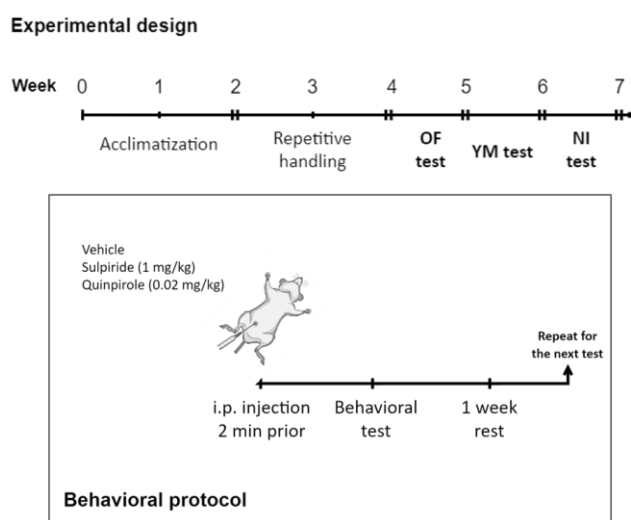


Figure 3.20. Time course of the behavioral experiments. 2-month-old female and male WT and CHL1 KO mice underwent a two-week acclimation period and were subjected to two weeks of repetitive handling. Behavioral tests were then performed in ascending order of stress with an interval of one week in between. Mice were treated with a single i.p. injection of vehicle (0.9% NaCl, 0.5% DMSO), sulpiride (1 mg/kg in vehicle solution), or quinpirole (0.02 mg/kg in vehicle solution) 2 min before each behavioral trial. Execution and analysis of the behavioral test were performed blindly.

3.4.1 Open field: locomotor, exploratory, and emotional evaluation

As mentioned earlier, spontaneous locomotion and exploration heavily rely on striatal and dopaminergic signaling, driven by motivational cues. The OF paradigm is commonly used to access how the animal's locomotor activity and spontaneous exploration are affected by its exposure to a new environment. This new environment can induce anxiety in mice due to social isolation during the test, agoraphobia from the arena's large proportions, and potentially high illumination levels^{317,340}. Thus, the locomotor and exploratory reactivity to the arena can be coupled to other tests to describe anxiety-like states. Often, the OF constitutes a reliable test to study the effects of stimulant or anxiolytic compounds over spontaneous locomotion and exploration.

To investigate whether CHL1 is important for the behavioral outcomes of D2DR signaling in terms of motor and explorative capabilities, female and male WT and CHL1 KO mice were acclimated to the behavioral room for 30 min prior to i.p. administration and vehicle, sulpiride, and quinpirole treatments

were administered 2 min before the respective trial. The activity was monitored over 30 min and locomotion and stereotypic behaviors were analyzed across different time intervals and compared between genotype, treatment, and sex.

First, spontaneous locomotion, distance moved, time moving, and average speed were explored. Female WT and CHL1 KO mice treated with vehicle did not show any differences in locomotion during the whole 30 min of the OF test. In contrast, male CHL1 KO mice had significantly lower activity than their WT littermates (Fig. 3.21 A). Sulpiride treatment significantly decreased activity by 18% only in CHL1 KO females relative to WT females and vehicle treatment groups of both genotypes, without affecting locomotion levels of WT and male CHL1 KO mice. Compared to the vehicle treatment, quinpirole treatment induced a general hypolocomotion effect with a decrease of activity of 25% and 36% in WT and CHL1 KO females and 36% and 22% in male WT and CHL1 KO mice. Overall, female mice were more active than males and significant differences were present between vehicle-treated CHL1 KO mice and sulpiride- and quinpirole-treated WT animals (Fig. 3.21 B).

Focusing on the first 10 min of the test, similar differences between the genotypes and treatments were observed (Fig. 3.22 A left). When comparing the distance moved between the genotypes for each treatment in 1 min time bins, vehicle-treated male CHL1 KO mice started moving less from the beginning of the trial (2-4 min), female CHL1 KO mice showed a general tendency to be less active with sulpiride treatment (4-5 min) and WT and CHL1 KO mice displayed the same level of motor activity with quinpirole treatment (Fig. 3.22 B). When comparing the D2DR-specific compounds to the vehicle treatment within the same genotype, WT and CHL1 KO mice treated with sulpiride moved a similar distance as vehicle-treated mice (Fig. 3.22 C right, blue/black graphs). For the quinpirole treatment (Fig. 3.22C right, red/black graphs), this comparison revealed an earlier hypolocomotion state in female and male WT mice starting at the 3 min of the test, relative to vehicle-treated WT mice. The same hypolocomotion state was induced in CHL1 KO animals at a later stage, at 7 min for the female and 9 min in the case of the male mice, compared with the vehicle-treated CHL1 KO mice.

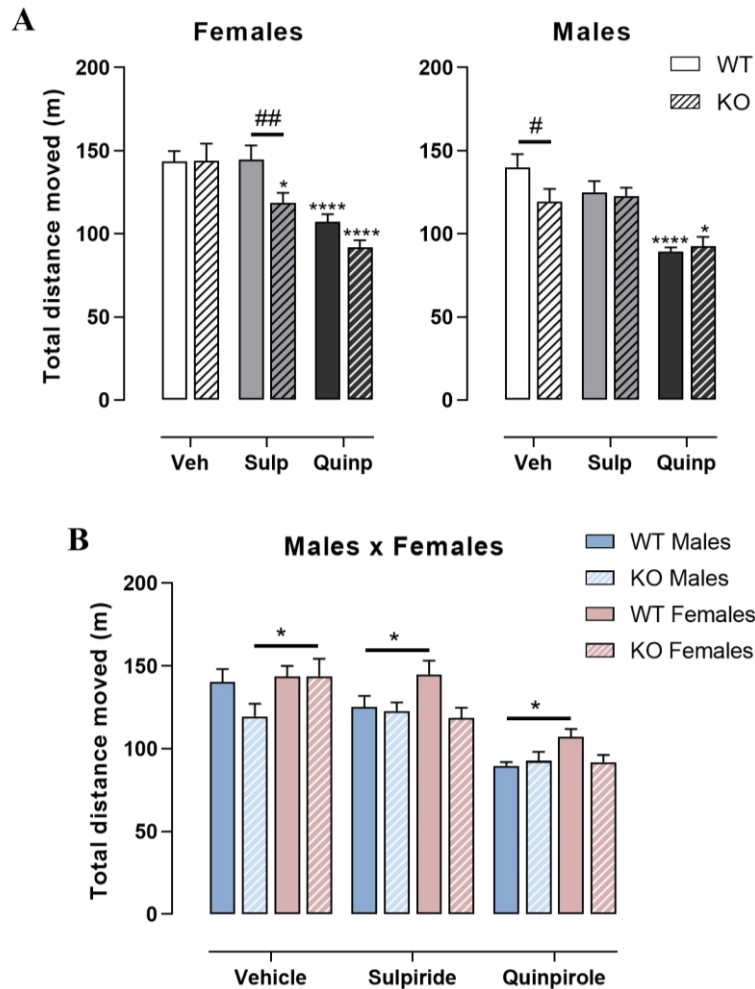


Figure 3.21. Locomotor activity is affected by sulpiride and quinpirole treatment in WT and CHL1 KO mice during 30 min of the OF test. 3-month-old female and male WT and CHL1 KO littermates were treated with a single i.p. injection of vehicle, sulpiride (1 mg/kg), or quinpirole (0.02 mg/kg) 2 min before the trial, and activity was tracked over 30 min. Total distance moved (m) was obtained for female and male mice (**A**) and was compared between sexes for each treatment (* $p < 0.05$) (**B**). Values are presented as mean + SEM ($n = 11-13$ mice per group) and were analyzed with three-way ANOVA ((A/B): genotype: $F(1,132) = 7.240$, $p = 0.008$; treatment: $F(2,132) = 44.277$, $p = 0.0001$; sex: $F(1,132) = 7.038$, $p = 0.009$; genotype x treatment x sex: $F(2,132)=3.417$ $p=0.036$) followed by Bonferroni correction post-hoc test (* $p < 0.05$, ** $p < 0.01$, **** $p < 0.0001$, statistical difference from vehicle-treated correspondent genotype; # in case of genotype difference within treatment).

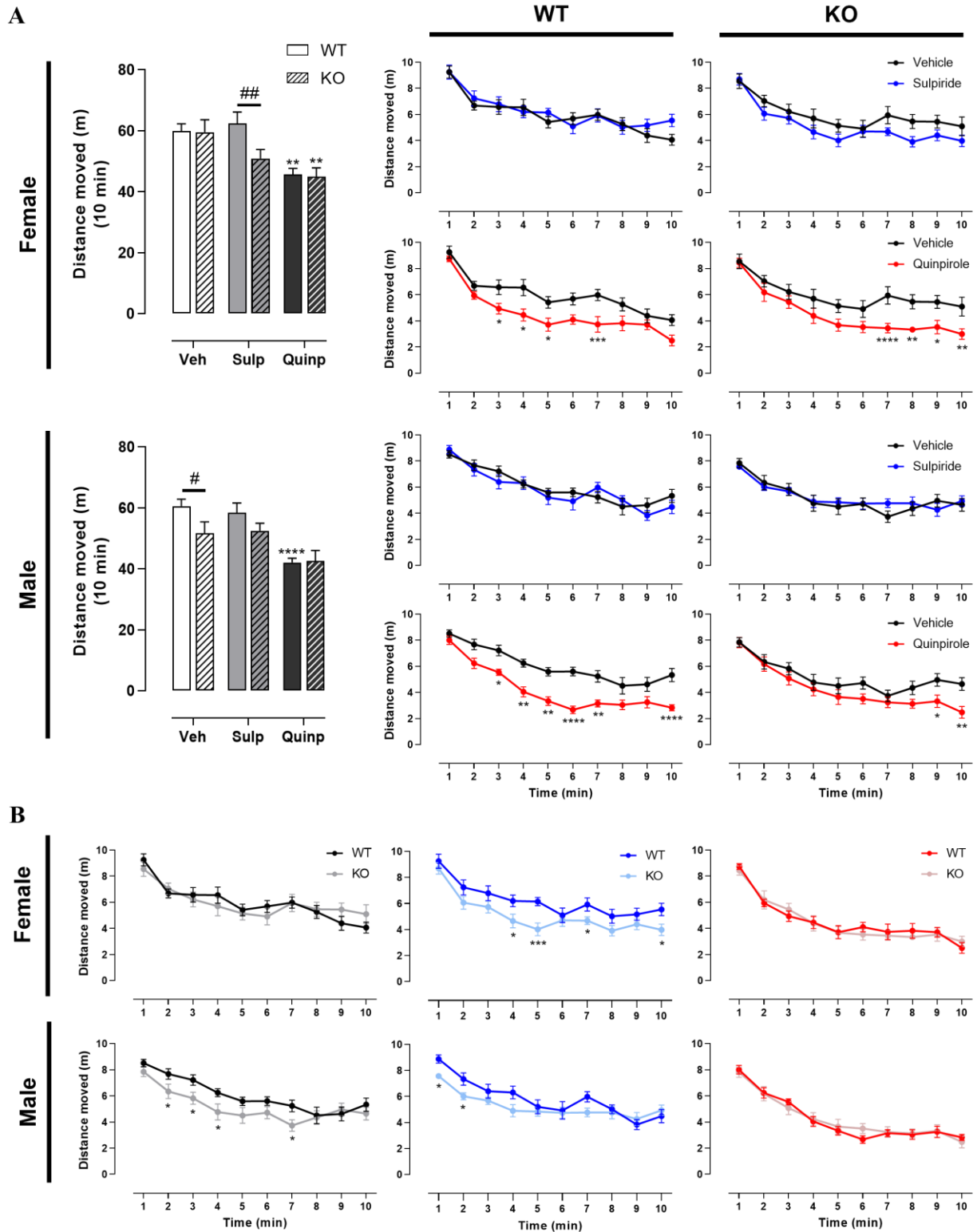


Figure 3.22. Locomotor activity is affected by sulpiride treatment in CHL1 KO females and quinpirole-induced hypocomotion is delayed in CHL1 KO mice in the first 10 min of the OF. 3-month-old female and male WT and CHL1 KO littermates were treated with a single i.p. injection of vehicle, sulpiride (1 mg/kg), or quinpirole (0.02 mg/kg) 2 min before the trial, and activity was tracked. **(A)** Distance moved (m) of female and male mice during the first 10 min of OF is shown and was compared in 1 min time-bins between DRD2-specific compounds and vehicle treatment for each genotype and sex group. **(B)** Distance moved (m) was compared between genotypes for each treatment and sex group in 1 min time-bins.

(Figure 3.22) Values are presented as mean + SEM (n = 11-13 mice per group) and were analyzed with three-way ANOVA ((A left): genotype: $F(1,132) = 6.814$, $p = 0.010$, treatment: $F(2,132) = 26.734$, $p = 0.0001$; followed by Bonferroni correction post-hoc test (* $p < 0.05$, ** $p < 0.01$, **** $p < 0.0001$, statistical difference from vehicle-treated correspondent genotype; # in case of genotype difference within treatment)) and three-way repeated measures ANOVA ((A right/B): genotype: $F(1,132) = 6.814$, $p = 0.01$, treatment: $F(2,132) = 26.734$, $p = 0.0001$; followed by Bonferroni correction post-hoc test (* $p < 0.05$, ** $p < 0.01$, *** $p < 0.001$, **** $p < 0.0001$)).

Equivalently, the behavioral effects found in the distance moved were also mimicked in the time moving parameter of the OF test. In the total duration of the trial, no differences between female and male WT and CHL1 KO mice treated with vehicle or sulpiride were detected, while quinpirole treatment induced a reduction of the activity for both genotypes and sexes, compared to vehicle treatment (Fig. 3.23 A). The same effects were already present in the first 10 min of the test where no differences were detected in vehicle and sulpiride treatments, and quinpirole decreased time moving in female WT and CHL1 KO mice and male WT mice, relative to vehicle treatment (Fig. 3.2 B left). When comparing the treatment with the D2DR-specific compounds to the vehicle treatment within the same genotype across 1 min time bins, WT and CHL1 KO animals showed the same levels of activity with sulpiride treatment, while quinpirole decreased moving time of WT animals starting at 5 min for female and 4 min for male mice and in CHL1 KO animals the reduction was delayed and only started at 7 min for female and 10 min for male mice (Fig. 3.23 B right).

Average speed is another parameter that reflected the effect of sulpiride and quinpirole on the locomotor aptitude of the animals. In the 30 min of the trial, female mice treated with vehicle did not show differences in average speed between genotypes, whilst male CHL1 KO mice move slower than the WT mice (Fig. 3.24 A). CHL1 KO females treated with sulpiride moved slower than WT mice and the respective vehicle-treated group, but no effects were detected in male mice. Quinpirole treatment reduced the average speed in WT and CHL1 KO mice for both sexes, relative to vehicle condition. The effects detected in the entire duration of the test were as well present in the first 10 min (Fig. 3.24 B).

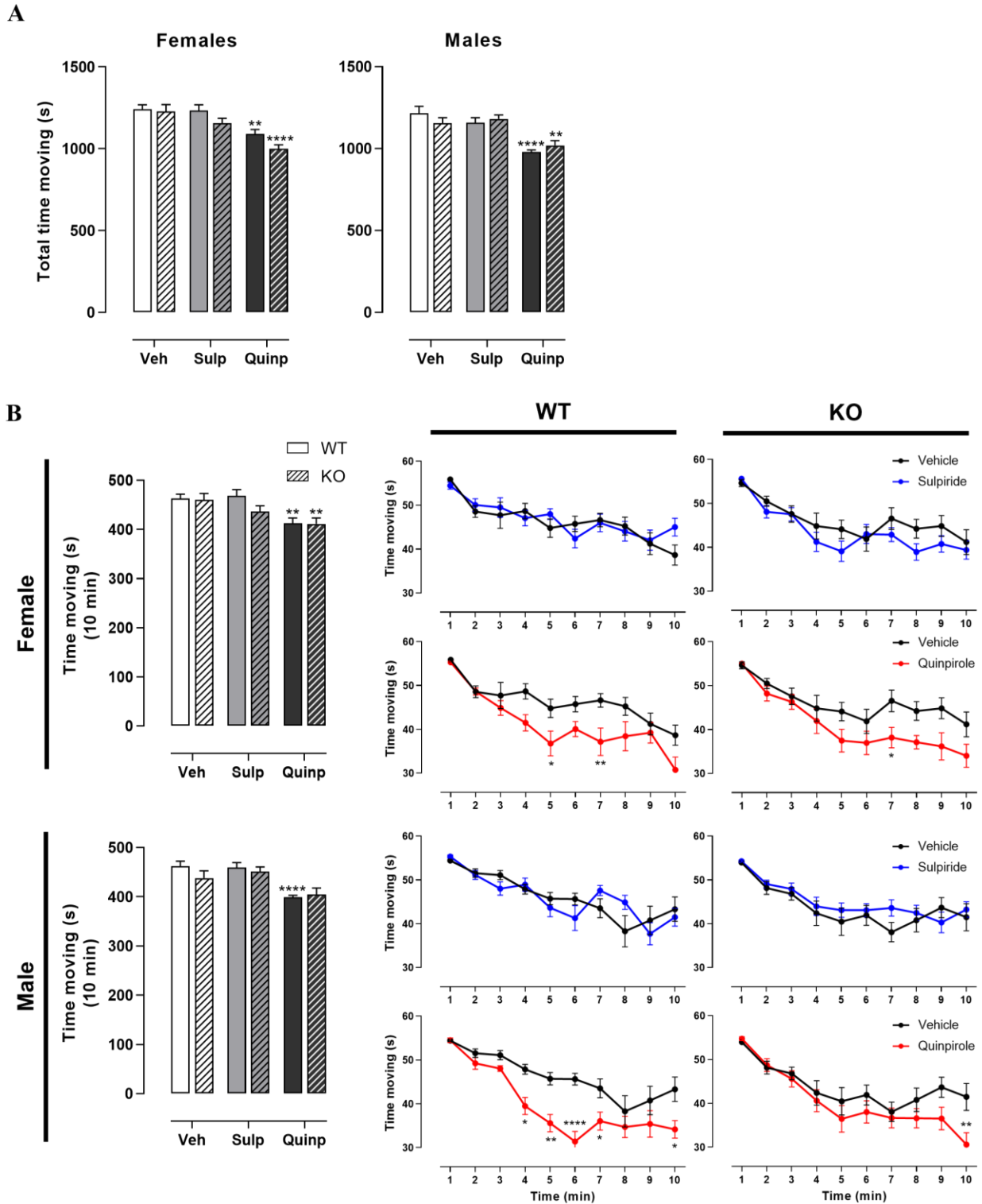


Figure 3.23. Time moving is not affected by sulpiride treatment but CHL1 KO females showed a delay in reduced time moving in the OF test after quinpirole treatment. 3-month-old female and male WT and CHL1 KO littermates were treated with a single i.p. injection of vehicle, sulpiride (1 mg/kg), or quinpirole (0.02 mg/kg) 2 min before the trial, and activity was tracked. **(A)** Total time moving (s) of female and male mice during 30 min of the OF. **(B)** Time moving (s) of female and male mice in the first 10 min of OF is shown and was compared in 1 min time-bins between DRD2-specific compounds and vehicle treatment for each genotype and sex group.

(Figure 3.23) Values are presented as mean + SEM (n = 11-13 mice per group) and were analyzed with three-way ANOVA ((A): treatment: $F(2,132) = 43.803$, $p = 0.0001$; (B left): treatment: $F(2,132) = 25.407$, $p = 0.0001$) followed by Bonferroni correction post-hoc test (** $p < 0.01$, **** $p < 0.0001$, statistical difference from vehicle-treated correspondent genotype) and three-way repeated measures ANOVA ((B right): treatment: $F(2,132) = 25.407$, $p = 0.0001$) followed by Bonferroni correction post-hoc test (* $p < 0.05$, ** $p < 0.01$, **** $p < 0.0001$).

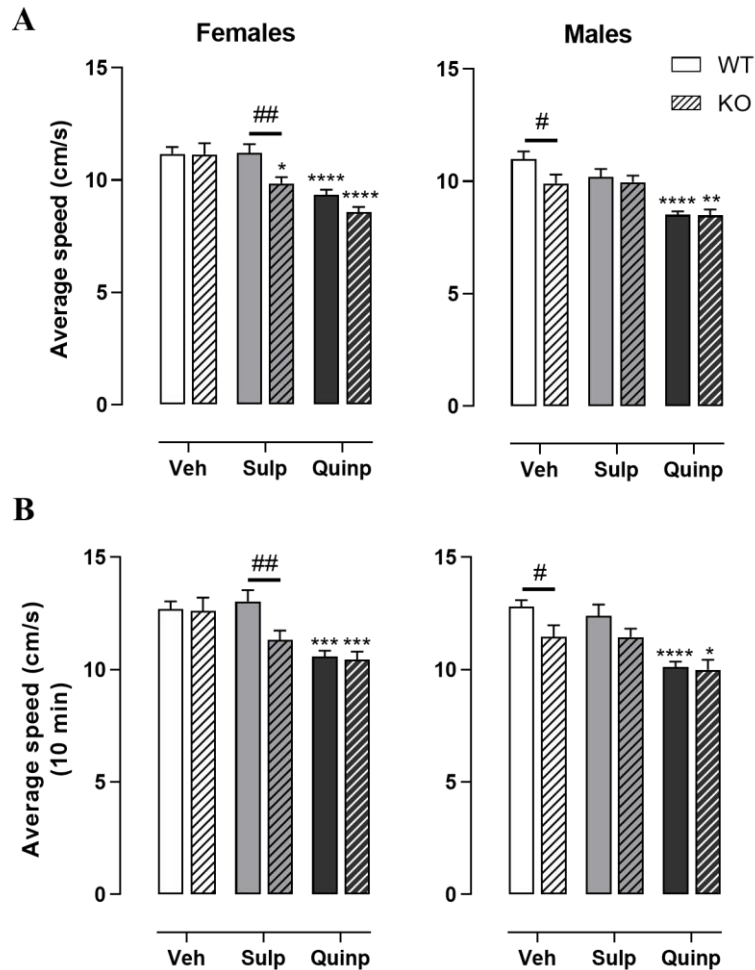


Figure 3.24. Sulpiride and quinpirole treatments affect the average speed of WT and CHL1 KO mice during the OF test. 3-month-old female and male WT and CHL1 KO littermates were treated with a single i.p. injection of vehicle, sulpiride (1 mg/kg), or quinpirole (0.02 mg/kg) 2 min before the trial, and activity was tracked. (A) Average speed (cm/s) of female and male mice during 30 min of the OF. (B) Average speed (cm/s) of female and male mice during the first 10 min of the OF. Values are presented as mean + SEM (n = 11-13 mice per group) and were analyzed with three-way ANOVA ((A): genotype: $F(1,132) = 9.891$, $p = 0.002$, treatment: $F(2,132) = 45.717$, $p = 0.0001$, genotype x treatment x sex: $F(2,132) = 3.243$, $p = 0.042$; (B): genotype: $F(1,132) = 9.269$, $p = 0.003$, treatment: $F(2,132) = 29.848$, $p = 0.0001$) followed by Bonferroni correction post-hoc test (* $p < 0.05$, ** $p < 0.01$, *** $p < 0.001$, **** $p < 0.0001$, statistical difference from vehicle-treated correspondent genotype; # in case of genotype difference within treatment).

Apart from locomotor aptitude, the exploratory pattern of mice can give an indication of the emotional state of the animal with parameters related to the exploration of the center zone of the OF. In the 30 min of the test, no differences were found in the percentage of time spent in the center between any of the groups (Fig. 3.25 A), except when looking at the sex of mice. Female WT mice showed a tendency to spend more time in the center than WT males reaching statistical significance in the case of quinpirole treatment (Fig. 3.25 B). No effects of genotype or treatment were detected in female mice, whilst sulpiride-treated CHL1 KO males moved longer time than WT mice and quinpirole treatment decreased this parameter in WT males, compared with CHL1 KO males and vehicle treatment (Fig. 3.25 C). Analysis of distance moved in the center also showed similar effects, with quinpirole treatment reducing distance moved by WT and female CHL1 KO mice relative to vehicle-treated mice and reducing drastically the distance moved by male WT mice, compared with the CHL1 KO group and vehicle treatment (Fig. 3.25 D). The average distance to the wall and latency to reach the central zone did not differ between mice (Fig. 3.25 E-G).

In the first 10 min of the test, percentage of time spent and time moving in the center of the arena were not affected by any of the treatments nor did they differ between genotypes (Fig. 3.26 A and B). Distance moved in the center was reduced in quinpirole-treated male WT mice relative to vehicle-treated mice (Fig. 3.26 C). Average distance to the wall was higher for CHL1 KO females treated with sulpiride than for female WT mice (Fig. 3.26 D).

The occurrence of fecal boli was as well monitored for the entire duration of the OF test and revealed no differences in female mice (Fig. 3.26 E). Male WT and CHL1 KO mice treated with quinpirole showed an increase in the deposition of fecal boli compared to vehicle-treated mice (Fig. 3.26 F).

Stereotypic behavior can reveal details about the willingness to explore and the emotional state of mice, specifically the rearing behavior in the first minutes of the test when the reactivity to novelty is highly triggered. During the first 10 min of the OF, the total rearing number was not affected by genotype, treatment, or sex (Fig. 3.27 A). Hence, a separate analysis for the unsupported/supported rearing was done.

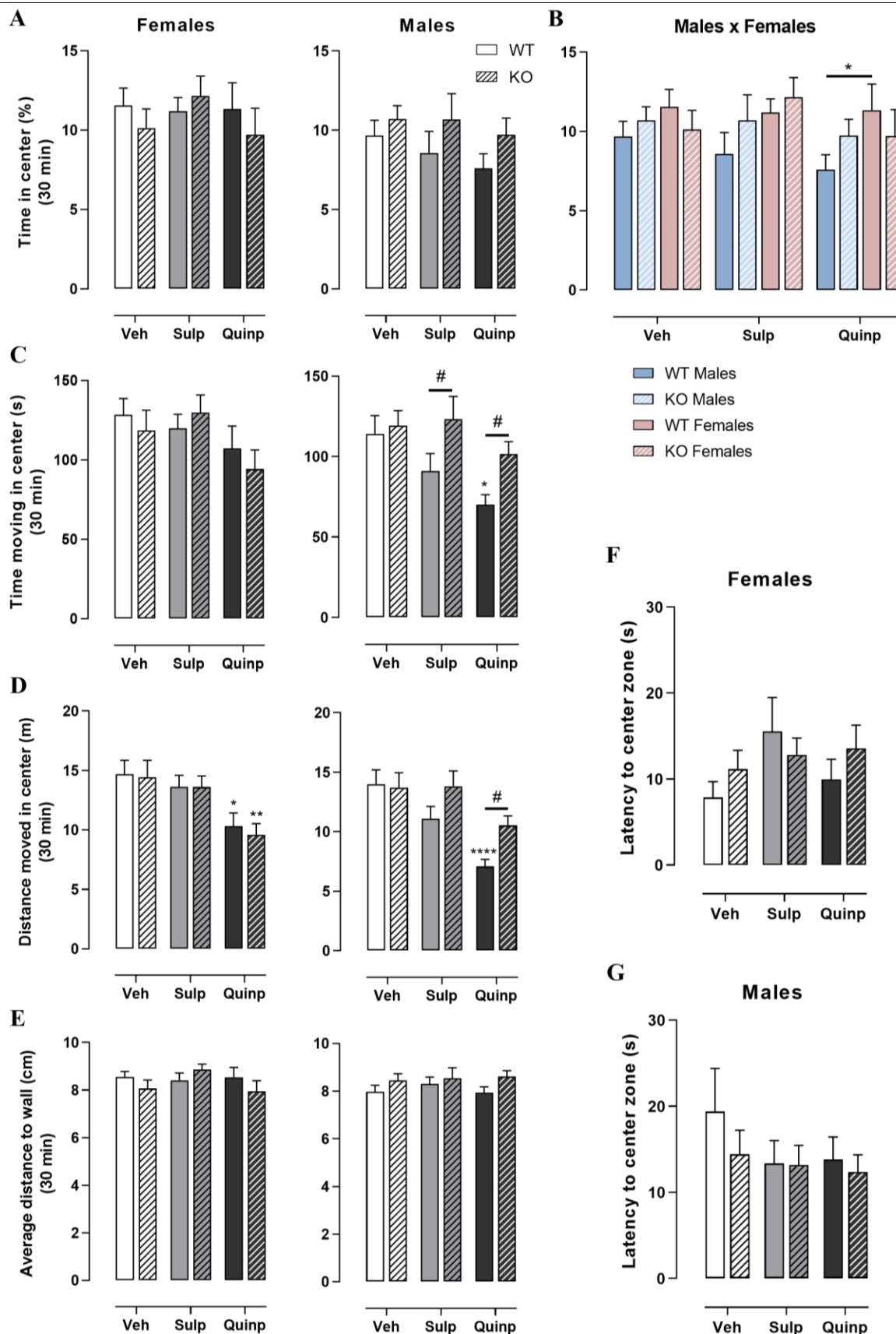


Figure 3.25. Exploration of the center zone by female mice is not affected by sulpiride treatment but is altered by sulpiride and quinpirole in male mice during 30 min of the OF test. 3-month-old female and male WT and CHL1 KO littermates were treated with a single i.p. injection of vehicle, sulpiride (1 mg/kg), or quinpirole (0.02 mg/kg) 2 min before the trial, and activity was tracked for 30 min.

(Figure 3.25) Percentage of time in the center is shown for female and male mice (**A**) and was compared between sexes for each treatment (* $p < 0.05$) (**B**). Total time moving (s) (**C**) and distance moved (m) (**D**) in the center are presented for female and male mice. The average distance to wall (cm) (**E**) and latency (s) (**F**, **G**) to reach the center zone were obtained for female and male mice. Values are presented as mean + SEM ($n = 11-13$ mice per group) and were analyzed with three-way ANOVA ((**B**): sex: $F(1,132) = 4.369$, $p = 0.039$; (**C**): treatment: $F(2,132) = 6.821$, $p = 0.002$, genotype x sex: $F(1,132) = 4.493$, $p = 0.036$; (**D**, females): treatment: $F(2,132) = 21.877$, $p = 0.0001$) or two-way ANOVA ((**D**, males): genotype: $F(1,66) = 5.161$, $p = 0.026$, treatment: $F(2,132) = 12.486$, $p = 0.0001$) followed by Bonferroni correction post-hoc test (* $p < 0.05$, ** $p < 0.01$, **** $p < 0.0001$, statistical difference from vehicle-treated correspondent genotype; # in case of genotype difference within treatment).

The unsupported rearing was considered whenever the mouse was lifted completely without any support (Fig. 3.27. B). CHL1 KO mice showed a general tendency to exhibit a higher number and time of unsupported rearing than WT mice since a strong statistical effect was detected for the genotype effect for both variables ($p = 0.0001$) (Fig. 3.27. C and D). However, statistical differences were only detected in number and time of unsupported rearings in sulpiride-treated CHL1 KO females and vehicle-treated CHL1 KO males. No differences were found in the latency (s) to the first unsupported rearing for the first time in female or male mice (Fig. 3.27. E and F). No differences or relevant effects were detected when comparing genotypes or treatments across time bins, therefore no graphs are presented for this matter.

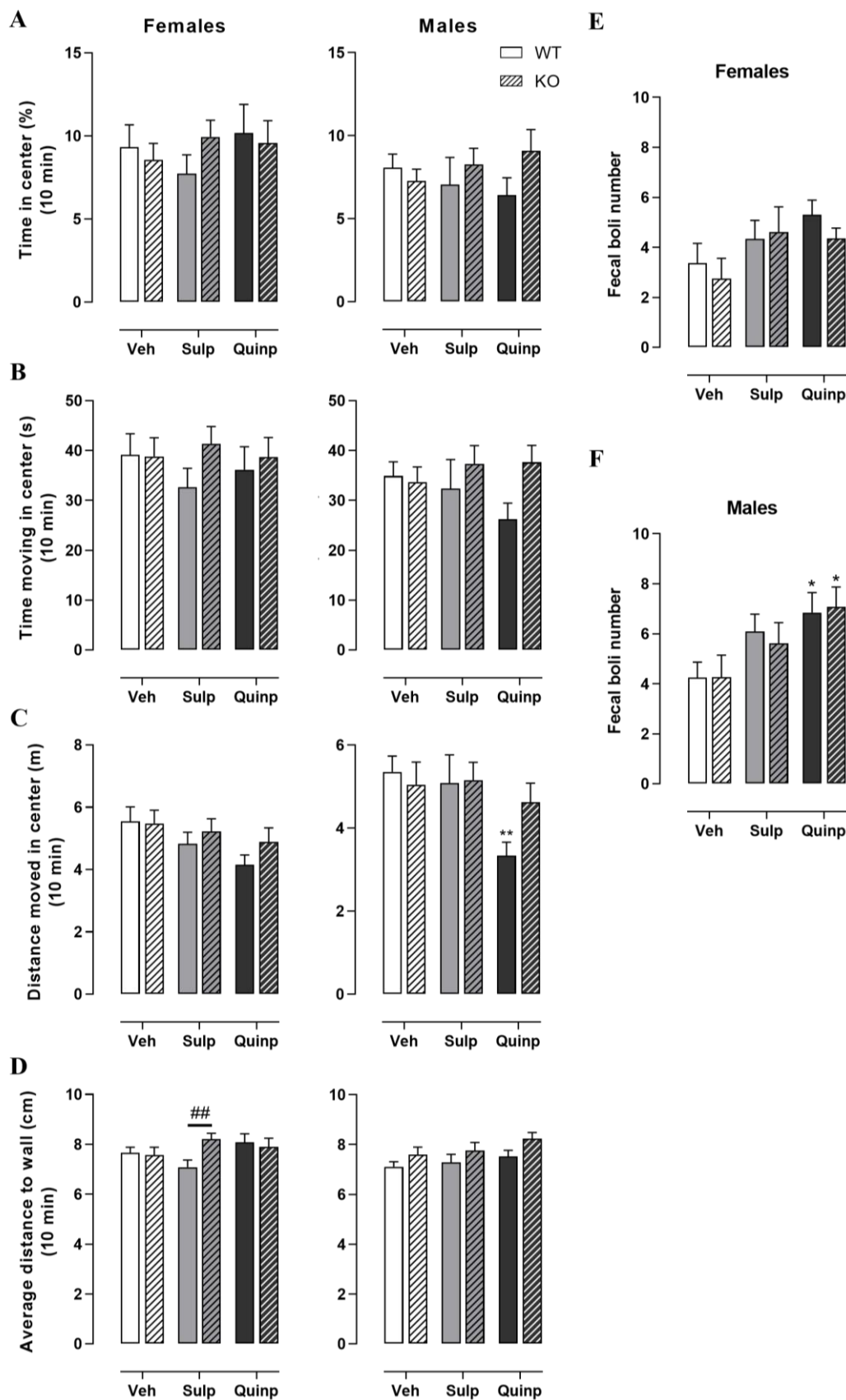


Figure 3.26. Sulpiride and quinpirole treatments do not affect exploration of the center zone in the first 10 min of the OF test. 3-month-old female and male WT and CHL1 KO littermates were treated with a single i.p. injection of vehicle, sulpiride (1 mg/kg), or quinpirole (0.02 mg/kg) 2 min before the trial, and activity was tracked for 10 min. Percentage of time in the center is shown for female and male mice (**A**). Total time moving (s) (**B**) and distance moved (m).

(Figure 3.26) (C) in the center are presented for female and male mice. (D) Average distance to wall (cm) for female and male mice. (E, F) Fecal boli numbers were counted female for and male mice for the entire duration of the test. Values are presented as mean + SEM (n = 11-13 mice per group) and were analyzed with three-way ANOVA ((C): treatment: $F(2,132) = 6.886$, $p = 0.001$; (D): genotype: $F(1,132) = 6.524$, $p = 0.0012$; (F): treatment: $F(2,132) = 8.646$, $p = 0.0001$) followed by Bonferroni correction post-hoc test (* $p < 0.05$, ** $p < 0.01$, statistical difference from vehicle-treated correspondent genotype; # in case of genotype difference within treatment).

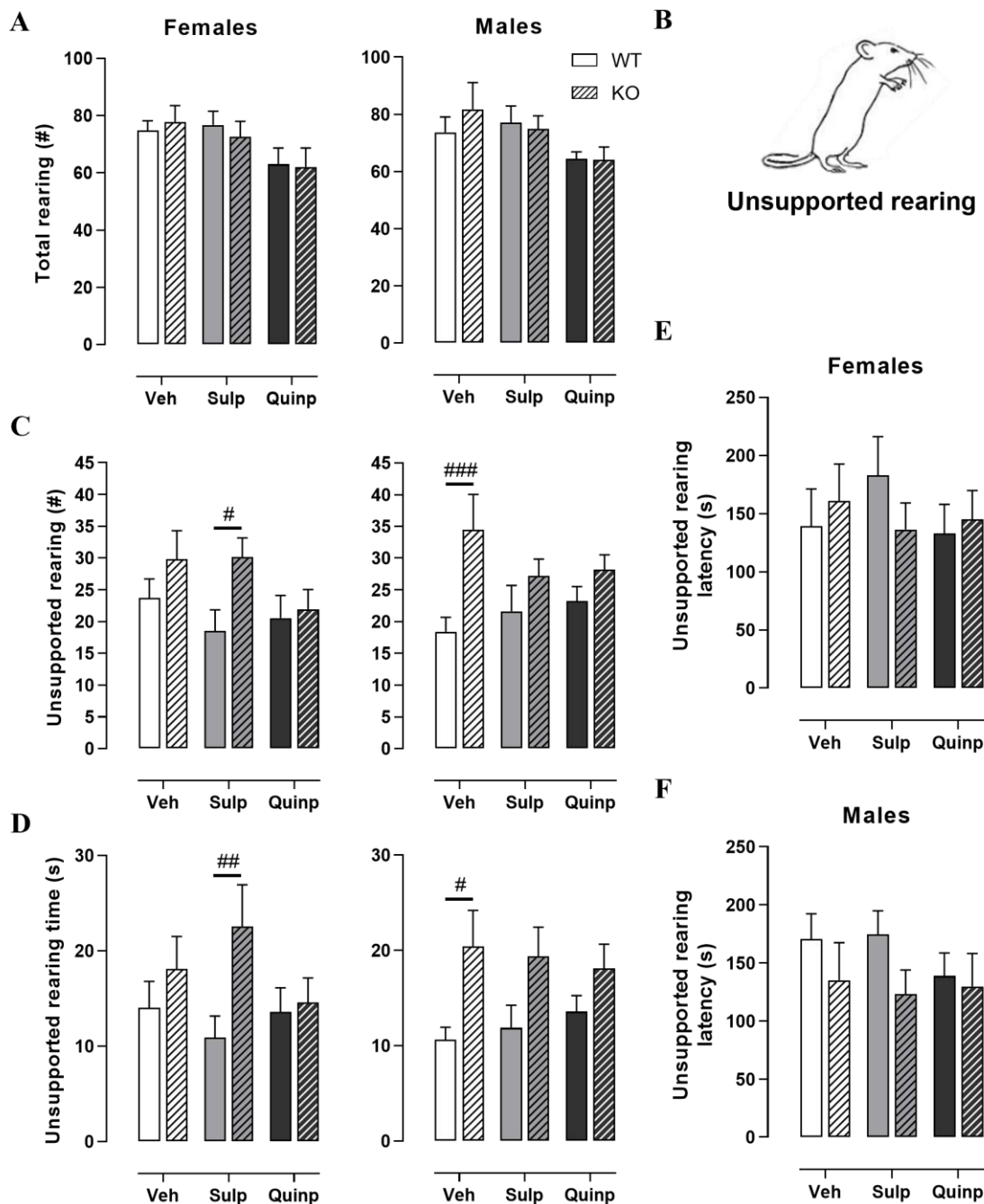


Figure 3.27. Unsupported rearing behavior in the OF tends to occur more often in CHL1 KO mice and is affected by sulpiride and quinpirole treatments. 3-month-old female and male WT and CHL1 KO littermates were treated with a single i.p. injection of vehicle, sulpiride (1 mg/kg), or quinpirole (0.02 mg/kg) 2 min before the trial, and rearing behavior was explored in the first 10 min of the test.

(Figure 3.27) 3-month-old female and male WT and CHL1 KO littermates were treated with a single i.p. injection of vehicle, sulpiride (1 mg/kg), or quinpirole (0.02 mg/kg) 2 min before the trial, and rearing behavior was explored in the first 10 min of the test. **(A)** Total rearing number is presented for female and male mice. **(B)** Representative figure of unsupported rearing adapted from Chaumont et al. (2019)*. Unsupported rearing number **(C)** and time (s) **(D)** were obtained for female and male mice. Latency (s) to the first unsupported rearing is shown for female **(E)** and male **(F)** mice. Values are presented as mean + SEM (n = 11-13 mice per group) and were analyzed with three-way ANOVA ((C): genotype: $F(1,132) = 15.118$, $p = 0.0001$; (D): genotype: $F(1,132) = 14.972$, $p = 0.0001$) followed by Bonferroni correction post-hoc test (* $p < 0.05$, ** $p < 0.01$, *** $p < 0.001$, statistical difference from vehicle-treated correspondent genotype; # in case of genotype difference within treatment).

Supported rearing was considered when the mouse lifts up with the support of the arena wall. Here, CHL1 KO mice showed a slight tendency to perform a lower number of supported rearings than the WT mice, which was statistically different for sulpiride-treated female mice (Fig. 3.28A left). When supported rearing was plotted across 1 min time bins, the same effect of sulpiride was present since CHL1 KO females showed a lower number of supported rearings than WT animals in the first minutes of the test (4-5 min) (Fig. 3.28 B). When comparing the mice with D2DR antagonist and agonist treatment to the vehicle treated mice of the same genotype across 2 min time bins, sulpiride treatment did not lead to any differences between WT or CHL1 KO mice, while quinpirole induced a reduction in supported rearing of WT animals at 4 min for female and 6 min for male mice (Fig. 3.28 A right). CHL1 KO animals showed a delayed reduction of supported rearing induced by quinpirole, which was starting at 8 min for female and 10 min for male mice.

The time of and the latency to perform the first supported rearing were not different between conditions (Fig. 3.29 A and B).

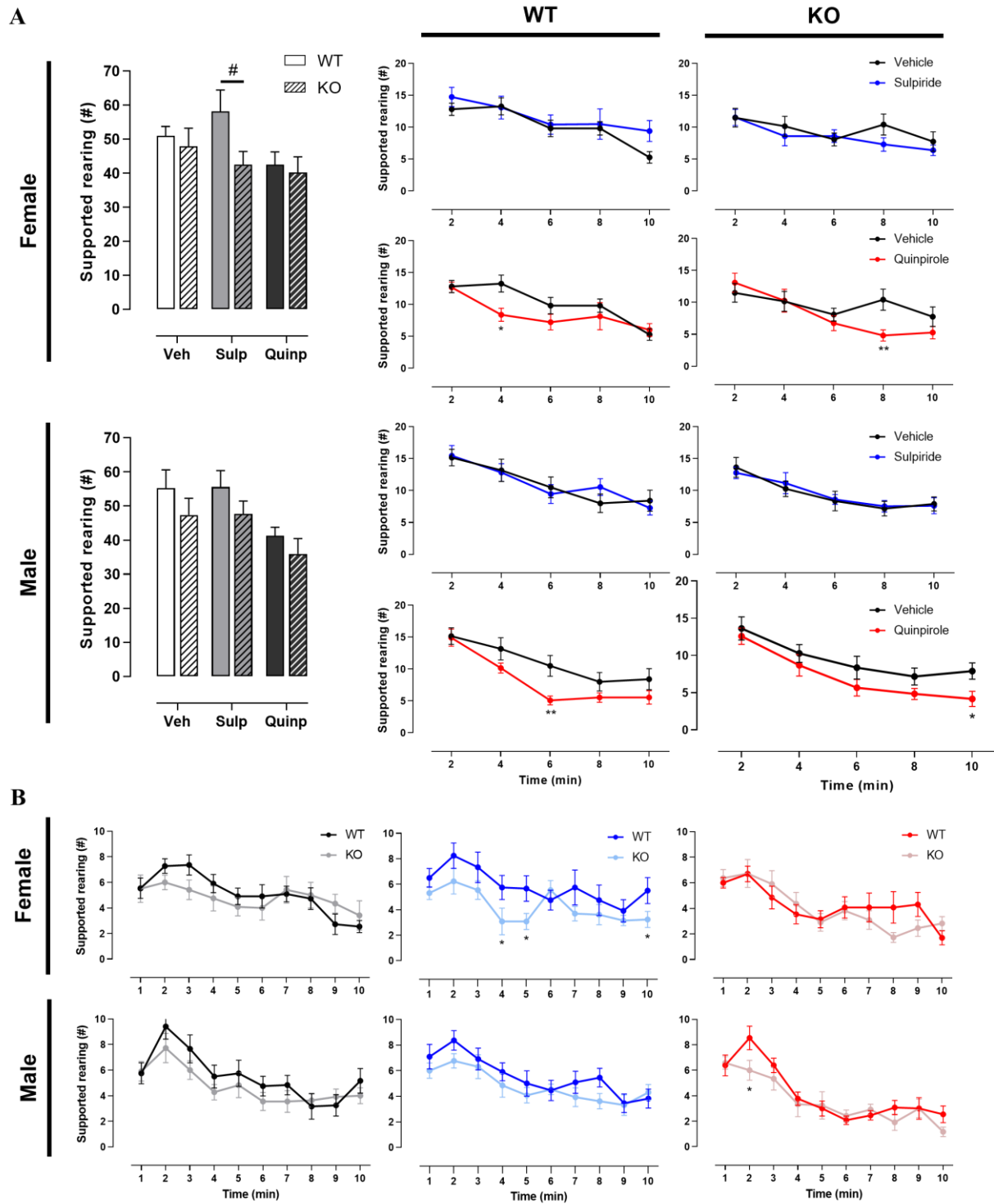


Figure 3.28. Sulpiride treatment affects supported rearing of CHL1 KO females and CHL1 KO mice show a delayed reduction of supported rearings after quinpirole treatment. 3-month-old female and male WT and CHL1 KO littermates were treated with a single i.p. injection of vehicle, sulpiride (1 mg/kg), or quinpirole (0.02 mg/kg) 2 min before the trial, and rearing behavior was explored in the first 10 min of the test. **(A)** Supported rearing number of female and male mice in the first 10 min of OF is shown and was compared in 2 min time-bins between mice treated with DRD2-specific compounds and vehicle treatment for each genotype and sex group. **(B)** Supported rearing number was compared between genotypes for each treatment and sex group in 1 min time-bins.

(**Figure 3.28**) Values are presented as mean + SEM (n = 11-13 mice per group) and were analyzed with three-way ANOVA ((A left): genotype: $F(1,132) = 7.393$, $p = 0.007$, treatment: $F(2,132) = 7.782$, $p = 0.001$) followed by Bonferroni correction post-hoc test ($\#p < 0.05$, genotype difference within treatment) and three-way repeated measures ANOVA ((B): genotype: $F(1,132) = 7.393$, $p = 0.007$, treatment: $F(2,132) = 7.782$, $p = 0.001$; (A right): treatment: $F(1,132) = 11.700$, $p = 0.001$) followed by Bonferroni correction post-hoc test ($*p < 0.05$, $**p < 0.01$).

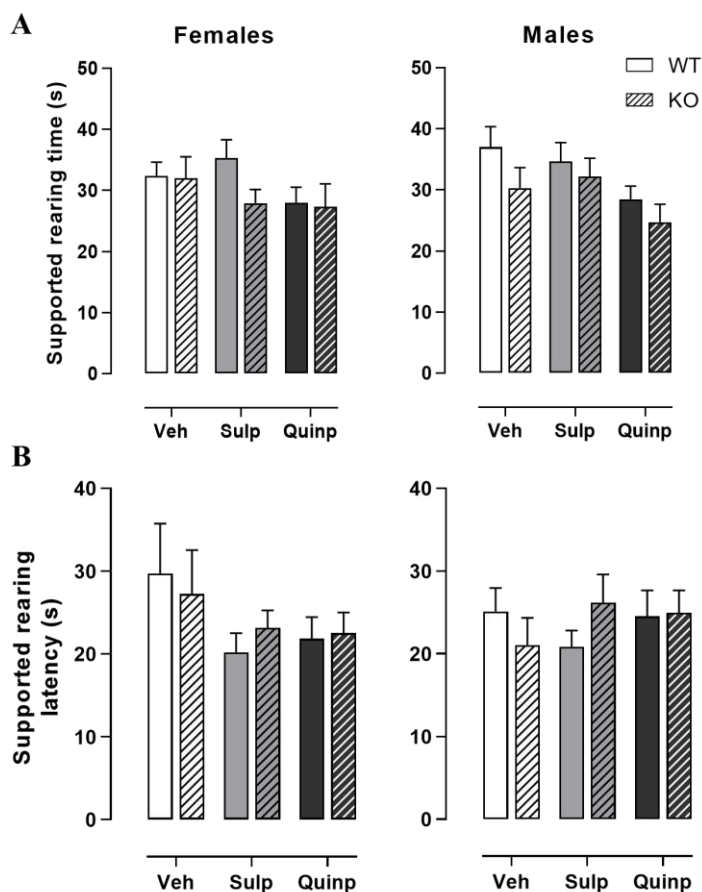


Figure 3.29. Sulpiride and quinpirole treatments do not affect supported rearing time or latency during the OF test. 3-month-old female and male WT and CHL1 KO littermates were treated with a single i.p. injection of vehicle, sulpiride (1 mg/kg), or quinpirole (0.02 mg/kg) 2 min before the trial, and rearing behavior was explored in the first 10 min of the test Supported rearing time (s) (A) and latency (s) (B) were obtained for female and male mice. Values are presented as mean + SEM (n = 11-13 mice per group) and were analyzed with three-way ANOVA ($p > 0.05$).

The amount of time mice spend self-grooming can be used as an indicator of anxiety- or depressive-like state, therefore the analysis of this stereotypic behavior was evaluated in the first 10 min of the OF. No differences were detected in grooming time between any of the groups (Fig. 3.30 A). However, the effect of the genotype factor was nearly significant ($p = 0.059$), which reflects the general tendency for a lower grooming time of CHL1 KO animals relative to WT animals. Despite no differences were found between treatments, the treatment factor had a significant effect ($p = 0.013$) shown by the tendency of

sulpiride and quinpirole to decrease grooming time of WT and CHL1 KO mice compared to vehicle treated mice. Female mice showed a tendency to spend less time grooming than males, which was statistically different in vehicle-treated CHL1 KO mice (Fig. 3.30 B). Grooming latency of female mice was not different, while vehicle-treated CHL1 KO males started grooming earlier than WT mice and quinpirole treated CHL1 KO males were the ones taking more time for the first grooming compared to vehicle treated mice (Fig. 3.30 C).

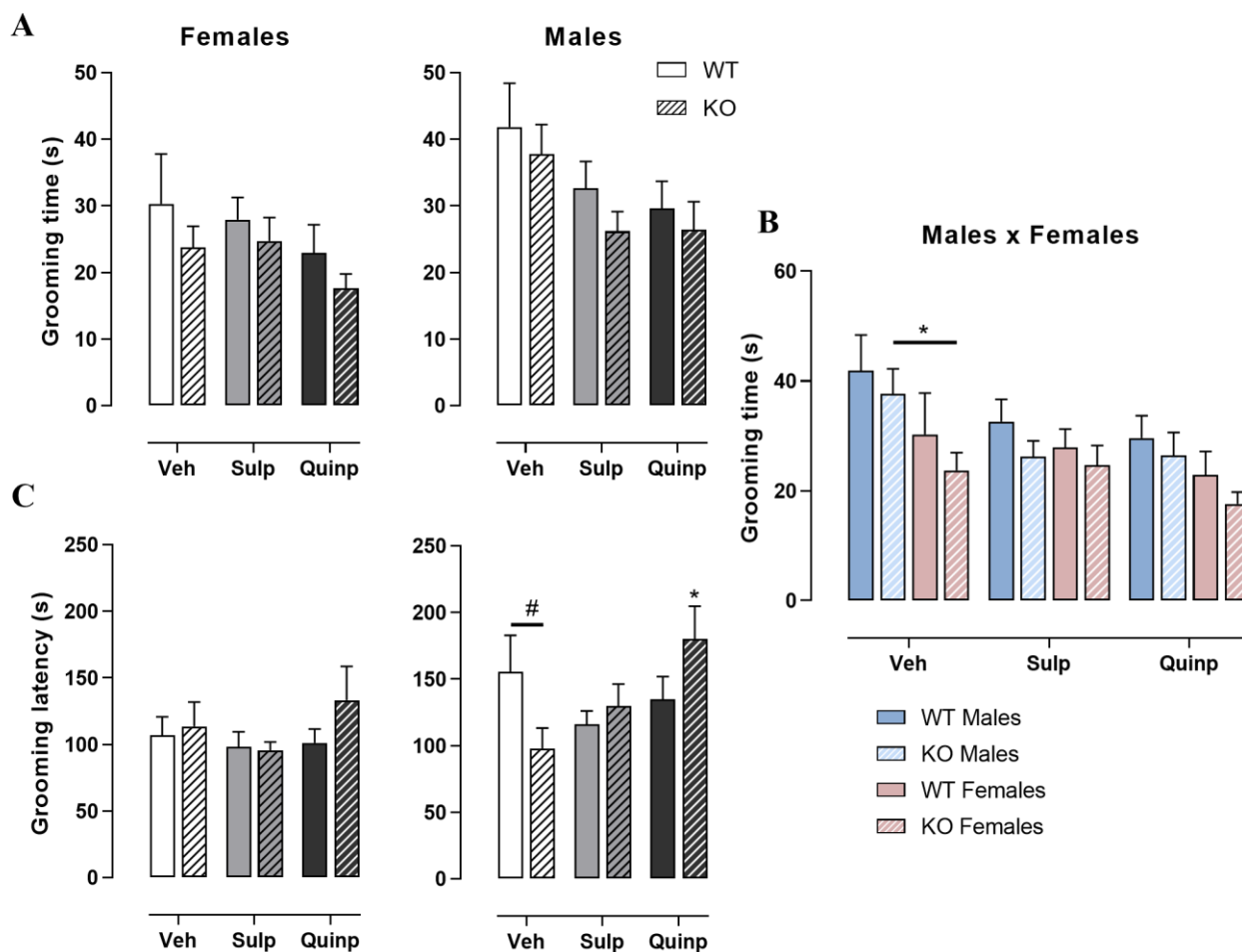


Figure 3.30. Grooming behavior tends to be lower in CHL1 KO mice and to decrease with sulpiride and quinpirole treatments in the OF test. 3-month-old female and male WT and CHL1 KO littermates were treated with a single i.p. injection of vehicle, sulpiride (1 mg/kg), or quinpirole (0.02 mg/kg) 2 min before the trial, and grooming behavior was explored in the first 10 min of the test. Grooming time (s) was obtained for female and male mice (A) and was compared between sexes for each treatment (* $p < 0.05$) (B). (C) Grooming latency (s) is presented for female and male mice. Values are presented as mean + SEM ($n = 11-13$ mice per group) and were analyzed with three-way ANOVA ((A/B): genotype: $F(1,132) = 3.627$, $p = 0.059$, treatment: $F(2,132) = 4.47$, $p = 0.013$, sex: $F(1,132) = 9.731$, $p = 0.002$; (C): three-way ANOVA, genotype x treatment: $F(2,132) = 3.386$, $p = 0.037$) followed by Bonferroni correction post-hoc test (* $p < 0.05$, statistical difference from vehicle-treated correspondent genotype; # in case of genotype difference within treatment).

The last stereotypic behavior analyzed was the jumping behavior against the wall which can be stress-induced during the first 10 min of the OF. Vehicle-treated females showed the same level of jumping and sulpiride treatment increased the number of wall jumpings in WT females relative to CHL1 KO females. Vehicle-treated WT males displayed a higher number of wall jumpings than CHL1 KO males but the same behavior was not present in sulpiride- or quinpirole-treated males (Fig. 3.31).

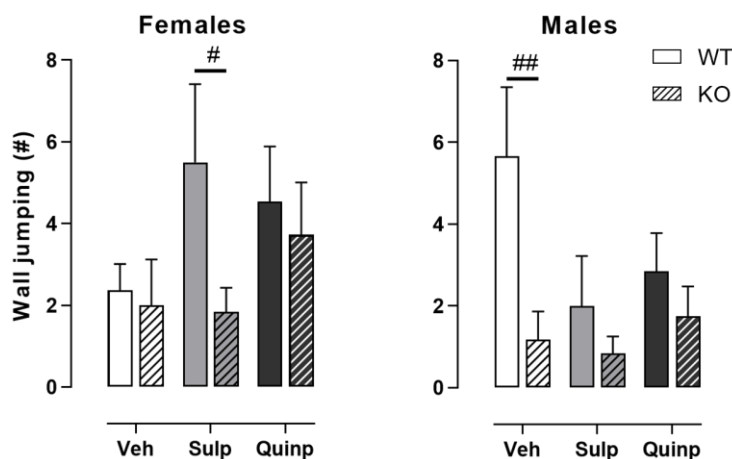


Figure 3.31. Sulpiride treatment impact wall jumping behavior in WT females and quinpirole treatment abolish the difference in jumping behavior between WT and CHL1 KO males in the OF test. 3-month-old female and male WT and CHL1 KO littermates were treated with a single i.p. injection of vehicle, sulpiride (1 mg/kg), or quinpirole (0.02 mg/kg) 2 min before the trial, and jumping behavior against the wall was quantified for female and male mice in the first 10 min of the test. Values are presented as mean + SEM (n = 11-13 mice per group) and were analyzed with three-way ANOVA (genotype: $F(1,132) = 8.618$, $p = 0.004$) followed by Bonferroni correction post-hoc test ($\#p < 0.05$, $##p < 0.01$, genotype difference within treatment).

The analysis of the locomotor activity revealed that while female WT and CHL1 KO mice did not differ in the level of activity, male CHL1 KO mice moved 15% less and at a slower rate than WT mice. The pharmacological modulation of DRD2 produced genotype- and sex-dependent effects on spontaneous locomotion, altering the behavior intrinsic to the CHL1 KO phenotype. DRD2 antagonism with sulpiride affected particularly the CHL1 KO females by decreasing the distance moved by 18% and the average speed compared to WT animals in the first 10 min and compared to the vehicle-treated mice during the entire 30 min of the test. Compared to the vehicle-treated mice, quinpirole treatment produced a hypolocomotion in all groups, reducing the distance moved by 25% for WT and 36% for CHL1 KO females, and 36% in WT and 22% in CHL1 KO males, along with a decrease in time moving and average speed for all groups. Furthermore, a delayed onset of quinpirole-induced hypolocomotion

was revealed in CHL1 KO animals since a decrease in distance moved or time moving occurs after 7 min of the test, a much later stage than in WT animals, where it occurs after 3 min.

The exploration of the center zone was not strongly affected by genotype or treatments, although some tendencies should be highlighted. Sulpiride treatment slightly increased the presence of CHL1 KO females in the center of the arena in the first 10 min of the test. With the same treatment, CHL1 KO males spent more time moving in the center than WT animals for the entire duration of the test. Similarly as seen for general locomotor activity, treatment with quinpirole decreased the level of activity in the central zone of female and male mice, with greater impact in the latter during the 30 min of the test.

Unsupported rearing behavior was performed more often by CHL1 KO animals than by WT mice, which was statistically significant for vehicle-treated CHL1 KO males and sulpiride-treated CHL1 KO females. Supported rearing behavior was different between WT and CHL1 KO females treated with sulpiride. Compared to vehicle treatment, quinpirole showed the tendency to decrease supported rearing numbers at similar levels between WT and CHL1 KO mice. Of note, during the time course of the test, this reduction occurred after 4 min in WT females and 6 min in WT males, whilst the same reduction was only evident much later in the case of the CHL1 KO mice (at 8 min for female and 10 min for male mice).

Despite no differences found in grooming time between genotypes or treatments, CHL1 KO animals showed a tendency to spend less time grooming than WT animals and in turn, sulpiride and quinpirole treatments seem to decrease this parameter. Jumping behavior is another parameter that was less prevalent in CHL1 KO males, being only statistically different between vehicle-treated males. Vehicle-treated females did not show differences, but sulpiride increased the wall jumping in WT females compared to CHL1 KO females. Fecal boli deposition was not different between genotypes; however, DRD2 agonism with quinpirole significantly increased its incidence in male mice.

Lastly, sex differences were detected in different parameters and showed that female mice moved significantly longer distances than male mice, with an increase of 20% for vehicle-treated CHL1 KO mice, 16% for sulpiride-treated WT mice, and 20% for quinpirole-treated WT mice. Additionally, female WT mice had the tendency to prefer the center zone more than male WT mice and the tendency to spend less time grooming.

3.4.2 Y-maze: short-term working spatial memory

Previous literature connects the ablation of CHL1 in mice with impairments in working memory duration, identifying a slower processing speed in a reinforced alternation task⁴⁵ and an intra-trial interval T-maze⁴⁴. The present test targets the capacity to retain and manipulate short-term memory, specifically spatial working memory, while accessing spontaneous alternation in a free-choice procedure. Due to an innate curiosity to explore previously unvisited areas, when rodents are placed in a three-arm maze, an intact working memory will make them remember the previously visited arm and mice will show a tendency to enter a less recently visited arm^{318–320}.

To investigate whether CHL1 modulates D2DR signaling and D2DR-mediated short-term working memory, female and male WT and CHL1 KO mice were acclimated to the behavioral room for 30 min prior to i.p. administration of vehicle, sulpiride, and quinpirole solution which were administered 2 min before the trial. Locomotor activity on the Y-maze was monitored over 15 min and spontaneous alternation was evaluated by considering the first 24 alternations within the 3 arms. An arm entry was considered when the mouse entered the arm with all four paws and a correct alternation was defined as the consecutive entry into the three different arms (Fig. 3.32 A). The percentage of correct alternations considering the first 24 alternations was then calculated.

The analysis of the correct number of alternations out of 24 showed differences between the genotypes: vehicle-treated female and male CHL1 KO mice completed a higher number of correct alternations compared to vehicle-treated WT animals (Fig. 3.32 B). Sulpiride treatment did not affect this behavior in female mice, but sulpiride-treated abolished the genotype difference between male WT and CHL1 KO mice. Quinpirole treatment tended to decrease the number of correct alternations in CHL1 KO mice to similar levels as seen for WT mice.

Calculation of the percentage of alternations and comparison with the chance level of 50% revealed that vehicle-treated CHL1 KO mice performed significantly better than the 50% chance level, whereas WT animals performed exactly at or only slightly above the chance level (Fig. 3.32 C). While sulpiride treatment did not affect this behavior in females, CHL1 KO males treated with the same compound showed a decrease in the percentage of correct alternations and performed at the same levels as male WT mice. WT and CHL1 KO females performed similarly close to the 50% chance level with quinpirole treatment, while only WT males had a correct alternation percentage above the 50% chance level.

(Figure 3.32) 3-month-old female and male WT and CHL1 KO littermates were treated with a single i.p. injection of vehicle, sulpiride (1 mg/kg), or quinpirole (0.02 mg/kg) 2 min before the trial, and activity was monitored over 15 min. **(A)** The level of spontaneous alternation was indicated by the consecutive entry of the mouse in the three different arms of the YM (correct alternation, A-B-C), and a repetitive entry into the previously visited arm was considered an incorrect alternation (e.g., A-B-C-B). **(B)** Number of correct alternations out of a total of 24 were analyzed for female and male mice. **(C)** Percentage of correct alternations was compared to the chance level of 50% for female and male mice. **(D)** Time to complete 24 alternations was obtained for female and male mice. **(E)** Fecal boli numbers were counted for the entire duration of the test. Values are presented as mean + SEM (n = 11-13 mice per group) and were analyzed with three-way ANOVA (B,E) ((B): genotype: $F(1,131) = 10.960$, $p = 0.001$, followed by Bonferroni correction test), and Brown-Forsythe ANOVA (D) ((female): $F(5, 50.028) = 15.460$, $p < 0.0001$; (male): $F(5, 57.705) = 8.992$, $p < 0.0001$, followed by Games-Howell post-hoc test) (* $p < 0.05$, ** $p < 0.01$ and **** $p < 0.0001$, statistical difference from vehicle-treated correspondent genotype; # in case of genotype difference within treatment). Student's t-test against the 50% chance level was also used (C)((female): veh KO ($t(11) = 3.554$, $p = 0.005$), sulp KO ($t(12) = 3.348$, $p = 0.006$); (male): veh KO ($t(10) = 3.365$, $p = 0.007$), quinp WT ($t(12) = 3.790$, $p = 0.005$) (*, significance against the 50% chance level).

In the time taken to complete the 24 alternations, no differences were detected between genotypes and vehicle or sulpiride treatments (Fig. 3.32 D). However, there was an increase in the time to complete the trial in female and male WT and female CHL1 KO mice treated with quinpirole. Furthermore, despite a greater tendency for elevated fecal boli deposits in quinpirole-treated animals, no differences were detected between groups (Fig. 3.32 E).

Locomotor activity during the 15 min of the YM test was analyzed and used as a control parameter of pharmacological efficacy of the administered drugs across the behavioral experiments. During the 15 min of the test, CHL1 KO males showed significantly lower activity than their WT littermates when they were treated with vehicle solution (Fig. 3.33 A left). Sulpiride treatment significantly decreased locomotor activity only in CHL1 KO females relative to WT animals and compared to vehicle treatment. Quinpirole treatment decreased the distance moved by female and male WT mice and female CHL1 KO mice relative to vehicle treatment as well. Distance moved across 3 min time bins in the YM showed that quinpirole treatment strongly reduced the activity of female and male WT mice when compared to vehicle treatment during the 15 min of the test. The same comparison in the CHL1 KO group revealed that the hypolocomotion induced by quinpirole was only present at a few time points in females, and was not detected in males (Fig. 3.33 A right). Differences between sexes were found between CHL1 KO mice treated with vehicle and WT mice treated with sulpiride (Fig. 3.33 B). The total time moving was lower in CHL1 KO males relative to their WT littermates treated with vehicle, and was decreased by quinpirole treatment in female and male WT and female CHL1 KO mice compared to the vehicle treatment (Fig. 3.33 C).

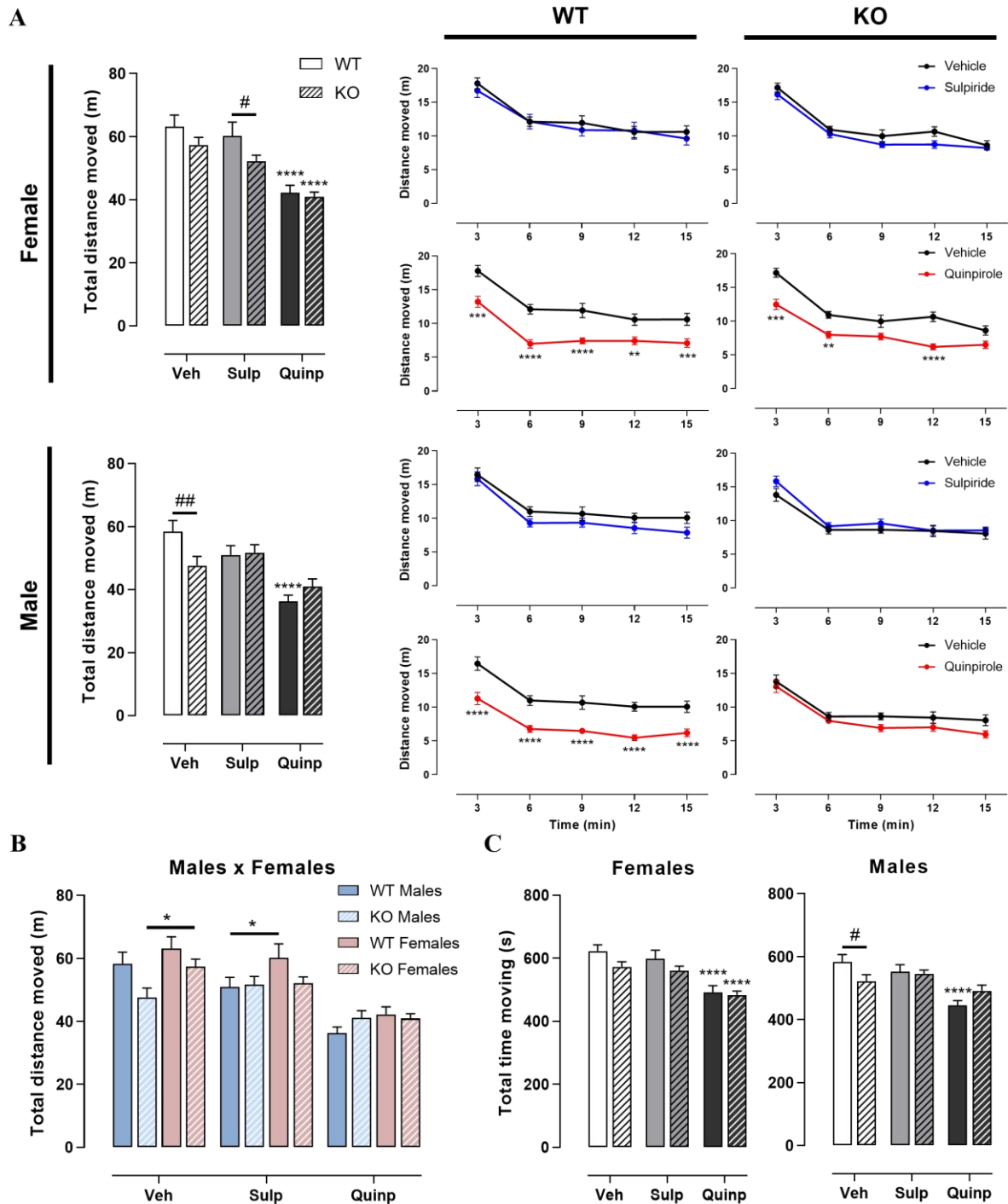


Figure 3.33. Total locomotor activity is affected by sulpiride treatment in CHL1 KO females and quinpirole-induced hypolocomotion is delayed in CHL1 KO mice of the YM test. 3-month-old female and male WT and CHL1 KO littermates were treated with a single i.p. injection of vehicle, sulpiride (1 mg/kg), or quinpirole (0.02 mg/kg) 2 min before the trial, and activity was monitored for 15 min. (A) Total distance moved (m) of female and male mice is shown and was compared in 3 min time-bins between DRD2-specific treatment and vehicle treatment for each genotype and sex group. (B) Total distance moved was compared between sexes for each treatment (* $p < 0.05$). (C) Total time moving was obtained for female and male mice.

(Figure 3.33) Values are presented as mean + SEM (n = 11-13 mice per group) and were analyzed with three-way ANOVA ((A left/B): genotype: $F(1,132) = 4.260$, $p = 0.041$, treatment: $F(2,132) = 39.211$, $p = 0.0001$, sex: $F(1,132) = 9.466$, $p = 0.003$, genotype x treatment: $F(2,132) = 3.085$, $p = 0.049$; (C): treatment: $F(2,132) = 31.791$, $p = 0.0001$, genotype x treatment: $F(2,132) = 3.848$, $p = 0.024$; followed by Bonferroni correction post-hoc test (* $p < 0.05$, ** $p < 0.01$, **** $p < 0.0001$, statistical difference from vehicle-treated correspondent genotype; # in case of genotype difference within treatment) and three-way repeated measures ANOVA ((A right): genotype: $F(1,132) = 4.260$, $p = 0.041$, treatment: $F(2,132) = 39.211$, $p = 0.0001$, genotype x treatment: $F(2,132) = 3.085$, $p = 0.049$, followed by Bonferroni correction post-hoc test (** $p < 0.01$, *** $p < 0.001$, **** $p < 0.0001$)).

The assessment of the short-term working spatial memory through the analysis of spontaneous alternations in a YM revealed that vehicle-treated CHL1 KO mice showed a better aptitude to complete the test with a higher number of correct alternations above the 50% chance level while taking the same time to complete it as the WT animals. Compared to vehicle treatment, sulpiride did not affect the performance of female WT or CHL1 KO mice, whereas CHL1 KO males performed just at the 50% chance level as WT animals. DRD2 agonism with quinpirole did not affect the level of correct alternations in female WT mice but reduced it in female CHL1 KO mice relative to vehicle treatment, causing as well an increase in the time taken to complete the trial for both genotypes. Of note, male WT mice showed a percentage of correct alternations above the 50% chance level with quinpirole treatment, despite a longer time taken to complete the 24 alternations. The same treatment of CHL1 KO males reduced the correct number of alternations to the chance level of 50% compared to vehicle treatment.

The analysis of spontaneous locomotion in the YM during the 15 min of the test revealed a pattern very similar to that found in the first 10 min of the OF test, the most important being the delayed and reduced hypolocomotion induced by quinpirole in CHL1 KO mice that was present at an earlier stage in case of the WT animals, compared to vehicle treatment.

3.4.3 Novelty-induced behavior: the spontaneous exploration of a novel object

Accumulating research has shown that D2DR pharmacological modulation or availability can directly impact novel stimulus and novelty-seeking behaviors^{341,342}. Ablation of CHL1 in mice has also been linked to mild impairment of novelty-seeking behavior: an initial hesitation to explore a new object was found but no effect on the total time of its exploration^{43,44}. Instead of a novel object test based on a previous recollection of an object (familiar object), my thesis focuses on a novelty-induced paradigm exclusively influenced by a new stimulus (stimulus novelty) without requiring any pre-existing recognition memory.

To investigate whether CHL1 and D2DR together influence risk-assessment behavior when animals are confronted with a completely new stimulus, like an object, female and male WT and CHL1 KO mice were acclimated to the behavioral room for 30 min prior to i.p. administration of vehicle, sulpiride, and quinpirole solution. The mice were placed in the corner of the arena with the new object located in the center. Locomotor activity and mouse-object interaction were monitored over 20 min. Interaction with the object was measured through distance and time moved by the nose (nose-point) in the area nearby the object (object zone) and the remaining area is represented by the outside zone (Fig. 3.34 A).

During the 20 min of the test, the total distance moved by the nose-point near the object was not affected by genotype vehicle- or sulpiride-treated mice (Fig. 3.34 B). However, CHL1 KO females showed a tendency to explore the object more than WT mice, as indicated by a $p = 0.154$ for the genotype factor. Quinpirole treatment did not change the activity in female mice but altered the activity between WT and male CHL1 KO mice. When comparing the sexes, a tendency for males to move more than females in the object zone was found, being statistically significant between CHL1 KO animals treated with quinpirole (Fig. 3.34 C). The distance moved across 2 min time bins did not differ between the different conditions (Fig. 3.34 D), although the tendency of CHL1 KO females to move more than WT females was present in the first minutes of the test. Significant effects were not detected in other time windows or time bins of the total distance moved.

Regarding the total time spent near the object, CHL1 KO mice tended to explore the object more than WT mice in all groups, as indicated by a $p = 0.007$ for the genotype factor (Fig. 3.35 A). However, only quinpirole-treated CHL1 KO males spent significantly more time near the object than WT males. When comparing the sexes, a tendency for males to move more than females in the object zone was found, being statistically significant between CHL1 KO animals treated with quinpirole (Fig. 3.35 B). Across the 2 min time bins, the tendency of CHL1 KO mice to explore the object more than WT animals was present throughout the test

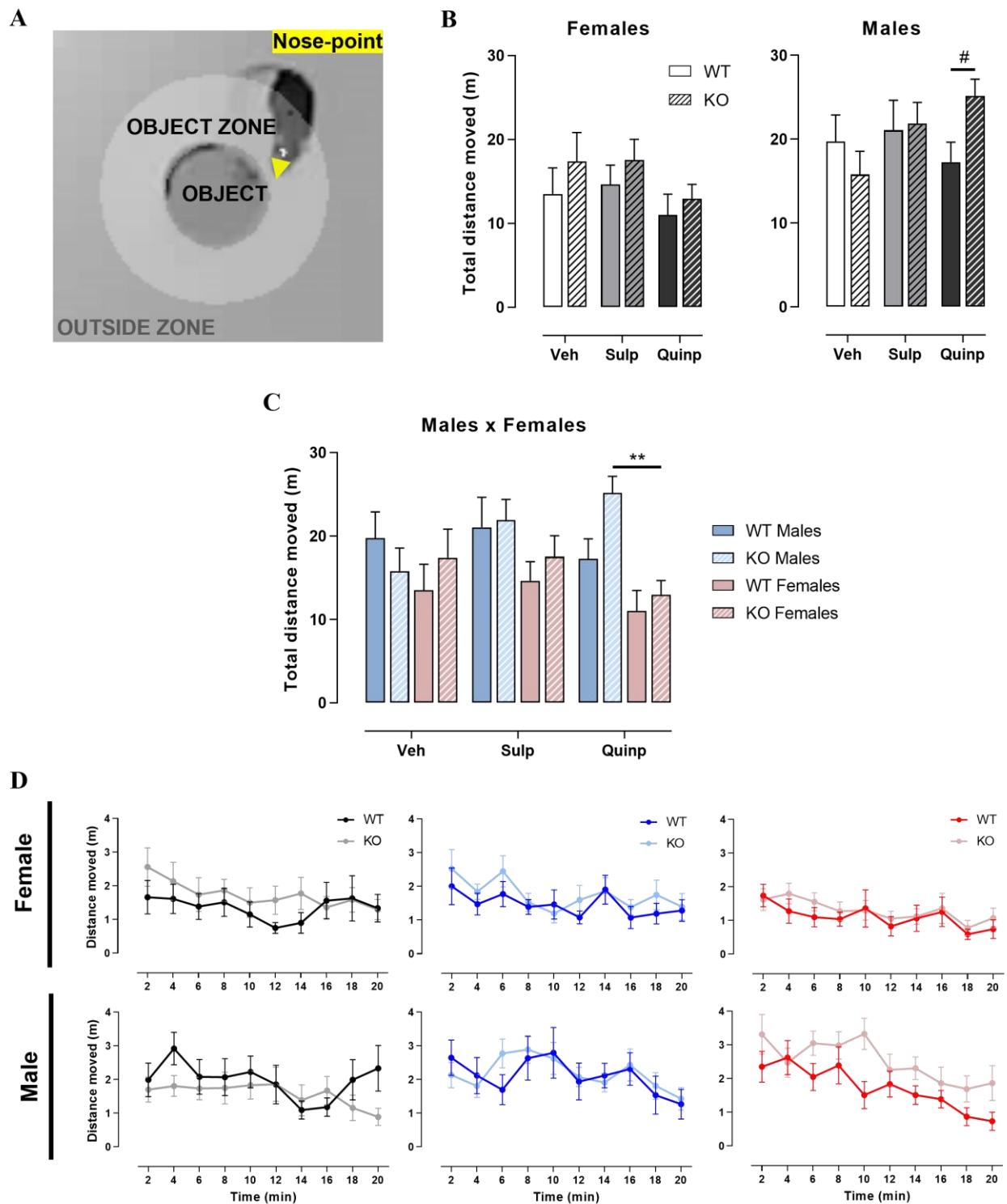


Figure 3.34. Novel object exploration is similar in female mice while quinpirole treatment altered the object exploration between male WT and CHL1 KO mice. 3-month-old female and male WT and CHL1 KO littermates were treated with a single i.p. injection of vehicle, sulpiride (1 mg/kg), or quinpirole (0.02 mg/kg) 2 min before the trial, and interaction of the mice with the object was monitored for 20 min. (A) A novel object was placed in the middle of the arena and the mice-object interaction was evaluated with the presence of the nose-point inside of the object zone. The remaining area is represented by the outside zone. Total distance moved by the nose-point in the object zone is shown for female and male mice (B) and was compared between sexes for each treatment (** $p < 0.01$) (C). (D) Total distance moved was compared between genotypes for each treatment and sex group in 2 min time-bins.

(Figure 3.34) Values are presented as mean + SEM (n = 11-13 mice per group) and were analyzed with three-way ANOVA ((B/C): sex: $F(1,132) = 13.081$, $p = 0.0001$, followed by Bonferroni correction post-hoc test and three-way repeated measures ANOVA (D) ($p > 0.05$).

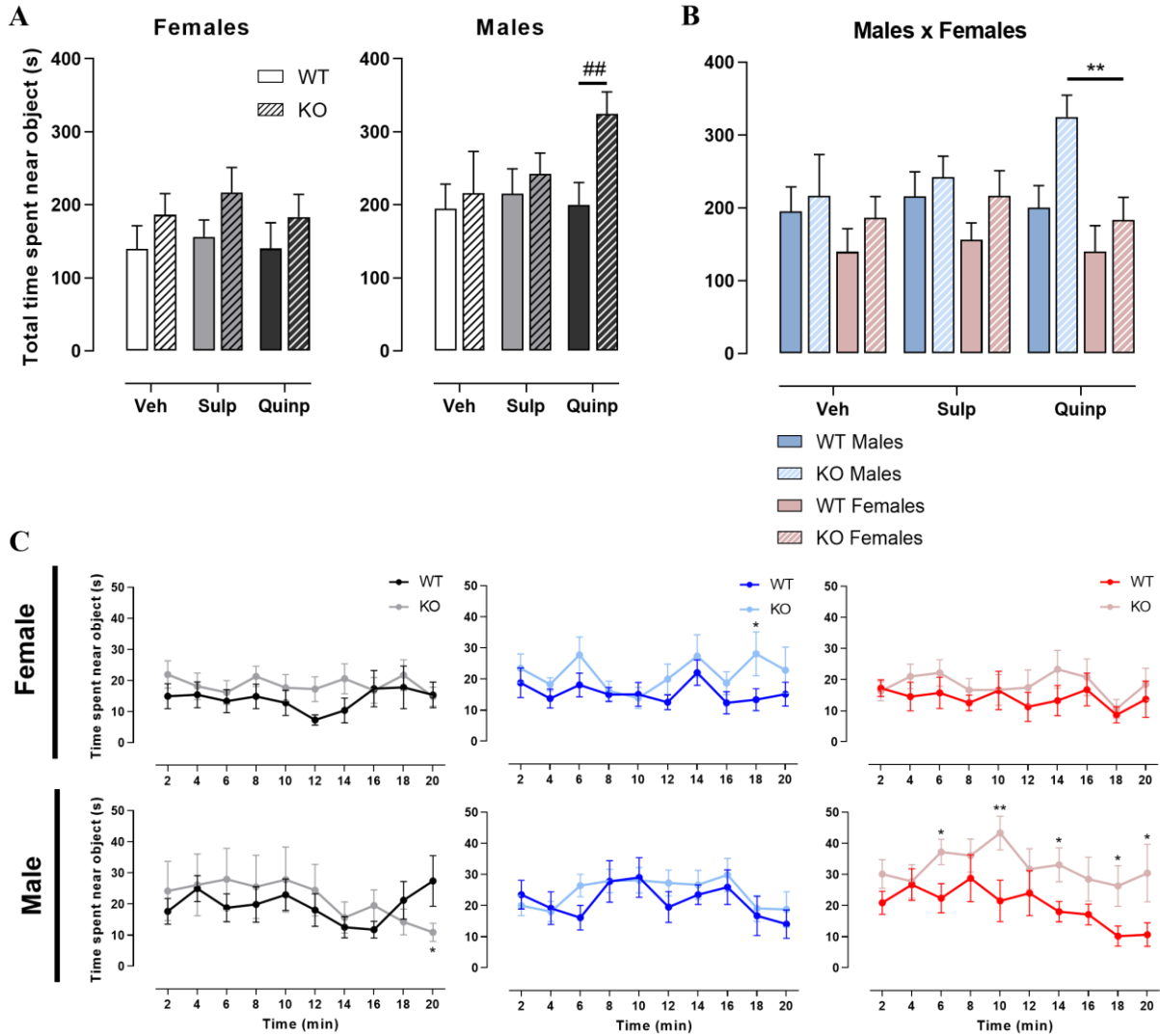


Figure 3.35. Time spent near the object is higher in quinpirole-treated CHL1 KO males. 3-month-old female and male WT and CHL1 KO littermates were treated with a single i.p. injection of vehicle, sulpiride (1 mg/kg), or quinpirole (0.02 mg/kg) 2 min before the trial, and interaction of the mice with the object was monitored for 20 min. Total time spent near the object by the nose-point is shown for female and male mice (A) and was compared between sexes for each treatment (** $p < 0.01$) (B). (C) Time spent near the object was compared between genotypes for each treatment and sex group in 2 min time-bins. Values are presented as mean + SEM (n = 11-13 mice per group) and were analyzed with three-way ANOVA ((A/B): genotype: $F(1,132) = 7.625$, $p = 0.007$, sex: $F(1,132) = 10.057$, $p = 0.002$, followed by Bonferroni correction post-hoc test ((A): $## p < 0.01$, genotype difference within treatment)) and three-way repeated measures ANOVA ((C): genotype: $F(1,132) = 7.625$, $p = 0.007$, sex: $F(1,132) = 10.057$, $p = 0.002$, followed by Bonferroni correction post-hoc test (* $p < 0.05$, ** $p < 0.01$)).

Analysis of total time moving near the object showed a general tendency for CHL1 KO animals to move longer time close to the object than WT mice (Fig. 3.36 A). Although vehicle- and sulpiride-treated CHL1 KO females tended to perceive the object more quickly than WT females, latency to first reach the object revealed no differences between genotype, treatment, or sex factors (Fig. 3.36 B). Fecal boli deposits were registered and showed no differences between genotypes or treatments in female and male mice (Fig. 3.36 C and D). A statistical difference is only detected in sulpiride-treated CHL1 KO mice just because vehicle-treated CHL1 KO mice tend to have higher occurrences of fecal boli.

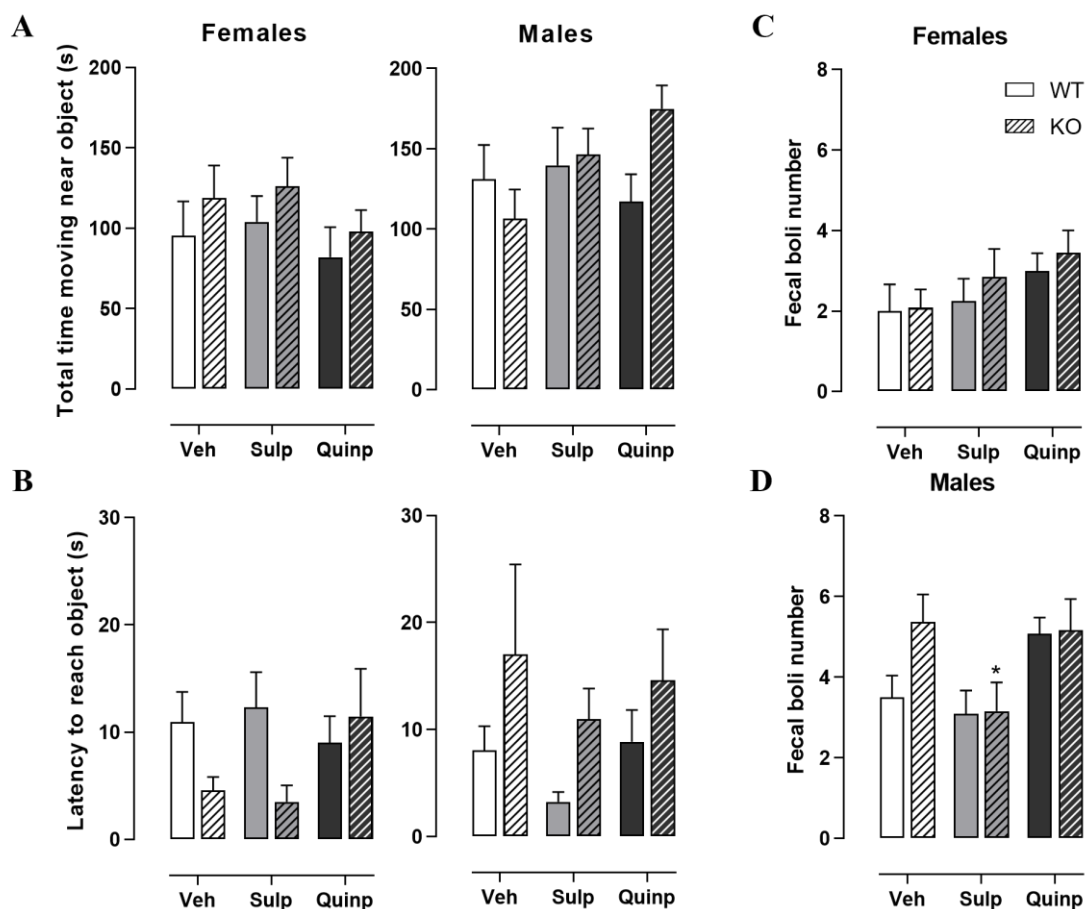


Figure 3.36. Effects of sulpiride and quinpirole treatments on parameters of novel-object exploration. 3-month-old female and male WT and CHL1 KO littermates were treated with a single i.p. injection of vehicle, sulpiride (1 mg/kg), or quinpirole (0.02 mg/kg) 2 min before the trial, and interaction of the mice with the object was monitored for 20 min. (A) Total time moving near the object by the nose-point is shown for female and male mice. (B) Latency to first reach the object was obtained for female and male mice. Fecal boli numbers were counted in female (C) and male (D) mice for the entire duration of the test. Values are presented as mean + SEM (n = 11-13 mice per group) and were analyzed with three-way ANOVA ((F): treatment: $F(2,132) = 5.359$, $p = 0.006$, followed by Bonferroni correction post-hoc test (* $p < 0.05$, statistical difference from vehicle-treated correspondent genotype)).

The distance moved by the nose-point during the 20 min of the novel object test was analyzed and used as a control parameter of DRD2-pharmacological efficacy across the behavioral experiments. Although the activity of WT and CHL1 KO mice was similar for both sexes treated with vehicle, male CHL1 KO mice show a tendency for lower locomotor activity relative to WT males ($p = 0.062$). Sulpiride treatment significantly decreased activity only in CHL1 KO females relative to WT females and compared to vehicle treatment. Quinpirole treatment decreased distance moved in female and male WT mice and female CHL1 KO mice relative to vehicle treatment as well. However, the same treatment elicits the tendency for CHL1 KO females to move less than WT females ($p = 0.056$) (Fig. 3.37 A left). Distance moved across 2 min time bins showed that quinpirole treatment reduced levels of activity in female WT mice and more strongly in CHL1 KO females compared to vehicle-treated mice (Fig. 3.37 A right). The same comparison in the male mice revealed that hypolocomotion induced by the treatment started at an earlier time point in WT males and was not present at all in CHL1 KO males. Focusing on sex differences, there is a general tendency for female mice to move less than male mice, and this was significant between CHL1 KO mice treated with sulpiride and quinpirole (Fig. 3.37 B). The total time moving was lower for CHL1 KO females relative to WT littermates treated with sulpiride treatment and was decreased by quinpirole treatment in female and male WT and female CHL1 KO mice compared to the vehicle-treated mice (Fig. 3.37 C).

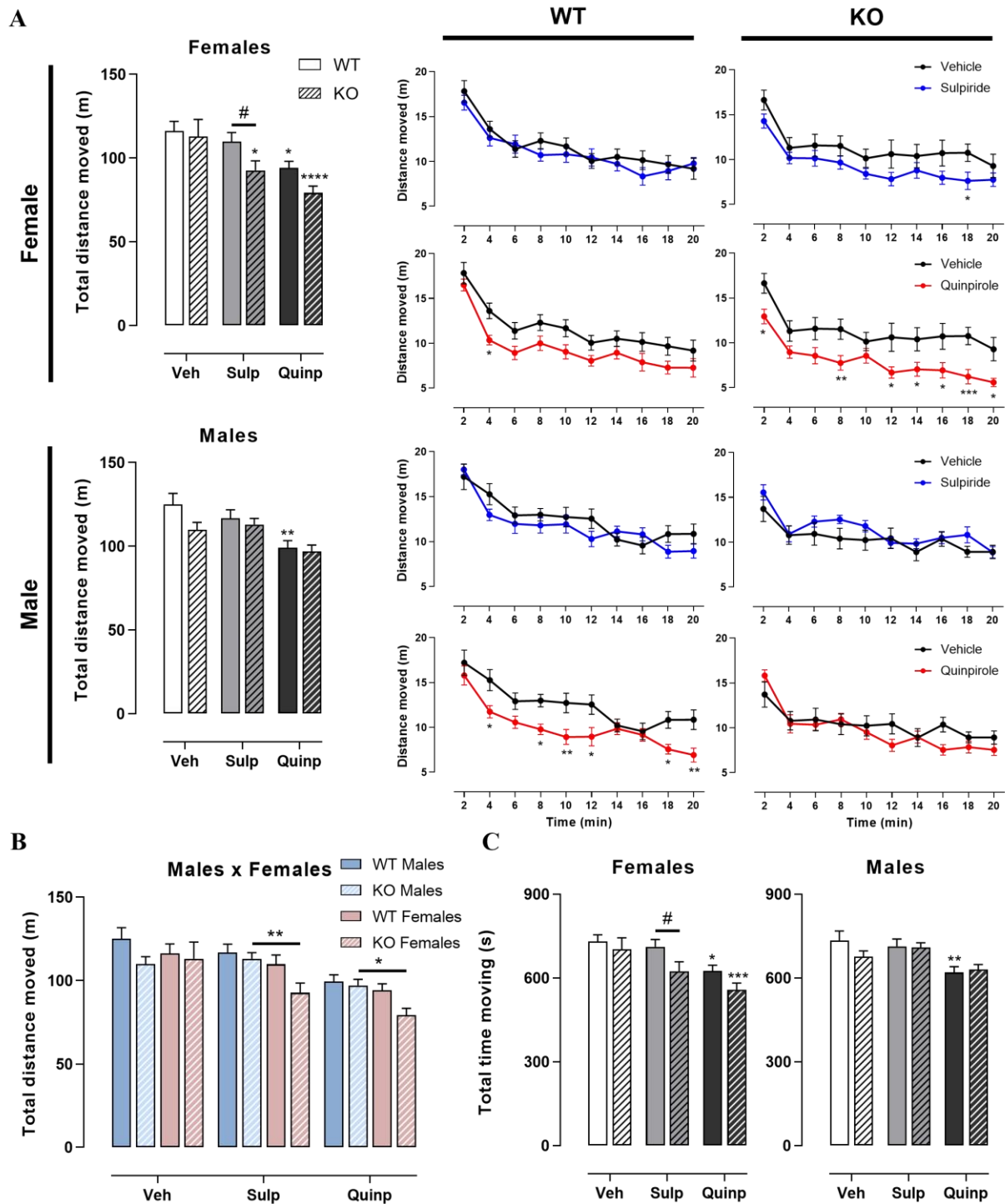


Figure 3.37. Locomotor activity of CHL1 KO females is decreased by sulpiride treatment and CHL1 KO males do not show hypolocomotion induced by quinpirole treatment. 3-month-old female and male WT and CHL1 KO littermates were treated with a single i.p. injection of vehicle, sulpiride (1 mg/kg), or quinpirole (0.02 mg/kg) 2 min before the trial, and locomotor activity was monitored for 20 min using the nose-point. **(A)** Total distance moved for female and male mice is shown and was compared in 2 min time-bins between DRD2-specific compounds and vehicle treatment for each genotype and sex group. **(B)** Total distance moved was compared between sexes for each treatment (* $p < 0.05$, ** $p < 0.01$). **(C)** Total time moving was obtained for female and male mice.

(Figure 3.37) Values are presented as mean + SEM (n = 11-13 mice per group) and were analyzed with three-way ANOVA ((A left/B): genotype: $F(1,131) = 8.814$, $p = 0.004$, treatment: $F(2,131) = 19.030$, $p = 0.0001$, sex: $F(1,131) = 8.500$, $p = 0.004$; (C): genotype: $F(1,131) = 6.483$, $p = 0.012$, treatment: $F(2,131) = 16.773$, $p = 0.0001$; followed by Bonferroni correction post-hoc test (* $p < 0.05$, ** $p < 0.01$, *** $p < 0.001$, **** $p < 0.0001$, statistical difference from vehicle-treated correspondent genotype; # in case of genotype difference within treatment)) and three-way repeated measures ANOVA ((A right): genotype: $F(1,132) = 10.124$, $p = 0.002$, treatment: $F(2,132) = 15.844$, $p = 0.0001$, followed by Bonferroni correction post-hoc test (* $p < 0.05$, ** $p < 0.01$, *** $p < 0.001$)).

The present results comprise different parameters that can help us to better understand the effect of the CHL1 and DRD2 interaction on behaviors induced by a novel external stimulus. Although not statistically significant, the first thing to point out is an overall tendency for CHL1 KO mice to engage more with the novel object than WT mice. Compared to WT mice, the total time spent near the object showed a tendency to be higher in vehicle-treated CHL1 KO females (25%) and males (8%), sulpiride-treated CHL1 KO females (28%) and males (11%), and quinpirole-treated CHL1 KO females (24%) and males (38%). This trend was more robust in vehicle- and sulpiride-treated CHL1 KO females since the total distance moved near the object was increased by 22% and 16% compared to WT females. Interestingly, these same groups were the only ones showing a tendency to perceive the object more quickly than WT females, which took 6.38 s or 8.81 s longer than vehicle- or sulpiride-treated CHL1 KO females. Overall, sulpiride treatment did not affect the natural tendency of the animals to explore the object. Quinpirole treatment showed a tendency to decrease activity near the object in WT males, whereas CHL1 KO males were not affected by the hypolocomotion effect induced by the treatment and therefore explored the object for a longer time than WT males.

The analysis of spontaneous locomotion in the outside zone during the NI test revealed a similar pattern to that found in the previous behavioral tests. DRD2 antagonism with sulpiride produced a reduction in the activity of CHL1 KO females compared to WT females and agonism with quinpirole caused an instant reduction of locomotion in male WT mice compared to vehicle treatment, while no effect was found in male CHL1 KO mice. Certain parameters are contradictory to previous results, such as: contrasting to WT females, CHL1 KO females did not show a delayed hypolocomotion state induced by quinpirole relative to vehicle treatment; and female mice tended to have lower levels of activity than male mice, which was also present in the sex differences of object exploration. Given that the activity of the mice near the object displayed a distinct exploratory pattern to that exhibited in the outside arena, this behavior can be considered to be specifically induced by the novel stimulus.

Chapter VI

Discussion

4 Discussion

The connection between CHL1 and the dopaminergic system is of interest due to CHL1's role in guiding and promoting the neuronal development of ventral midbrain structures, thereby contributing significantly to the development of dopaminergic pathways^{20,74}. Furthermore, *CALL* polymorphisms are linked to neuropsychiatric disorders like ASD and schizophrenia^{49,51,52,343}, which share behavioral and physiological similarities with CHL1 deficiency^{27,44,46,47}, which has sparked interest in investigating this relationship in more detail. Of note, ASD and schizophrenia both involve impairments in DRD2 signaling, suggesting that CHL1's interaction with DRD2 could serve as a conceivable mechanism by which CHL1 influences the dopaminergic system. Notably, previous research of our group confirmed CHL1's direct interaction with DRD2, a differential role of CHL1 in the internalization of the short versus long DRD2 isoforms, and the impact of CHL1 deficiency on pre- and postsynaptic dopaminergic signaling in the striatum³⁸. However, the functional consequences of the CHL1-dependent modulation of dopaminergic signaling through DRD2 had yet to be explored.

My thesis aimed to comprehensively study the functional interaction between CHL1 and DRD2. The results reveal that CHL1 interacts with DRD2 in presynaptic dopaminergic neurons and postsynaptic striatal neurons, both *in vivo* and *in vitro*. While the absence of CHL1 in these neurons does not affect their normal physiological functions, it impacts DRD2-related functions like presynaptic signal transduction and postsynaptic neuronal and synaptic morphology. Behavioral analysis of CHL1 KO animals revealed genotype- and sex-specific responses to the DRD2 antagonist sulpiride or agonist quinpirole. Moreover, the absence of CHL1 notably reduced the behavioral sensitivity to the DRD2 agonist quinpirole, with a distinct time window effect between WT and CHL1 KO mice.

4.1 CHL1 and DRD2 interact in presynaptic dopaminergic and postsynaptic striatal neurons

In addition to the discovery of the direct binding of the extracellular domain of CHL1 to the first extracellular domain of DRD2, previous data from our laboratory have shown that this interaction can be detected in striatal sections of adult WT mice³⁴⁴. CHL1 expression has also been reported in developing dopaminergic neurons of the ventral midbrain^{20,30}. To investigate the CHL1 and DRD2 interaction and its impact on pre- and postsynaptic dopaminergic signaling, the close proximity of CHL1 and DRD2 was determined with PLA and simultaneous immunostaining of dopaminergic markers (TH or DARPP-32) to stain striatal sections of adult WT males and primary neurons from ventral midbrain or striatal cultures. My results confirm the presence of CHL1 and DRD2 in close proximity in TH-positive neurons of the striatal tissue and cultured ventral midbrain neurons, indicating

the presynaptic existence of this interaction in dopaminergic neurons and their terminals in the striatum³⁸. Similarly, the same observation was made in DARPP-32-positive neurons of striatal tissue and cultured striatal neurons, suggesting an interaction of CHL1 and DRD2 postsynaptically in the striatal MSNs³⁸.

The co-localization of CHL1 and both DRD2 isoforms was also confirmed in transfected HEK293 cells expressing CHL1 and either DRD2_S or DRD2_L³⁸. Additionally, studies exploring the expression and behavioral functions of these DRD2 isoforms support distinct roles: DRD2_S is primarily expressed presynaptically and plays a role in presynaptic dopaminergic neurons of the ventral midbrain, while DRD2_L is predominantly postsynaptically expressed and regulates dopaminergic-induced signaling in striatal MSNs^{119,133,138}. My findings, which demonstrate the co-localization of CHL1 and DRD2 in striatal tissue and primary neurons, not only complement the observations of CHL1's interaction with both DRD2 isoforms in HEK293 cells but also provide a biological context for understanding the significance of this interaction. These findings suggest that CHL1 might regulate the functions of DRD2_S presynaptically in dopaminergic neurons and their axonal projections to the striatum. In addition, CHL1 potentially regulates postsynaptic functions of DRD2_L in MSNs.

Previously, CHL1 has been detected at the presynaptic axonal plasma membrane of cultured inhibitory and excitatory hippocampal neurons³⁴. At synaptic vesicles in these terminals, CHL1 recruits and interacts with the heat shock cognate 70 kDa protein (Hsc70) to regulate clathrin uncoating from clathrin-coated vesicles³⁴. Upon synaptic activation, CHL1 and Hsc70 are endocytosed, and the disruption of the CHL1-Hsc70 complex leads to an abnormal accumulation of clathrin-coated synaptic vesicles. Additionally, CHL1 forms protein complexes with Hsc70 and other chaperones, aiding in the assembly of the SNARE complex to induce synaptic vesicle exocytosis³⁵. These findings highlight the regulatory role of CHL1 during presynaptic activity, particularly in promoting synaptic vesicle endocytosis through their recycling via a clathrin-dependent pathway. Furthermore, in HEK293 cells, CHL1 has been shown to prevent quinpirole-induced internalization of DRD2_S³⁸, suggesting its potential role in regulating clathrin-dependent presynaptic DRD2 internalization. As dopaminergic terminals from the ventral midbrain mainly express DRD2_S^{119,133} and considering CHL1's function as a presynaptic regulatory protein, my thesis aimed to investigate the impact of CHL1 binding to DRD2 on presynaptic dopaminergic neuron signaling.

My results show for the first time a connection between CHL1 and the postsynaptic DRD2 in MSNs³⁸. The extracellular domain of CHL1 was demonstrated to trans-interact with HEK293 cells expressing either DRD2_S or DRD2_L, suggesting that presynaptic and postsynaptic CHL1 might bind to the DRD2 isoforms at opposite presynaptic and postsynaptic sites. Additionally, CHL1 was found in striatal parvalbumin-positive GABAergic interneurons and might also trans-interact with DRD2-expressing MSNs³⁷, which provide a feedforward inhibitory control to approximately 25-75% of MSNs^{345,346}. While the literature on the postsynaptic functions of CHL1 is limited, CHL1 KO adult

mice exhibited increased numbers of excitatory synapses and disrupted synaptic strength in the postsynaptic membrane of pyramidal cortical neurons³⁶. As CHL1 in presynaptic dopaminergic terminals or other striatal neurons can interact with postsynaptic DRD2 in MSNs and has been shown to induce postsynaptic changes in pyramidal cortical neurons, this thesis aimed to investigate how CHL1's binding to the receptor influences DRD2-dependent neurotransmission in striatal MSNs.

4.2 Functional impact of the CHL1 interaction with pre- and postsynaptic DRD2

4.2.1 CHL1 modulates agonist-induced responses of presynaptic DRD2 while basal DRD2 signaling remains unaffected *in vitro*

Presynaptic DRD2 plays a crucial role in maintaining optimal dopamine levels in the synaptic cleft through a negative feedback mechanism involving dopamine uptake and synthesis¹⁷⁸. As a rate-limiting enzyme in dopamine synthesis, TH serves as a dopaminergic marker used to assess the initiation of dopaminergic signaling cascades. The activation of the cAMP/PKA pathway, inhibited by DRD2 activation, leads to TH phosphorylation at Ser40. Therefore, measuring cAMP levels allows to assess the activity of DRD2¹⁸³. Additionally, DRD2 is involved in the regulation of the GSK3 and ERK1/2 pathways, thus phosphorylation of these proteins can be additionally assessed to investigate DRD2 modulation^{294,347}. Here, analysis of vehicle-treated primary ventral midbrain neurons (basal condition) showed similar basal TH phosphorylation at Ser40 levels in both WT and CHL1 KO neurons. There was a tendency for lower cAMP levels in CHL1 KO neurons compared to WT neurons, but no significant differences were found in phosphorylated and total GSK3 β and ERK1/2 levels. I suggest that the absence of CHL1 in the ventral midbrain neurons does not affect the presynaptic DRD2 signaling under basal conditions.

Compared to vehicle-treated WT and CHL1 KO neurons, the DRD2 antagonist sulpiride and agonist quinpirole reduced TH phosphorylation in both WT and CHL1 KO neurons. CHL1 KO neurons showed a more pronounced decrease in pTH with sulpiride treatment than WT neurons, while quinpirole had similar effects on neurons from both genotypes. While cAMP levels were not significantly altered by the treatments relative to the vehicle condition, CHL1 KO neurons exhibited lower cAMP levels than WT neurons following sulpiride and quinpirole treatment. No significant differences were observed between the genotypes in phosphorylated and total GSK3 β and ERK1/2 levels after sulpiride or quinpirole treatments.

Sulpiride, a selective DRD2 ligand with some affinity for DRD3, is frequently employed as an antagonist in binding assays, competing with dopamine and other DRD2 agonists like quinpirole^{311,348,349}. In DRD2_S-expressing PC12 cells, sulpiride prevented quinpirole's inhibitory

impact on dopamine release and TH activity after 40 minutes of co-incubation, with no observable impact from sulpiride incubation alone¹⁸⁴. Another study using rat striatal slices reported that sulpiride increased TH activity only under depolarizing conditions when slices were maintained in a K⁺-enriched medium (60 mM), but no effects were observed under normal conditions³⁵⁰. DRD2 ligands, including sulpiride, have previously been categorized as antagonists but were later found to possess inverse agonistic properties³⁵¹. Thus, depending on the condition, sulpiride can either act as a blocker or induce the opposite effect of a DRD2 agonist, including increased TH activity, dopamine release, and reduced dopamine uptake through its impact on DAT function^{184,352,353}. Consequently, by blocking DRD2 activation or inducing agonist-opposite effects, sulpiride reverses dopamine-induced inhibition of cAMP synthesis, leading to cAMP accumulation in the cytosol^{354,355}. Additionally, sulpiride promotes the activation of other pathways, leading to the deactivation of GSK3 β by increasing its phosphorylation³⁴⁷.

Based on the available literature, my findings suggest that sulpiride treatment in ventral midbrain primary neurons failed to produce the expected effect of antagonism or inverse agonism on presynaptic DRD2 signaling, regardless of the genotype of the mice. Nonetheless, the results are in line with the findings in PC12 cells expressing DRD2_s, which were not affected when treated with sulpiride alone¹⁸⁴. To conclude, the effect of sulpiride in my experimental setting remains inconclusive. It can be argued that the experimental conditions might not have been optimal for analyzing the effects of sulpiride. Previous functional studies of DRD2 signaling in other cell or neuronal systems have employed different conditions for sulpiride treatment, ranging from 10-40 μ M for 30-45 min^{184,296,297}. In my experiments, concentrations lower than the one used (30 μ M) did not produce any observable effects. As the concentration used here falls within the range employed in the literature, the 20 min incubation period might not have been long enough for neurons to respond to sulpiride action adequately. Additionally, the lack of full maturation of ventral midbrain neurons at the time of treatment (7 div) could have contributed to sulpiride's results. While literature often focuses on DRD2-related functions in ventral midbrain cultures after 5-10 days in culture^{356,357}, one study indicated that extracellular dopamine levels at 7 div are more likely to be governed by VMAT or DAT rather than DRD2, evident from the lack of sulpiride's impact³⁵⁸. Furthermore, the binding of sulpiride to DRD2 is dependent on the presence of Na⁺ ions^{359,360} and their binding affinity was shown to increase \approx 23-fold in the presence of Na⁺³⁶¹. The binding of Na⁺ to cytoplasmic allosteric binding sites within DRD2 induces conformational changes that modulate ligand binding at the orthosteric site³⁶². This phenomenon has been demonstrated to enhance the binding affinity of antagonists such as sulpiride to the receptor³⁵⁹. Conversely, the lack of Na⁺ leads to unstable conformations of sulpiride within the binding pocket, as shown by molecular dynamics simulations³⁶³. While the culture medium used for the primary cultures is presumed to provide an abundant concentration of Na⁺ necessary for the regular development and functioning of the cells, it is also plausible to speculate that the experimental conditions could have

limited the ventral midbrain neurons from achieving the required cytoplasmic Na⁺ levels for sulpiride to effectively induce DRD2 signaling. Therefore, to understand the impact of sulpiride on WT and CHL1 KO ventral midbrain neurons, it would be important to further investigate extended incubation periods and *in vitro* growth. Additionally, considering the concentration of Na⁺ as a factor in the experimental conditions could provide insights into whether lower or higher Na⁺ levels affect the current setup and impact the binding of sulpiride to DRD2.

Quinpirole-induced DRD2 inhibition has been reported to decrease cAMP levels in non-neuronal cell models^{364,365}, or to either not affect basal cAMP levels or inhibit forskolin-enhanced cAMP levels in cortical neurons³⁶⁶. Additionally, in DRD2_s-expressing PC12 cells and striatal slices from male WT rats and female WT/DRD2_L KO mice the DRD2-mediated inhibition of the cAMP pathway by quinpirole leads to a decrease in TH phosphorylation at Ser40^{119,183,184}. Moreover, quinpirole treatment promotes the activation of GSK3 β by decreasing its phosphorylation in mouse renal proximal tubule cells and enhances the phosphorylation of ERK1/2 in dopaminergic neurons^{294,347}. In the current experiments, quinpirole reduced pTH levels in both WT and CHL1 KO neurons. Additionally, CHL1 KO neurons exhibited a more substantial reduction in pTH relative to their basal conditions compared to WT neurons (18.2% vs. 13.8%, respectively). As the cAMP pathway serves as a conventional transduction pathway for GPCRs, the limited impact of quinpirole on cAMP levels relative to the vehicle condition could be indicative of a rapid and transient effect that is still present in CHL1 KO neurons.

While CHL1 does not influence the DRD2 signaling pathway in ventral midbrain neurons under basal conditions (vehicle treatment), it is worth noting that the absence of CHL1 increases the sensitivity of the neurons to DRD2 modulation, especially from sulpiride, even though no alterations in phosphorylated levels of GSK3 β or ERK1/2 are observed.

4.2.2 Sex- and genotype-dependent modulation of TH phosphorylation in the striatum by DRD2 agonism

The DRD2-dependent signaling was also investigated in the striatal tissue of adult WT/CHL1 KO female and male mice. My results indicate that WT and CHL1 KO mice show comparable levels of phosphorylated and total TH, GSK3 β and ERK1/2 proteins. Previously, reduced TH phosphorylated levels were found in the dorsal striatum, but not ventral striatum of male CHL1 KO mice³⁸. In my research, the analysis of the whole striatum did not find any disparities in protein content between genotypes in female and male mice, aligning with the *in vitro* findings with WT and CHL1 KO ventral midbrain cultures. It is possible that analyzing the whole striatal tissue masked the difference present in the dorsal striatum. It is also worth noting that Kotarska et al. (2020)³⁸ employed a different sacrifice method, and the animals did not have prior exposure to behavioral tests, which can explain the different

findings. In agreement with the tests using ventral midbrain cultures, the levels of phosphorylated and total GSK3 β and ERK1/2 proteins are similar between genotypes. Therefore, it can be concluded that in female and male mice lacking CHL1 the amounts of proteins involved in DRD2 signaling and their phosphorylation remains within the normal range in the whole striatal tissue.

When mice were sacrificed 15 minutes after treatment with DRD2-specific compounds, the analysis of the striatal protein content exposed genotype- and sex-dependent effects of the compounds on TH phosphorylation. Namely, TH phosphorylation levels decreased in response to sulpiride treatment in WT females compared to the vehicle condition, whereas prior studies report that sulpiride incubation in striatal slices of male rats does not affect TH activity³⁵⁰. Although quinpirole incubation induced a reduction in TH phosphorylation in striatal slices of male WT rats and female WT and DRD2_L KO mice^{119,183}, my findings here demonstrate that quinpirole treatment selectively decreased pTH levels in male CHL1 KO mice compared to WT mice and the respective vehicle group. This genotype-dependent effect suggests that the absence of CHL1 in male mice results in an enhanced sensitivity to the low dose of quinpirole, which might stem from the absence of a negative regulatory mechanism exerted by CHL1 on DRD2 presynaptic dopaminergic transmission in WT males. Furthermore, the sex-dependent decrease in TH phosphorylation observed in CHL1 KO males is in line with previous findings indicating that female rats exhibit a lower sensitivity to both biochemical and behavioral effects of quinpirole^{367,368}. For instance, quinpirole was less effective at inhibiting striatal dopamine release in females than in males, which aligns with males displaying a higher susceptibility to the locomotor depressant effects of the compound.

The analysis of the striatal protein content in mice supports the observations in ventral midbrain primary neurons, providing further evidence that the initial effects of sulpiride and quinpirole treatments on the DRD2 signaling pathway exhibit sex-dependent characteristics, with the impact of quinpirole being influenced by the presence of CHL1.

4.2.3 CHL1 and DRD2 stimulation alters complexity of cultured MSNs

Prior research has shown that disruptions in DRD2 signaling can lead to varying changes in synaptic transmission through structural modifications of neuronal morphology or of dendritic spines. *In vivo* mouse studies with striatal postsynaptic DRD2 upregulation or ablation found a reduced arbor complexity in MSNs^{173,369}. In turn, selective presynaptic DRD2 ablation in dopaminergic neurons increased neuronal tree complexity in SNc neurons¹⁷⁶. CHL1 is involved in controlling similar processes in several neuronal types^{36,331}. Hence, I evaluated the impact of CHL1 presence or absence on dendritic and spine morphological changes induced by DRD2 modulation in striatal MSNs.

The neuronal tree of cultured MSNs was examined at intermediate (12 div) and advanced (21 div) stages of development and vehicle-treated WT and CHL1 KO MSNs showed no gross differences in

the neuronal architecture and dendritic spine morphology at both stages. However, CHL1 KO neurons at 12 div displayed a reduced dendritic complexity compared to WT neurons, suggesting that CHL1's absence in cultured MSNs affects neuronal tree development but not dendritic spine composition under basal conditions.

Previous literature described how homo- and heterophilic interactions of CHL1 regulate neurite outgrowth of cerebellar and dopaminergic neurons. Under non-stimulating conditions, neurite length was found to be similar between WT and CHL1 KO neurons^{20,23}. This aligns with my findings that CHL1 does not change the dendritic tree of cultured MSNs to a strong extent. Interestingly, while comparing the dendritic arbor at 12 and 21 div, a lower complexity of the neuronal tree of CHL1 KO neurons was observed at 12 div. The absence of this observation at 21 div suggests a potential compensatory mechanism possibly involving other CAMs coming into play when CHL1 is absent and also that development is delayed in the absence of CHL1. Compensatory mechanisms of CAMs during development were commonly observed in loss-of-function studies and suggested to take place due to the functional overlap of CAMs, which could explain the presence of only mild defects when an individual CAM is deleted^{20,30,370}. For instance, CHL1's involvement in neuronal morphogenesis of primary dopaminergic neurons did not lead to aberrant changes in dopaminergic pathways in the ventral midbrain²⁰. On the other hand, the period of 12 div, starting at E16, coincides with a critical stage of development when CHL1 expression reaches its peak (E18 to P7)^{9,17}. CHL1's absence during the developmental period where its expression normally peaks could show the strongest effect at this time period and underly the reduced complexity observed in CHL1 KO neurons at 12 div. In contrast, the developmental stage at 21 div corresponds with the developmental stage well after P7, when CHL1 expression declines to lower levels also seen in adulthood^{9,17}. This extended period provides an opportunity for the neuronal tree to respond and potentially recover from the lack of CHL1 through possible compensatory mechanisms, resulting in smaller or no alterations when CHL1 is not present. Lastly, cortical neurons from adult CHL1 KO mice contained a higher percentage of thin spines and a lower percentage of stubby and mushroom spines on their apical dendrites when compared to WT neurons³⁶. My analysis revealed that the lack of CHL1 did not lead to alterations of the dendritic spine classes in cultured MSNs, suggesting that MSNs might be influenced differently by the lack of CHL1 as cortical neurons, or CHL1 is more important for spine morphology in adult mice.

These findings indicate that CHL1 might exert an influence on the dendritic development of MSNs, since at specific time points CHL1 seems to play a role in ensuring proper arborization and development of MSNs. Despite potential compensatory mechanisms that could mitigate the effects of CHL1's absence, certain neuronal processes might still be impaired later on.

When dendritic arborization after sulpiride and quinpirole treatment of MSNs at 12 div was analysed, no significant effect was observed but sulpiride and quinpirole notably increased the

arborization in the distal part of CHL1 KO neurons compared to WT and vehicle-treated CHL1 KO neurons, while there was no significant change observed between vehicle- and sulpiride/quinpirole-treated WT neurons. In mature neurons at 21 div, sulpiride increased the arborization complexity in both WT and CHL1 KO neurons, while quinpirole boosted overall dendritic complexity in WT neurons compared to the vehicle-treated group. In contrast, no differences were detected between quinpirole- and vehicle-treated CHL1 KO neurons. Collectively, these findings reveal that CHL1's absence enhances the reactivity of immature MSNs to both sulpiride and quinpirole treatments, while mature WT and CHL1 KO neurons react similarly to sulpiride but differently to quinpirole.

Prior research has shown that disruptions in DRD2 signaling can lead to varying changes in synaptic transmission through structural modifications of neuronal morphology or dendritic spines. *In vivo* mouse studies with striatal postsynaptic DRD2 upregulation or ablation found a reduced arbor complexity in MSNs^{173,369}. In turn, selective presynaptic DRD2 ablation in dopaminergic neurons increased neuronal tree complexity in SNc neurons¹⁷⁶ and reduced dendritic length in primary dopaminergic neurons¹⁵³. Chronic quinpirole treatment in DRD2 KO dopaminergic neurons only extended neuronal length of TH-positive WT neurons¹⁵³. Interestingly, TH-positive dopaminergic neurons chronically treated with higher quinpirole doses (10 μ M) increased dendritic arborization and lower doses (1 μ M) decreased axonal terminal numbers, while sulpiride had no impact on neuronal morphology alone but prevented the quinpirole effects^{177,371}.

My experiments show an overall increase in neuronal complexity, mostly in mature WT MSNs, induced by sulpiride and quinpirole. Quinpirole increases arbor complexity in previous studies involving chronic DRD2 stimulation of dopaminergic neurons^{153,371}, whereas a single 10 μ M quinpirole treatment for 24 hours in postnatal striatal MSNs resulted in a decrease of neurite length and branching¹⁷⁴. The latter study employed similar conditions as I used here (20 μ M for 24 hours at 21 div), but the use of postnatal striatal cultures at day 0 is probably responsible for differing quinpirole effects observed due to differences in DRD2 expression³⁷². Indeed, different maturation stages at E17 or postnatal day 0 were described to result in distinct axonal morphogenesis in Purkinje cells³⁷³. Nonetheless, employing E16.5 embryonic cultures results in fewer cholinergic interneurons, enabling a more focused examination of MSN responses and yielding a higher neuronal survival rate compared to postnatal neurons in dissociated cultures²⁸⁸. Concerning sulpiride, while there is no prior information on its effect on striatal dendritic morphology, sulpiride (4-5 μ M) did not influence morphological parameters in mesencephalic neurons^{177,371}. However, these studies employed low concentrations of sulpiride in chronic treatments, which differ entirely from the high single dose (30 μ M for 30 min or 24 hours) used here.

Another significant observation is that at 21 div, there was an increase in neuronal complexity in WT MSNs treated with both sulpiride and quinpirole, while in CHL1 KO MSNs only sulpiride had an impact. At 12 div, WT neurons were unresponsiveness to the treatments, whereas sulpiride and

quinpirole caused an increase in neuronal complexity in CHL1 KO MSNs relative to their vehicle-treated group. Given that CHL1 KO MSNs displayed reduced baseline neuronal complexity at 12 div, this characteristic might contribute to their increased sensitivity to the morphological effects of quinpirole at this developmental point. Despite the 12 div stage being marked by robust neuronal connectivity²⁹², the absence of CHL1 at this point could amplify the reactivity of MSNs to the postsynaptic DRD2 modulation. As previous studies suggest a stable dendritic and spine maturation in MSNs at 21 div^{290,293}, the notion of compensatory mechanisms gains weight. It is conceivable that CHL1 KO neurons employ these mechanisms to recover from the slightly lower neuronal complexity from 12 div to 21 div at basal conditions, contributing to a similar response to DRD2 modulation of both WT and CHL1 KO MSNs at the later stage. Although quinpirole-treated WT and CHL1 KO MSNs showed a comparable neuronal tree, it is worth noting that, compared to basal conditions, CHL1 KO neurons suffered less morphological changes at 21 div than WT neurons. Therefore, CHL1 KO neurons were less influenced by quinpirole-induced DRD2 stimulation, suggesting that if compensatory mechanisms are at play to help neurons to react and recover from the absence of CHL1, they might not be fully effective when postsynaptic MSNs are exposed to pharmacological modulation.

The understanding of these compensatory strategies is essential as striatal functional connectivity has been linked to conditions like schizophrenia and Parkinson's disease, potentially influencing specific symptoms or disease progression^{374,375}. To test this theory, future studies could use CRISPR/Cas9-mediated gene knock-down³⁷⁶ of binding partners of CHL1 or CAMs that could compensate for CHL1 to gain valuable insights into whether compensatory strategies are activated in MSNs when CHL1 is absent. Investigating the impacts of DRD2 pharmacological modulation in these knock-down models at different developmental stages would also be interesting, given the developmental stage-dependent effects observed in CHL1 KO neurons. Additionally, electrophysiological studies using optogenetic stimulation³⁷⁷ could be applied to observe inhibitory postsynaptic currents of striatal neurons in response to dopaminergic stimuli. This approach could help determine whether the absence of CHL1 alters the synaptic transmission and functionality of MSNs.

Quantitative and morphological analyses of dendritic spines revealed no significant impact of the compounds compared to the vehicle condition. However, punctual genotype-dependent differences in MSNs' response to DRD2 modulation were found. Sulpiride-treated CHL1 KO neurons showed a reduced percentage of long thin spines and increased mushroom spine volume compared to WT neurons, although there were no significant changes compared to vehicle-treated CHL1 KO neurons. Quinpirole-treated CHL1 KO neurons contained significantly increased mushroom spine density and all morphological parameters (mean/total area, length, neck length, and volume) of CHL1 KO neurons compared to WT neurons, even though no significant distinctions were noted when compared to

vehicle-treated CHL1 KO neurons. Moreover, both DRD2-specific compounds induced a significant reduction in PSD95 levels in WT MSNs, but this effect was absent in CHL1 KO MSNs.

Earlier research reported a lower total spine number in acute striatal slices from mice with selective postsynaptic DRD2 ablation³⁶⁹. In mutant mice, spine numbers remained unchanged post-quinpirole treatment, whereas WT neurons exhibited an increase. Using a similar quinpirole treatment (10 μ M for 24 hours), another study noted a reduced spine density and PSD95 downregulation due to DRD2 stimulation in postnatal striatal cultures at P0¹⁷⁴.

The detailed spine morphology analysis performed here proved to be valuable in uncovering specific effects on dendritic spines. While quinpirole treatment (20 μ M for 24 hours) did not alter total spine density, CHL1 KO neurons exhibited an increased mushroom spine density, along with an increase of all morphological parameters, compared to WT neurons. CHL1 KO long thin spines were also moderately affected by quinpirole treatment. Mushroom spines are linked to mature and stable synapses, also called memory synapses, while long thin spines are transient and form or disappear based on synaptic activity levels and they are known as learning spines. Both spine types are considered more mature than stubby or filopodia structures^{378,379}. Moreover, the increased spine dimensions in these types can influence synaptic activity by retaining more molecules like PSD95 and Ca^{2+} in their heads, leading to enhanced synaptic activation^{378,379}. Hence, my results suggest that CHL1 has an impact on the DRD2-induced modulation of synaptic activity in postsynaptic MSNs, as its absence seems to facilitate the morphological synaptic maturation mirrored by the dynamic alterations in mushroom and long thin spines following quinpirole treatment.

Reinforcing this notion is my finding that PSD95 levels in CHL1 KO neurons were not affected by quinpirole, while WT neurons experienced a pronounced reduction in PSD95 levels. PSD95, crucial for synaptic structure and plasticity in excitatory synapses, directly interacts with DISC1³³⁹. Intriguingly, DISC1 is a binding partner of CHL1, influencing neurite outgrowth of cortical neurons³³¹, and DRD2, which, when overactivated, binds to DISC1 and downregulates PSD95 levels in striatal neurons¹⁷⁴. On one side, CHL1's interaction with DRD2 might facilitate DISC1 binding to the receptor upon activation, explaining the lowered PSD95 levels in WT neurons. On the other side, in CHL1's absence, the receptor activation might not suffice to trigger DISC1 binding to DRD2, leaving DISC1 free to interact with PSD95 without altering its levels. Alternatively, mechanisms involving NMDA receptors might also be in effect, given that PSD95 directly interacts with NMDA receptors³⁸⁰ and DRD2 inhibits NMDA receptor currents by interacting with GluN2B subunits in MSNs and hippocampal neurons^{175,381}. Additionally, PSD95 was found to interact with DRD1 and DRD2 in HEK293 cells³⁸², and PSD95 acts as a molecular brake to limit the interaction of DRD1 with NMDA receptors³⁸³. Hence, CHL1 might similarly interfere with DRD2-NMDA receptors interaction, potentially influencing PSD95 levels in MSNs. While much remains to be explored to comprehend the

intricate interplay among these elements, the present findings position CHL1 as a modulator of postsynaptic DRD2 functions in MSNs' synaptic plasticity.

The brain's plasticity and adaptability stem from its constant reshaping of the neuronal architecture, optimizing functions and integrating new experiences, knowledge, and skills, a fundamental process that enables learning, recovery from injuries or leads to diseases, and adaptation to external environmental changes. Changes and plasticity in the neuronal and spine structure are closely interconnected with synaptic function³⁸⁴. My detailed assessment of neuronal tree and dendritic spine architecture reveals that CHL1 significantly impacts DRD2-dependent modulation of neuronal morphology and synaptic plasticity in MSNs, warranting further investigation into its biological implication. In a prior study that measured spontaneous Ca^{2+} signals during methamphetamine treatment, inhibition of the neuronal activity in ventral midbrain neurons was prevented and even increased above the basal level through DRD2 blockade with sulpiride³⁸⁵. Additionally, in dopaminergic terminals within the NAc, sulpiride increased dopamine release evoked by electrical wave pulses, whereas quinpirole decreased dopamine release upon single and wave pulses³⁵². Hence, employing similar methodologies to quantify the impact of CHL1 on DRD2-dependent neuronal activity or dopamine efflux following DRD2 antagonism or agonism could also be applied to assess whether the morphological effects also translate into observable alterations in synaptic transmission.

4.2.4 Interpreting the CHL1 modulation of pre- and postsynaptic DRD2 functions

4.2.4.1 CHL1 might act as an allosteric modulator of DRD2 in response to an agonist

In my previous findings, CHL1's absence did not notably impact presynaptic neurons or postsynaptic neuron morphology under basal conditions. Nevertheless, it influenced sulpiride-induced DRD2 signaling in ventral midbrain neurons and quinpirole-induced morphological effects, highlighting its potential role in modulating both pre- and postsynaptic DRD2 functions, particularly in the presence of DRD2-specific compounds.

The enhanced sensitivity of DRD2 to dopaminergic effects induced by psychostimulants like amphetamine or 3,4-methylenedioxymetamphetamine (MDMA) has been reported in a mouse model of schizophrenia, particularly in trace amine-associated receptor 1 (TAAR1) KO mice^{386,387}, and was associated with an increase in striatal high-affinity state DRD2³⁸⁶. Later research uncovered a direct interaction between TAAR1 and DRD2, which form a heterodimer that modulates cAMP levels³⁸⁸. Moreover, studies on DRD2_S KO and DRD2_L KO mice found normal basal pre- and postsynaptic DRD2-mediated functions but disrupted dopaminergic signaling upon treatment with DRD2 agonist quinpirole and antagonist haloperidol¹³⁸. Additionally, a small compound was discovered to interact

with DRD2 outside the orthosteric binding site and to negatively modulate its signaling in the presence of certain agonists, without affecting basal dopamine responses³⁸⁹. Similarly, endogenous ligands like small hormones, neurotransmitters, or proteins function as allosteric modulators through extracellular interactions outside of the GPCR orthosteric site, inducing structural changes that impact the affinity and/or effectiveness of orthosteric ligand binding to receptors³⁹⁰. Given the absence of DRD2 signaling impairments at basal conditions in CHL1 KO ventral midbrain cultures, coupled with the altered neuronal response to DRD2 stimulation by quinpirole, it is conceivable that CHL1 might act as an allosteric ligand of DRD2 influencing its functionality only when certain ligands bind to the receptor.

The extracellular domain of CHL1 interacts with the first extracellular loop (EL1) of DRD2³⁸, which contains a critical residue responsible for stabilizing a binding pocket's conformation exclusive to DRD2³⁹¹. As predicted in molecular dynamics simulations, the conformational dynamics of EL1 in DRD2, DRD3, and DRD4, are responsible for and sensitive to ligand binding and might also provide a structural space for allosteric ligands within DRD2^{363,392}. Using the crystalized structure of DRD2 with risperidone, this method predicted that the helical conformation of EL2 contributes to the high energy state of the receptor, while its elongated conformation interacts with EL1 constraining its dynamics³⁶³. The potential involvement of EL1 in constituting or contributing to a DRD2 allosteric binding site, coupled with CHL1's ability to influence DRD2's response to specific agonists while avoiding receptor activation under physiological conditions, strengthens the hypothesis that CHL1 functions as an allosteric modulator, thereby exerting an influence over DRD2's functionality.

The characterization of the effects of CHL1 binding to the allosteric binding site of DRD2, stands as a promising avenue for future studies. Performing targeted mutations on residues within the predicted allosteric binding site of DRD2 and evaluating the impact on CHL1's ability to modulate DRD2-mediated responses to agonists can as well be a strategy. This could be done with live-cell imaging techniques such as fluorescence or bioluminescence resonance energy transfer (FRET/BRET) by quantifying the interaction of CHL1 with the mutated variants of DRD2.

4.2.4.2 CHL1 might contribute to the maturation of DRD2-dependent signaling during embryonic stages

In alignment with prior research, my thesis demonstrates that modulation of DRD2 leads to alterations within the neuronal architecture of cultured MSNs and the impact of CHL1's absence varies with the neuronal developmental stage. In younger MSNs at 12 div, while no impact is observed in WT neurons, dendritic arborization of CHL1 KO neurons is altered by DRD2-specific compounds. In contrast, mature WT neurons at 21 div show a higher sensitivity to the increasing neuronal complexity effects induced by the treatments. While DRD2 modulation in presynaptic dopaminergic neurons at 7 div lacks a significant impact on the signaling pathway, CHL1 KO neurons show a tendency to be more sensitive to the DRD2-induced reduction of pTH. This raises the possibility that the observed disparities

between younger WT and CHL1 KO MSNs could stem from distinct expression profiles of DRD2 on the cell surface or a different ratio of DRD2 low/high conformational states.

CHL1's involvement in processes like neurite outgrowth, migration, and differentiation of primary dopaminergic neurons has been established but *in vivo* mouse studies found no abnormal changes in ventral midbrain dopaminergic neurons²⁰. In the striatum, CHL1 KO mice displayed reduced DRD2 levels in the dorsal striatum, while the NAc remained unaffected³⁸. Given this distinct local DRD2 expression in the striatum of adult CHL1 KO mice and CHL1's role in dopaminergic pathway development, investigating whether CHL1 deficiency affects the temporal and/or spatial DRD2 expression during circuit development would be intriguing. Changes in DRD2 availability within the striatum have been implicated to underly the disruption of dopaminergic function observed across various neuropsychiatric conditions. For instance, in schizophrenia, patients often exhibit an elevated density of DRD2, whereas in cases of drug addiction, a decreased striatal DRD2 density is linked to enhanced drug consumption¹¹⁷. Interestingly, the overexpression of DRD2 in MSNs during development is enough to trigger cognitive impairments in later life. Reversing the developmental overexpression of DRD2 in MSNs solely during adulthood is not sufficient to effectively ameliorate working memory deficits but it can successfully reverse the decrease in motivation^{232,241}. Furthermore, transiently inducing overexpression of the serotonin receptor 5-HT1A during embryonic to perinatal stages, but not thereafter, led to alterations in anxiety-related behavior and memory tasks in adult mice^{393,394}. Therefore, if CHL1 influences the temporal and/or spatial expression of DRD2 during development, the resulting consequences could impact the behavior of mice at later stages of life.

In addition, it is plausible to speculate that the absence of CHL1 in MSNs or ventral midbrain neurons might produce conformational shifts in DRD2, potentially enhancing its binding affinity for quinpirole. This alteration could result in more sustained and prolonged currents, thus contributing to more pronounced DRD2-induced effects like the decrease in TH phosphorylation and morphological alterations. Previously, a higher binding affinity of quinpirole to DRD2 compared to dopamine³⁹⁵ was described to result in more prolonged inhibitory postsynaptic currents in VTA slices, with a slower rate of rise and decay, compared to the currents elicited by dopamine³⁹⁶. These conformational changes within DRD2 might correspond to its interconvertible affinity states: the G protein-coupled DRD2^{high} with enhanced agonist binding affinity and the G protein-uncoupled DRD2^{low} with reduced agonist binding affinity³⁹⁷, and this states can be influenced by mutations, ligands, or allosteric modulators. Mutations in the TM5 of DRD2_{long} did not disrupt the receptor's overall conformation but differentially impacted the binding affinity of distinct agonists³⁹⁸. Histamine receptor agonists were found to particularly decrease DRD2's affinity for quinpirole in striatal membrane preparations, while amphetamine treatment enhanced the expression of DRD2^{high} in striatal slices^{399,400}. Furthermore, allosteric modulators of DRD2 can alter the receptor's affinity for ligands and even exert control over the dimerization of DRD2 with other receptors, such as the adenosine A2A receptor^{401,402}. Therefore,

if CHL1's potential role as an allosteric modulator of DRD2 is taken into account, it is reasonable to consider that this interaction could influence the conformational state of DRD2. Indeed, alterations in the binding affinity state of DRD2 have been linked to numerous animal models of schizophrenia and are believed to hold significance in the disorder's pathophysiology^{403–405}.

In conclusion, if the observed changes in sensitivity of CHL1 KO neurons compared to WT neurons are influenced by alterations in the expression or binding affinity state of DRD2 receptors during specific developmental windows, the consequences could lead to either compensatory mechanisms or impairments in adulthood. Investigating the role of CHL1 in modulating these aspects can offer insights into new mechanisms that contribute to impairments in dopaminergic transmission, providing a deeper understanding of their effects on brain function.

4.2.4.3 Advantages and limitations of the *in vitro* models

To investigate the influence of CHL1 on DRD2-dependent functions, primary neuronal cultures were employed, enabling a controlled manipulation of experimental conditions and cellular targets. Cultures enriched in MSNs or ventral midbrain neurons allow to determine the effect of CHL1, quinpirole and sulpiride on DRD2 function and signaling specifically in these cells. The *in vitro* neuronal models effectively generated consistent and replicable data, demonstrating a high degree of sensitivity in detecting genotype differences but could not fully replicate the complexity of *in vivo* interactions.

Studying signaling pathways in primary cultures presents known challenges due to the absence of fully interconnected circuits involving diverse neuron types and glial cells, limiting their complete functionality⁴⁰⁶. Non-specific binding of quinpirole and sulpiride within the experimental setup presents a limitation that must be taken into account, as it has the potential to introduce bias into the assessment of signaling pathways. The incomplete maturation of neurons or the lack of medium constituents might have influenced the cellular response. Consequently, conducting a thorough investigation of these factors is essential to gain a more profound insight into their potential influence. In addition, the antagonistic impact of sulpiride could be further explored by studying its effects in the presence of an agonist, assessing the extent to which sulpiride blocks the activation of the signaling pathway.

Using monocultures of striatal MSNs in my thesis offers the advantage of a higher cell count and simplified morphology for subsequent analysis. However, the absence of intercommunication with other neural circuits might reduce treatment responsiveness. While my methods revealed CHL1's influence on DRD2 signaling and functions, future research could benefit from co-culture systems to better mimic *in vivo* scenarios. One such approach is the co-culture with glial cells, particularly astrocytes, which express CHL1 and are known to provide metabolic and structural support to neurons⁴⁰⁷. Cortical astrocytes cultured with dopaminergic primary neurons were reported to grant

neuroprotective mechanisms to the neurons and mediate neurostimulation and neurite outgrowth⁴⁰⁷. The presence of a small number of astrocytes or the use of previously conditioned media from astroglia cultures can also improve the development and survival of co- or mono- cultures of MSNs²⁹⁰. In the context of MSNs culture, the co-culture with cortical neurons can yield higher density of dendritic spines and provide a more comprehensive representation of the native neuronal network^{290,293}. Furthermore, astrocytes are known to be activated by dopamine and to modulate perisynaptic concentrations of ions and neurotransmitters⁴⁰⁸, which might also affect the response of MSNs to quinpirole and sulpiride. In addition, drug incubation effects could be studied using brain slices or organotypic brain slice cultures, preserving the tissue's three-dimensional structure, but a significant drawback is decreased neuronal survival over time⁴⁰⁹ and compound's permeability into the tissue. By mimicking *in vivo* interconnected neural circuits, these co-culture models could provide more precise insight into signaling cascades and cellular responses in a biologically relevant environment, potentially enhancing our understanding of CHL1's impact on DRD2-related processes. Nevertheless, the primary challenge with these approaches lies in differentiating MSN-specific effects from those on other cells, and this distinction constitutes a key advantage of the present approach.

4.3 Behavioral characterization of the CHL1 and DRD2 interaction

In this thesis, I supplemented the functional analysis of the CHL1 and DRD2 interaction with a comprehensive behavioral assessment of striatal-dependent functions, including locomotor activity, exploration and emotionality, working memory, and novelty-seeking behavior— parameters heavily influenced by DRD2 signaling. Both female and male WT and CHL1 KO mice received treatments with a vehicle solution, a low-dose sulpiride (1 mg/kg), or quinpirole (0.02 mg/kg). These low doses were chosen to specifically target presynaptic DRD2.

4.3.1 CHL1 modulates locomotor activity and influences postsynaptic effects of DRD2 antagonism and presynaptic effects of DRD2 agonism in a sex-dependent manner

Voluntary movement is primarily regulated by dopamine releases from the SNc to the dorsal striatum. Locomotor activity was evaluated and compared using three behavioral tests: OF, YM, and NI. Throughout the entire duration of these tests, vehicle-treated WT and CHL1 KO females exhibited similar levels of spontaneous locomotion, while CHL1 KO males moved less and at a slower pace than WT males. Prior studies reported lower locomotor activity of both female and male CHL1 KO mice compared to their respective controls in the OF arena, aligning with my findings with male mice^{37,43}. The difference between genotypes is unlikely to be linked to motor impairments, as CHL1 KO mice show no motor deficits in tests of motor ability and coordination, such as rotarod or balance pole^{27,44,45}. Similarly to CHL1 KO males, male mice lacking the postsynaptic DRD2 in MSNs display reduced

basal motor activity, unlike mice expressing either both DRD2 isoforms or only the postsynaptic DRD2 which show no impairments^{137,139}. This suggests that the specific interplay of CHL1 with postsynaptic DRD2 is crucial for controlling striatal-dependent behaviors and it seems to have a greater impact in males than in females, as only CHL1 KO males show locomotor impairments. Interestingly, CHL1 KO males showed reduced DRD2 and pTH levels in the dorsal striatum³⁸, associated with an overactivation of the striatal indirect pathway. Therefore, a genotype- and sex-dependent mechanism could be implied.

Sulpiride notably reduced locomotor activity of CHL1 KO females compared to WT females within the first 10 to 15 min and relative to vehicle-treated CHL1 KO females after 20 min in all three tests, whilst no observable effects on CHL1 KO males were detected. Quinpirole reduced locomotion of both WT and CHL1 KO females to a similar extent throughout the tests, but decreased the activity of WT males in the first 20 min, while CHL1 KO males exhibited reduced activity only after 30 min in the OF. Within the initial 10 min of OF testing, WT mice responded more quickly to the treatment than CHL1 KO mice. Quinpirole-induced hypolocomotion was observed in WT females and males at 3 min, whereas the effect appeared at 7 and 9 min in CHL1 KO females and males. CHL1 KO males consistently displayed the delayed quinpirole effect in all tests, whereas CHL1 KO females showed a reduced but noticeable effect in the initial YM minutes, disappearing in the NI.

These results demonstrate that CHL1 deficiency in females increases their response to sulpiride, leading to decreased locomotor activity. Low doses of sulpiride (0.5 to 5 mg/kg) were shown to exhibit no impact on the spontaneous activity of rodents regardless of the sex^{225,410,411}, which is in line with my current findings in all male mice and WT females. In female rats, higher doses of sulpiride (10 mg/kg) did not affect motor activity, whereas at 40 mg/kg, it either decreased motor activity only in diestrus females or had no impact independently of the estrous cycle^{412,413}. On the contrary, male rats treated with the same sulpiride doses show consistent catalepsy and reduced locomotion^{225,228,412}. Given the absence of noticeable effects on the locomotion of female rodents at low doses of sulpiride, coupled with the lack of influence from the estrous cycle, this suggests that the estrous cycle is not a relevant factor in my experimental setup. Instead, the reduced locomotion observed in sulpiride-treated CHL1 KO females appears to be a sex-dependent effect linked to the absence of CHL1.

Fundamentally, the inhibition of motor activity arises from the activation of the striatal indirect pathway, initiated by reduced signaling of postsynaptic DRD2 or its blockage in the iMSNs. In contrast, the blockade of presynaptic DRD2 leads to dopamine release in the striatum, activating postsynaptic DRD2 and promoting an increase in spontaneous locomotion. As low doses of sulpiride specifically block DRD2_s^{222,223}, and I observed decreased activity instead of an increase, it can be suggested that the absence of CHL1 in females prevents the action of sulpiride on presynaptic DRD2, promotes the blockade of postsynaptic DRD2 and the activation of the striatal indirect pathway. This could be attributed to either impaired presynaptic signaling due to a shift in sulpiride's binding affinity, favoring

antagonistic action at the postsynaptic DRD2 or an enhanced sensitivity of postsynaptic DRD2 to the antagonist.

Quinpirole treatment induced hypolocomotion regardless of genotype or sex, although with a consistent delayed effect on CHL1 KO males and a stronger effect on WT males than females. Similarly to sulpiride, quinpirole elicits a dose-dependent biphasic locomotor response by initially selectively stimulating presynaptic DRD2^{138,139}. Multiple studies using male rodents consistently show that high doses of quinpirole (> 0.1 mg/kg) initially reduce locomotion within minutes after administration, leading to a sustained hyperactive state. Low doses (0.02-0.03 mg/kg) cause a rapid decline in locomotor activity within the first 5 min of treatment, persisting for over 2 hours^{136,137,219,414}. In my experimental setup, the low quinpirole dose consistently induced a prolonged hypolocomotive state in WT mice, observable from 3 to 30 min in the OF. This observation is in agreement with prior literature and substantiates the initial goal of targeting presynaptic DRD2-specific behaviors. Intriguingly, quinpirole-induced hypolocomotion was also observed in CHL1 KO mice, but at a significantly later stage compared to WT mice, suggesting that the absence of CHL1 impacts the presynaptic or postsynaptic DRD2 responsiveness to quinpirole in an initial time-window. This phenomenon could stem from lower density/levels of the pre- or post-synaptic DRD2, or due to alterations in receptor conformational states, which notably aligns with theories already explored in the preceding section when interpreting the functional regulation of CHL1 over DRD2 signaling *in vitro* (section 4.2.4).

One possible explanation could involve reduced levels of either presynaptic or postsynaptic DRD2 in CHL1's absence, leading to delayed hypolocomotion induced by quinpirole due to either the decreased presynaptic DRD2 availability for quinpirole binding or lower postsynaptic DRD2 levels that leads to a slower response to quinpirole-induced presynaptic effects (striatal dopamine reduction). Alternatively, reduced levels of both presynaptic and postsynaptic DRD2 receptors might be involved as well. A prior study in male rats with lower presynaptic DRD2 expression exhibited a delayed quinpirole effect, accompanied by lower postsynaptic DRD2 levels that resulted in a blunted response to quinpirole²⁴⁵. Instead of a blunted response to the treatment, quinpirole-treated WT and CHL1 KO mice showed similar levels of total locomotion throughout all the tests. Nonetheless, the possibility of reduced levels of postsynaptic DRD2 cannot be ruled out, as evidenced by the lower tonic activity observed in CHL1 KO males but not in females, which reflects a basal overactivity of the striatal indirect pathway in a sex-dependent manner. This hypothesis finds support in previous studies revealing reduced DRD2 and pTH levels in the dorsal striatum of CHL1 KO males and *in vitro* experiments indicating that CHL1's absence leads to a higher quinpirole-triggered internalization of DRD2s, but not on DRD2L³⁸. Relying solely on the hypothesis of presynaptic DRD2 downregulation would impose high extracellular dopamine levels and spontaneous hyperlocomotion²¹⁸, which is not present in either female or male CHL1 KO mice. Additionally, variations in DRD2 expression impact the recruitment of crucial elements for DRD2 signal transduction and internalization, such as G α_{i1} and

β -arrestin 2⁴¹⁵. Given the potential modulation of presynaptic DRD2 internalization and/or postsynaptic DRD2 signaling by CHL1, this could lead to changes in surface expression levels and, consequently, impact the responses to dopaminergic compounds. Hence, I propose that CHL1 KO mice exhibit a concurrent downregulation in the expression of both pre- and postsynaptic DRD2, with CHL1 KO females experiencing a relatively low impact on postsynaptic DRD2. This hypothesis supports the decreased tonic locomotion observed only in CHL1 KO males, the higher postsynaptic sensitivity of CHL1 KO females to sulpiride, and the delayed hypolocomotion effect of quinpirole in CHL1 KO mice, indicating a sex-dependent dopaminergic regulation.

Another plausible explanation is that CHL1's absence might not reduce DRD2 levels but could induce conformational changes, potentially altering the receptor's affinity for quinpirole. The finding that CHL1 KO neurons maintain normal basal properties but exhibit increased sensitivity to quinpirole, implies a potential upregulation of high-affinity DRD2. Of note, elevated expression of high-affinity DRD2 in the striatum has been associated with schizophrenia in animal models and patients^{386,387,403–405}. However, based on the current behavioral results, an alternative scenario can be proposed: the delayed quinpirole effect could be attributed to a reduced affinity of the compound to presynaptic and/or postsynaptic DRD2 due to a higher proportion of low-affinity DRD2. It is also plausible that CHL1 acts as an allosteric ligand for DRD2, inducing conformational changes that affect the receptor's function in the presence of specific ligands. This notion gains support from findings of disrupted dopaminergic signaling in response to quinpirole treatment specifically in DRD2_S KO and DRD2_L KO mice¹³⁸, as well as the identification of an allosteric binder that selectively modulates DRD2 signaling in the presence of certain agonists while not affecting basal dopamine actions³⁸⁹.

Therefore, CHL1's absence leads to enhanced sensitivity of postsynaptic DRD2 to sulpiride effects in females, while presynaptic DRD2 agonism affects both sexes. However, males exhibit greater resistance to presynaptic DRD2 agonism. CHL1 modulates both types of DRD2-mediated locomotor responses with sex-dependent variations.

4.3.2 CHL1's role in emotional homeostasis and its influence on sex-specific sensitivity to DRD2 antagonism in females and DRD2 agonism in males

A new open arena constitutes a source of anxiety for mice, eliciting various stressors like social isolation, novelty, brightness, and agoraphobia^{317,340}. Spontaneous alternation, exploratory patterns, and stereotypic behaviors are influenced by these motivational cues, relying on the dopaminergic signaling in the dorsal/ventral striatum to expose the emotional reactivity in mice^{340,416}. The exploratory pattern in the arena indicates heightened stress or anxiety when mice avoid the center and exhibit increased thigmotaxis⁴¹⁷. Rearing is an exploratory behavior often observed as a response to novelty shortly after exposure to a new environment, and unsupported/supported rearing distinction adds layers

of information, as they have been associated with emotionality and activity, respectively⁴¹⁸. Defecation and stereotypic behaviors such as self-grooming or jumping are stress indicators negatively correlated with anxiety-like behaviors⁴¹⁸⁻⁴²⁰.

CHL1 KO females display emotionality levels similar to those of WT females, with no differences in their exploration of the center zone, unsupported rearing, grooming, wall jumping, or defecation. While unsupported rearing is more frequently performed by CHL1 KO males than by WT males, both groups demonstrate similar center zone exploration and defecation patterns, along with a reduced grooming latency and fewer wall jumping of CHL1 KO males. These findings suggest that CHL1 differently influences stress-related parameters in female and male mice when exposed to a novel environment: while CHL1 deficiency does not impact the emotional reactivity of females, it reduces reactivity and stress-related behavior of males. Indeed, previous behavioral assessments of CHL1 KO males in various tests have reported no significant alterations in anxiety levels, but they consistently described a general state of reduced stress or anxiety^{27,43-45}. Furthermore, different tests indicated that this state might reflect a different exploratory reaction to a novel environment rather than literal reduced anxiety. In the Morris water maze, CHL1 KO males showed a swim path which was different from the path of WT littermates, but their escape latency and swimming distance were similar, indicating normal spatial learning of CHL1 KO males²⁷. In addition to a different spatial exploration in the OF arena, CHL1 KO females and males showed less interest in novel objects placed in the arena although they spent more time nearby⁴³. A subsequent study characterized CHL1 KO males with reduced rearing, decreased reactivity in spontaneous alternation and olfactory tasks, and delayed responses in social tests such as urine marking, resident-intruder, and social preference⁴⁴. Additionally, in a light/dark discrimination test, CHL1 KO mice spent more time in the lighted part of the box⁴⁵. These behaviors confirm a reduced and delayed responsiveness of CHL1 KO males to environmental and social stimuli, suggesting a diminished novelty perception and a less anxious state, possibly linked to attention and sensory gating deficits^{27,43,44}. Of note, sensorimotor gating deficits were observed in CHL1 KO females⁴⁷, a behavioral marker of schizophrenia linked to a prolonged decrease in attention. Although reduced rearing of CHL1 KO males in the first 2 min of the OF was previously associated with lower novelty reactivity^{44,421}, it is worth noting that my study's handling protocol might have contributed to a decrease in overall anxiety levels, as indicated by the increased unsupported rearing and unchanged supported rearing. This finding further strengthens the unaltered anxiety state reported for CHL1 KO mice⁴⁴. Nevertheless, in comparison to WT animals, CHL1 KO females exhibit greater emotional balance than CHL1 KO males.

Sulpiride treatment did not change emotional behavior relative to the vehicle treatment but WT females showed a decrease the occurrence of unsupported rearing and an increase in wall jumping relative to CHL1 KO females, whereas quinpirole equally decreased distance moved in the center for

both genotypes. Increased unsupported rearing seen by vehicle-treated CHL1 KO males relative to WT males, only persisted as a tendency after sulpiride and quinpirole treatments. In addition, quinpirole reduced center zone activity of WT males relative to CHL1 KO males and vehicle-treated WT males, enhanced the grooming latency of CHL1 KO males compared to WT males and increased similarly the fecal boli deposition from both genotypes. The results indicate that sulpiride did not affect male mice and CHL1 KO females, but WT females exhibited a higher level of stress-like behavior compared to CHL1 KO females. Quinpirole treatment reduced the center exploration only in WT males but did not impact the emotionality or stress-related behavior of WT and CHL1 KO mice.

As a benzamide, sulpiride induces a dose-dependent anxiolytic-like state at 10-20 mg/kg administered dose with no impact on rearing behavior of male mice^{422,423}. In rats, a 10 mg/kg sulpiride dose had no effect on rearing or grooming behavior of females or males, but at 40 mg/kg, it reduced these behaviors and decreased motor activity of male rats and females in the diestrus phase⁴¹². While female rats in estrus treated with the same dose exhibited a decrease exclusively in grooming behavior⁴¹², recent findings indicate that rearing behavior remains unchanged by high sulpiride doses (20-40 mg/kg) regardless of the estrous cycle⁴¹³. In my study, the low-dose of sulpiride had no impact on the emotion of male mice, aligning with previous results and suggesting a minor role for CHL1 in this behavior. How the estrous cycle affects sulpiride-induced effects remains unclear but only high sulpiride doses were able to induce an anxiolytic-like state in female rodents, likely linked to reduced locomotion⁴¹². My results revealed that 1 mg/kg sulpiride had no impact on the anxiety of WT and CHL1 KO females, although WT females show higher levels of stress than CHL1 KO females after treatment and this difference is not present between the vehicle-treated genotypes. This effect suggests that following sulpiride treatment, CHL1 KO females might be less responsive to stimulus-induced stress in comparison to WT females. Of note, the observed decrease in locomotion of CHL1 KO females due to sulpiride is accompanied by a reduction in supported rearing compared to sulpiride-treated WT females, drawing attention to the significance of differentiating between these two rearing behaviors.

Different studies with male rodents analysing vertical behaviors (e.g., rearing and grooming) reported a decrease of these behaviors in a dose-dependent manner upon quinpirole treatment with 0.03, 0.25 and 0.5 mg/kg^{219,423,424}. In some cases, statistical differences were only reached with 0.25-0.5 mg/kg doses but not with lower doses⁴²³. Quinpirole dose from 0.05-0.1 mg/kg did not change rearing, grooming or jumping behavior of male mice, while treatment with 1 mg/kg increased rearing and jumping after 60 min of treatment⁴²⁵. In these studies, rearing was not segregated and was consistently accompanied by reduced motor activity. Similarly, the overall decline in center exploration observed in quinpirole-treated WT mice and CHL1 KO females analyzed here reflected the locomotor activity and is likely linked to the quinpirole-induced hypolocomotion. In fact, supported rearings are closely associated to motor activity, and relative to vehicle-treated mice, quinpirole treatment caused a

delayed reduction in supported rearing of CHL KO mice compared to WT mice, as already observed for the locomotor parameter. This underscores once more the greater impact of quinpirole on WT mice and its delayed effect on CHL KO mice. Furthermore, the more pronounced decrease in center exploration observed for WT males compared to WT females was also present in the locomotor analysis, reinforcing the notion that center exploration and supported rearing mirror the quinpirole-dependent locomotor effects and that quinpirole does not impact the emotional behavior of WT and CHL1 KO mice. Nevertheless, it is worth noting that quinpirole increased the grooming latency and tended to reduce unsupported rearing of CHL1 KO males but not WT males compared to the vehicle condition. Given that quinpirole had a more pronounced impact on locomotor activity of WT males, this slightly elevated stress state of CHL1 KO males could reflect that CHL1 ablation affects the ability to control changes in dopamine levels, potentially making them more susceptible to minor emotional shifts following quinpirole treatment.

In summary, the behavioral analysis show that CHL1 plays a role in maintaining the tonic homeostasis of emotion and stress-related behaviors, particularly in males. However, the absence of CHL1 slightly turns females less responsive to stimulus-induced stress after sulpiride treatment and males more sensitive to stress after quinpirole treatment.

4.3.3 Impact of dopaminergic modulation on spontaneous alternation of CHL1 KO mice: working memory is more vulnerable to changes in dopamine triggered by sulpiride in males and by quinpirole in females and males

Spatial working memory was evaluated through a spontaneous alternation task in a free-trial Y-maze procedure, providing a deeper understanding of DRD2-mediated mechanisms within the context of CHL1 ablation. This behavior is driven by rodents' innate curiosity to explore previously unvisited areas, with the dorsomedial striatum playing a key role^{199,426}. An intact working memory enables them to remember the previously visited arm and show a preference for entering a less recently visited one^{319,320}.

In the Y-maze, vehicle-treated WT mice performed at chance level and CHL1 KO mice performed generally better with a reduced number of errors within the same period to complete the trial. Learning capabilities of CHL1 mutant mice were normal in several behavioral paradigms^{27,44-46}, cognitive impairments were observed and have been linked to altered aspects of working memory. In a T-maze spontaneous alternation task with an inter-trial interval, CHL1 KO mice performed above the chance level as WT animals, but in a T-maze reinforced alternation task they did not achieve above chance performance^{44,45}. However, both tests showed that CHL1 KO animals exhibited impaired working memory duration, as they took more time to complete trials, indicating a slower processing speed compared to WT animals^{44,45}. Additionally, male CHL1 KO mice were described to attend to relevant

task cues but struggled to integrate spatial and temporal information in a complex radial maze task⁴⁶. Here, no slower processing speed or short-term retention difference were observed in the spatial working memory during the spontaneous alternation task. CHL1 KO mice showed a better performance within the same time to complete the trial than WT mice. This outcome might be influenced by the overall reduced stress-like state observed in CHL1 KO mice, as anxiety traits can impact cognitive-motor planning when adjusting walking movements⁴²⁷. An interesting observation is that an anxiolytic and anti-depressant-like mouse model, the TAAR5 KO line, exhibits elevated dopamine levels in the striatum and an enhanced cognitive performance in working memory tasks⁴²⁸. Given the potential influence of anxiety and stress levels on working memory, it is plausible to consider that the current results could reflect the reduced baseline stress imposed by the overall behavioral procedure on the mice, rather than indicating improved cognitive performance. Moreover, the literature reports impaired working memory only in the context of the most challenging paradigms. When considering data from the first inter-trial interval (either 5 or 30 seconds) in a spontaneous alternation test or the first alternate arm choices in two 8-arm radial mazes, CHL1 KO mice did not exhibit differences from WT animals^{44,45}. This suggests that working memory discrepancies become apparent only under the highest cognitive load conditions, and it is conceivable that in a relatively simple spontaneous alternation task, such as the one used here, CHL1 ablation might not lead to notable working memory impairments in either female or male mice.

Regarding working memory, striatal DRD2 signaling acts as a gating mechanism that facilitates or prevents the access of new working memory information into the PFC, relying on a prefrontal-basal ganglia model consisting of a "go" circuit mediated by DRD1 (striatal direct pathway) and a "no-go" circuit mediated by DRD2 (striatal indirect pathway)^{233,234}. There is a U-shaped relationship between working memory and striatal dopamine levels: intermediate tonic levels promote optimal gating (selective target updating); high tonic levels lead to over updating, causing interference from distractors; low tonic levels result in overall poor updating, even for essential information^{235,429}. However, the working memory effects of DRD2 antagonism or agonism depends on the individual baseline levels of dopamine in the striatum (e.g., high-span individuals show higher baseline dopamine levels) and on the concentrations of DRD2-specific compounds targeting pre- and postsynaptic effects^{233,234}. For example, sulpiride's differential DRD2 pre- and postsynaptic effects contribute differently to spatial working memory. A high dose of sulpiride administered to healthy volunteers caused impairments in spatial working memory only at more complex paradigms (higher "no-go" signaling)²³⁶. Lower doses were found to either produce fewer correct sequences during the first exposure to a sequence generation task or show no effect on working memory performance (reduced "no-go" signaling)^{237,238}. While it is essential to consider both pre- and postsynaptic mechanisms, studies have emphasized the importance of baseline dopamine levels, especially when using a potent

DRD2 agonist like cabergoline, in the context of working memory^{233,234}. For instance, low-span individuals with a reduced baseline of dopamine suffered an enhancement of working memory in a standard task, but an impaired one when distractors were present because of the lower threshold for updating working memory and increase in distractibility (mimics a striatal dopamine level increase). Individuals with a high-span are more susceptible to the reduction of presynaptic DA bursts which cause a less optimal performance of working memory relative to their usual level of distractor-filtering ability^{233,234}.

Based on my findings, the above change level performance of CHL1 KO mice but not of WT mice was still noticeable between sulpiride-treated WT and CHL1 KO females, whereas sulpiride did not affect WT males but tended to decrease CHL1 KO males' performance to the same level as WT males, though the effect was not distinct from vehicle-treated CHL1 KO males. This suggests that WT mice and females with CHL1 ablation did not respond to the presynaptic DRD2 blockade and the subsequent increase in striatal dopamine or the treatment did not produce increased striatal dopamine levels, showing normal spatial working memory. The absence of effects aligns with previous studies with healthy subjects, where the lowest doses of sulpiride failed to induce any working memory effects²³⁸. Nevertheless, the tendency towards poorer performance of sulpiride-treated CHL1 KO males relative to the vehicle-treated group could indicate a specific impact of sulpiride on working memory in males when CHL1 is absent. In turn, quinpirole treatment did not affect WT mice's performance but seemed to slightly worsen CHL1 KO mice's percentage of correct alternations, bringing their performance in line with that of WT mice (at chance level). Quinpirole-induced hypolocomotion was reflected by an extended time required for WT mice and CHL1 KO females to complete alternations. In contrast, this effect was not observed in CHL1 KO males, indicating their reduced sensitivity to quinpirole-induced motor inhibition. It is plausible that WT mice have normal striatal dopamine levels and effective balancing mechanisms, which would lead to a reduction in striatal dopamine levels caused by presynaptic DRD2 stimulation, mainly enhancing "no-go" signaling inducing motor activity suppression (resulting in longer completion times) but this might not be enough to affect spatial working memory in the simplified Y-maze task. Regarding CHL1 KO mice, their slightly inferior performance after quinpirole treatment could be due to an increased sensitivity to the decrease of striatal dopamine triggered by presynaptic DRD2 stimulation. The increased "no-go" signaling leads to the subsequent suppression of motor activity as in WT animals but also extends its impact by decreasing update-checking behavior in spatial working memory. With sulpiride treatment, increased striatal dopamine levels lead to increased updating behavior, making CHL1 KO males more susceptible to distractions in spatial working memory, a response that WT mice can better manage. It is plausible that a presynaptic downregulation of DRD2 or a higher proportion of low-affinity DRD2 in CHL1 KO mice could disrupt the balance of dopamine regulation within the working memory circuits. WT mice retain

the ability to counteract these dopamine changes and are less susceptible to working memory deficits, whereas CHL1 KO mice lack this compensatory mechanism.

Hence, the enhanced spatial working memory performance of CHL1 KO mice could have been enabled by the relaxed-like state. Additionally, DRD2 modulation had no impact on spatial working memory of WT animals. Interestingly, sulpiride tended to worsen the performance of CHL1 KO males in the Y-maze, while quinpirole negatively affected the performance of CHL1 KO females and males. These results support the downregulation or a higher proportion of low-affinity DRD2 in CHL1 KO mice that could cause an imbalance in working memory.

4.3.4 CHL1 does not impact novelty-seeking behavior

Novelty-seeking behavior is linked to the motivation for new experiences and to the reward system, with a significant impact from dopaminergic projections from the VTA to the NAc, the SN to the striatum tail, and the VTA-hippocampus neuronal loop^{199,430}. My thesis focused on stimulus novelty, where the striatum plays a significant role due to the absence of pre-existing recognition memory, rather than contextual novelty based on prior recollection of familiar objects^{321,322}. Following a pre-habituation period in the arena, the mice's reactivity and interest in a novel object were assessed using the NI test.

While analyzing mouse activity near a novel object in the arena, no significant differences in exploration existed between WT and CHL1 KO mice. CHL1 KO females only exhibited a tendency for enhanced exploration and quicker approaches to the novel object, in contrast to CHL1 KO males, who tended to exhibit reduced movement and delayed approaches but an equivalent amount of time near the object. CHL1 ablation in mice has been linked to mild impairments in novelty-seeking behavior, characterized by initial hesitation when exploring a new object without significant changes in its exploration time^{43,44}. Additionally, decreased responsiveness to environmental and social stimuli has been observed, including reduced reactions to a novel open field arena and delayed responses to social stimuli in tests like urine marking, resident-intruder, and social preference^{37,44}. Interestingly, these results are in line with the observation that CHL1 KO males tended to explore less and take more time to perceive the novel object compared to WT males, although it is worth considering that the overall reduction in stress levels could have contributed to an enhanced environmental perception, explaining the lack of statistical significance relative to WT males. These reduced and delayed novelty perception could be linked to attention and sensory gating deficits, supported by an impaired prepulse inhibition of the acoustic startle response, indicating difficulties in gating sensorimotor information, as well as an impaired interval timing and a reduced latent inhibition⁴⁶⁻⁴⁸. However, the tendency for a higher novelty-induced behavior exhibited by CHL1 KO females did not correspond to the previous findings. With this novelty-inducing paradigm, the earlier hypotheses suggesting that the deletion of

CHL1 results in less disruption of dopaminergic balance and a reduced impact of postsynaptic DRD2 impairment in females compared to males gain further support. Interestingly, there is an inverse relationship between novelty-seeking behavior and the availability of DRD2 in the ventral midbrain, observed in both humans and rodents^{244,245}. Indeed, mice lacking DRD2 in dopaminergic neurons display hyperactivity in novel environments and increased motivation to seek rewards²¹⁸. Additionally, rodents with high responsiveness to novelty exhibit higher levels of extracellular dopamine in the NAc both under baseline conditions and when stimulated^{246,247}. Consequently, these individuals show increased dopamine release mediated by presynaptic DRD2 that are less sensitive to agonists inhibition²⁴⁵. Therefore, while the enhanced novelty responsiveness of CHL1 KO females remains a tendency, it further supports the notion of a slightly altered phenotype in both females and males following CHL1 deletion. Specifically, females seem to exhibit a tighter dopaminergic regulation despite a probable downregulation of presynaptic DRD2, while males display a greater imbalance with reduced basal locomotion.

Unlike the previous behavioral parameters, the DRD2 modulation had no impact on the novelty-induced behavior of WT and CHL1 KO mice. It is important to highlight that the performance of quinpirole-treated CHL1 KO males might suggest an increased interest in the novel object compared to WT males, but this likely mirrors the delayed hypolocomotor effect of quinpirole particularly present in CHL1 KO males.

The stimulus novelty from an unfamiliar object typically triggers risk-assessment behavior, influencing the animal's decision to engage or avoid the object. This behavior is closely tied to fluctuations in striatal dopamine levels^{321,322}. Enhanced reactivity to novelty often correlates with elevated striatal dopamine levels, which can be attributed to a reduced availability of presynaptic DRD2 in midbrain axon terminals in healthy individuals and rats, or postsynaptic DRD2 in the caudate nucleus of monkeys^{244,245,342}. Prior research about DRD2 modulation's impact on recognition memory revealed that high doses of the DRD2 antagonist sulpiride had no effect on object recognition in male rats, while haloperidol improved object recognition in mice with mildly elevated striatal dopamine levels^{341,431}. Simultaneous activation of DRD1 and DRD2 with the mutual agonist apomorphine in humans increased the sensitivity of the brain to novelty, while administering a high dose of quinpirole to male rats did not result in memory impairments^{432,433}. The behavioral paradigm employed in this study aimed to assess reactivity towards novel stimuli, and neither DRD2 blockage nor stimulation affected this behavior in WT and CHL1 KO mice. Since object recognition behavior remains unaffected even with higher doses of DRD2-specific compounds, it is reasonable to assume that lower doses would have no impact on a less intricate cognitive behavior such as reactivity to novel stimuli. In addition, DAT-deficient mice, characterized by hyperdopaminergia, displayed normal locomotor activity in the absence of environmental stimuli but showed novelty-induced hyperlocomotion, which was only fully

reversed by high doses of haloperidol, a DRD2 antagonist⁴³⁴. The authors suggested that the ineffectiveness of lower haloperidol doses might result from increased synaptic dopamine levels and DRD2 downregulation, reducing haloperidol's potency⁴³⁴. Therefore, the absence of effects of sulpiride and quinpirole on CHL1 KO mice relative to WT animals suggests that, despite the potential mild impairments in dopaminergic signaling, these are not substantial to significantly impact their reactivity to novel stimuli.

4.3.5 Sex-dependent behaviors and final assumptions

Neuropsychiatric disorders marked by dopaminergic impairment, such as schizophrenia, ASD, major depressive disorder, Parkinson's disease, and addiction, incorporate sex as a vital biological factor, yet a comprehensive understanding of its implications remains elusive. Incorporating sex as a variable in the study of dopaminergic-mediated behaviors is crucial because the dopaminergic system exhibits significant sex-based distinctions in its anatomy, regulation, and function. In this study, I aimed to address these gaps by investigating potential sex-related behaviors resulting from CHL1 ablation in mice and their potential influence on the regulation of DRD2-mediated dopaminergic signaling.

As ovarian hormones fluctuation can interfere with dopaminergic signaling in the striatum⁴³⁵, it is important to establish in advance whether the estrous cycle might interfere with the behavior studied. Previous studies on C57BL/6J mice consistently found minimal estrous cycle impact on locomotor and anxiety-related parameters (assessed via the open field test, rotarod, or elevated plus maze), depression-like behavior (evaluated with sucrose preference, marble burying, tail suspension, or forced swimming tests), cognitive parameters (examined in motor learning and working memory recognition), and social motivation (tested using the resident-intruder or social interaction tests)⁴³⁶⁻⁴³⁹. Nevertheless, an influence of the estrous cycle on anxiety- and depression-like behaviors has been reported, but results are inconsistent⁴⁴⁰. While some studies suggested a higher anxiety-like state in females during the diestrus stage^{440,441}, many failed to detect the estrous cycle's effect^{437-439,442}. Considering this, the present behavioral setting used housing conditions promoting estrous cycle synchronization via the Whitten effect, where virgin female and male mice were maintained in the same behavioral room in cages with 3 to 4 animals. The exposure to volatile pheromones from male urine induces females to enter the estrus phase by the third day of exposure^{443,444}. This method is sufficient to reinstate cyclicity across grouped female mice to ensure a higher probability of all females being at the same estrous phase when tested^{445,446}.

Neuroanatomical differences between sexes begin to develop before any influence of gonadal hormones⁴⁴⁷ and persist into adulthood, shaping the anatomy, organization, and circuitry of the dopamine system. For example, female rats have fewer SNc but more VTA dopaminergic neurons than males^{448,449}, while female mice exhibit only a higher number of VTA dopaminergic neurons⁴⁵⁰. Sex-specific aspects of the dopaminergic system include the regulation of dopamine clearance, release, and

signaling for controlling extracellular dopamine levels. Female rodents exhibit enhanced dopamine clearance in the striatum relative to males, attributed to increased DAT and VMAT2 activity/efficiency^{451–454}, a finding supported by binding and uptake studies in rats and humans^{455–457}. Interestingly, DRD2 was reported to couple with DAT to promote its phosphorylation and recruitment to the membrane⁴⁵⁸, a regulation that was found only in the dorsal striatum of males and in the ventral striatum of female mice⁴⁵⁹. Additionally, female rats show increased responses to cocaine-induced DAT blockage and haloperidol-induced DRD2 blockage, resulting in elevated striatal dopamine release compared to males, alongside reduced sensitivity to the DRD2 agonist quinpirole, which is less effective at inhibiting dopamine release in the dorsal striatum^{367,368}. These results are in line with increased cocaine-induced locomotion in female rats and reduced sensitivity of female rats/monkeys to the hypolocomotor and other behavioral effects of quinpirole at lower doses^{367,368,460–462}, suggesting enhanced presynaptic DRD2 function in females with a near-maximal activation at baseline, rendering subsequent DRD2 activation ineffective in further reducing dopamine release. This reduced quinpirole sensitivity is further accentuated during the estrus phase⁴⁶². While studies on DRD2 expression or affinity in the striatum did not reveal sex differences in humans or rats^{124,125,128}, female rats exhibit higher DRD1-DRD2 heteromer expression in the CPu and NAc, along with lower DRD1 expression in the NAc compared to males¹²⁸. The lower DRD1 expression in females might contribute to reduced GABA feedback on dopamine terminals, potentially elevating dopamine levels⁴⁶³. In summary, the literature suggests enhanced stimulus-driven dopamine release in females, balanced by increased presynaptic DRD2 tonic activation that promotes a tighter and efficient dopamine clearance/repackaging via DAT and VMAT2. Additionally, sustained presynaptic DRD2 activation limits further stimulation and reduces self-inhibition over dopamine release, working in conjunction with reduced GABA-negative feedback to elevate basal dopamine levels in females.

In the present thesis the distinct neuroanatomy and dopamine regulation in female and male mice lead to sex-based disparities in animal behavior, cognition, and motor abilities, potentially explaining sex-dependent disparities in CHL1 ablation and DRD2 pharmacological modulation outcomes.

In my behavioral analysis, WT mice consistently show no differences in motor activity levels across all tests, consistent with previous reports on motor performance in C57BL/6 mice^{464,465}. Nonetheless, across various mouse and rat strains, females consistently display higher ambulation levels compared to males, with variations in sex hormones, particularly increased estrogen and decreased testosterone levels in females, contributing to their enhanced activity and exploratory behavior^{466,467}. In the case of CHL1 ablation, CHL1 KO males exhibit lower baseline motor activity compared to females in both the OF and YM tests, with both sexes displaying a delayed response to quinpirole. This could result from the downregulation of both pre- and postsynaptic DRD2, though in a sex-dependent manner. I suggest that the decreased presynaptic DRD2 activity could potentially diminish dopamine's presynaptic

inhibition, while the reduced availability of postsynaptic DRD2 might render them less effective at inhibiting the striatal indirect pathway relative to WT males, resulting in decreased locomotion and reduced responsiveness to increased striatal dopamine levels. In CHL1 KO females, the downregulation of presynaptic DRD2 could be counteracted by their innately enhanced tonic dopaminergic activity of release and clearance and by a less pronounced impact on postsynaptic DRD2 relative to males. This combination could lead to greater inhibition of the striatal indirect pathway, serving as a preventive mechanism against the increased presynaptic DRD2 autoinhibition that would otherwise be induced by CHL1's ablation. Interestingly, CHL1 KO males were previously shown to exhibit lower motor activity and a tendency for poorer performance on the rotarod compared to females⁴³. These findings could potentially reflect as well the sex-dependent motor behavior I observed as a consequence of CHL1 deficiency. It is worth noting that tail handling, a common practice for lifting mice, has been reported to induce higher stress levels in males, whereas female mice tend to experience stress when subjected to low handling frequency⁴⁶⁸. Given these sex-specific responses to handling, the consistent and gentle handling protocol employed in my experimental setup might have contributed to a lower stress state in CHL1 KO females, thereby facilitating the detection of this motor behavior that is dependent on both genotype and sex.

The distinct tonic dopaminergic activity between sexes was similarly observed following presynaptic DRD2 activation with quinpirole. Despite reducing motor activity in WT mice starting at the same time (3 min into testing), the decline was more pronounced in WT males compared to WT females, both in comparison to the vehicle-treated group during the first 10 min of the OF and to each other during the 30 min of testing. Indeed, this sex-dependent effect of quinpirole in female rats was previously reported, as they display lower sensitivity than males to quinpirole's hypolocomotor effects at lower doses due to reduced efficacy of the drug to inhibit dopamine release from dopaminergic terminals in females^{367,368,461,462}. Furthermore, the delayed hypolocomotor effect induced by quinpirole in CHL1 KO mice took longer to manifest in males, becoming evident 9 min after the start of the OF, while in females, it was observed after 7 min. I suspect that this sex difference could be attributed to the pronounced reduction of postsynaptic DRD2 availability in CHL1 KO males, resulting in decreased responsiveness to changes in striatal dopamine levels and rendering males less susceptible than females to quinpirole's effects, ultimately leading to a delayed locomotor reduction.

Another sex-dependent effect consistently observed in all tests was the decreased motor activity among CHL1 KO females following sulpiride treatment, which could potentially be attributed to the comparatively lower impact on postsynaptic DRD2 in CHL1 KO females compared to males. Despite employing a sulpiride concentration targeting presynaptic DRD2 effects, the reduction of presynaptic DRD2 in both CHL1 KO females and males could facilitate the binding of sulpiride to postsynaptic DRD2. The proposed higher availability of postsynaptic DRD2 in CHL1 KO females relative to males could render females more susceptible to the postsynaptic effects of sulpiride, leading to increased

activation of the striatal indirect pathway and subsequent reduction in locomotion. Moreover, other contributing factors might play a role in this outcome. Considering that previous research has indicated that sulpiride binding to DRD2 is dependent on and enhanced by Na⁺ ions^{360,361}, it is plausible that an accentuated reduced availability of DRD2 in CHL1 KO mice, whether through decreased higher conformational state or expression, could result in altered sensitivity to Na⁺ ions, ultimately weakening the binding of sulpiride to postsynaptic DRD2.

My behavioral analysis revealed a tendency for only CHL1 KO females to show reduced responsiveness to stimulus-induced stress compared to males and WT females after sulpiride treatment. It is worth noting that sulpiride at higher doses has been reported to induce an anxiolytic-like state in both female and male rodents^{412,422}. Additionally, it was proposed that sulpiride might possess a higher affinity for DRD2 in the mesolimbic pathway (from VTA to NAc)⁴⁶⁹, a characteristic shared with the structurally and functionally similar compound, amisulpride⁴⁷⁰. Female rats have previously displayed increased responses to haloperidol-induced catalepsy^{367,471} and have shown higher sensitivity to sulpiride's effects on fear conditioning during the estrus phase⁴¹³. Similarly, methylphenidate administration in women has been observed to elicit an enhanced dopamine release only in the NAc⁴⁷². Furthermore, the regulation of DAT expression in the NAc seems to be under the control of presynaptic DRD2 only in female rats⁴⁵⁹. Therefore, in addition to the sex-specific effects of sulpiride on the locomotion of CHL1 KO females, which could be attributed to the higher availability of postsynaptic DRD2 compared to males, it could also be of value to explore the hypothesis of a sex- and region-specific impairment of postsynaptic DRD2 in CHL1 mice within the striatum. In CHL1 KO females, the decreased availability of presynaptic DRD2 in the NAc could potentially lead to changes in DAT expression, dopaminergic homeostasis, and/or ion content. These altered mechanisms in CHL1 KO females might result in a higher susceptibility to sulpiride's effects within the NAc compared to WT females. Notably, the NAc, along with the dorsal striatum, contributes to motor function²¹⁵, so increased postsynaptic DRD2 sensitivity in the NAc aligns with the observed reduction in locomotion induced by sulpiride only in CHL1 KO females.

This comprehensive study has unveiled intriguing sex-dependent differences arising from CHL1 ablation, subsequently triggering a genotype- and sex-specific modulation of DRD2 functions. The absence of CHL1 in males is associated with basal locomotor impairments and a reduced sensitivity to quinpirole-induced hypolocomotion, whereas in females, the diminished quinpirole sensitivity is less pronounced. On the other hand, the absence of CHL1 heightens female responsiveness to sulpiride, resulting in reduced locomotion and a slight decrease to stimulus-induced stress responsiveness. In conclusion, I propose that CHL1 KO mice exhibit a compromised function or availability of both DRD2 isoforms, impacting behavior primarily governed by dopaminergic projections to the dorsal striatum - the nigrostriatal pathway, in both females and males. In females, the impairment of postsynaptic DRD2 might be less pronounced and could extend across the entire striatum or be limited to the NAc. Thus,

the potential for region-specific postsynaptic DRD2 impairment in CHL1 mice within the striatum requires further investigation through the use of postsynaptic DRD2 targeting doses or localized intra-striatal injections, alongside behavioral paradigms focused on the limbic system, such as those related to reward and punishment-based learning.

Chapter V

Conclusion

5 Conclusion

This thesis provided a functional characterization of the CHL1 and DRD2 interaction by investigating how their interplay influences pre- and postsynaptic dopaminergic mechanisms, ranging from neuronal biochemistry processes to the evaluation of striatal-dependent behaviors in mice. Biological models of WT and transgenic CHL1 KO mice, together with the pharmacological inhibition/blockage of DRD2-dependent functions with sulpiride or quinpirole, were used to study such interaction.

The biochemical findings revealed that CHL1 interacts with DRD2 in presynaptic dopaminergic neurons and postsynaptic striatal neurons, both *in vivo* and *in vitro*. Here, ventral midbrain primary neurons were used to model presynaptic dopaminergic transmission, while striatal primary neurons were used to represent the postsynaptic MSNs-expressing DRD2. CHL1 ablation had no significant impact on the basal signaling of both DRD2 isoforms; however, it induced alterations in sulpiride-induced DRD2 signaling in ventral midbrain neurons and influenced the effects of quinpirole on DRD2-dependent neuronal morphology in a manner that depended on developmental stages.

These results suggest that the normal functioning of pre- and post-synaptic DRD2-dependent functions is not significantly disrupted by the absence of CHL1. Instead, was observed that the sensitivity of receptors to the pharmacological modulation undergoes notable changes, unveiling CHL1's role as a modulator in the dopaminergic neurotransmission, through its interaction with DRD2. Based on the altered sensitivity of DRD2 when interacting with exogenous ligands in the absence of CHL1, I propose that CHL1 might function as an allosteric modulator, exerting influence over the structural conformation and functionality of DRD2. Furthermore, developmental-dependent alterations in the morphological responses of cultured MSNs to postsynaptic DRD2 modulation were observed in the absence of CHL1. This suggests that CHL1 could play a role in the temporal and/or spatial expression of DRD2 during striatal development, similar to its developmental role in the ventral midbrain dopaminergic pathways²⁰.

Ascertaining the role of CHL1 as an allosteric modulator of DRD2 in future studies could advance our understanding of DRD2's conformational dynamics in the dopaminergic pathways. The interaction between an endogenous allosteric ligand and a receptor provides valuable insights into the receptor's diverse biological conformations, potentially serving as inspiration for the design of structure-based compounds. Considering CHL1's functions as a cell adhesion molecule and its involvement in the development of ventral midbrain dopaminergic neurons²⁰, it is plausible that CHL1 plays a role in the development of dopaminergic signaling in MSNs. This has the potential to result in atypical striatal connectivity, which could impact mouse behavior in subsequent stages of life.

The behavioral assessment of striatal-dependent functions focused on evaluating the effects of pharmacological modulation of presynaptic DRD2, which included parameters of locomotor activity, exploration, emotionality, working memory, and novelty-seeking, revealed intriguing sex-dependent differences resulting from CHL1 ablation. CHL1 KO males exhibited reduced locomotor activity and a slightly more relaxed emotional state or reduced reactivity to external stimuli, aligning with the previously documented behavioral phenotype. In contrast, CHL1 ablation in females had no significant impact on their motor activity or emotional reactivity to stimuli. The DRD2 agonist quinpirole induced a hypolocomotor effect in both WT and CHL1 KO mice but with CHL1 KO mice showing a comparatively delay. Notably, the hyposensitivity to quinpirole was more pronounced in CHL1 KO males compared to females. Moreover, the DRD2 antagonist sulpiride led to a reduction in locomotor activity and a slight decrease in stimulus-induced stress responsiveness exclusively in CHL1 KO females.

Based on these findings, I suggest that CHL1's ablation simultaneously disrupts the functioning or availability of pre- and postsynaptic DRD2, possibly by altering its higher conformational state or surface expression. Notably, CHL1 KO females exhibit a relatively lower impact on postsynaptic DRD2 compared to males, hinting at a potential region-specific postsynaptic DRD2 impairment within the striatum of CHL1 mice. This hypothesis supports the decreased tonic locomotion observed particularly in CHL1 KO males, the enhanced postsynaptic sensitivity of CHL1 KO females to sulpiride, and the differential delayed hypolocomotor effect of quinpirole in CHL1 KO mice. Thus, CHL1 appears to modulate DRD2 signaling in striatal-dependent behaviors regulated by the dorsal striatum in both females and males and possibly by the ventral striatum exclusively in females. Nevertheless, it is important to acknowledge that the divergent sex impact of CHL1 on the DRD2 signaling might also stem from various other factors that are inherently associated with the sexual dimorphism present in the neurobiology and anatomy of the dopaminergic system.

Notably, it has been documented that sexual dimorphism plays a substantial role in the onset of neuropsychiatric diseases, the severity of their symptoms, and even in the responsiveness to antidepressant and antipsychotic treatments, with women typically exhibiting greater sensitivity and requiring lower medication doses than men^{473,474}. Given the substantial body of evidence linking genetic or functional abnormalities in DRD2 to a range of neurological conditions, including schizophrenia, ASD, and major depressive disorder, it becomes essential to gain a comprehensive understanding of the intricate interactions between DRD2 and other physiological binding partners, such as CHL1. As a result, my thesis provides valuable insights into the complex biochemical and behavioral outcomes that emerge from the interplay between CHL1 and both DRD2 isoforms, emphasizing the critical role of considering sex as a significant biological variable in future studies.

Abbreviations

5-HT2c	serotonin 2c	CTLD	C-type lectin-like domain
AC	adenylyl cyclase	Cy	cyanine fluorescent dye
ACC	anterior cingulate cortex	DA	dopamine
ADAM8	a disintegrin and metalloproteinase	DAG	diacylglycerol
Akt	protein kinase B	DAPI	4',6-diamidino-2-phenylindole
Ala	alanine	DAT	dopamine transporter
AMPA	α -amino-3-hydroxy-5-methyl-4- isoxazolepropionic acid	DNA	deoxyribonucleic acid
AMY	amygdala	DARPP-32	dopamine- and cAMP-regulated phosphoprotein 32 kDa
ANOVA	analysis of variance	dH₂O	distilled water
AP	alkaline phosphatase	ddH₂O	double distilled water
AP2	clathrin adaptor protein 2	DISC1	disrupted-in-schizophrenia 1
Arg	arginine	div	days <i>in vitro</i>
ASD	autism spectrum disorders	DGEA	Asp-Gly-Glu-Ala peptide
Asp	aspartic acid	DMEM	dulbecco's modified eagle Medium
ATP	adenosine triphosphate	dMSNs	direct pathway medium spiny neurons
BACE1	β -site amyloid precursor proteincleaving enzyme 1	DMSO	dimethyl sulfoxide
BCA	bicinchoninic acid protein	DNA	deoxyribonucleic acid
BRET	bioluminescence resonance energy transfer	DNase	deoxyribonuclease
BSA	bovine serum albumin	DRD1	dopamine receptor type-1
CALL	human ortholog gene of CHL1	DRD2	dopamine receptor type-2
CAM	cell adhesion molecule	DRD2_L	DRD2 long isoform
CaMKII	calcium/calmodulin-dependent PK II	DRD2_S	DRD2 short isoform
cAMP	cyclic adenosine monophosphate	DRD3	dopamine receptor type-3
cDNA	complementary DNA	DRD4	dopamine receptor type-4
CDK5	cyclin-dependent kinase 5	DRD5	dopamine receptor type-5
CHL1	close homolog of L1	dSTR	dorsal striatum
CHL1 KO	CHL1 knock-out	E	embryonic day
CNS	central nervous system	ECL	enhanced chemiluminescence
CNTN4	Contactin-4 gene	ECM	extracellular matrix
CPu	caudate putamen	EDTA	ethylenediaminetetraacetic acid
CRBN	Cereblon gene	EGTA	ethylene glycol tetraacetic acid
CREB	cAMP response element-binding protein	EL1/2	extracellular loop 1 or 2
CTCF	corrected total cell fluorescence	ELISA	enzyme-linked immunosorbent assay
		ERK1/2	extracellular signal-regulated kinase 1/2
		ERM	ezrin-radixin-moesin

ETC	entorhinal cortex	KO	knock-out
FBS	fetal bovine serum	Leu	leucine
FIGAY	Phe-Ile-Gly-Ala-Tyr peptide	LHb	lateral habenula
FIGQY	Phe-Ile-Gly- Gln-Tyr peptide	LRR	leucine-rich repeat
FN-III	fibronectin type III	MAP2	microtubule-associated protein 2
FRET	fluorescence resonance energy transfer	MDMA	3,4-methylenedioxymetamphetamine
G$\alpha_{i/o}$	inhibitory G α subunits	min	minute/s
Gα_s	excitatory G α subunits	mRNA	messenger ribonucleic acid
GABA	γ -aminobutyric acid	MSNs	medium spiny neurons
GAPDH	glyceraldehyde-3-phosphate dehydrogenase	NAc	nucleus accumbens
Glu	glutamic acid	NCAM	neural cell adhesion molecule
Gly	glycine	NF	neurofascin
GDP	guanosine diphosphate	NF186	186 kDa isoform of neurofascin
GIRKs	G protein-coupled inwardly rectifying potassium channels	NGF-β	nerve growth factor β
GPCR	G protein coupled receptor	NI	novelty-induced test
GPe	externus globus pallidus	NMDA	N-methyl-D-aspartate
GPi	internus globus pallidus	NPCs	neuronal progenitor cells
GRK	G protein-coupled receptor kinase	NrCAM	neuron-glia-related CAM
GSK3	glycogen synthase kinase 3 (α and β)	NSF-1	neural survival factor-1
GTP	guanosine triphosphate	OF	open field test
HBSS	hanks' balanced salt solution	OT	olfactory tubercle
HRP	horseradish peroxidase	P	postnatal day
Hsc70	heat shock cognate 70 kDa protein	PAT	proline-, alanine-, threonine
HYP	hippocampus	PBS	phosphate-buffered saline
ICC	immunocytochemistry	PCR	polymerase chain reaction
ICL	intracellular loop	pDARPP-32	phosphorylated DARPP-32
Ig	immunoglobulin	PDK	phosphatidyl-dependent kinases
IgSF	immunoglobulin superfamily	PDL	poly-D-lysine
IHC	immunohistochemistry	pERK1/2	phosphorylated extracellular signal-regulated kinase 1/2
iMSNs	indirect pathway medium spiny neurons	PET	positron emission tomography
i.p.	intraperitoneal	PFA	paraformaldehyde
IP3	inositol trisphosphate	PFC	prefrontal cortex
IRDye	infrared dye	pGSK3β	phosphorylates glycogen synthase kinase 3 β (Ser9)
Kir2	inward rectifying potassium 2	PI3K	phosphoinositol-3 kinase
KGE	Lys-Gly-Glu peptide	PIP2	phosphatidylinositol 4,5-bisphosphate

PIP3	phosphatidylinositol 3,4,5-trisphosphate	SN	substantia nigra
PP2A	protein phosphatase-2A	SNC	substantia nigra pars compacta
PTEN	phosphatase and tensin homolog	SNP	single nucleotide polymorphism
PKA	protein kinase A	SNr	substantia nigra pars reticulata
PKC	protein kinase C	SSRI	selective serotonin reuptake inhibitors
PLA	proximity ligation assay	STh	subthalamic nucleus
PLC	phospholipase C	Sulp	sulpiride
PMSF	phenylmethylsulfonyl fluoride	TAAR1	trace amine-associated receptor 1
PNC	peripheral nervous system	TAE	tris-acetate-ethylenediaminetetraacetic acid buffer
PNBM	primary neuron basal medium	TBS	tris-buffered saline
PNGM	primary neuron growth medium	TBS-T	tris-buffered saline with Tween 20
PP1	protein phosphatase 1	TH	tyrosine hydroxylase
PP2B	phosphatase calcineurin/protein phosphatase 2B	Thr	threonine
PSD95	postsynaptic density 95	Tris	trisaminomethane
PTCH1	hedgehog receptor patched-1	Tyr	tyrosine
pTH	phosphorylated tyrosine hydroxylase (Ser40)	v	volume
Quinp	quinpirole	Veh	vehicle
RGS	regulators of G protein signaling protein	VGluT2	vesicular-glutamate transporter 2
RGD	Arg-Gly-Asp peptide	VMAT	vesicular monoamine transporter
RIPA	radioimmunoprecipitation assay	VTA	ventral tegmental area
RNA	ribonucleic acid	w	weight
RrF	retrobulbar field	WB	western Blot
RSLE	Arg-Ser-Leu-Glu peptide	WT	wild-type
RTK	receptor tyrosine kinases	YM	Y-maze test
SAP	synapse-associated protein		
SD	standard deviation		
SDS	sodium dodecyl sulfate		
SDS-PAGE	SDS-polyacrylamide gel electrophoresis		
SEM	standard error of the mean		
Sema3A	semaphorin 3A		
Ser	serine		
SI	social interaction		
SMC	sensorimotor cortex		
SNARE	receptor of soluble N-ethylmaleimide-sensitive factor attachment protein		

References

1. Togashi H, Sakisaka T, Takai Y. Cell adhesion molecules in the central nervous system. *Cell Adh Migr*. 2009;3(1):29-35. doi:10.4161/cam.3.1.6773
2. Petruzzelli L, Takami M, Humes HD. Structure and function of cell adhesion molecules. *Am J Med*. 1999;106(4):467-476. doi:10.1016/S0002-9343(99)00058-3
3. Shapiro L, Love J, Colman DR. Adhesion Molecules in the Nervous System: Structural Insights into Function and Diversity. *Annu Rev Neurosci*. 2007;30(1):451-474. doi:10.1146/annurev.neuro.29.051605.113034
4. Horstkorte R, Fuss B. Cell Adhesion Molecules. In: *Basic Neurochemistry*. Elsevier; 2012:165-179. doi:10.1016/B978-0-12-374947-5.00009-2
5. Moreland T, Poulain FE. To Stick or Not to Stick: The Multiple Roles of Cell Adhesion Molecules in Neural Circuit Assembly. *Front Neurosci*. 2022;16(April):1-16. doi:10.3389/fnins.2022.889155
6. Maness PF, Schachner M. Neural recognition molecules of the immunoglobulin superfamily: Signaling transducers of axon guidance and neuronal migration. *Nat Neurosci*. 2007;10(1):19-26. doi:10.1038/nn1827
7. Irintchev A, Schachner M. The Injured and Regenerating Nervous System. *Neurosci*. 2012;18(5):452-466. doi:10.1177/1073858411419047
8. Leshchyns'ka I, Sytnyk V. Reciprocal Interactions between Cell Adhesion Molecules of the Immunoglobulin Superfamily and the Cytoskeleton in Neurons. *Front Cell Dev Biol*. 2016;4(February):1-10. doi:10.3389/fcell.2016.00009
9. Holm J, Hillenbrand R, Steuber V, et al. Structural Features of a Close Homologue of L1 (CHL1) in the Mouse: A New Member of the L1 Family of Neural Recognition Molecules. *Eur J Neurosci*. 1996;8(8):1613-1629. doi:10.1111/j.1460-9568.1996.tb01306.x
10. Kurolap A, Kreuder F, Gonzaga-Jauregui C, et al. Bi-allelic variants in neuronal cell adhesion molecule cause a neurodevelopmental disorder characterized by developmental delay, hypotonia, neuropathy/spasticity. *Am J Hum Genet*. 2022;109(3):518-532. doi:10.1016/j.ajhg.2022.01.004
11. Buhusi M, Midkiff BR, Gates AM, Richter M, Schachner M, Maness PF. Close Homolog of L1 Is an Enhancer of Integrin-mediated Cell Migration. *J Biol Chem*. 2003;278(27):25024-25031. doi:10.1074/jbc.M303084200
12. Schlatter MC, Buhusi M, Wright AG, Maness PF. CHL1 promotes Sema3A-induced growth cone collapse and neurite elaboration through a motif required for recruitment of ERM proteins to the plasma membrane. *J Neurochem*. 2007;104(3):071108171001015-??? doi:10.1111/j.1471-4159.2007.05013.x
13. Falk J, Thoumine O, Dequidt C, Choquet D, Faivre-Sarrailh C. NrCAM Coupling to the Cytoskeleton Depends on Multiple Protein Domains and Partitioning into Lipid Rafts. *Mol Biol Cell*. 2004;15(10):4695-4709. doi:10.1091/mbc.e04-03-0171
14. Dirks P, Thomas U, Montag D. The cytoplasmic domain of NrCAM binds to PDZ domains of synapse-associated proteins SAP90/PSD95 and SAP97. *Eur J Neurosci*. 2006;24(1):25-31. doi:10.1111/j.1460-9568.2006.04899.x
15. Naus S, Richter M, Wildeboer D, Moss M, Schachner M, Bartsch JW. Ectodomain Shedding of the Neural Recognition Molecule CHL1 by the Metalloprotease-disintegrin ADAM8 Promotes Neurite Outgrowth and Suppresses Neuronal Cell Death. *J Biol Chem*. 2004;279(16):16083-16090. doi:10.1074/jbc.M400560200
16. Barão S, Gärtner A, Leyva-Díaz E, et al. Antagonistic Effects of BACE1 and APH1B- γ -Secretase Control Axonal Guidance by Regulating Growth Cone Collapse. *Cell Rep*. 2015;12(9):1367-1376. doi:10.1016/j.celrep.2015.07.059
17. Hillenbrand R, Molthagen M, Montag D, Schachner M. The close homologue of the neural adhesion molecule L1 (CHL1): Patterns of expression and promotion of neurite outgrowth by heterophilic interactions. *Eur J Neurosci*. 1999;11(3):813-826. doi:10.1046/j.1460-9568.1999.00496.x
18. Human Protein Atlas. <https://www.proteinatlas.org/>
19. Nikonenko AG, Sun M, Lepsveridze E, et al. Enhanced perisomatic inhibition and impaired long-term potentiation in the CA1 region of juvenile CHL1-deficient mice. *Eur J Neurosci*. 2006;23(7):1839-1852. doi:10.1111/j.1460-9568.2006.04710.x
20. Alsanie WF, Penna V, Schachner M, Thompson LH, Parish CL. Homophilic binding of the neural cell adhesion molecule CHL1 regulates development of ventral midbrain dopaminergic pathways. *Sci Rep*. 2017;7(1):9368. doi:10.1038/s41598-017-09599-y
21. Frints SGM, Marynen P, Hartmann D, et al. CALL interrupted in a patient with non-specific mental retardation: Gene dosage-dependent alteration of murine brain development and behavior. *Hum Mol Genet*. 2003;12(13):1463-1474. doi:10.1093/hmg/ddg165
22. Tsuboyama M, Iqbal MA. CHL1 deletion is associated with cognitive and language disabilities – Case report and review of literature. *Mol Genet Genomic Med*. 2021;9(7):3-9. doi:10.1002/mgg3.1725
23. Jakovcevski I, Wu J, Karl N, et al. Glial Scar Expression of CHL1, the Close Homolog of the Adhesion Molecule L1, Limits Recovery after Spinal Cord Injury. *J Neurosci*. 2007;27(27):7222-7233. doi:10.1523/JNEUROSCI.0739-07.2007
24. Chen S, Mantei N, Dong L, Schachner M. Prevention of neuronal cell death by neural adhesion molecules L1 and CHL1. *J Neurobiol*. 1999;38(3):428-439. doi:10.1002/(SICI)1097-4695(19990215)38:3<428::AID-NEU10>3.0.CO;2-6
25. Katic J, Loers G, Kleene R, et al. Interaction of the Cell Adhesion Molecule CHL1 with Vitronectin, Integrins, and the Plasminogen Activator Inhibitor-2 Promotes CHL1-Induced Neurite Outgrowth and Neuronal Migration. *J Neurosci*. 2014;34(44):14606-14623. doi:10.1523/JNEUROSCI.3280-13.2014

26. Ango F, Wu C, Van der Want JJ, Wu P, Schachner M, Huang ZJ. Bergmann Glia and the Recognition Molecule CHL1 Organize GABAergic Axons and Direct Innervation of Purkinje Cell Dendrites. Ghosh A, ed. *PLoS Biol.* 2008;6(4):e103. doi:10.1371/journal.pbio.0060103
27. Montag-Sallaz M, Schachner M, Montag D. Misguided Axonal Projections, Neural Cell Adhesion Molecule 180 mRNA Upregulation, and Altered Behavior in Mice Deficient for the Close Homolog of L1. *Mol Cell Biol.* 2002;22(22):7967-7981. doi:10.1128/MCB.22.22.7967-7981.2002
28. Demyanenko GP, Schachner M, Anton E, et al. Close Homolog of L1 Modulates Area-Specific Neuronal Positioning and Dendrite Orientation in the Cerebral Cortex. *Neuron.* 2004;44(3):423-437. doi:10.1016/j.neuron.2004.10.016
29. Wright AG, Demyanenko GP, Powell A, et al. Close Homolog of L1 and Neuropilin 1 Mediate Guidance of Thalamocortical Axons at the Ventral Telencephalon. *J Neurosci.* 2007;27(50):13667-13679. doi:10.1523/JNEUROSCI.2888-07.2007
30. Bye CR, Rytova V, Alsanie WF, Parish CL, Thompson LH. Axonal Growth of Midbrain Dopamine Neurons is Modulated by the Cell Adhesion Molecule ALCAM Through Trans-Heterophilic Interactions with L1cam, Chl1, and Semaphorins. *J Neurosci.* 2019;39(34):6656-6667. doi:10.1523/JNEUROSCI.0278-19.2019
31. Jakovcevski I, Siering J, Hargus G, et al. Close homologue of adhesion molecule L1 promotes survival of Purkinje and granule cells and granule cell migration during murine cerebellar development. *J Comp Neurol.* 2009;513(5):496-510. doi:10.1002/cne.21981
32. Huang X, Zhu L, Zhao T, et al. CHL1 negatively regulates the proliferation and neuronal differentiation of neural progenitor cells through activation of the ERK1/2 MAPK pathway. *Mol Cell Neurosci.* 2011;46(1):296-307. doi:10.1016/j.mcn.2010.09.013
33. Katic J, Loers G, Tosic J, Schachner M, Kleene R. The cell adhesion molecule CHL1 interacts with patched-1 to regulate apoptosis during postnatal cerebellar development. *J Cell Sci.* 2017;130(15):2606-2619. doi:10.1242/jcs.194563
34. Leshchynska I, Sytnyk V, Richter M, Andreyeva A, Puchkov D, Schachner M. The Adhesion Molecule CHL1 Regulates Uncoating of Clathrin-Coated Synaptic Vesicles. *Neuron.* 2006;52(6):1011-1025. doi:10.1016/j.neuron.2006.10.020
35. Andreyeva A, Leshchynska I, Knepper M, et al. CHL1 Is a Selective Organizer of the Presynaptic Machinery Chaperoning the SNARE Complex. Kleinschmitz C, ed. *PLoS One.* 2010;5(8):e12018. doi:10.1371/journal.pone.0012018
36. Mohan V, Wade SD, Sullivan CS, et al. Close Homolog of L1 Regulates Dendritic Spine Density in the Mouse Cerebral Cortex Through Semaphorin 3B. *J Neurosci.* 2019;39(32):6233-6250. doi:10.1523/JNEUROSCI.2984-18.2019
37. Kleene R, Chaudhary H, Karl N, et al. Interaction between CHL1 and serotonin receptor 2c regulates signal transduction and behavior in mice. *J Cell Sci.* 2015;128(24):4642-4652. doi:10.1242/jcs.176941
38. Kotarska A, Fernandes L, Kleene R, Schachner M. Cell adhesion molecule close homolog of L1 binds to the dopamine receptor D2 and inhibits the internalization of its short isoform. *FASEB J.* 2020;34(4):4832-4851. doi:10.1096/fj.201900577RRRR
39. Zhang J, Forkstam C, Engel JA, Svensson L. Role of dopamine in prepulse inhibition of acoustic startle. *Psychopharmacology (Berl).* 2000;149(2):181-188. <http://www.embase.com/search/results?subaction=viewrecord&from=export&id=L30238957>
40. Chaisuksunt V, Campbell G, Zhang Y, Schachner M, Lieberman AR, Anderson PN. The cell recognition molecule CHL1 is strongly upregulated by injured and regenerating thalamic neurons. *J Comp Neurol.* 2000;425(3):382-392. doi:10.1002/1096-9861(20000925)425:3<382::AID-CNE4>3.0.CO;2-N
41. Guseva D, Jakovcevski I, Irintchev A, et al. Cell Adhesion Molecule Close Homolog of L1 (CHL1) Guides the Regrowth of Regenerating Motor Axons and Regulates Synaptic Coverage of Motor Neurons. *Front Mol Neurosci.* 2018;11(May):1-14. doi:10.3389/fnmol.2018.00174
42. Schmalbach B, Lepsveridze E, Djogo N, et al. Age-dependent loss of parvalbumin-expressing hippocampal interneurons in mice deficient in CHL1, a mental retardation and schizophrenia susceptibility gene. *J Neurochem.* 2015;135(4):830-844. doi:10.1111/jnc.13284
43. Pratte M, Rougon G, Schachner M, Jamon M. Mice deficient for the close homologue of the neural adhesion cell L1 (CHL1) display alterations in emotional reactivity and motor coordination. *Behav Brain Res.* 2003;147(1-2):31-39. doi:10.1016/S0166-4328(03)00114-1
44. Morellini F, Lepsveridze E, Kähler B, Dityatev A, Schachner M. Reduced reactivity to novelty, impaired social behavior, and enhanced basal synaptic excitatory activity in perforant path projections to the dentate gyrus in young adult mice deficient in the neural cell adhesion molecule CHL1. *Mol Cell Neurosci.* 2007;34(2):121-136. doi:10.1016/j.mcn.2006.10.006
45. Kolata S, Wu J, Light K, Schachner M, Matzel LD. Impaired Working Memory Duration But Normal Learning Abilities Found in Mice That Are Conditionally Deficient in the Close Homolog of L1. *J Neurosci.* 2008;28(50):13505-13510. doi:10.1523/JNEUROSCI.2127-08.2008
46. Buhusi M, Scripa I, Williams CL, Buhusi C V. Impaired Interval Timing and Spatial-Temporal Integration in Mice Deficient in CHL1, a Gene Associated with Schizophrenia. *Timing Time Percept.* 2013;1(1):21-38. doi:10.1163/22134468-00002003
47. Irintchev A, Koch M, Needham LK, Maness P, Schachner M. Impairment of sensorimotor gating in mice deficient in the cell adhesion molecule L1 or its close homologue, CHL1. *Brain Res.* 2004;1029(1):131-134. doi:10.1016/j.brainres.2004.09.042
48. Buhusi M, Obray D, Guercio B, Bartlett MJ, Buhusi C V. Chronic mild stress impairs latent inhibition and induces region-specific neural activation in CHL1-deficient mice, a mouse model of schizophrenia. *Behav Brain Res.* 2017;333:1-8. doi:10.1016/j.bbr.2017.06.033
49. Salyakina D, Cukier HN, Lee JM, et al. Copy Number Variants in Extended Autism Spectrum Disorder Families Reveal Candidates Potentially Involved in Autism Risk. Zwick ME, ed. *PLoS One.* 2011;6(10):e26049.

doi:10.1371/journal.pone.0026049

50. Morag A, Pasmanik-Chor M, Oron-Karni V, Rehavi M, Stingl JC, Gurwitz D. Genome-wide expression profiling of human lymphoblastoid cell lines identifies CHL1 as a putative SSRI antidepressant response biomarker. *Pharmacogenomics*. 2011;12(2):171-184. doi:10.2217/pgs.10.185
51. Chu TT, Liu Y. An integrated genomic analysis of gene-function correlation on schizophrenia susceptibility genes. *J Hum Genet*. 2010;55(5):285-292. doi:10.1038/jhg.2010.24
52. Tam GWC, van de Lagemaat LN, Redon R, et al. Confirmed rare copy number variants implicate novel genes in schizophrenia. *Biochem Soc Trans*. 2010;38(2):445-451. doi:10.1042/BST0380445
53. Onate-Quiroz K V., Nwosu BU, Salemi P. Novel duplication of the cell adhesion molecule L1-like gene in an individual with cognitive impairment, tall stature, and obesity: A case report. *Front Neurol*. 2023;14(April):1-5. doi:10.3389/fneur.2023.1104649
54. Fu J, Wang T, Fu Z, et al. Case Report: A Case Report and Literature Review of 3p Deletion Syndrome. *Front Pediatr*. 2021;9(February). doi:10.3389/fped.2021.618059
55. Shoukier M, Fuchs S, Schwaibold E, et al. Microduplication of 3p26.3 in Nonsyndromic Intellectual Disability Indicates an Important Role of CHL1 for Normal Cognitive Function. *Neuropediatrics*. 2013;44(05):268-271. doi:10.1055/s-0033-1333874
56. Fernandez T, Morgan T, Davis N, et al. Disruption of Contactin 4 (CNTN4) Results in Developmental Delay and Other Features of 3p Deletion Syndrome. *Am J Hum Genet*. 2008;82(6):1385. doi:10.1016/j.ajhg.2008.04.021
57. Dijkhuizen T, van Essen T, van der Vlies P, et al. FISH and array-CGH analysis of a complex chromosome 3 aberration suggests that loss of CNTN4 and CRBN contributes to mental retardation in 3pter deletions. *Am J Med Genet Part A*. 2006;140A(22):2482-2487. doi:10.1002/ajmg.a.31487
58. Tassano E, Biancheri R, Denegri L, et al. Heterozygous deletion of CHL1 gene: Detailed array-CGH and clinical characterization of a new case and review of the literature. *Eur J Med Genet*. 2014;57(11-12):626-629. doi:10.1016/j.ejmg.2014.09.007
59. Bertini V, Azzarà A, Toschi B, Gana S, Valetto A. 3p26.3 terminal deletions: a challenge for prenatal genetic counseling. *Prenat Diagn*. 2017;37(2):197-200. doi:10.1002/pd.4978
60. Palumbo O, Fischetto R, Palumbo P, et al. De novo microduplication of CHL1 in a patient with non-syndromic developmental phenotypes. *Mol Cytogenet*. 2015;8(1):66. doi:10.1186/s13039-015-0170-3
61. Li C, Liu C, Zhou B, Hu C, Xu X. Novel microduplication of CHL1 gene in a patient with autism spectrum disorder: a case report and a brief literature review. *Mol Cytogenet*. 2016;9(1):51. doi:10.1186/s13039-016-0261-9
62. Gandawijaya J, Bamford RA, Burbach JPH, Oguro-Ando A. Cell Adhesion Molecules Involved in Neurodevelopmental Pathways Implicated in 3p-Deletion Syndrome and Autism Spectrum Disorder. *Front Cell Neurosci*. 2021;14(January). doi:10.3389/fncel.2020.611379
63. Fabbri C, Crisafulli C, Calati R, et al. Neuroplasticity and second messenger pathways in antidepressant efficacy: pharmacogenetic results from a prospective trial investigating treatment resistance. *Eur Arch Psychiatry Clin Neurosci*. 2017;267(8):723-735. doi:10.1007/s00406-017-0766-1
64. Bartova L, Dold M, Kautzky A, et al. Results of the European Group for the Study of Resistant Depression (GSRD) — basis for further research and clinical practice. *World J Biol Psychiatry*. 2019;20(6):427-448. doi:10.1080/15622975.2019.1635270
65. TANDON R, KESHAVAN M, NASRALLAH H. Schizophrenia, “Just the Facts” What we know in 2008. 2. Epidemiology and etiology. *Schizophr Res*. 2008;102(1-3):1-18. doi:10.1016/j.schres.2008.04.011
66. Patel KR, Cherian J, Gohil K, Atkinson D. Schizophrenia: overview and treatment options. *P T*. 2014;39(9):638-645. <http://www.ncbi.nlm.nih.gov/pubmed/25210417>
67. Sakurai K, Migita O, Toru M, Arinami T. An association between a missense polymorphism in the close homologue of L1 (CHL1, CALL) gene and schizophrenia. *Mol Psychiatry*. 2002;7(4):412-415. doi:10.1038/sj.mp.4000973
68. Shaltout TE, Alali KA, Bushra S, et al. Significant association of close homologue of L1 gene polymorphism rs2272522 with schizophrenia in Qatar. *Asia-Pacific Psychiatry*. 2013;5(1):17-23. doi:10.1111/appy.12014
69. Chen Q-Y, Chen Q, Feng G-Y, et al. Case-control association study of the close homologue of L1 (CHL1) gene and schizophrenia in the Chinese population. *Schizophr Res*. 2005;73(2-3):269-274. doi:10.1016/j.schres.2004.06.001
70. Winship IR, Dursun SM, Baker GB, et al. An Overview of Animal Models Related to Schizophrenia. *Can J Psychiatry*. 2019;64(1):5-17. doi:10.1177/0706743718773728
71. Braff DL, Geyer MA, Swerdlow NR. Human studies of prepulse inhibition of startle: normal subjects, patient groups, and pharmacological studies. *Psychopharmacology (Berl)*. 2001;156(2-3):234-258. doi:10.1007/s002130100810
72. Navari S, Dazzan P. Do antipsychotic drugs affect brain structure? A systematic and critical review of MRI findings. *Psychol Med*. 2009;39(11):1763-1777. doi:10.1017/S0033291709005315
73. Knable MB, Barci BM, Webster MJ, Meador-Woodruff J, Torrey EF. Molecular abnormalities of the hippocampus in severe psychiatric illness: postmortem findings from the Stanley Neuropathology Consortium. *Mol Psychiatry*. 2004;9(6):609-620. doi:10.1038/sj.mp.4001471
74. Brignani S, Pasterkamp RJ. Neuronal subset-specific migration and axonal wiring mechanisms in the developing midbrain dopamine system. *Front Neuroanat*. 2017;11(July):1-18. doi:10.3389/fnana.2017.00055
75. Mandic-Maravic V, Grujicic R, Milutinovic L, Munjiza-Jovanovic A, Pejovic-Milovancevic M. Dopamine in Autism Spectrum Disorders—Focus on D2/D3 Partial Agonists and Their Possible Use in Treatment. *Front Psychiatry*. 2022;12(February):1-9. doi:10.3389/fpsy.2021.787097

76. McCutcheon RA, Abi-Dargham A, Howes OD. Schizophrenia, Dopamine and the Striatum: From Biology to Symptoms. *Trends Neurosci.* 2019;42(3):205-220. doi:10.1016/j.tins.2018.12.004
77. De Diego-Balaguer R, Couette M, Dolbeau G, Durr A, Youssov K, Bachoud-Levi A-C. Striatal degeneration impairs language learning: evidence from Huntington's disease. *Brain.* 2008;131(11):2870-2881. doi:10.1093/brain/awn242
78. Wittmann BC, Bunzeck N, Dolan RJ, Düzel E. Anticipation of novelty recruits reward system and hippocampus while promoting recollection. *Neuroimage.* 2007;38(1):194-202. doi:10.1016/j.neuroimage.2007.06.038
79. Ellenbroek B., Budde S, Cools A. Prepulse inhibition and latent inhibition: the role of dopamine in the medial prefrontal cortex. *Neuroscience.* 1996;75(2):535-542. doi:10.1016/0306-4522(96)00307-7
80. Xiao M-F, Xu J-C, Tereshchenko Y, Novak D, Schachner M, Kleene R. Neural Cell Adhesion Molecule Modulates Dopaminergic Signaling and Behavior by Regulating Dopamine D 2 Receptor Internalization. *J Neurosci.* 2009;29(47):14752-14763. doi:10.1523/JNEUROSCI.4860-09.2009
81. Vallone D, Picetti R, Borrelli E. Structure and function of dopamine receptors. *Neurosci Biobehav Rev.* 2000;24(1):125-132. doi:10.1016/S0149-7634(99)00063-9
82. Jang JY, Jang M, Kim SH, et al. Regulation of dopaminergic neuron firing by heterogeneous dopamine autoreceptors in the substantia nigra pars compacta. *J Neurochem.* 2011;116(6):966-974. doi:10.1111/j.1471-4159.2010.07107.x
83. Faure A, Haberland U, Condé F, Massioui N El. Lesion to the Nigrostriatal Dopamine System Disrupts Stimulus-Response Habit Formation. *J Neurosci.* 2005;25(11):2771-2780. doi:10.1523/JNEUROSCI.3894-04.2005
84. Mannella F, Mirolli M, Baldassarre G. Goal-Directed Behavior and Instrumental Devaluation: A Neural System-Level Computational Model. *Front Behav Neurosci.* 2016;10(OCT). doi:10.3389/fnbeh.2016.00181
85. Alcaro A, Huber R, Panksepp J. Behavioral functions of the mesolimbic dopaminergic system: An affective neuroethological perspective. *Brain Res Rev.* 2007;56(2):283-321. doi:10.1016/j.brainresrev.2007.07.014
86. Floresco SB, Magyar O. Mesocortical dopamine modulation of executive functions: beyond working memory. *Psychopharmacology (Berl).* 2006;188(4):567-585. doi:10.1007/s00213-006-0404-5
87. Bromberg-Martin ES, Matsumoto M, Hikosaka O. Dopamine in Motivational Control: Rewarding, Aversive, and Alerting. *Neuron.* 2010;68(5):815-834. doi:10.1016/j.neuron.2010.11.022
88. Cools R, D'Esposito M. Inverted-U-Shaped Dopamine Actions on Human Working Memory and Cognitive Control. *Biol Psychiatry.* 2011;69(12):e113-e125. doi:10.1016/j.biopsych.2011.03.028
89. Puig MV, Antzoulatos EG, Miller EK. Prefrontal dopamine in associative learning and memory. *Neuroscience.* 2014;282(6):217-229. doi:10.1016/j.neuroscience.2014.09.026
90. Lyons DJ, Hellysaz A, Broberger C. Prolactin Regulates Tuberoinfundibular Dopamine Neuron Discharge Pattern: Novel Feedback Control Mechanisms in the Lactotrophic Axis. *J Neurosci.* 2012;32(23):8074-8083. doi:10.1523/JNEUROSCI.0129-12.2012
91. Björklund A, Dunnett SB. Dopamine neuron systems in the brain: an update. *Trends Neurosci.* 2007;30(5):194-202. doi:10.1016/j.tins.2007.03.006
92. Wise RA. Roles for nigrostriatal—not just mesocorticolimbic—dopamine in reward and addiction. *Trends Neurosci.* 2009;32(10):517-524. doi:10.1016/j.tins.2009.06.004
93. Lerner TN, Shilyansky C, Davidson TJ, et al. Intact-Brain Analyses Reveal Distinct Information Carried by SNc Dopamine Subcircuits. *Cell.* 2015;162(3):635-647. doi:10.1016/j.cell.2015.07.014
94. Beier KT, Steinberg EE, DeLoach KE, et al. Circuit Architecture of VTA Dopamine Neurons Revealed by Systematic Input-Output Mapping. *Cell.* 2015;162(3):622-634. doi:10.1016/j.cell.2015.07.015
95. Fraser KM, Pribut HJ, Janak PH, Keiflin R. From Prediction to Action: Dissociable Roles of Ventral Tegmental Area and Substantia Nigra Dopamine Neurons in Instrumental Reinforcement. *bioRxiv.* Published online 2022:2022.08.15.501890. <https://www.biorxiv.org/content/10.1101/2022.08.15.501890v1> [https://www.biorxiv.org/content/10.1101/2022.08.15.501890v1](https://www.biorxiv.org/content/10.1101/2022.08.15.501890v1.abstract) <https://www.biorxiv.org/content/10.1101/2022.08.15.501890v1>
96. Morales M, Root DH. Glutamate neurons within the midbrain dopamine regions. *Neuroscience.* 2014;282:60-68. doi:10.1016/j.neuroscience.2014.05.032
97. Morello F, Partanen J. Diversity and development of local inhibitory and excitatory neurons associated with dopaminergic nuclei. *FEBS Lett.* 2015;589(24PartA):3693-3701. doi:10.1016/j.febslet.2015.10.001
98. Cai J, Tong Q. Anatomy and Function of Ventral Tegmental Area Glutamate Neurons. *Front Neural Circuits.* 2022;16(May). doi:10.3389/fncir.2022.867053
99. Antal M, Beneduce BM, Regehr WG. The Substantia Nigra Conveys Target-Dependent Excitatory and Inhibitory Outputs from the Basal Ganglia to the Thalamus. *J Neurosci.* 2014;34(23):8032-8042. doi:10.1523/JNEUROSCI.0236-14.2014
100. Stamatakis AM, Jennings JH, Ung RL, et al. A Unique Population of Ventral Tegmental Area Neurons Inhibits the Lateral Habenula to Promote Reward. *Neuron.* 2013;80(4):1039-1053. doi:10.1016/j.neuron.2013.08.023
101. Root DH, Mejias-Aponte CA, Zhang S, et al. Single rodent mesohabenular axons release glutamate and GABA. *Nat Neurosci.* 2014;17(11):1543-1551. doi:10.1038/nn.3823
102. Yamaguchi T, Wang H-L, Li X, Ng TH, Morales M. Mesocorticolimbic Glutamatergic Pathway. *J Neurosci.* 2011;31(23):8476-8490. doi:10.1523/JNEUROSCI.1598-11.2011

103. Zhang S, Qi J, Li X, et al. Dopaminergic and glutamatergic microdomains in a subset of rodent mesoaccumbens axons. *Nat Neurosci.* 2015;18(3):386-392. doi:10.1038/nn.3945
104. Morikawa H, Paladini CA. Dynamic regulation of midbrain dopamine neuron activity: intrinsic, synaptic, and plasticity mechanisms. *Neuroscience.* 2011;198:95-111. doi:10.1016/j.neuroscience.2011.08.023
105. Tepper JM, Lee CR. GABAergic control of substantia nigra dopaminergic neurons. In: *Progress in Brain Research.* Vol 160. ; 2007:189-208. doi:10.1016/S0079-6123(06)60011-3
106. Faget L, Osakada F, Duan J, et al. Afferent Inputs to Neurotransmitter-Defined Cell Types in the Ventral Tegmental Area. *Cell Rep.* 2016;15(12):2796-2808. doi:10.1016/j.celrep.2016.05.057
107. Kaushik P, Naudé J, Raju SB, Alexandre F. A VTA GABAergic computational model of dissociated reward prediction error computation in classical conditioning. *Neurobiol Learn Mem.* 2022;193:107653. doi:10.1016/j.nlm.2022.107653
108. Dong J, Hawes S, Wu J, Le W, Cai H. Connectivity and Functionality of the Globus Pallidus Externa Under Normal Conditions and Parkinson's Disease. *Front Neural Circuits.* 2021;15(March):1-19. doi:10.3389/fncir.2021.645287
109. Bentivoglio M, Morelli M. Chapter I The organization and circuits of mesencephalic dopaminergic neurons and the distribution of dopamine receptors in the brain. In: Vol 21. ; 2005:1-107. doi:10.1016/S0924-8196(05)80005-3
110. Pandey P, Mersha MD, Dhillon HS. A synergistic approach towards understanding the functional significance of dopamine receptor interactions. *J Mol Signal.* 2013;8:13. doi:10.1186/1750-2187-8-13
111. Ben-Jonathan N. *Dopamine, Endocrine and Oncogenic Functions.* Vol 6. CRC Press; 2020. doi:10.1201/9780429402272
112. Beaulieu J-M, Gainetdinov RR. The Physiology, Signaling, and Pharmacology of Dopamine Receptors. Sibley DR, ed. *Pharmacol Rev.* 2011;63(1):182-217. doi:10.1124/pr.110.002642
113. Gurevich E. Distribution of Dopamine D3 Receptor Expressing Neurons in the Human Forebrain Comparison with D2 Receptor Expressing Neurons. *Neuropsychopharmacology.* 1999;20(1):60-80. doi:10.1016/S0893-133X(98)00066-9
114. Meador-Woodruff JH, Damask SP, Wang J, Haroutunian V, Davis KL, Watson SJ. Dopamine receptor mRNA expression in human striatum and neocortex. *Neuropsychopharmacology.* 1996;15(1):17-29. doi:10.1016/0893-133X(95)00150-C
115. Surmeier DJ, Carrillo-Reid L, Vargas J. Dopaminergic modulation of striatal neurons, circuits, and assemblies. *Neuroscience.* 2011;198(1):3-18. doi:10.1016/j.neuroscience.2011.08.051
116. Centonze D, Grande C, Usiello A, et al. Receptor Subtypes Involved in the Presynaptic and Postsynaptic Actions of Dopamine on Striatal Interneurons. *J Neurosci.* 2003;23(15):6245-6254. doi:10.1523/JNEUROSCI.23-15-06245.2003
117. Gallo EF. Disentangling the diverse roles of dopamine D2 receptors in striatal function and behavior. *Neurochem Int.* 2019;125(3):35-46. doi:10.1016/j.neuint.2019.01.022
118. Gagnon D, Petryszyn S, Sanchez MG, et al. Striatal Neurons Expressing D1 and D2 Receptors are Morphologically Distinct and Differently Affected by Dopamine Denervation in Mice. *Sci Rep.* 2017;7(1):41432. doi:10.1038/srep41432
119. Lindgren N, Usiello A, Gojny M, et al. Distinct roles of dopamine D2L and D2S receptor isoforms in the regulation of protein phosphorylation at presynaptic and postsynaptic sites. *Proc Natl Acad Sci.* 2003;100(7):4305-4309. doi:10.1073/pnas.0730708100
120. Li X, Qi J, Yamaguchi T, Wang H-L, Morales M. Heterogeneous composition of dopamine neurons of the rat A10 region: molecular evidence for diverse signaling properties. *Brain Struct Funct.* 2013;218(5):1159-1176. doi:10.1007/s00429-012-0452-z
121. Bamford NS, Zhang H, Schmitz Y, et al. Heterosynaptic Dopamine Neurotransmission Selects Sets of Corticostriatal Terminals. *Neuron.* 2004;42(4):653-663. doi:10.1016/S0896-6273(04)00265-X
122. Higley MJ, Sabatini BL. Competitive regulation of synaptic Ca²⁺ influx by D2 dopamine and A2A adenosine receptors. *Nat Neurosci.* 2010;13(8):958-966. doi:10.1038/nn.2592
123. Kaasinen V, Nägren K, Hietala J, Farde L, Rinne JO. Sex Differences in Extrastriatal Dopamine D₂-Like Receptors in the Human Brain. *Am J Psychiatry.* 2001;158(2):308-311. doi:10.1176/appi.ajp.158.2.308
124. Pohjalainen T, Rinne JO, Nägren K, Syvälahti E, Hietala J. Sex differences in the striatal dopamine D2 receptor binding characteristics in vivo. *Am J Psychiatry.* 1998;155(6):768-773.
125. Farde L, Hall H, Pauli S, Halldin C. Variability in D2-dopamine receptor density and affinity: A PET study with [¹¹C]raclopride in man. *Synapse.* 1995;20(3):200-208. doi:10.1002/syn.890200303
126. Wong DF, Wagner HN, Dannals RF, et al. Effects of Age on Dopamine and Serotonin Receptors Measured by Positron Tomography in the Living Human Brain. *Science (80-).* 1984;226(4681):1393-1396. doi:10.1126/science.6334363
127. Orendain-Jaime EN, Ortega-Ibarra JM, López-Pérez SJ. Evidence of sexual dimorphism in D1 and D2 dopaminergic receptors expression in frontal cortex and striatum of young rats. *Neurochem Int.* 2016;100:62-66. doi:10.1016/j.neuint.2016.09.001
128. Hasbi A, Nguyen T, Rahal H, et al. Sex difference in dopamine D1-D2 receptor complex expression and signaling affects depression- and anxiety-like behaviors. *Biol Sex Differ.* 2020;11(1):8. doi:10.1186/s13293-020-00285-9
129. Andersen SL, Teicher MH. Sex differences in dopamine receptors and their relevance to ADHD. *Neurosci Biobehav Rev.* 2000;24(1):137-141. doi:10.1016/S0149-7634(99)00044-5
130. Giros B, Sokoloff P, Martres M-P, Riou J-F, Emorine LJ, Schwartz J-C. Alternative splicing directs the expression of two D2 dopamine receptor isoforms. *Nature.* 1989;342(6252):923-926. doi:10.1038/342923a0
131. Montmayeur JP, Bausero P, Amlaiky N, Maroteaux L, Hen R, Borrelli E. Differential expression of the mouse D₂ dopamine receptor isoforms. *FEBS Lett.* 1991;278(2):239-243. doi:10.1016/0014-5793(91)80125-M

132. Żuk J, Bartuzi D, Matosiuk D, Kaczor AA. Preferential Coupling of Dopamine D2S and D2L Receptor Isoforms with Gi1 and Gi2 Proteins—In Silico Study. *Int J Mol Sci.* 2020;21(2):436. doi:10.3390/ijms21020436
133. Khan ZU, Mrzljak L, Gutierrez A, De La Calle A, Goldman-Rakic PS. Prominence of the dopamine D2 short isoform in dopaminergic pathways. *Proc Natl Acad Sci U S A.* 1998;95(13):7731-7736. doi:10.1073/pnas.95.13.7731
134. Mercuri NB, Saiardi A, Bonci A, et al. Loss of autoreceptor function in dopaminergic neurons from dopamine D2 receptor deficient mice. *Neuroscience.* 1997;79(2):323-327. doi:10.1016/s0306-4522(97)00135-8
135. L'hirondel M, Chéramy A, Godeheu G, et al. Lack of autoreceptor-mediated inhibitory control of dopamine release in striatal synaptosomes of D2 receptor-deficient mice. *Brain Res.* 1998;792(2):253-262. doi:10.1016/S0006-8993(98)00146-2
136. Usiello A, Baik J, Rougé-Pont F, et al. Distinct functions of the two isoforms of dopamine D2 receptors. *Nature.* 2000;408(6809):199-203. doi:10.1038/35041572
137. Wang Y, Xu R, Sasaoka T, Tonegawa S, Kung M-P, Sankoorikal E-B. Dopamine D2 Long Receptor-Deficient Mice Display Alterations in Striatum-Dependent Functions. *J Neurosci.* 2000;20(22):8305-8314. doi:10.1523/JNEUROSCI.20-22-08305.2000
138. Radl D, Chiacchiaretta M, Lewis RG, Brami-Cherrier K, Arcuri L, Borrelli E. Differential regulation of striatal motor behavior and related cellular responses by dopamine d2l and d2s isoforms. *Proc Natl Acad Sci U S A.* 2018;115(1):198-203. doi:10.1073/pnas.1717194115
139. Anzalone A, Lizardi-Ortiz JE, Ramos M, et al. Dual Control of Dopamine Synthesis and Release by Presynaptic and Postsynaptic Dopamine D2 Receptors. *J Neurosci.* 2012;32(26):9023-9034. doi:10.1523/JNEUROSCI.0918-12.2012
140. Gantz SC, Robinson BG, Buck DC, et al. Distinct regulation of dopamine D2S and D2L autoreceptor signaling by calcium. *Elife.* 2015;4(AUGUST2015):1-19. doi:10.7554/eLife.09358
141. Glukhova A, Draper-Joyce CJ, Sunahara RK, Christopoulos A, Wootten D, Sexton PM. Rules of Engagement: GPCRs and G Proteins. *ACS Pharmacol Transl Sci.* 2018;1(2):73-83. doi:10.1021/acspsci.8b00026
142. Jiang M, Spicher K, Boulay G, Wang Y, Birnbaumer L. Most central nervous system D2 dopamine receptors are coupled to their effectors by Go. *Proc Natl Acad Sci.* 2001;98(6):3577-3582. doi:10.1073/pnas.051632598
143. Cordeaux Y, Nickolls SA, Flood LA, Graber SG, Strange PG. Agonist Regulation of D2 Dopamine Receptor/G Protein Interaction. *J Biol Chem.* 2001;276(31):28667-28675. doi:10.1074/jbc.M008644200
144. Gazi L, Nickolls SA, Strange PG. Functional coupling of the human dopamine D 2 receptor with Gα i1 , Gα i2 , Gα i3 and Gα o G proteins: evidence for agonist regulation of G protein selectivity. *Br J Pharmacol.* 2003;138(5):775-786. doi:10.1038/sj.bjp.0705116
145. Grünewald S, Reiländer H, Michel H. In Vivo Reconstitution of Dopamine D 2S Receptor-Mediated G Protein Activation in Baculovirus-Infected Insect Cells: Preferred Coupling to G i1 versus G i2. *Biochemistry.* 1996;35(48):15162-15173. doi:10.1021/bi960757w
146. Marcott PF, Gong S, Donthamsetti P, et al. Regional Heterogeneity of D2-Receptor Signaling in the Dorsal Striatum and Nucleus Accumbens. *Neuron.* 2018;98(3):575-587.e4. doi:10.1016/j.neuron.2018.03.038
147. Beaulieu J-M, Espinoza S, Gainetdinov RR. Dopamine receptors - IUPHAR Review 13. *Br J Pharmacol.* 2015;172(1):1-23. doi:10.1111/bph.12906
148. Greengard P, Allen PB, Nairn AC. Beyond the Dopamine Receptor. *Neuron.* 1999;23(3):435-447. doi:10.1016/S0896-6273(00)80798-9
149. Connelly WM, Errington AC, Giovanni G Di, Crunelli V. Metabotropic regulation of extrasynaptic GABAA receptors. *Front Neural Circuits.* 2013;7(October):1-8. doi:10.3389/fncir.2013.00171
150. Flores-Hernandez J, Hernandez S, Snyder GL, et al. D(1) dopamine receptor activation reduces GABA(A) receptor currents in neostriatal neurons through a PKA/DARPP-32/PP1 signaling cascade. *J Neurophysiol.* 2000;83(5):2996-3004. doi:10.1152/jn.2000.83.5.2996
151. Beom S, Cheong D, Torres G, Caron MG, Kim K-M. Comparative Studies of Molecular Mechanisms of Dopamine D2 and D3 Receptors for the Activation of Extracellular Signal-regulated Kinase. *J Biol Chem.* 2004;279(27):28304-28314. doi:10.1074/jbc.M403899200
152. Santini E, Feyder M, Gangarossa G, Bateup HS, Greengard P, Fisone G. Dopamine- and cAMP-regulated phosphoprotein of 32-kDa (DARPP-32)-dependent activation of extracellular signal-regulated kinase (ERK) and mammalian target of rapamycin complex 1 (mTORC1) signaling in experimental parkinsonism. *J Biol Chem.* 2012;287(33):27806-27812. doi:10.1074/jbc.M112.388413
153. Sung YK, Kyou CC, Min SC, et al. The dopamine D2 receptor regulates the development of dopaminergic neurons via extracellular signal-regulated kinase and Nurr1 activation. *J Neurosci.* 2006;26(17):4567-4576. doi:10.1523/JNEUROSCI.5236-05.2006
154. Bolan EA, Kivell B, Jaligam V, et al. D2 receptors regulate dopamine transporter function via an extracellular signal-regulated kinases 1 and 2-dependent and phosphoinositide 3 kinase-independent mechanism. *Mol Pharmacol.* 2007;71(5):1222-1232. doi:10.1124/mol.106.027763
155. Bibb JA, Snyder GL, Nishi A, et al. Phosphorylation of DARPP-32 by Cdk5 modulates dopamine signalling in neurons. *Nature.* 1999;402(6762):669-671. doi:10.1038/45251
156. Hernández-López S, Tkatch T, Perez-Garci E, et al. D 2 Dopamine Receptors in Striatal Medium Spiny Neurons Reduce L-Type Ca²⁺ Currents and Excitability via a Novel PLCβ1–IP 3 –Calcineurin-Signaling Cascade. *J Neurosci.* 2000;20(24):8987-

8995. doi:10.1523/JNEUROSCI.20-24-08987.2000

157. Lüscher C, Slesinger PA. Emerging roles for G protein-gated inwardly rectifying potassium (GIRK) channels in health and disease. *Nat Rev Neurosci.* 2010;11(5):301-315. doi:10.1038/nrn2834
158. Gurevich V V., Gurevich E V. GPCR Signaling Regulation: The Role of GRKs and Arrestins. *Front Pharmacol.* 2019;10(FEB):1-11. doi:10.3389/fphar.2019.00125
159. Rashid AJ, So CH, Kong MMC, et al. D1–D2 dopamine receptor heterooligomers with unique pharmacology are coupled to rapid activation of G_q/11 in the striatum. *Proc Natl Acad Sci.* 2007;104(2):654-659. doi:10.1073/pnas.0604049104
160. Pack TF, Orlen MI, Ray C, Peterson SM, Caron MG. The dopamine D2 receptor can directly recruit and activate GRK2 without G protein activation. *J Biol Chem.* 2018;293(16):6161-6171. doi:10.1074/jbc.RA117.001300
161. Namkung Y, Dipace C, Javitch JA, Sibley DR. G Protein-coupled Receptor Kinase-mediated Phosphorylation Regulates Post-endocytic Trafficking of the D2 Dopamine Receptor. *J Biol Chem.* 2009;284(22):15038-15051. doi:10.1074/jbc.M900388200
162. Peterson SM, Pack TF, Wilkins AD, et al. Elucidation of G-protein and β -arrestin functional selectivity at the dopamine D2 receptor. *Proc Natl Acad Sci.* 2015;112(22):7097-7102. doi:10.1073/pnas.1502742112
163. Del'Guidice T. Role of beta-arrestin 2 downstream of dopamine receptors in the basal ganglia. *Front Neuroanat.* 2011;5(September):1-11. doi:10.3389/fnana.2011.00058
164. Beaulieu J-M, Sotnikova TD, Marion S, Lefkowitz RJ, Gainetdinov RR, Caron MG. An Akt/ β -Arrestin 2/PP2A Signaling Complex Mediates Dopaminergic Neurotransmission and Behavior. *Cell.* 2005;122(2):261-273. doi:10.1016/j.cell.2005.05.012
165. Beaulieu J-M, Tirotta E, Sotnikova TD, et al. Regulation of Akt Signaling by D 2 and D 3 Dopamine Receptors In Vivo. *J Neurosci.* 2007;27(4):881-885. doi:10.1523/JNEUROSCI.5074-06.2007
166. Mannoury la Cour C, Salles M-J, Pasteau V, Millan MJ. Signaling Pathways Leading to Phosphorylation of Akt and GSK-3 β by Activation of Cloned Human and Rat Cerebral D 2 and D 3 Receptors. *Mol Pharmacol.* 2011;79(1):91-105. doi:10.1124/mol.110.065409
167. Beaulieu J-M, Sotnikova TD, Yao W-D, et al. Lithium antagonizes dopamine-dependent behaviors mediated by an AKT/glycogen synthase kinase 3 signaling cascade. *Proc Natl Acad Sci.* 2004;101(14):5099-5104. doi:10.1073/pnas.0307921101
168. Beaulieu J-M, Gainetdinov RR, Caron MG. The Akt–GSK-3 signaling cascade in the actions of dopamine. *Trends Pharmacol Sci.* 2007;28(4):166-172. doi:10.1016/j.tips.2007.02.006
169. Lan H, Liu Y, Bell MI, Gurevich W, Neve KA. Erratum: A dopamine D2 receptor mutant capable of G protein-mediated signaling but deficient in Arrestin Binding (Molecular Pharmacology (2009) 75 (113-123)). *Mol Pharmacol.* 2009;75(3):729. doi:10.1124/mol.75.3.729
170. Crandall JE, McCarthy DM, Araki KY, Sims JR, Ren JQ, Bhide PG. Dopamine receptor activation modulates GABA neuron migration from the basal forebrain to the cerebral cortex. *J Neurosci.* 2007;27(14):3813-3822. doi:10.1523/JNEUROSCI.5124-06.2007
171. Mishra A, Singh S, Shukla S. Physiological and Functional Basis of Dopamine Receptors and Their Role in Neurogenesis: Possible Implication for Parkinson's disease. *J Exp Neurosci.* 2018;12:117906951877982. doi:10.1177/1179069518779829
172. Kippin TE, Kapur S, Van Der Kooy D. Dopamine specifically inhibits forebrain neural stem cell proliferation, suggesting a novel effect of antipsychotic drugs. *J Neurosci.* 2005;25(24):5815-5823. doi:10.1523/JNEUROSCI.1120-05.2005
173. Cazorla M, Shegda M, Ramesh B, Harrison NL, Kellendonk C. Striatal D2 Receptors Regulate Dendritic Morphology of Medium Spiny Neurons via Kir2 Channels. *J Neurosci.* 2012;32(7):2398-2409. doi:10.1523/JNEUROSCI.6056-11.2012
174. Zheng P, Su QP, Jin D, Yu Y, Huang X-F. Prevention of Neurite Spine Loss Induced by Dopamine D2 Receptor Overactivation in Striatal Neurons. *Front Neurosci.* 2020;14(June):1-12. doi:10.3389/fnins.2020.00642
175. Jia J-M, Zhao J, Hu Z, Lindberg D, Li Z. Age-dependent regulation of synaptic connections by dopamine D2 receptors. *Nat Neurosci.* 2013;16(11):1627-1636. doi:10.1038/nn.3542
176. Giguère N, Delignat-Lavaud B, Herborg F, et al. Increased vulnerability of nigral dopamine neurons after expansion of their axonal arborization size through D2 dopamine receptor conditional knockout. *PLoS Genet.* 2019;15(8):1-26. doi:10.1371/journal.pgen.1008352
177. Fasano C, Poirier A, DesGroseillers L, Trudeau LE. Chronic activation of the D2 dopamine autoreceptor inhibits synaptogenesis in mesencephalic dopaminergic neurons in vitro. *Eur J Neurosci.* 2008;28(8):1480-1490. doi:10.1111/j.1460-9568.2008.06450.x
178. Ford CP. The role of D2-autoreceptors in regulating dopamine neuron activity and transmission. *Neuroscience.* 2014;282:13-22. doi:10.1016/j.neuroscience.2014.01.025
179. Cardozo DL, Bean BP. Voltage-dependent calcium channels in rat midbrain dopamine neurons: modulation by dopamine and GABAB receptors. *J Neurophysiol.* 1995;74(3):1137-1148. doi:10.1152/jn.1995.74.3.1137
180. Ikeda SR. Voltage-dependent modulation of N-type calcium channels by G-protein beta gamma subunits. *Nature.* 1996;380(6571):255-258. doi:10.1038/380255a0
181. Benoit-Marand M, Ballion B, Borrelli E, Boraud T, Gonon F. Inhibition of dopamine uptake by D2 antagonists: an in vivo study. *J Neurochem.* 2011;116(3):449-458. doi:10.1111/j.1471-4159.2010.07125.x
182. Sonders MS, Zhu S-J, Zahniser NR, Kavanaugh MP, Amara SG. Multiple Ionic Conductances of the Human Dopamine Transporter: The Actions of Dopamine and Psychostimulants. *J Neurosci.* 1997;17(3):960-974. doi:10.1523/JNEUROSCI.17-03-00960.1997

183. Lindgren N, Xu ZQD, Herrera-Marschitz M, Haycock J, Hökfelt T, Fisone G. Dopamine D2 receptors regulate tyrosine hydroxylase activity and phosphorylation at Ser40 in rat striatum. *Eur J Neurosci*. 2001;13(4):773-780. doi:10.1046/j.0953-816X.2000.01443.x
184. Pothos EN, Przedborski S, Davila V, Schmitz Y, Sulzer D. D2-like dopamine autoreceptor activation reduces quantal size in PC 12 cells. *J Neurosci*. 1998;18(15):5575-5585. doi:10.1523/jneurosci.18-15-05575.1998
185. Truong JG, Newman AH, Hanson GR, Fleckenstein AE. Dopamine D2 receptor activation increases vesicular dopamine uptake and redistributes vesicular monoamine transporter-2 protein. *Eur J Pharmacol*. 2004;504(1-2):27-32. doi:10.1016/j.ejphar.2004.09.049
186. Dobbs LK, Lemos JC, Alvarez VA. Restructuring of basal ganglia circuitry and associated behaviors triggered by low striatal D2 receptor expression: implications for substance use disorders. *Genes, Brain Behav*. 2017;16(1):56-70. doi:10.1111/gbb.12361
187. Ford CP, Gantz SC, Phillips PEM, Williams JT. Control of extracellular dopamine at dendrite and axon terminals. *J Neurosci*. 2010;30(20):6975-6983. doi:10.1523/JNEUROSCI.1020-10.2010
188. Courtney NA, Mamaligas AA, Ford CP. Species Differences in Somatodendritic Dopamine Transmission Determine D2-Autoreceptor-Mediated Inhibition of Ventral Tegmental Area Neuron Firing. *J Neurosci*. 2012;32(39):13520-13528. doi:10.1523/JNEUROSCI.2745-12.2012
189. Rifkin RA, Huyghe D, Li X, et al. GIRK currents in VTA dopamine neurons control the sensitivity of mice to cocaine-induced locomotor sensitization. *Proc Natl Acad Sci*. 2018;115(40):E9479-E9488. doi:10.1073/pnas.1807788115
190. Claing A. Endocytosis of G protein-coupled receptors: roles of G protein-coupled receptor kinases and β -arrestin proteins. *Prog Neurobiol*. 2002;66(2):61-79. doi:10.1016/S0301-0082(01)00023-5
191. Namkung Y, Sibley DR. Protein Kinase C Mediates Phosphorylation, Desensitization, and Trafficking of the D2 Dopamine Receptor. *J Biol Chem*. 2004;279(47):49533-49541. doi:10.1074/jbc.M408319200
192. Brizuela M, Antipov A, Blessing WW, Ootsuka Y. Activating dopamine D2 receptors reduces brown adipose tissue thermogenesis induced by psychological stress and by activation of the lateral habenula. *Sci Rep*. 2019;9(1):19512. doi:10.1038/s41598-019-56125-3
193. Soares-Cunha C, Coimbra B, Sousa N, Rodrigues AJ. Reappraising striatal D1- and D2-neurons in reward and aversion. *Neurosci Biobehav Rev*. 2016;68:370-386. doi:10.1016/j.neubiorev.2016.05.021
194. Gangarossa G, Espallergues J, Mailly P, et al. Spatial distribution of D1R- and D2R-expressing medium-sized spiny neurons differs along the rostro-caudal axis of the mouse dorsal striatum. *Front Neural Circuits*. 2013;7(JUL):1-16. doi:10.3389/fncir.2013.00124
195. Gangarossa G, Espallergues J, de Kerchove d'Exaerde A, et al. Distribution and compartmental organization of GABAergic medium-sized spiny neurons in the mouse nucleus accumbens. *Front Neural Circuits*. 2013;7(FEBRUARY 2013):1-20. doi:10.3389/fncir.2013.00022
196. Muñoz-Manchado AB, Bengtsson Gonzales C, Zeisel A, et al. Diversity of Interneurons in the Dorsal Striatum Revealed by Single-Cell RNA Sequencing and PatchSeq. *Cell Rep*. 2018;24(8):2179-2190.e7. doi:10.1016/j.celrep.2018.07.053
197. Simpson EH, Gallo EF, Balsam PD, Javitch JA, Kellendonk C. How changes in dopamine D2 receptor levels alter striatal circuit function and motivation. *Mol Psychiatry*. 2022;27(1):436-444. doi:10.1038/s41380-021-01253-4
198. Florio TM, Scarnati E, Rosa I, et al. The Basal Ganglia: More than just a switching device. *CNS Neurosci Ther*. 2018;24(8):677-684. doi:10.1111/cns.12987
199. Chen AP, Chen L, Kim TA, Xiong Q. Integrating the Roles of Midbrain Dopamine Circuits in Behavior and Neuropsychiatric Disease. *Biomedicines*. 2021;9(6):647. doi:10.3390/biomedicines9060647
200. Fuccillo M V. Striatal Circuits as a Common Node for Autism Pathophysiology. *Front Neurosci*. 2016;10(FEB). doi:10.3389/fnins.2016.00027
201. Shin JH, Kim D, Jung MW. Differential coding of reward and movement information in the dorsomedial striatal direct and indirect pathways. *Nat Commun*. 2018;9(1):404. doi:10.1038/s41467-017-02817-1
202. Nonomura S, Nishizawa K, Sakai Y, et al. Monitoring and Updating of Action Selection for Goal-Directed Behavior through the Striatal Direct and Indirect Pathways. *Neuron*. 2018;99(6):1302-1314.e5. doi:10.1016/j.neuron.2018.08.002
203. Tarantino IS, Sharp RF, Geyer MA, Meves JM, Young JW. Working memory span capacity improved by a D2 but not D1 receptor family agonist. *Behav Brain Res*. 2011;219(2):181-188. doi:10.1016/j.bbr.2010.12.037
204. Duvarci S, Simpson EH, Schneider G, Kandel ER, Roeper J, Sigurdsson T. Impaired recruitment of dopamine neurons during working memory in mice with striatal D2 receptor overexpression. *Nat Commun*. 2018;9(1):2822. doi:10.1038/s41467-018-05214-4
205. Chernysheva M, Sych Y, Fomins A, et al. Striatum-projecting prefrontal cortex neurons support working memory maintenance. *bioRxiv*. Published online January 1, 2021:2021.12.03.471159. doi:10.1101/2021.12.03.471159
206. Vicente AM, Galvão-Ferreira P, Tecuapetla F, Costa RM. Direct and indirect dorsolateral striatum pathways reinforce different action strategies. *Curr Biol*. 2016;26(7):R267-R269. doi:10.1016/j.cub.2016.02.036
207. Bergstrom HC, Lipkin AM, Lieberman AG, et al. Dorsolateral Striatum Engagement Interferes with Early Discrimination Learning. *Cell Rep*. 2018;23(8):2264-2272. doi:10.1016/j.celrep.2018.04.081
208. Floresco SB. The Nucleus Accumbens: An Interface Between Cognition, Emotion, and Action. *Annu Rev Psychol*. 2015;66(1):25-52. doi:10.1146/annurev-psych-010213-115159

209. Lobo MK, Covington HE, Chaudhury D, et al. Cell Type–Specific Loss of BDNF Signaling Mimics Optogenetic Control of Cocaine Reward. *Science* (80-). 2010;330(6002):385-390. doi:10.1126/science.1188472
210. Kravitz A V, Tye LD, Kreitzer AC. Distinct roles for direct and indirect pathway striatal neurons in reinforcement. *Nat Neurosci*. 2012;15(6):816-818. doi:10.1038/nn.3100
211. Kupchik YM, Brown RM, Heinsbroek JA, Lobo MK, Schwartz DJ, Kalivas PW. Coding the direct/indirect pathways by D1 and D2 receptors is not valid for accumbens projections. *Nat Neurosci*. 2015;18(9):1230-1232. doi:10.1038/nn.4068
212. Verharen JPH, Adan RAH, Vanderschuren LJMJ. Differential contributions of striatal dopamine D1 and D2 receptors to component processes of value-based decision making. *Neuropsychopharmacology*. 2019;44(13):2195-2204. doi:10.1038/s41386-019-0454-0
213. Kwak S, Jung MW. Distinct roles of striatal direct and indirect pathways in value-based decision making. *Elife*. 2019;8:1-16. doi:10.7554/eLife.46050
214. Gallo EF, Salling MC, Feng B, et al. Upregulation of Dopamine D2 Receptors in the Nucleus Accumbens Indirect Pathway Increases Locomotion but Does Not Reduce Alcohol Consumption. *Neuropsychopharmacology*. 2015;40(7):1609-1618. doi:10.1038/npp.2015.11
215. Lemos JC, Friend DM, Kaplan AR, et al. Enhanced GABA Transmission Drives Bradykinesia Following Loss of Dopamine D2 Receptor Signaling. *Neuron*. 2016;90(4):824-838. doi:10.1016/j.neuron.2016.04.040
216. Baik JH, Picetti R, Saiardi A, et al. Parkinsonian-like locomotor impairment in mice lacking dopamine D2 receptors. *Nature*. 1995;377(6548):424-428. doi:10.1038/377424a0
217. Nakamura T, Sato A, Kitsukawa T, Momiyama T, Yamamori T, Sasaoka T. Distinct motor impairments of dopamine D1 and D2 receptor knockout mice revealed by three types of motor behavior. *Front Integr Neurosci*. 2014;8(JUL):1-11. doi:10.3389/fnint.2014.00056
218. Bello EP, Mateo Y, Gelman DM, et al. Cocaine supersensitivity and enhanced motivation for reward in mice lacking dopamine D2 autoreceptors. *Nat Neurosci*. 2011;14(8):1033-1038. doi:10.1038/nn.2862
219. Eilam D, Szechtman H. Biphasic effect of D-2 agonist quinpirole on locomotion and movements. *Eur J Pharmacol*. 1989;161(2-3):151-157. doi:10.1016/0014-2999(89)90837-6
220. Castro SW, Strange PG. Differences in the Ligand Binding Properties of the Short and Long Versions of the D 2 Dopamine Receptor. *J Neurochem*. 1993;60(1):372-375. doi:10.1111/j.1471-4159.1993.tb05863.x
221. Einsiedel J, Thomas C, Hübner H, Gmeiner P. Phenylloxazoles and phenylthiazoles as benzamide bioisosteres: Synthesis and dopamine receptor binding profiles. *Bioorganic Med Chem Lett*. 2000;10(17):2041-2044. doi:10.1016/S0960-894X(00)00405-4
222. Kuroki T, Meltzer HY, Ichikawa J. Effects of antipsychotic drugs on extracellular dopamine levels in rat medial prefrontal cortex and nucleus accumbens. *J Pharmacol Exp Ther*. 1999;288(2):774-781. <http://jpet.aspetjournals.org/content/288/2/774.abstract>
223. Ohmann HA, Kuper N, Wacker J. A low dosage of the dopamine D2-receptor antagonist sulpiride affects effort allocation for reward regardless of trait extraversion. *Personal Neurosci*. 2020;3:e7. doi:10.1017/pen.2020.7
224. Tagliamonte A, DeMontis G, Olanas M, Vargiu L, Corsini GU, Gessa GL. Selective increase of brain dopamine synthesis by sulpiride. *J Neurochem*. 1975;24(4):707-710. doi:10.1111/j.1471-4159.1975.tb11667.x
225. Fujiwara H. Comparative studies of sulpiride and classical neuroleptics on induction of catalepsy, locomotor activity, and brain dopamine metabolism in mice. *Pharmacol Biochem Behav*. 1992;41(2):301-308. doi:10.1016/0091-3057(92)90102-L
226. Boschen SL, Andreatini R, da Cunha C. Activation of postsynaptic D2 dopamine receptors in the rat dorsolateral striatum prevents the amnesic effect of systemically administered neuroleptics. *Behav Brain Res*. 2015;281:283-289. doi:10.1016/j.bbr.2014.12.040
227. Eisenegger C, Naef M, Linszen A, et al. Role of Dopamine D2 Receptors in Human Reinforcement Learning. *Neuropsychopharmacology*. 2014;39(10):2366-2375. doi:10.1038/npp.2014.84
228. Frantz KJ, Van Hartesveldt C. Sulpiride antagonizes the biphasic locomotor effects of quinpirole in weanling rats. *Psychopharmacology (Berl)*. 1995;119(3):299-304. doi:10.1007/BF02246295
229. Stuchlik A, Rehakova L, Rambousek L, Svoboda J, Vales K. Manipulation of D2 receptors with quinpirole and sulpiride affects locomotor activity before spatial behavior of rats in an active place avoidance task. *Neurosci Res*. 2007;58(2):133-139. doi:10.1016/j.neures.2007.02.006
230. Jones C, Watson D, Fone K. Animal models of schizophrenia. *Br J Pharmacol*. 2011;164(4):1162-1194. doi:10.1111/j.1476-5381.2011.01386.x
231. Laruelle M. Imaging dopamine transmission in schizophrenia. A review and meta-analysis. *Q J Nucl Med*. 1998;42(3):211-221. doi:9796369
232. Kellendonk C, Simpson EH, Polan HJ, et al. Transient and Selective Overexpression of Dopamine D2 Receptors in the Striatum Causes Persistent Abnormalities in Prefrontal Cortex Functioning. *Neuron*. 2006;49(4):603-615. doi:10.1016/j.neuron.2006.01.023
233. Frank MJ, O'Reilly RC. A mechanistic account of striatal dopamine function in human cognition: Psychopharmacological studies with cabergoline and haloperidol. *Behav Neurosci*. 2006;120(3):497-517. doi:10.1037/0735-7044.120.3.497
234. Broadway JM, Frank MJ, Cavanagh JF. Dopamine D2 agonist affects visuospatial working memory distractor interference depending on individual differences in baseline working memory span. *Cogn Affect Behav Neurosci*. 2018;18(3):509-520. doi:10.3758/s13415-018-0584-6

235. Slagter HA, Tomer R, Christian BT, et al. PET Evidence for a Role for Striatal Dopamine in the Attentional Blink: Functional Implications. *J Cogn Neurosci*. 2012;24(9):1932-1940. doi:10.1162/jocn_a_00255
236. Naef M, Müller U, Linssen A, Clark L, Robbins TW, Eisenegger C. Effects of dopamine D2/D3 receptor antagonism on human planning and spatial working memory. *Transl Psychiatry*. 2017;7(4):e1107-e1107. doi:10.1038/tp.2017.56
237. Mehta MA, Sahakian BJ, McKenna PJ, Robbins TW. Systemic sulpiride in young adult volunteers simulates the profile of cognitive deficits in Parkinson's disease. *Psychopharmacology (Berl)*. 1999;146(2):162-174. doi:10.1007/s002130051102
238. Mehta M. Systemic sulpiride modulates striatal blood flow: relationships to spatial working memory and planning. *Neuroimage*. 2003;20(4):1982-1994. doi:10.1016/j.neuroimage.2003.08.007
239. Risinger FO, Freeman PA, Rubinstein M, Low MJ, Grandy DK. Lack of operant ethanol self-administration in dopamine D2 receptor knockout mice. *Psychopharmacology (Berl)*. 2000;152(3):343-350. doi:10.1007/s002130000548
240. Soto PL, Grandy DK, Hursh SR, Katz JL. Behavioral economics of food reinforcement and the effects of prefeeding, extinction, and eticlopride in dopamine D2 receptor mutant mice. *Psychopharmacology (Berl)*. 2011;215(4):775-784. doi:10.1007/s00213-011-2173-z
241. Drew MR, Simpson EH, Kellendonk C, et al. Transient Overexpression of Striatal D 2 Receptors Impairs Operant Motivation and Interval Timing. *J Neurosci*. 2007;27(29):7731-7739. doi:10.1523/JNEUROSCI.1736-07.2007
242. Ward RD, Simpson EH, Richards VL, et al. Dissociation of Hedonic Reaction to Reward and Incentive Motivation in an Animal Model of the Negative Symptoms of Schizophrenia. *Neuropsychopharmacology*. 2012;37(7):1699-1707. doi:10.1038/npp.2012.15
243. Trifilieff P, Feng B, Urizar E, et al. Increasing dopamine D2 receptor expression in the adult nucleus accumbens enhances motivation. *Mol Psychiatry*. 2013;18(9):1025-1033. doi:10.1038/mp.2013.57
244. Zald DH, Cowan RL, Riccardi P, et al. Midbrain Dopamine Receptor Availability Is Inversely Associated with Novelty-Seeking Traits in Humans. *J Neurosci*. 2008;28(53):14372-14378. doi:10.1523/JNEUROSCI.2423-08.2008
245. Tournier BB, Steimer T, Millet P, et al. Innately low D2 receptor availability is associated with high novelty-seeking and enhanced behavioural sensitization to amphetamine. *Int J Neuropsychopharmacol*. 2013;16(8):1819-1834. doi:10.1017/S1461145713000205
246. Stacy Hooks M, Colvin AC, Juncos JL, Justice JB. Individual differences in basal and cocaine-stimulated extracellular dopamine in the nucleus accumbens using quantitative microdialysis. *Brain Res*. 1992;587(2):306-312. doi:10.1016/0006-8993(92)91012-4
247. Norbury A, Husain M. Sensation-seeking: Dopaminergic modulation and risk for psychopathology. *Behav Brain Res*. 2015;288:79-93. doi:10.1016/j.bbr.2015.04.015
248. WHO, World Health Organization. <https://www.who.int/>
249. Brisch R, Saniotis A, Wolf R, et al. The Role of Dopamine in Schizophrenia from a Neurobiological and Evolutionary Perspective: Old Fashioned, but Still in Vogue. *Front Psychiatry*. 2014;5(May):1-11. doi:10.3389/fpsy.2014.00047
250. Zakzanis KK, Hansen KT. Dopamine D2 densities and the schizophrenic brain. *Schizophr Res*. 1998;32(3):201-206. doi:10.1016/S0920-9964(98)00041-3
251. Kestler LP, Walker E, Vega EM. Dopamine receptors in the brains of schizophrenia patients: a meta-analysis of the findings. *Behav Pharmacol*. 2001;12(5):355-371. doi:10.1097/00008877-200109000-00007
252. Miyamoto S, Duncan GE, Marx CE, Lieberman JA. Treatments for schizophrenia: a critical review of pharmacology and mechanisms of action of antipsychotic drugs. *Mol Psychiatry*. 2005;10(1):79-104. doi:10.1038/sj.mp.4001556
253. Rampino A, Marakhovskaia A, Soares-Silva T, Torretta S, Veneziani F, Beaulieu JM. Antipsychotic Drug Responsiveness and Dopamine Receptor Signaling; Old Players and New Prospects. *Front Psychiatry*. 2019;9(January):1-13. doi:10.3389/fpsy.2018.00702
254. Seeman P, Hall FS, Uhl G. Increased dopamine D2High receptors in knockouts of the dopamine transporter and the vesicular monoamine transporter may contribute to spontaneous hyperactivity and dopamine supersensitivity. *Synapse*. 2007;61(7):573-576. doi:10.1002/syn.20402
255. Seeman P, Schwarz J, Chen J, et al. Psychosis pathways converge via D2High dopamine receptors. *Synapse*. 2006;60(4):319-346. doi:10.1002/syn.20303
256. Novak G, Seeman P. Hyperactive mice show elevated D2 High receptors, a model for schizophrenia: Calcium/calmodulin-dependent kinase II alpha knockouts. *Synapse*. 2010;800(October 2009):NA-NA. doi:10.1002/syn.20786
257. Bertolino A, Taurisano P, Pisciotto NM, et al. Genetically Determined Measures of Striatal D2 Signaling Predict Prefrontal Activity during Working Memory Performance. Aleman A, ed. *PLoS One*. 2010;5(2):e9348. doi:10.1371/journal.pone.0009348
258. Leonard CJ, Kaiser ST, Robinson BM, et al. Toward the Neural Mechanisms of Reduced Working Memory Capacity in Schizophrenia. *Cereb Cortex*. 2013;23(7):1582-1592. doi:10.1093/cercor/bhs148
259. Bertolino A, Fazio L, Caforio G, et al. Functional variants of the dopamine receptor D2 gene modulate prefronto-striatal phenotypes in schizophrenia. *Brain*. 2009;132(2):417-425. doi:10.1093/brain/awn248
260. Gluskin BS, Mickey BJ. Genetic variation and dopamine D2 receptor availability: a systematic review and meta-analysis of human in vivo molecular imaging studies. *Transl Psychiatry*. 2016;6(3):e747-e747. doi:10.1038/tp.2016.22
261. Luykx JJ, Broersen JL, de Leeuw M. The DRD2 rs1076560 polymorphism and schizophrenia-related intermediate phenotypes: A systematic review and meta-analysis. *Neurosci Biobehav Rev*. 2017;74:214-224. doi:10.1016/j.neubiorev.2017.01.006

262. D'Ambrosio E, Pergola G, Pardiñas AF, et al. A polygenic score indexing a DRD2-related co-expression network is associated with striatal dopamine function. *Sci Rep*. 2022;12(1):12610. doi:10.1038/s41598-022-16442-6
263. Bouvier M, Fehsel K, Schmitt A, Meisenzahl-Lechner E, Gaebel W, Wilmsdorff M. Sex-dependent alterations of dopamine receptor and glucose transporter density in rat hypothalamus under long-term clozapine and haloperidol medication. *Brain Behav*. 2020;10(8):1-11. doi:10.1002/brb3.1694
264. Schuck RK, Flores RE, Fung LK. Brief Report: Sex/Gender Differences in Symptomology and Camouflaging in Adults with Autism Spectrum Disorder. *J Autism Dev Disord*. 2019;49(6):2597-2604. doi:10.1007/s10803-019-03998-y
265. de Giambattista C, Ventura P, Trerotoli P, Margari F, Margari L. Sex Differences in Autism Spectrum Disorder: Focus on High Functioning Children and Adolescents. *Front Psychiatry*. 2021;12(July):1-13. doi:10.3389/fpsy.2021.539835
266. Brandenburg C, Soghomonian J, Zhang K, et al. Increased Dopamine Type 2 Gene Expression in the Dorsal Striatum in Individuals With Autism Spectrum Disorder Suggests Alterations in Indirect Pathway Signaling and Circuitry. *Front Cell Neurosci*. 2020;14(November):1-13. doi:10.3389/fncel.2020.577858
267. Karayannis T, Au E, Patel JC, et al. Cntnap4 differentially contributes to GABAergic and dopaminergic synaptic transmission. *Nature*. 2014;511(7508):236-240. doi:10.1038/nature13248
268. Belujon P, Grace AA. Dopamine System Dysregulation in Major Depressive Disorders. *Int J Neuropsychopharmacol*. 2017;20(12):1036-1046. doi:10.1093/ijnp/pyx056
269. Peciña M, Sikora M, Avery ET, et al. Striatal dopamine D2/3 receptor-mediated neurotransmission in major depression: Implications for anhedonia, anxiety and treatment response. *Eur Neuropsychopharmacol*. 2017;27(10):977-986. doi:10.1016/j.euroneuro.2017.08.427
270. Shah PJ, Ogilvie AD, Goodwin GM, Ebmeier KP. Clinical and psychometric correlates of dopamine D2 binding in depression. *Psychol Med*. 1997;27(6):1247-1256. doi:10.1017/s0033291797005382
271. Thiele S, Sörensen A, Weis J, et al. Deep Brain Stimulation of the Medial Forebrain Bundle in a Rodent Model of Depression: Exploring Dopaminergic Mechanisms with Raclopride and Micro-PET. *Stereotact Funct Neurosurg*. 2020;98(1):8-20. doi:10.1159/000504860
272. Reekes TH, Higginson CI, Ledbetter CR, Sathivadivel N, Zweig RM, Disbrow EA. Sex specific cognitive differences in Parkinson disease. *npj Park Dis*. 2020;6(1):7. doi:10.1038/s41531-020-0109-1
273. Jurado-Coronel JC, Cabezas R, Ávila Rodríguez MF, Echeverría V, García-Segura LM, Barreto GE. Sex differences in Parkinson's disease: Features on clinical symptoms, treatment outcome, sexual hormones and genetics. *Front Neuroendocrinol*. 2018;50(September):18-30. doi:10.1016/j.yfrne.2017.09.002
274. Klein MO, Battagello DS, Cardoso AR, Hauser DN, Bittencourt JC, Correa RG. Dopamine: Functions, Signaling, and Association with Neurological Diseases. *Cell Mol Neurobiol*. 2019;39(1):31-59. doi:10.1007/s10571-018-0632-3
275. Hentosh S, Zhu L, Patino J, Furr JW, Rocha NP, Furr Stimming E. Sex Differences in Huntington's Disease: Evaluating the Enroll-HD Database. *Mov Disord Clin Pract*. 2021;8(3):420-426. doi:10.1002/mdc3.13178
276. McColgan P, Tabrizi SJ. Huntington's disease: a clinical review. *Eur J Neurol*. 2018;25(1):24-34. doi:10.1111/ene.13413
277. Bozzi Y, Borrelli E. Dopamine in neurotoxicity and neuroprotection: what do D2 receptors have to do with it? *Trends Neurosci*. 2006;29(3):167-174. doi:10.1016/j.tins.2006.01.002
278. Paoletti P, Vila I, Rifé M, Lizcano JM, Alberch J, Ginés S. Dopaminergic and Glutamatergic Signaling Crosstalk in Huntington's Disease Neurodegeneration: The Role of p25/Cyclin-Dependent Kinase 5. *J Neurosci*. 2008;28(40):10090-10101. doi:10.1523/JNEUROSCI.3237-08.2008
279. Macpherson T, Hikida T. Role of basal ganglia neurocircuitry in the pathology of psychiatric disorders. *Psychiatry Clin Neurosci*. 2019;73(6):289-301. doi:10.1111/pcn.12830
280. Williams OOF, Coppolino M, George SR, Perreault ML. Sex Differences in Dopamine Receptors and Relevance to Neuropsychiatric Disorders. *Brain Sci*. 2021;11(9):1199. doi:10.3390/brainsci11091199
281. Brown AK, Mandelkern MA, Farahi J, et al. Sex differences in striatal dopamine D2/D3 receptor availability in smokers and non-smokers. *Int J Neuropsychopharmacol*. 2012;15(07):989-994. doi:10.1017/S1461145711001957
282. Okita K, Petersen N, Robertson CL, Dean AC, Mandelkern MA, London ED. Sex Differences in Midbrain Dopamine D2-Type Receptor Availability and Association with Nicotine Dependence. *Neuropsychopharmacology*. 2016;41(12):2913-2919. doi:10.1038/npp.2016.105
283. Volkow ND, Wang G-J, Fowler JS, Tomasi D, Telang F. Addiction: Beyond dopamine reward circuitry. *Proc Natl Acad Sci*. 2011;108(37):15037-15042. doi:10.1073/pnas.1010654108
284. Trifilieff P, Martinez D. Imaging addiction: D2 receptors and dopamine signaling in the striatum as biomarkers for impulsivity. *Neuropharmacology*. 2014;76(1):498-509. doi:10.1016/j.neuropharm.2013.06.031
285. Egervari G, Cicciocioppo R, Jentsch JD, Hurd YL. Shaping vulnerability to addiction – the contribution of behavior, neural circuits and molecular mechanisms. *Neurosci Biobehav Rev*. Published online May 2017. doi:10.1016/j.neubiorev.2017.05.019
286. Choi W-S, Kim H-W, Xia Z. Preparation of Primary Cultured Dopaminergic Neurons from Mouse Brain. In: Zhou R, Mei L, eds. *Neural Development: Methods and Protocols, Methods in Molecular Biology*. Vol 1018. Methods in Molecular Biology. Humana Press; 2013:61-69. doi:10.1007/978-1-62703-444-9_6
287. Weinert M, Selvakumar T, Tierney TS, Alavian KN. Isolation, Culture and Long-Term Maintenance of Primary Mesencephalic Dopaminergic Neurons From Embryonic Rodent Brains. *J Vis Exp*. 2015;(96):1-5. doi:10.3791/52475
288. Schock SC, Jolin-Dahel KS, Schock PC, Staines WA, Garcia-Munoz M, Arbuthnott GW. Striatal interneurons in dissociated

- cell culture. *Histochem Cell Biol.* 2010;134(1):1-12. doi:10.1007/s00418-010-0707-9
289. Deyts C, Galan-Rodriguez B, Martin E, et al. Dopamine D2 receptor stimulation potentiates polyQ Huntingtin-induced mouse striatal neuron dysfunctions via Rho/ROCK-II activation. *PLoS One.* 2009;4(12). doi:10.1371/journal.pone.0008287
 290. Penrod RD, Kourrich S, Kearney E, Thomas MJ, Lanier LM. An embryonic culture system for the investigation of striatal medium spiny neuron dendritic spine development and plasticity. *J Neurosci Methods.* 2011;200(1):1-13. doi:10.1016/j.jneumeth.2011.05.029
 291. Neely MD, Schmidt DE, Deutch AY. Cortical regulation of dopamine depletion-induced dendritic spine loss in striatal medium spiny neurons. *Neuroscience.* 2007;149(2):457-464. doi:10.1016/j.neuroscience.2007.06.044
 292. Naia L, Rego AC. Isolation and Maintenance of Striatal Neurons. *Bio-Protocol.* 2018;8(8):1-10. doi:10.21769/bioprotoc.2823
 293. Penrod RD, Campagna J, Panneck T, Preese L, Lanier LM. The presence of cortical neurons in striatal-cortical co-cultures alters the effects of dopamine and BDNF on medium spiny neuron dendritic development. *Front Cell Neurosci.* 2015;9(July):1-14. doi:10.3389/fncel.2015.00269
 294. Yoon S, Baik J-H. Dopamine D2 Receptor-mediated Epidermal Growth Factor Receptor Transactivation through a Disintegrin and Metalloprotease Regulates Dopaminergic Neuron Development via Extracellular Signal-related Kinase Activation. *J Biol Chem.* 2013;288(40):28435-28446. doi:10.1074/jbc.M113.461202
 295. Mutti V, Bono F, Tomasoni Z, et al. Structural Plasticity of Dopaminergic Neurons Requires the Activation of the D3R-nAChR Heteromer and the PI3K-ERK1/2/Akt-Induced Expression of c-Fos and p70S6K Signaling Pathway. *Mol Neurobiol.* 2022;59(4):2129-2149. doi:10.1007/s12035-022-02748-z
 296. Chen HT, Ruan NY, Chen JC, Lin TY. Dopamine D2 receptor-mediated Akt/PKB signalling: Initiation by the D2S receptor and role in quinpirole-induced behavioural activation. *ASN Neuro.* 2012;4(6):371-382. doi:10.1042/AN20120013
 297. Chun LS, Vekariya RH, Free RB, et al. Structure-Activity Investigation of a G Protein-Biased Agonist Reveals Molecular Determinants for Biased Signaling of the D2 Dopamine Receptor. *Front Synaptic Neurosci.* 2018;10(FEB):1-18. doi:10.3389/fnsyn.2018.00002
 298. Hansson E, Von Euler G, Fuxe K, Hansson T. Toluene induces changes in the morphology of astroglia and neurons in striatal primary cell cultures. *Toxicology.* 1988;49(1):155-163. doi:10.1016/0300-483X(88)90188-6
 299. Sun Y, Lim Y, Li F, et al. ProBDNF Collapses Neurite Outgrowth of Primary Neurons by Activating RhoA. Obukhov AG, ed. *PLoS One.* 2012;7(4):e35883. doi:10.1371/journal.pone.0035883
 300. Håkansson K, Galdi S, Hendrick J, Snyder G, Greengard P, Fisone G. Regulation of phosphorylation of the GluR1 AMPA receptor by dopamine D 2 receptors. *J Neurochem.* 2006;96(2):482-488. doi:10.1111/j.1471-4159.2005.03558.x
 301. Bateup HS, Svenningsson P, Kuroiwa M, et al. Cell type-specific regulation of DARPP-32 phosphorylation by psychostimulant and antipsychotic drugs. *Nat Neurosci.* 2008;11(8):932-939. doi:10.1038/nn.2153
 302. Cai G, Zhen X, Uryu K, Friedman E. Activation of Extracellular Signal-Regulated Protein Kinases Is Associated with a Sensitized Locomotor Response to D 2 Dopamine Receptor Stimulation in Unilateral 6-Hydroxydopamine-Lesioned Rats. *J Neurosci.* 2000;20(5):1849-1857. doi:10.1523/JNEUROSCI.20-05-01849.2000
 303. Phamluong K, Darcq E, Wu S, Sakhai SA, Ron D. Fyn Signaling Is Compartmentalized to Dopamine D1 Receptor Expressing Neurons in the Dorsal Medial Striatum. *Front Mol Neurosci.* 2017;10(August). doi:10.3389/fnmol.2017.00273
 304. Gomes I, Sierra S, Devi LA. Detection of Receptor Heteromerization Using In Situ Proximity Ligation Assay. In: *Current Protocols in Pharmacology.* Vol 118. John Wiley & Sons, Inc.; 2016:2.16.1-2.16.31. doi:10.1002/cpph.15
 305. Langhammer CG, Previtera ML, Sweet ES, Sran SS, Chen M, Firestein BL. Automated Sholl analysis of digitized neuronal morphology at multiple scales: Whole cell Sholl analysis versus Sholl analysis of arbor subregions. *Cytom Part A.* 2010;77A(12):1160-1168. doi:10.1002/cyto.a.20954
 306. Palombo M, Ligneul C, Najac C, et al. New paradigm to assess brain cell morphology by diffusion-weighted MR spectroscopy in vivo. *Proc Natl Acad Sci.* 2016;113(24):6671-6676. doi:10.1073/pnas.1504327113
 307. Wilson MD, Sethi S, Lein PJ, Keil KP. Valid statistical approaches for analyzing sholl data: Mixed effects versus simple linear models. *J Neurosci Methods.* 2017;279:33-43. doi:10.1016/j.jneumeth.2017.01.003
 308. Ferreira TA, Blackman A V, Oyrer J, et al. Neuronal morphometry directly from bitmap images. *Nat Methods.* 2014;11(10):982-984. doi:10.1038/nmeth.3125
 309. Imaris. Classify Spines Xtension In Imaris Tutorial. Published 2013. <https://imaris.oxinst.com/learning/view/article/classify-spines-xtension>
 310. Boschen SL, Wietzikoski EC, Winn P, Cunha C Da. The role of nucleus accumbens and dorsolateral striatal D2 receptors in active avoidance conditioning. *Neurobiol Learn Mem.* 2011;96(2):254-262. doi:10.1016/j.nlm.2011.05.002
 311. Guo N, Guo W, Kralikova M, et al. Impact of D2 Receptor Internalization on Binding Affinity of Neuroimaging Radiotracers. *Neuropsychopharmacology.* 2010;35(3):806-817. doi:10.1038/npp.2009.189
 312. Bepalov A, Jongen-Rêlo A-L, van Gaalen M, Harich S, Schoemaker H, Gross G. Habituation Deficits Induced by Metabotropic Glutamate Receptors 2/3 Receptor Blockade in Mice: Reversal by Antipsychotic Drugs. *J Pharmacol Exp Ther.* 2007;320(2):944-950. doi:10.1124/jpet.106.110684
 313. Deutsch-Feldman M, Picetti R, Seip-Cammack K, Zhou Y, Kreek MJ. Effects of handling and vehicle injections on adrenocorticotrophic and corticosterone concentrations in Sprague-Dawley compared with Lewis rats. *J Am Assoc Lab Anim Sci.* 2015;54(1):35-39. <http://www.ncbi.nlm.nih.gov/pubmed/25651089>
 314. Ding JX, Rudak PT, Inoue W, Haeryfar SMM. Physical restraint mouse models to assess immune responses under stress with

- or without habituation. *STAR Protoc.* 2021;2(4):100838. doi:10.1016/j.xpro.2021.100838
315. Gouveia K, Hurst JL. Improving the practicality of using non-aversive handling methods to reduce background stress and anxiety in laboratory mice. *Sci Rep.* 2019;9(1):20305. doi:10.1038/s41598-019-56860-7
 316. Gould TD, Dao DT, Kovacsics CE. *Mood and Anxiety Related Phenotypes in Mice.* Vol 42. (Gould TD, ed.). Humana Press; 2009. doi:10.1007/978-1-60761-303-9
 317. Prut L, Belzung C. The open field as a paradigm to measure the effects of drugs on anxiety-like behaviors: a review. *Eur J Pharmacol.* 2003;463(1-3):3-33. doi:10.1016/S0014-2999(03)01272-X
 318. Miedel CJ, Patton JM, Miedel AN, Miedel ES, Levenson JM. Assessment of Spontaneous Alternation, Novel Object Recognition and Limb Claspings in Transgenic Mouse Models of Amyloid- β ; and Tau Neuropathology. *J Vis Exp.* 2017;2017(123):1-8. doi:10.3791/55523
 319. Kraeuter A-K, Guest PC, Sarnyai Z. The Y-Maze for Assessment of Spatial Working and Reference Memory in Mice. In: *Methods in Molecular Biology.* Vol 1916. ; 2019:105-111. doi:10.1007/978-1-4939-8994-2_10
 320. Lalonde R. The neurobiological basis of spontaneous alternation. *Neurosci Biobehav Rev.* 2002;26(1):91-104. doi:10.1016/S0149-7634(01)00041-0
 321. Akiti K, Tsutsui-Kimura I, Xie Y, et al. Striatal dopamine explains novelty-induced behavioral dynamics and individual variability in threat prediction. *Neuron.* 2022;110(22):3789-3804.e9. doi:10.1016/j.neuron.2022.08.022
 322. Barto A, Mirolli M, Baldassarre G. Novelty or Surprise? *Front Psychol.* 2013;4(DEC):1-15. doi:10.3389/fpsyg.2013.00907
 323. Lanciego JL, Luquin N, Obeso JA. Functional Neuroanatomy of the Basal Ganglia. *Cold Spring Harb Perspect Med.* 2012;2(12):a009621-a009621. doi:10.1101/cshperspect.a009621
 324. Matamales M, Bertran-Gonzalez J, Salomon L, et al. Striatal medium-sized spiny neurons: Identification by nuclear staining and study of neuronal subpopulations in BAC transgenic mice. *PLoS One.* 2009;4(3). doi:10.1371/journal.pone.0004770
 325. Prestoz L, Jaber M, Gaillard A. Dopaminergic axon guidance: Which makes what? *Front Cell Neurosci.* 2012;6(JULY 2012):1-13. doi:10.3389/fncel.2012.00032
 326. Gille G, Rausch W-D, Hung S-T, et al. Pergolide protects dopaminergic neurons in primary culture under stress conditions. *J Neural Transm.* 2002;109(5-6):633-643. doi:10.1007/s007020200052
 327. Choi WS, Kruse SE, Palmiter RD, Xia Z. Mitochondrial complex I inhibition is not required for dopaminergic neuron death induced by rotenone, MPP+, or paraquat. *Proc Natl Acad Sci U S A.* 2008;105(39):15136-15141. doi:10.1073/pnas.0807581105
 328. Gaven F, Marin P, Claeysen S. Primary culture of mouse dopaminergic neurons. *J Vis Exp.* 2014;(91):1-11. doi:10.3791/51751
 329. Ebdrup BH, Glenthøj B, Rasmussen H, et al. Hippocampal and caudate volume reductions in antipsychotic-naïve first-episode schizophrenia. *J Psychiatry Neurosci.* 2010;35(2):95-104. doi:10.1503/jpn.090049
 330. Zaja-Milatovic S, Milatovic D, Schantz AM, et al. Dendritic degeneration in neostriatal medium spiny neurons in Parkinson disease. *Neurology.* 2005;64(3):545-547. doi:10.1212/01.WNL.0000150591.33787.A4
 331. Ren J, Zhao T, Xu Y, Ye H. Interaction between DISC1 and CHL1 in regulation of neurite outgrowth. *2016.* 2016;1648:290-297. doi:10.1016/j.brainres.2016.06.033
 332. Solis O, Vázquez-Roque RA, Camacho-Abrego I, et al. Decreased dendritic spine density of neurons of the prefrontal cortex and nucleus accumbens and enhanced amphetamine sensitivity in postpubertal rats after a neonatal amygdala lesion. *Synapse.* 2009;63(12):1143-1153. doi:10.1002/syn.20697
 333. Ying L, Zhao J, Ye Y, et al. Regulation of Cdc42 signaling by the dopamine D2 receptor in a mouse model of Parkinson's disease. *Aging Cell.* 2022;21(5):1-16. doi:10.1111/accel.13588
 334. Coley AA, Gao W-J. PSD-95 deficiency disrupts PFC-associated function and behavior during neurodevelopment. *Sci Rep.* 2019;9(1):9486. doi:10.1038/s41598-019-45971-w
 335. Yusifov R, Tippmann A, Staiger JF, Schlüter OM, Löwel S. Spine dynamics of PSD-95-deficient neurons in the visual cortex link silent synapses to structural cortical plasticity. *Proc Natl Acad Sci.* 2021;118(10):1-9. doi:10.1073/pnas.2022701118
 336. Zhao B, Zhu J, Dai D, et al. Differential dopaminergic regulation of inwardly rectifying potassium channel mediated subthreshold dynamics in striatal medium spiny neurons. *Neuropharmacology.* 2016;107:396-410. doi:10.1016/j.neuropharm.2016.03.037
 337. Ehrlich I, Klein M, Rumpel S, Malinow R. PSD-95 is required for activity-driven synapse stabilization. *Proc Natl Acad Sci U S A.* 2007;104(10):4176-4181. doi:10.1073/pnas.0609307104
 338. Park SW, Lee CH, Cho HY, et al. Effects of antipsychotic drugs on the expression of synaptic proteins and dendritic outgrowth in hippocampal neuronal cultures. *Synapse.* 2013;67(5):224-234. doi:10.1002/syn.21634
 339. Hayashi-Takagi A, Takaki M, Graziane N, et al. Disrupted-in-Schizophrenia 1 (DISC1) regulates spines of the glutamate synapse via Rac1. *Nat Neurosci.* 2010;13(3):327-332. doi:10.1038/nn.2487
 340. Ramos A. Animal models of anxiety: do I need multiple tests? *Trends Pharmacol Sci.* 2008;29(10):493-498. doi:10.1016/j.tips.2008.07.005
 341. França ASC, Muratori L, Nascimento GC, Pereira CM, Ribeiro S, Lobão-Soares B. Object recognition impairment and rescue by a dopamine D2 antagonist in hyperdopaminergic mice. *Behav Brain Res.* 2016;308:211-216. doi:10.1016/j.bbr.2016.04.009
 342. Czoty PW, Gage HD, Nader MA. Differences in D2 dopamine receptor availability and reaction to novelty in socially housed male monkeys during abstinence from cocaine. *Psychopharmacology (Berl).* 2010;208(4):585-592. doi:10.1007/s00213-009-1756-4

343. Xue L, Geng Y, Li M, et al. The effects of D3R on TLR4 signaling involved in the regulation of METH-mediated mast cells activation. *Int Immunopharmacol*. 2016;36:187-198. doi:10.1016/j.intimp.2016.04.030
344. Kotarska A. Cell adhesion molecule close homolog of L1 regulates internalization of the dopamine receptor D2 and formation of the mesolimbic dopaminergic pathway in mice (*Mus musculus* Linnaeus, 1758). Published online 2019.
345. Tepper JM, Wilson CJ, Koós T. Feedforward and feedback inhibition in neostriatal GABAergic spiny neurons. *Brain Res Rev*. 2008;58(2):272-281. doi:10.1016/j.brainresrev.2007.10.008
346. Owen SF, Berke JD, Kreitzer AC. Fast-Spiking Interneurons Supply Feedforward Control of Bursting, Calcium, and Plasticity for Efficient Learning. *Cell*. 2018;172(4):683-695.e15. doi:10.1016/j.cell.2018.01.005
347. Han F, Konkalmatt P, Mokashi C, et al. Dopamine D2 receptor modulates Wnt expression and control of cell proliferation. *Sci Rep*. 2019;9(1):16861. doi:10.1038/s41598-019-52528-4
348. Hall H, Sällemark M, Jerning E. Effects of Remoxipride and some Related New Substituted Salicylamides on Rat Brain Receptors. *Acta Pharmacol Toxicol (Copenh)*. 1986;58(1):61-70. doi:10.1111/j.1600-0773.1986.tb00071.x
349. Sokoloff P, Andrieux M, Besançon R, et al. Pharmacology of human dopamine D3 receptor expressed in a mammalian cell line: comparison with D2 receptor. *Eur J Pharmacol Mol Pharmacol*. 1992;225(4):331-337. doi:10.1016/0922-4106(92)90107-7
350. Mestikawy S, Glowinski J, Hamon M. Presynaptic Dopamine Autoreceptors Control Tyrosine Hydroxylase Activation in Depolarized Striatal Dopaminergic Terminals. *J Neurochem*. 1986;46(1):12-22. doi:10.1111/j.1471-4159.1986.tb12919.x
351. Hall DA, Strange PG. Evidence that antipsychotic drugs are inverse agonists at D 2 dopamine receptors. *Br J Pharmacol*. 1997;121(4):731-736. doi:10.1038/sj.bjp.0701196
352. Fawaz CS, Martel P, Leo D, Trudeau L-E. Presynaptic action of neurotensin on dopamine release through inhibition of D2 receptor function. *BMC Neurosci*. 2009;10(1):96. doi:10.1186/1471-2202-10-96
353. Fazeli G, Oli RG, Schupp N, Stopper H. The Role of the Dopamine Transporter in Dopamine-Induced DNA Damage. *Brain Pathol*. 2011;21(3):237-248. doi:10.1111/j.1750-3639.2010.00440.x
354. Albert PR, Neve KA, Bunzow JR, Civelli O. Coupling of a cloned rat dopamine-D2 receptor to inhibition of adenylyl cyclase and prolactin secretion. *J Biol Chem*. 1990;265(4):2098-2104. doi:10.1016/S0021-9258(19)39945-4
355. Rodriguez-Contreras D, Condon AF, Buck DC, et al. Signaling-Biased and Constitutively Active Dopamine D2 Receptor Variant. *ACS Chem Neurosci*. 2021;12(11):1873-1884. doi:10.1021/acchemneuro.0c00712
356. Richardson BD, Saha K, Krout D, et al. Membrane potential shapes regulation of dopamine transporter trafficking at the plasma membrane. *Nat Commun*. 2016;7(1):10423. doi:10.1038/ncomms10423
357. Dagra A, Miller DR, Lin M, et al. α -Synuclein-induced dysregulation of neuronal activity contributes to murine dopamine neuron vulnerability. *npj Park Dis*. 2021;7(1):76. doi:10.1038/s41531-021-00210-w
358. Murase S, McKay RD. A Specific Survival Response in Dopamine Neurons at Most Risk in Parkinson's Disease. *J Neurosci*. 2006;26(38):9750-9760. doi:10.1523/JNEUROSCI.2745-06.2006
359. Neve KA, Cox BA, Henningsen RA, Spanoyannis A, Neve RL. Pivotal role for aspartate-80 in the regulation of dopamine D2 receptor affinity for drugs and inhibition of adenylyl cyclase. *Mol Pharmacol*. 1991;39(6):733-739. <http://www.ncbi.nlm.nih.gov/pubmed/1828858>
360. Newton CL, Wood MD, Strange PG. Examining the Effects of Sodium Ions on the Binding of Antagonists to Dopamine D2 and D3 Receptors. Lodola A, ed. *PLoS One*. 2016;11(7):e0158808. doi:10.1371/journal.pone.0158808
361. Michino M, Free RB, Doyle TB, Sibley DR, Shi L. Structural basis for Na⁺ -sensitivity in dopamine D2 and D3 receptors. *Chem Commun*. 2015;51(41):8618-8621. doi:10.1039/C5CC02204E
362. Ericksen SS, Cummings DF, Weinstein H, Schetz JA. Ligand Selectivity of D 2 Dopamine Receptors Is Modulated by Changes in Local Dynamics Produced by Sodium Binding. *J Pharmacol Exp Ther*. 2009;328(1):40-54. doi:10.1124/jpet.108.141531
363. Lane JR, Abramyan AM, Adhikari P, et al. Distinct inactive conformations of the dopamine D2 and D3 receptors correspond to different extents of inverse agonism. *Elife*. 2020;9:1-26. doi:10.7554/eLife.52189
364. Nir I, Harrison JM, Haque R, et al. Dysfunctional light-evoked regulation of cAMP in photoreceptors and abnormal retinal adaptation in mice lacking dopamine D4 receptors. *J Neurosci*. 2002;22(6):2063-2073. doi:10.1523/JNEUROSCI.22-06-02063.2002
365. Huang Y, Chen C-C, Wang T-T, Qiu Y-H, Peng Y-P. Dopamine receptors modulate T lymphocytes via inhibition of cAMP-CREB signaling pathway. *Neuro Endocrinol Lett*. 2016;37(7):491-500. <http://www.ncbi.nlm.nih.gov/pubmed/28326743>
366. Montezinho LP, Mørk A, Duarte CB, Penschuck S, Gerales CFGC, Castro MMCA. Effects of mood stabilizers on the inhibition of adenylate cyclase via dopamine D 2 -like receptors. *Bipolar Disord*. 2007;9(3):290-297. doi:10.1111/j.1399-5618.2007.00354.x
367. Walker QD, Ray R, Kuhn CM. Sex Differences in Neurochemical Effects of Dopaminergic Drugs in Rat Striatum. *Neuropsychopharmacology*. 2006;31(6):1193-1202. doi:10.1038/sj.npp.1300915
368. Schindler CW, Carmona GN. Effects of dopamine agonists and antagonists on locomotor activity in male and female rats. *Pharmacol Biochem Behav*. 2002;72(4):857-863. doi:10.1016/S0091-3057(02)00770-0
369. Shioda N, Yabuki Y, Wang Y, et al. Endocytosis following dopamine D2 receptor activation is critical for neuronal activity and dendritic spine formation via Rabex-5/PDGFR β signaling in striatopallidal medium spiny neurons. *Mol Psychiatry*. 2017;22(8):1205-1222. doi:10.1038/mp.2016.200
370. Li J, Monk KR. Healthy attachments: Cell adhesion molecules collectively control myelin integrity. *J Cell Biol*.

- 2019;218(9):2824-2825. doi:10.1083/jcb.201907077
371. Collo G, Zanetti S, Missale C, Spano P. Dopamine D3 receptor-preferring agonists increase dendrite arborization of mesencephalic dopaminergic neurons via extracellular signal-regulated kinase phosphorylation. *Eur J Neurosci.* 2008;28(7):1231-1240. doi:10.1111/j.1460-9568.2008.06423.x
 372. Jung AB, Bennett JP. Development of striatal dopaminergic function. I. Pre- and postnatal development of mRNAs and binding sites for striatal D1 (D1a) and D2 (D2a) receptors. *Dev Brain Res.* 1996;94(2):109-120. doi:10.1016/S0165-3806(96)80002-2
 373. de Luca A, Vassallo S, Benitez-Temino B, Menichetti G, Rossi F, Buffo A. Distinct Modes of Neuritic Growth in Purkinje Neurons at Different Developmental Stages: Axonal Morphogenesis and Cellular Regulatory Mechanisms. Amédée T, ed. *PLoS One.* 2009;4(8):e6848. doi:10.1371/journal.pone.0006848
 374. Carruzzo F, Kaiser S, Tobler PN, Kirschner M, Simon JJ. Increased ventral striatal functional connectivity in patients with schizophrenia during reward anticipation. *NeuroImage Clin.* 2022;33:102944. doi:10.1016/j.nicl.2022.102944
 375. Nandhagopal R, Kuramoto L, Schulzer M, et al. Longitudinal evolution of compensatory changes in striatal dopamine processing in Parkinson's disease. *Brain.* 2011;134(11):3290-3298. doi:10.1093/brain/awr233
 376. Straub C, Granger AJ, Saulnier JL, Sabatini BL. CRISPR/Cas9-Mediated Gene Knock-Down in Post-Mitotic Neurons. Tang Y-P, ed. *PLoS One.* 2014;9(8):e105584. doi:10.1371/journal.pone.0105584
 377. Adrover MF, Shin JH, Alvarez VA. Glutamate and Dopamine Transmission from Midbrain Dopamine Neurons Share Similar Release Properties But Are Differentially Affected by Cocaine. *J Neurosci.* 2014;34(9):3183-3192. doi:10.1523/JNEUROSCI.4958-13.2014
 378. Bourne J, Harris KM. Do thin spines learn to be mushroom spines that remember? *Curr Opin Neurobiol.* 2007;17(3):381-386. doi:10.1016/j.conb.2007.04.009
 379. Guo H, Ali T, Que J, Zhou Y, Bai Y. Dendritic spine dynamics in associative memory: A comprehensive review. *FASEB J.* 2023;37(5):e22896. doi:10.1096/fj.202202166R
 380. Kim E, Sheng M. PDZ domain proteins of synapses. *Nat Rev Neurosci.* 2004;5(10):771-781. doi:10.1038/nrn1517
 381. Liu X-Y, Chu X-P, Mao L-M, et al. Modulation of D2R-NR2B Interactions in Response to Cocaine. *Neuron.* 2006;52(5):897-909. doi:10.1016/j.neuron.2006.10.011
 382. Sun P, Wang J, Gu W, et al. PSD-95 regulates D1 dopamine receptor resensitization, but not receptor-mediated Gs-protein activation. *Cell Res.* 2009;19(5):612-624. doi:10.1038/cr.2009.30
 383. Zhang J, Saur T, Duke AN, et al. Motor Impairments, Striatal Degeneration, and Altered Dopamine-Glutamate Interplay in Mice Lacking PSD-95. *J Neurogenet.* 2014;28(1-2):98-111. doi:10.3109/01677063.2014.892486
 384. Bosch M, Hayashi Y. Structural plasticity of dendritic spines. *Curr Opin Neurobiol.* 2012;22(3):383-388. doi:10.1016/j.conb.2011.09.002
 385. Miller DR, Lebowitz JJ, Guenther DT, et al. Methamphetamine regulation of activity and topology of ventral midbrain networks. *PLoS One.* 2019;14(9):1-19. doi:10.1371/journal.pone.0222957
 386. Wolinsky TD, Swanson CJ, Smith KE, et al. The Trace Amine 1 receptor knockout mouse: an animal model with relevance to schizophrenia. *Genes, Brain Behav.* 2007;6(7):628-639. doi:10.1111/j.1601-183X.2006.00292.x
 387. Di Cara B, Maggio R, Aloisi G, et al. Genetic Deletion of Trace Amine 1 Receptors Reveals Their Role in Auto-Inhibiting the Actions of Ecstasy (MDMA). *J Neurosci.* 2011;31(47):16928-16940. doi:10.1523/JNEUROSCI.2502-11.2011
 388. Espinoza S, Salahpour A, Masri B, et al. Functional Interaction between Trace Amine-Associated Receptor 1 and Dopamine D2 Receptor. *Mol Pharmacol.* 2011;80(3):416-425. doi:10.1124/mol.111.073304
 389. Rossi M, Fasciani I, Marampon F, Maggio R, Scarselli M. The First Negative Allosteric Modulator for Dopamine D 2 and D 3 Receptors, SB269652 May Lead to a New Generation of Antipsychotic Drugs. *Mol Pharmacol.* 2017;91(6):586-594. doi:10.1124/mol.116.107607
 390. Latorraca NR, Venkatakrishnan AJ, Dror RO. GPCR Dynamics: Structures in Motion. *Chem Rev.* 2017;117(1):139-155. doi:10.1021/acs.chemrev.6b00177
 391. Wang S, Che T, Levit A, Shoichet BK, Wacker D, Roth BL. Structure of the D2 dopamine receptor bound to the atypical antipsychotic drug risperidone. *Nature.* 2018;555(7695):269-273. doi:10.1038/nature25758
 392. Žuk J, Bartuzi D, Silva AG, et al. Allosteric modulation of dopamine D2L receptor in complex with Gi1 and Gi2 proteins: the effect of subtle structural and stereochemical ligand modifications. *Pharmacol Reports.* 2022;74(2):406-424. doi:10.1007/s43440-021-00352-x
 393. Kusserow H, Davies B, Hörtnagl H, et al. Reduced anxiety-related behaviour in transgenic mice overexpressing serotonin1A receptors. *Mol Brain Res.* 2004;129(1-2):104-116. doi:10.1016/j.molbrainres.2004.06.028
 394. Bert B, Dere E, Wilhelmi N, et al. Transient overexpression of the 5-HT1A receptor impairs water-maze but not hole-board performance. *Neurobiol Learn Mem.* 2005;84(1):57-68. doi:10.1016/j.nlm.2005.03.005
 395. Levant B, Grigoriadis DE, DeSouza EB. Characterization of [3H]quinpirole binding to D2-like dopamine receptors in rat brain. *J Pharmacol Exp Ther.* 1992;262(3):929-935. <http://jpet.aspetjournals.org/content/262/3/929.abstract>
 396. Ford CP, Phillips PEM, Williams JT. The time course of dopamine transmission in the ventral tegmental area. *J Neurosci.* 2009;29(42):13344-13352. doi:10.1523/JNEUROSCI.3546-09.2009
 397. Skinbjerg M, Sibley DR, Javitch JA, Abi-Dargham A. Imaging the high-affinity state of the dopamine D2 receptor in vivo: Fact or fiction? *Biochem Pharmacol.* 2012;83(2):193-198. doi:10.1016/j.bcp.2011.09.008

398. Fowler JC, Bhattacharya S, Urban JD, Vaidehi N, Mailman RB. Receptor Conformations Involved in Dopamine D₂L Receptor Functional Selectivity Induced by Selected Transmembrane-5 Serine Mutations. *Mol Pharmacol*. 2012;81(6):820-831. doi:10.1124/mol.111.075457
399. Ferrada C, Ferré S, Casadó V, et al. Interactions between histamine H₃ and dopamine D₂ receptors and the implications for striatal function. *Neuropharmacology*. 2008;55(2):190-197. doi:10.1016/j.neuropharm.2008.05.008
400. Wang M, Pei L, Fletcher PJ, Kapur S, Seeman P, Liu F. Schizophrenia, amphetamine-induced sensitized state and acute amphetamine exposure all show a common alteration: Increased dopamine D₂ receptor dimerization. *Mol Brain*. 2010;3(1):1-9. doi:10.1186/1756-6606-3-25
401. Lane JR, Powney B, Wise A, Rees S, Milligan G. Protean agonism at the dopamine D₂ receptor: (S)-3-(3-hydroxyphenyl)-N-propylpiperidine is an agonist for activation of G_{o1} but an antagonist/inverse agonist for Gi₁, G_{i2}, and Gi₃. *Mol Pharmacol*. 2007;71(5):1349-1359. doi:10.1124/mol.106.032722
402. Fuxe K, Marcellino D, Leo G, Agnati LF. Molecular integration via allosteric interactions in receptor heteromers. A working hypothesis. *Curr Opin Pharmacol*. 2010;10(1):14-22. doi:10.1016/j.coph.2009.10.010
403. Seeman P, Weinschenker D, Quirion R, et al. Dopamine supersensitivity correlates with D₂ High states, implying many paths to psychosis. *Proc Natl Acad Sci*. 2005;102(9):3513-3518. doi:10.1073/pnas.0409766102
404. Seeman P. All Roads to Schizophrenia Lead to Dopamine Supersensitivity and Elevated Dopamine D₂High Receptors. *CNS Neurosci Ther*. 2011;17(2):118-132. doi:10.1111/j.1755-5949.2010.00162.x
405. Kubota M, Nagashima T, Takano H, et al. Affinity States of Striatal Dopamine D₂ Receptors in Antipsychotic-Free Patients with Schizophrenia. *Int J Neuropsychopharmacol*. 2017;20(11):928-935. doi:10.1093/ijnp/pyx063
406. Jalink P, Caiazzo M. Brain Organoids: Filling the Need for a Human Model of Neurological Disorder. *Biology (Basel)*. 2021;10(8):740. doi:10.3390/biology10080740
407. Keller S, Polanski WH, Enzensperger C, Reichmann H, Hermann A, Gille G. 9-Methyl- β -carboline inhibits monoamine oxidase activity and stimulates the expression of neurotrophic factors by astrocytes. *J Neural Transm*. 2020;127(7):999-1012. doi:10.1007/s00702-020-02189-9
408. Berezhnov A V., Fedotova EI, Sergeev AI, Teplov IY, Abramov AY. Dopamine controls neuronal spontaneous calcium oscillations via astrocytic signal. *Cell Calcium*. 2021;94(January):102359. doi:10.1016/j.ceca.2021.102359
409. Croft CL, Futch HS, Moore BD, Golde TE. Organotypic brain slice cultures to model neurodegenerative proteinopathies. *Mol Neurodegener*. 2019;14(1):45. doi:10.1186/s13024-019-0346-0
410. Simón V., Parra A, Miñarro J, Arenas M., Vinader-Caerols C, Aguilar M. Predicting how equipotent doses of chlorpromazine, haloperidol, sulpiride, raclopride and clozapine reduce locomotor activity in mice. *Eur Neuropsychopharmacol*. 2000;10(3):159-164. doi:10.1016/S0924-977X(00)00070-5
411. Karami M, Zarrindast MR. Morphine sex-dependently induced place conditioning in adult Wistar rats. *Eur J Pharmacol*. 2008;582(1-3):78-87. doi:10.1016/j.ejphar.2007.12.010
412. Díaz-Véliz G, Benavides MS, Butrón S, Dussaubat N, Mora S. Behavioral Effects of Dopamine Agonists and Antagonists. *Pharmacol Biochem Behav*. 1999;62(1):21-29. doi:10.1016/S0091-3057(98)00097-5
413. de Oliveira Alves C, Reimer AE, de Oliveira AR. Involvement of D₂-like dopaminergic receptors in contextual fear conditioning in female rats: influence of estrous cycle. *Front Behav Neurosci*. 2022;16(November):1-12. doi:10.3389/fnbeh.2022.1033649
414. Hartesveldt C Van, Cottrell GA, Potter T, Meyer ME. Effects of intracerebral quinpirole on locomotion in rats. *Eur J Pharmacol*. 1992;214(1):27-32. doi:10.1016/0014-2999(92)90091-H
415. Ferraiolo M, Atik H, Ponthot R, Koener B, Hanson J, Hermans E. Dopamine D₂L receptor density influences the recruitment of β -arrestin2 and Gi₁ induced by antiparkinsonian drugs. *Neuropharmacology*. 2022;207:108942. doi:10.1016/j.neuropharm.2022.108942
416. McDermott TJ, Berg H, Touthang J, et al. Striatal reactivity during emotion and reward relates to approach–avoidance conflict behaviour and is altered in adults with anxiety or depression. *J Psychiatry Neurosci*. 2022;47(5):E311-E322. doi:10.1503/jpn.220083
417. La-Vu M, Tobias BC, Schuette PJ, Adhikari A. To Approach or Avoid: An Introductory Overview of the Study of Anxiety Using Rodent Assays. *Front Behav Neurosci*. 2020;14(August):1-7. doi:10.3389/fnbeh.2020.00145
418. Sturman O, Germain PL, Bohacek J. Exploratory rearing: a context- and stress-sensitive behavior recorded in the open-field test. *Stress*. 2018;21(5):443-452. doi:10.1080/10253890.2018.1438405
419. Ramos A, Mormède P. Stress and emotionality: a multidimensional and genetic approach. *Neurosci Biobehav Rev*. 1997;22(1):33-57. doi:10.1016/S0149-7634(97)00001-8
420. Kalueff A V, Stewart AM, Song C, Berridge KC, Graybiel AM, Fentress JC. Neurobiology of rodent self-grooming and its value for translational neuroscience. *Nat Rev Neurosci*. 2016;17(1):45-59. doi:10.1038/nrn.2015.8
421. Montag-Sallaz M, Baarke A, Montag D. Aberrant neuronal connectivity in CHL1-deficient mice is associated with altered information processing-related immediate early gene expression. *J Neurobiol*. 2003;57(1):67-80. doi:10.1002/neu.10254
422. Bruhwyler J, Chleide E, Liégeois J-F, Delarge J, Mercier M. Anxiolytic potential of sulpiride, clozapine and derivatives in the open-field test. *Pharmacol Biochem Behav*. 1990;36(1):57-61. doi:10.1016/0091-3057(90)90125-2
423. Rodgers RJ, Nikulina EM, Cole JC. Dopamine D₁ and D₂ receptor ligands modulate the behaviour of mice in the elevated plus-maze. *Pharmacol Biochem Behav*. 1994;49(4):985-995. doi:10.1016/0091-3057(94)90253-4
424. Horvitz JC, Williams G, Joy R. Time-dependent actions of D₂ family agonist quinpirole on spontaneous behavior in the rat:

- dissociation between sniffing and locomotion. *Psychopharmacology (Berl)*. 2001;154(4):350-355. doi:10.1007/s002130000677
425. Luque-Rojas MJ, Galeano P, Suárez J, et al. Hyperactivity induced by the dopamine D2/D3 receptor agonist quinpirole is attenuated by inhibitors of endocannabinoid degradation in mice. *Int J Neuropsychopharmacol*. 2013;16(03):661-676. doi:10.1017/S1461145712000569
426. Chernysheva M, Sych Y, Fomins A, et al. Striatum-projecting prefrontal cortex neurons support working memory maintenance. *bioRxiv*. Published online 2021:2021.12.03.471159. doi:10.1101/2021.12.03.471159
427. Schiavo A, Martins LA, Wearick-Silva LE, Orso R, Xavier LL, Mestriner RG. Can anxiety-like behavior and spatial memory predict the extremes of skilled walking performance in mice? An exploratory, preliminary study. *Front Behav Neurosci*. 2023;17(February):1-11. doi:10.3389/fnbeh.2023.1059029
428. Maggi S, Bon C, Gustincich S, Tucci V, Gainetdinov RR, Espinoza S. Improved cognitive performance in trace amine-associated receptor 5 (TAAR5) knock-out mice. *Sci Rep*. 2022;12(1):14708. doi:10.1038/s41598-022-18924-z
429. Dodds CM, Clark L, Dove A, et al. The dopamine D2 receptor antagonist sulpiride modulates striatal BOLD signal during the manipulation of information in working memory. *Psychopharmacology (Berl)*. 2009;207(1):35-45. doi:10.1007/s00213-009-1634-0
430. Valjent E, Gangarossa G. The Tail of the Striatum: From Anatomy to Connectivity and Function. *Trends Neurosci*. 2021;44(3):203-214. doi:10.1016/j.tins.2020.10.016
431. Besheer J, Short KR, Bevins RA. Dopaminergic and cholinergic antagonism in a novel-object detection task with rats. *Behav Brain Res*. 2001;126(1-2):211-217. doi:10.1016/S0166-4328(01)00245-5
432. Rangel-Gomez M, Hickey C, van Amelsvoort T, Bet P, Meeter M. The Detection of Novelty Relies on Dopaminergic Signaling: Evidence from Apomorphine's Impact on the Novelty N2. *PLoS One*. 2013;8(6). doi:10.1371/journal.pone.0066469
433. de Lima MNM, Presti-Torres J, Dornelles A, et al. Modulatory influence of dopamine receptors on consolidation of object recognition memory. *Neurobiol Learn Mem*. 2011;95(3):305-310. doi:10.1016/j.nlm.2010.12.007
434. Spielewoy C, Roubert C, Hamon M, Nosten M, Betancur C, Giros B. Behavioural disturbances associated with hyperdopaminergia in dopamine-transporter knockout mice. *Behav Pharmacol*. 2000;11(3 & 4):279-290. doi:10.1097/00008877-200006000-00011
435. Meitzen J, Meisel RL, Mermelstein PG. Sex differences and the effects of estradiol on striatal function. *Curr Opin Behav Sci*. 2018;23(1):42-48. doi:10.1016/j.cobeha.2018.03.007
436. Meziane H, Ouagazzal AM, Aubert L, Wietrzyk M, Krezel W. Estrous cycle effects on behavior of C57BL/6J and BALB/cByJ female mice: Implications for phenotyping strategies. *Genes, Brain Behav*. 2007;6(2):192-200. doi:10.1111/j.1601-183X.2006.00249.x
437. Chari T, Griswold S, Andrews NA, Fagiolini M. The Stage of the Estrus Cycle Is Critical for Interpretation of Female Mouse Social Interaction Behavior. *Front Behav Neurosci*. 2020;14(June):1-9. doi:10.3389/fnbeh.2020.00113
438. Zhao W, Li Q, Ma Y, et al. Behaviors Related to Psychiatric Disorders and Pain Perception in C57BL/6J Mice During Different Phases of Estrous Cycle. *Front Neurosci*. 2021;15(April):1-10. doi:10.3389/fnins.2021.650793
439. Zeng P-Y, Tsai Y-H, Lee C-L, Ma Y-K, Kuo T-H. Minimal influence of estrous cycle on studies of female mouse behaviors. *Front Mol Neurosci*. 2023;16(July):1-17. doi:10.3389/fnmol.2023.1146109
440. Lovick TA, Zangrossi H. Effect of Estrous Cycle on Behavior of Females in Rodent Tests of Anxiety. *Front Psychiatry*. 2021;12(August):1-20. doi:10.3389/fpsy.2021.711065
441. Rocks D, Cham H, Kundakovic M. Why the estrous cycle matters for neuroscience. *Biol Sex Differ*. 2022;13(1):62. doi:10.1186/s13293-022-00466-8
442. Francois M, Delgado IC, Shargorodsky N, Leu CS, Zeltser L. Assessing the effects of stress on feeding behaviors in laboratory mice. *Elife*. 2022;11:1-20. doi:10.7554/ELIFE.70271
443. McClintock MK. Social Control of the Ovarian Cycle and the Function of Estrous Synchrony. *Am Zool*. 1981;21(1):243-256. doi:10.1093/icb/21.1.243
444. Gangrade BK, Dominic CJ. Studies of the Male-Originating Pheromones Involved in the Whitten Effect and Bruce Effect in Mice. *Biol Reprod*. 1984;31(1):89-96. doi:10.1095/biolreprod31.1.89
445. Ma W. Induction of Estrus in Grouped Female Mice (*Mus domesticus*) by Synthetic Analogues of Preputial Gland Constituents. *Chem Senses*. 1999;24(3):289-293. doi:10.1093/chemse/24.3.289
446. Dalal SJ, Estep JS, Valentin-Bon IE, Jerse AE. Standardization of the Whitten Effect to induce susceptibility to *Neisseria gonorrhoeae* in female mice. *Contemp Top Lab Anim Sci*. 2001;40(2):13-17. <http://www.ncbi.nlm.nih.gov/pubmed/11300681>
447. Dewing P, Shi T, Horvath S, Vilain E. Sexually dimorphic gene expression in mouse brain precedes gonadal differentiation. *Mol Brain Res*. 2003;118(1-2):82-90. doi:10.1016/S0169-328X(03)00339-5
448. Dewing P, Chiang CWK, Sinchak K, et al. Direct regulation of adult brain function by the male-specific factor SRY. *Curr Biol*. 2006;16(4):415-420. doi:10.1016/j.cub.2006.01.017
449. Kritzer MF, Creutz LM. Region and Sex Differences in Constituent Dopamine Neurons and Immunoreactivity for Intracellular Estrogen and Androgen Receptors in Mesocortical Projections in Rats. *J Neurosci*. 2008;28(38):9525-9535. doi:10.1523/JNEUROSCI.2637-08.2008
450. Tanida T, WARITA K, MITSUHASHI T, et al. Morphological Analyses of Sex Differences and Age-Related Changes in C3H Mouse Midbrain. *J Vet Med Sci*. 2009;71(7):855-863. doi:10.1292/jvms.71.855

451. Walker QD, Rooney MB, Wightman RM, Kuhn CM. Dopamine release and uptake are greater in female than male rat striatum as measured by fast cyclic voltammetry. *Neuroscience*. 1999;95(4):1061-1070. doi:10.1016/S0306-4522(99)00500-X
452. Bhatt SD, Dluzen DE. Dopamine transporter function differences between male and female CD-1 mice. *Brain Res*. 2005;1035(2):188-195. doi:10.1016/j.brainres.2004.12.013
453. Dluzen DE, McDermott JL. Sex Differences in Dopamine- and Vesicular Monoamine-Transporter Functions. *Ann NY Acad Sci*. 2008;1139(1):140-150. doi:10.1196/annals.1432.010
454. Brundage JN, Mason CP, Wadsworth HA, et al. Regional and sex differences in spontaneous striatal dopamine transmission. *J Neurochem*. 2022;160(6):598-612. doi:10.1111/jnc.15473
455. Morissette M, Paolo T Di. Effect of Chronic Estradiol and Progesterone Treatments of Ovariectomized Rats on Brain Dopamine Uptake Sites. *J Neurochem*. 1993;60(5):1876-1883. doi:10.1111/j.1471-4159.1993.tb13415.x
456. Rivest R, Falardeau P, Di Paolo T. Brain dopamine transporter: gender differences and effect of chronic haloperidol. *Brain Res*. 1995;692(1-2):269-272. doi:10.1016/0006-8993(95)00611-S
457. Harper Mozley L, Gur RC, Mozley RD, Gur RE. Striatal dopamine transporters and cognitive functioning in healthy men and women. *Am J Psychiatry*. 2001;158(9):1492-1499. doi:10.1176/appi.ajp.158.9.1492
458. Lee FJS, Pei L, Moszczynska A, Vukusic B, Fletcher PJ, Liu F. Dopamine transporter cell surface localization facilitated by a direct interaction with the dopamine D2 receptor. *EMBO J*. 2007;26(8):2127-2136. doi:10.1038/sj.emboj.7601656
459. Stewart A, Mayer FP, Gowrishankar R, et al. Sex and Circuit Specific Dopamine Transporter Regulation Underlies Unique Behavioral Trajectories of Functional SLC6A3 Coding Variation. *bioRxiv*. Published online January 1, 2021. doi:10.1101/2021.11.02.466932
460. Becker JB. Gender Differences in Dopaminergic Function in Striatum and Nucleus Accumbens. *Pharmacol Biochem Behav*. 1999;64(4):803-812. doi:10.1016/S0091-3057(99)00168-9
461. Martelle SE, Nader SH, Czoty PW, et al. Further Characterization of Quinpirole-Elicited Yawning as a Model of Dopamine D3 Receptor Activation in Male and Female Monkeys. *J Pharmacol Exp Ther*. 2014;350(2):205-211. doi:10.1124/jpet.114.214833
462. Calipari ES, Juarez B, Morel C, et al. Dopaminergic dynamics underlying sex-specific cocaine reward. *Nat Commun*. 2017;8:1-15. doi:10.1038/ncomms13877
463. Roberts BM, Doig NM, Brimblecombe KR, et al. GABA uptake transporters support dopamine release in dorsal striatum with maladaptive downregulation in a parkinsonism model. *Nat Commun*. 2020;11(1):4958. doi:10.1038/s41467-020-18247-5
464. Sedelis M, Hofele K, Auburger GW, Morgan S, Huston JP, Schwarting RKW. Behav Genet 2000 Sedelis.pdf. 2000;30(3):171-182.
465. Vöikar V, Kõks S, Vasar E, Rauvala H. Strain and gender differences in the behavior of mouse lines commonly used in transgenic studies. *Physiol Behav*. 2001;72(1-2):271-281. doi:10.1016/S0031-9384(00)00405-4
466. Rosenfeld CS. Sex-dependent differences in voluntary physical activity. *J Neurosci Res*. 2017;95(1-2):279-290. doi:10.1002/jnr.23896
467. Borbélyová V, Janišová K, Mysliveček J, Riljak V. Sex-Related Differences in Locomotion and Climbing of C57Bl/6NTac Mice in a Novel Environment. *Physiol Res*. 2019;68:S353-S359. doi:10.33549/physiolres.934348
468. Sensini F, Inta D, Palme R, et al. The impact of handling technique and handling frequency on laboratory mouse welfare is sex-specific. *Sci Rep*. 2020;10(1):17281. doi:10.1038/s41598-020-74279-3
469. Mo VM, Zapparoli HR, Reimer AE, Brandão ML, de Oliveira AR. Dopamine D2 receptors in the expression and extinction of contextual and cued conditioned fear in rats. *Exp Brain Res*. 2021;239(6):1963-1974. doi:10.1007/s00221-021-06116-6
470. Schoemaker H, Claustre Y, Fage D, et al. Neurochemical characteristics of amisulpride, an atypical dopamine D2/D3 receptor antagonist with both presynaptic and limbic selectivity. *J Pharmacol Exp Ther*. 1997;280(1):83-97. <http://www.ncbi.nlm.nih.gov/pubmed/8996185>
471. Campbell A, Baldessarini RJ, Cremens MC. Dose-catalepsy response to haloperidol in rat: Effects of strain and sex. *Neuropharmacology*. 1988;27(11):1197-1199. doi:10.1016/0028-3908(88)90018-4
472. Manza P, Shokri-Kojori E, Wiers CE, et al. Sex differences in methylphenidate-induced dopamine increases in ventral striatum. *Mol Psychiatry*. 2022;27(2):939-946. doi:10.1038/s41380-021-01294-9
473. Biskup E, Martinkova J, Ferretti MT. Gender medicine: Towards a gender-specific treatment of neuropsychiatric disorders. In: *Handbook of Clinical Neurology*. Vol 175. 1st ed. Elsevier B.V.; 2020:437-448. doi:10.1016/B978-0-444-64123-6.00029-1
474. Cahill B, Poelker-Wells S, Prather JF, Li Y. A Glimpse Into the Sexual Dimorphisms in Major Depressive Disorder Through Epigenetic Studies. *Front Neural Circuits*. 2021;15(October):1-10. doi:10.3389/fncir.2021.768571

Acknowledgements

First and foremost, I would like to express my sincere gratitude to my thesis supervisor, Prof. Dr. Matthias Kneussel. His support and willingness to step into this role without hesitation have been instrumental in this journey. I am immensely thankful for his guidance and assistance during the challenging phases of my PhD.

I extend my heartfelt thanks to the members of my thesis committee, Dr. Bernreuther and Prof. Dr. Fester. Their advice and guidance during pivotal moments of my project have greatly contributed to its success.

I would also like to extend my deepest gratitude to Prof. Dr. Schachner for the great opportunity she gave me to pursue a PhD in her research group.

Dr. Ralf Kleene and Dr. Gabriele Loers deserve my heartfelt gratitude for their mentorship, supervision, and guidance throughout the entirety of the five-year research adventure. Their constant availability to discuss questions, their expert advice, and their support during the writing process have been indispensable. I deeply appreciate Dr. Ralf Kleene's patience in discussing and explaining topics, assistance with experimental planning, and dedicated efforts to improve working conditions for PhD students. Dr. Gabriele Loers' endless availability to hear and clarify doubts, suggestions, shared knowledge, assistance with experiment planning, and support during critical moments have been invaluable. I would also like to extend a special thanks to Ute Bork for her help in the laboratory and for always bringing some laughs and friendliness.

My heartfelt appreciation goes out to all my colleagues in our research group. Your constant support, whether technical, theoretical, emotional, mental, or cultural, has been a cornerstone of my journey. I am grateful for our much-needed breaks over lunch, coffee, or sweets, and for your encouragement and friendship. In no particular order, I want to express my gratitude to Viviana Granato, Laura Amores-Bonet, and Ludovica Congiu. I want to extend my thanks to my former colleagues, Maria Girbes-Minguez and Gaston Castillo, who warmly welcomed me and generously shared their knowledge. I want also to express my deep gratitude to my dear friend and countrywoman, Rita Marques, for all her support, advice, friendship, and for always checking on me.

I would like to thank the entire ZMNH community, especially the Ph.D. students, post-docs, and technicians within Prof. Kneussel's group, for their invaluable technical support. I'm also grateful to Dr. Freitag for her extensive assistance with the behavioral experiments, and to Dr. Muhia for her expert guidance in statistics.

Additionally, I'm grateful to Dr. Failla and Dr. Zobiak for generously allowing me to use their microscope at the UKE Microscopy Imaging Facility and for their support throughout the process.

Last but certainly not least, my deepest appreciation is reserved for my parents, brothers, grandmother, Belita, Laura, friends and my Alex. To my parents, I am grateful for their enduring love and support, even from afar, and for continually empowering me to surpass my limits. To all of them, I'm grateful for the cherished moments we've shared whenever we gather in Portugal, where time seems to stand still. And, above all, I want to express my boundless thanks and gratitude to my boyfriend, Alex, for his care, love, unwavering support, culinary skills, encouragement, and for the beautiful life we share together.

Curriculum Vitae

Personal data

Name Luciana Fernandes

Place of birth Portugal

Education

Oct 2018 – Feb 2024 **Ph.D.-Programm Nicht-Medizin**

Senior Group Biosynthesis of Neural Structures at Zentrum für Molekulare Neurobiologie Hamburg, Universitätsklinikum Hamburg-Eppendorf

Project: Animal behavioral assessment and implementation of biochemical methods to study protein interactions, neuronal signaling pathways, and morphological parameters *in vivo* and *in vitro*, using specific dopaminergic compounds

Sept 2015 – Sept 2017 **MSc. Medicinal chemistry**

Department of Chemistry at Faculty of Sciences and Technology, University of Coimbra, Portugal

Project: Impact of substance abuse on mouse behavior and consequent biochemical analysis of dopaminergic-induced toxicity

Sept 2012 – Sept 2015 **BSc. Medicinal chemistry**

Department of Chemistry at Faculty of Sciences and Technology, University of Coimbra, Portugal

Sept 2009 – Sept 2012 **High School for Science and Technology**

Group of Schools Dr. Mário Sacramento, Aveiro, Portugal

Main subjects: Mathematics, Biology, and Chemistry

Eidesstattliche Erklärung

Ich versichere ausdrücklich, dass ich die Arbeit selbständig und ohne fremde Hilfe verfasst, andere als die von mir angegebenen Quellen und Hilfsmittel nicht benutzt und die aus den benutzten Werken wörtlich oder inhaltlich entnommenen Stellen einzeln nach Ausgabe (Auflage und Jahr des Erscheinens), Band und Seite des benutzten Werkes kenntlich gemacht habe.

Ferner versichere ich, dass ich die Dissertation bisher nicht einem Fachvertreter an einer anderen Hochschule zur Überprüfung vorgelegt oder mich anderweitig um Zulassung zur Promotion beworben habe.

Ich erkläre mich einverstanden, dass meine Dissertation vom Dekanat der Medizinischen Fakultät mit einer gängigen Software zur Erkennung von Plagiaten überprüft werden kann.

30.09.2023, Hamburg

Unterschrift